Connecting metabolic networks

-

The role of the

Mitochondrial Carrier Family in plants

Inauguraldissertation

zur Erlangung des Doktorgrades
der Mathematisch-Naturwissenschaftlichen Fakultät
der Heinrich-Heine-Universität Düsseldorf

vorgelegt von

Björn Hielscher

aus Mülheim an der Ruhr

Düsseldorf, August 2018

aus dem Institut für Biochemie der Pflanzen
der Heinrich-Heine-Universität Düsseldorf

Gedruckt mit der Genehmigung der
Mathematisch-Naturwissenschaftlichen Fakultät der Heinrich-Heine-Universität Düsseldorf

Referent: PD Dr. Nicole Linka

Korreferent: Prof. Dr. Peter Westhoff

Tag der mündlichen Prüfung: 17.12.2018

Erklärung

Ich versichere an Eides Statt, dass ich die vorliegende Dissertation eigenständig und ohne unerlaubte Hilfe unter Beachtung der „Grundsätze zur Sicherung guter wissenschaftlicher Praxis“ an der Heinrich-Heine-Universität Düsseldorf angefertigt habe. Die Dissertation habe ich in der dieser oder in ähnlicher Form noch bei keiner anderen Institution eingereicht.
Ich habe bisher keine erfolglosen Promotionsversuche unternommen

Düsseldorf, den

_____

Björn Hielscher

Table of contents

I. Preface

This thesis is divided into independent sections with two submission-ready manuscripts and three previously published works. Manuscript 1 describes the identification and biochemical characterization of two transport proteins probably involved in photorespiration and β-oxidation. Comparative co-expression analysis of C3, C4 and intermediate Flaveria transcriptomes was used to identify 34 candidate genes linked to photorespiration in Arabidopsis. Two selected Arabidopsis proteins from the mitochondrial carrier family (MCF) localized in peroxisomes were biochemically characterized. Arabidopsis loss-of-function mutants were established using the CRISPR/Cas9 system. Manuscript 2 focuses on the phenotypic analysis of two Arabidopsis T-DNA insertion lines impaired in the expression of the MCF member and mitochondrial phosphate transporter AtPHT3;3. Each manuscript concludes with an outlook section. Both manuscripts are included in section V. Section VI summarizes the results of Manuscript 1 and 2. Section VII contains three previously published manuscripts. Manuscript 3 is a method paper on the analysis of peroxisomal β-oxidation in Arabidopsis seeds during early germination published as Hielscher et al. (2017). Manuscript 4 describes the biochemical characterization of the Arabidopsis MCF transporters AtUCP1 and AtUCP2 and was published as Monné et al. (2018). Manuscript 5 describes the function of two *Cichorium intybus* enzymes CiSHT1 and CiSHT2 and was published as Delporte et al. (2018).

References

Delporte, M., Bernard, G., Legrand, G., Hielscher, B., Lanoue, A., Moliné, R., Rambaud, C., Mathiron, D., Sébastien, B., Linka, N., Hilbert, J.-L., and Gagneul, D. (2018). Neofunctionalization within the BAHD family results in the production of tetrahydroxycinnamoyl spermine in the pollen coat of the Asteraceae family. (Accepted at Journal of Experimental Botany at the time of submission)

Hielscher, B., Charton, L., Mettler-Altmann, T., and Linka, N. (2017). Analysis of Peroxisomal β-Oxidation During Storage Oil Mobilization in Arabidopsis thaliana Seedlings. Methods Mol. Biol. **1595**: 291–304.

Monné, M., Daddabbo, L., Gagneul, D., Obata, T., Hielscher, B., Palmieri, L., Miniero, D.V., Fernie, A.R., Weber, A.P.M., and Palmieri, F. (2018). Uncoupling proteins 1 and 2 (UCP1 and UCP2) from Arabidopsis thaliana are mitochondrial transporters of aspartate, glutamate, and dicarboxylates. J. Biol. Chem. **293**: 4213–4227.

II.1 Summary

The subcellular compartmentalization of plant cells led to functional separation of genes, cell structures and metabolic pathways and the evolution of compartments. However, in-depth analyses have shown that these compartments are highly interconnected and that organellar metabolic pathways are part of a dynamic metabolic network that connects numerous cell compartments (Heinig et al., 2013). Metabolites need to be shuttled between these compartments and across impermeable organellar membranes. Essential components of this shuttle are transport proteins (Carraretto et al., 2016; Eisenhut et al., 2015). Transport proteins regulate the import of most metabolites and evolved into numerous transporter families. These transporter families are usually categorized by specific protein sequence structures or substrate specificity.

An essential protein family is the mitochondrial carrier family (MCF) with 58 known members in Arabidopsis (Picault et al., 2004). MCF proteins are localized in mitochondria, peroxisomes, plastids, the endoplasmic reticulum (ER) or the plasma membrane and shuttle substrates like nucleotides, carboxylates and amino acids (Palmieri et al., 2011; Haferkamp and Linka, 2012). They share a highly conserved tripartite sequence of 100 repeating amino acids with two α-helices per repeat. Each repeat is separated by a hydrophilic loop and contains the signature PFAM PF00153 motif (Palmieri, 1994).

This study focuses on the characterization of MCF members in Arabidopsis. Manuscript 1 describes the identification of transporters co-regulated with photorespiratory enzymes in C3 to C4 species of Flaveria. AtPPR1;1 and AtPPR1;2, two peroxisomal MCF members, have been identified to be upregulated in the C3 species *Tarenaya hassleriana* compared to the related C4 species *Gynandropsis gynandra* and under photorespiratory CO_2 conditions in Arabidopsis. Tissue-specific expression data revealed higher transcript levels in mature seeds of *T. hassleriana* and Arabidopsis. Biochemical analysis of both transporters revealed a substrate affinity for the dicarboxylic acid malate. Evidences suggest that AtPPR1;1 and AtPPR1;2 are involved in the peroxisomal malate/oxaloacetate shuttle. This shuttle is crucial for NAD^+/NADH regeneration in plant peroxisomes. Malate is converted to oxaloacetate via the peroxisomal malate dehydrogenase (MDH) releasing NADH in the process (Antonenkov and Hiltunen, 2012). NAD^+/NADH is involved in β-oxidation and photorespiration (Pracharoenwattana et al., 2007; Timm et al., 2011). AtPPR1;1 and AtPPR1;2 might fuel β-oxidation and peroxisomal photorespiration with reducing equivalents during early seed germination and photosynthesis. Further studies need to verify additional substrates to elucidate the role of these proteins in Arabidopsis.

Manuscript 2 describes the phenotypic characterization of the MCF transporter AtPHT3;3 in Arabidopsis. The PHT3 family is localized in plant mitochondria and is thought to fuel ATP synthase with inorganic phosphate for ATP production (Junge and Nelson, 2015).

While AtPHT3;1 and AtPHT3;2 have been shown to transport phosphate (Hamel et al., 2004), the function of AtPHT3;3 has not been shown yet. AtPHT3;3 is ubiquitously expressed but shows higher transcript levels in the shoot apical meristem (SAM) and in reproductive tissues. AtPHT3;3 T-DNA insertion lines do not show any impairment in pollen viability but embryo development. Siliques contain a higher number of smaller aborted seeds and empty seed positions indicating a defect during seed production. Indeed, aborted seeds contain no embryos or embryos stuck in early stages of development. Analysis of fatty acid content revealed no impairment of storage or degradation processes. Homologues of Arabidopsis PHT3 proteins in yeast and mammals (ScPic2 and SLC25A3, respectively) have been shown to use copper as primary substrate (Vest et al., 2013; Boulet et al., 2018). These proteins refill the mitochondrial copper pool, which is required for a COX/Complex IV assembly and therefore a functional electron transport chain (Cobine et al., 2004; Mansilla et al., 2018). Defects in this pathway usually lead to lethal embryos or severe growth defects (Attallah et al., 2011; Radin et al., 2015). Arabidopsis PHT3 proteins might play a role in mitochondrial copper transport. Yet, further analyses need to provide data about the biochemical function of AtPHT3;3 and substrate specificities for the PHT3 family in Arabidopsis.

Much progress has been made on the function of MCF members and their role during plant development. Proteins of this family are localized in various subcellular compartments and plant tissues. Compared to other organisms, plants contain a high number of diverse MCF proteins. With this, the MCF and the associated pathways are a prime example of complex intracellular metabolic networks.

II.2 Zusammenfassung

Die Kompartimentierung pflanzlicher Zellen führte zur funktionalen Trennung Genen, Zellstrukturen und Stoffwechselwegen und der Entwicklung von Kompartimenten. Studien zeigten jedoch, dass diese Kompartimente miteinander verbunden und die meisten Stoffwechselwege Teil eines hochdynamischen Netzwerks sind, das diese Kompartimente miteinander verbindet (Heinig et al., 2013)., Metabolite müssen zwischen diesen Kompartimenten transportiert und durch zumeist impermeable Membranen gebracht werden. Wichtige Bestandteile dieses Transports sind membranständige Transportproteine (Carraretto et al., 2016; Eisenhut et al., 2015). Transportproteine regulieren den Einstrom von Metaboliten und haben sich in zahlreichen Proteinfamilien manifestiert. Diese Proteinfamilien werden entsprechend ihrer Struktur oder ihrer Substratspezifität eingeordnet.

Eine wichtige Proteinfamilie bildet die Mitochondriale Carrier Familie (MCF) mit 58 identifizierten Proteinen in Arabidopsis (Picault et al., 2004). MCF Proteine sind in Mitochondrien, Peroxisomen, Plastiden, im endoplasmatischen Retikulum (ER) oder in der Plasmamembran lokalisiert. Sie transportieren Substrate wie Nukleotide, Carbonsäuren oder Aminosäuren (Palmieri et al., 2011; Haferkamp and Linka, 2012). MCF Proteine besitzen einen für diese Familie charakteristischen Aufbau: Eine konservierte dreiteilige Struktur von etwa 100 Aminosäuren langen Sequenzwiederholungen. Jede Sequenzwiederholung besitzt zwei α-Helices und das charakteristische PFAM PF00153 Motiv. Jede Sequenzwiederholung wird von einer hydrophoben Sequenz unterbrochen (Palmieri, 1994).

Diese Arbeit beschreibt die Charakterisierung von MCF Proteinen in Arabidopsis. Manuskript 1 beschreibt die Identifizierung von Transportern, welche mit photorespiratorischen Enzymen in C3 und C4 Flaveria-Spezies co-reguliert sind. Zwei peroxisomale MCF Proteine, AtPPR1;1 und AtPPR1;2, wurden identifiziert. Im Vergleich zur C4 Spezies *Gynandropsis gynandra*, ist die Expression beider Proteine in der C3 Spezies *Tarenaya hassleriana* hochreguliert. Auch in Arabidopsis ist die Expression unter photorespiratorischen CO_2 Bedingungen erhöht. Weiterhin zeigen gewebespezifische Expressionsanalysen, dass reife Samen höhere Transkriptmengen beinhalten. Eine biochemische Analyse beider Transporter zeigt, dass beide Proteine die Dicarbonsäure Malat als Substrat akzeptieren. Diese Ergebnisse weisen darauf hin, dass AtPPR1;1 und AtPPR1;2 eine Rolle im peroxisomalen Malat/Oxaloacetat-Transportweg spielen könnten. Dieser Transportweg für die Regeneration von NAD^+/NADH durch die Malatdehydrogenase (MDH) von Bedeutung (Antonenkov and Hiltunen, 2012). NAD^+/NADH sind Cofaktoren der β-Oxidation und der Photorespiration (Pracharoenwattana et al., 2007; Timm et al., 2011). AtPPR1;1 und AtPPR1;2 könnten die β-Oxidation und den peroxisomalen Teil der Photorespiration indirekt mit NAD^+/NADH versorgen. Weitere Untersuchungen sind erforderlich, um die physiologische Rolle dieser Proteine in Arabidopsis zu erforschen.

Manuskript 2 beschreibt die phänotypische Analyse des MCF Proteins AtPHT3;3 in Arabidopsis. Proteine der PHT3 Familie befinden sich in der inneren mitochondrialen Membran. Zur Produktion von ATP versorgen sie die ATP-Synthase mit anorganischem Phosphat (Junge and Nelson, 2015). Für AtPHT3;1 und AtPHT3;2 konnte der Transport von Phosphat nachgewiesen werden (Hamel et al., 2004). Das bevorzugte Substrat von AtPHT3;3 ist bislang unbekannt. AtPHT3;3 ist in allen Geweben von Arabidopsis exprimiert, zeigt jedoch eine höhere Transkriptmenge im Sprossapikalmeristem und in Reproduktionsgeweben. AtPHT3;3 T-DNA Insertionslinien zeigen keine Beeinträchtigung der Pollenaktivität. Jedoch ist die Samenproduktion gestört. Es zeigt sich eine erhöhte Anzahl verkümmerter Samen und leerer Samenpositionen. Verkümmerte Samen beinhalten keine Embryos oder Embryos, deren Entwicklung in einer frühen Phase abgebrochen wurde. Eine Analyse des Fettsäuregehalts in Arabidopsissamen zeigte keine Störung der Fettsäuremenge oder des Fettsäureabbaus. Homologe Proteine in Hefe und Säugetieren (ScPic2 und SLC25A) bevorzugen Kupfer als Substrat (Vest et al., 2013; Boulet et al., 2018). ScPic2 und SLC25A füllen den mitochondrialer Kupferpool, welcher für die Korrekte Zusammensetzung und Funktion des COX/Komplex IV der Elektronentransportkette nötig ist (Cobine et al., 2004; Mansilla et al., 2018). Eine Störung dieses Mechanismus führt häufig zu nicht überlebensfähigen Embryos oder schweren Wachstumsdefiziten (Attallah et al., 2011; Radin et al., 2015). Arabidopsis PHT3 Proteine spielen möglicherweise eine zusätzliche Rolle im mitochondrialen Kupfertransport. Weitere Studien sind jedoch nötig, um die biochemische Funktion von AtPHT3;3 und die Substratspezifität der PHT3 Familie aufzuklären.

Große Fortschritte wurden auf dem Gebiet der MCF Proteine und deren Rolle während der pflanzlichen Entwicklung gemacht. Proteine dieser Proteinfamilie befinden sich in verschiedenen subzellulären Kompartimenten und Geweben. Verglichen mit anderen Organsimen, beinhalten Pflanzen eine vergleichsweise hohe Anzahl an verschiedenen MCF Proteinen. Sie sind ein Musterbeispiel für komplexe intrazelluläre Stoffwechselwege.

References

Antonenkov, V.D. and Hiltunen, J.K. (2012). Transfer of metabolites across the peroxisomal membrane. Biochim. Biophys. Acta - Mol. Basis Dis. **1822**: 1374–1386.

Attallah, C. V., Welchen, E., Martin, A.P., Spinelli, S. V., Bonnard, G., Palatnik, J.F., and Gonzalez, D.H. (2011). Plants contain two SCO proteins that are differentially involved in cytochrome c oxidase function and copper and redox homeostasis. J. Exp. Bot. **62**: 4281–4294.

Boulet, A. et al. (2018). The mammalian phosphate carrier SLC25A3 is a mitochondrial copper transporter required for cytochrome c oxidase biogenesis. J. Biol. Chem. **293**: 1887–1896.

Carraretto, L., Teardo, E., Checchetto, V., Finazzi, G., Uozumi, N., and Szabo, I. (2016). Ion Channels in Plant Bioenergetic Organelles, Chloroplasts and Mitochondria: From Molecular Identification to Function. Mol. Plant **9**: 371–395.

Cobine, P.A., Ojeda, L.D., Rigby, K.M., and Winge, D.R. (2004). Yeast Contain A Non-proteinaceous Pool of Copper in the Mitochondrial Matrix. J. Biol. Chem. **279**: 14447–14455.

Eisenhut, M., Hocken, N., and Weber, A.P.M. (2015). Plastidial metabolite transporters integrate photorespiration with carbon, nitrogen, and sulfur metabolism. Cell Calcium **58**: 98–104.

Haferkamp, I. and Linka, N. (2012). Functional expression and characterisation of membrane transport proteins. Plant Biol. **14**: 675–690.

Hamel, P., Saint-Georges, Y., De Pinto, B., Lachacinski, N., Altamura, N., and Dujardin, G. (2004). Redundancy in the function of mitochondrial phosphate transport in Saccharomyces cerevisiae and Arabidopsis thaliana. Mol. Microbiol. **51**: 307–317.

Heinig, U., Gutensohn, M., Dudareva, N., and Aharoni, A. (2013). The challenges of cellular compartmentalization in plant metabolic engineering. Curr. Opin. Biotechnol. **24**: 239–246.

Junge, W. and Nelson, N. (2015). ATP Synthase. Annu. Rev. Biochem. **84**: 631–657.

Mansilla, N., Racca, S., Gras, D.E., Gonzalez, D.H., and Welchen, E. (2018). The complexity of mitochondrial complex iv: An update of cytochrome c oxidase biogenesis in plants. Int. J. Mol. Sci. **19**.

Palmieri, F. (1994). Mitochondrial carrier proteins. FEBS Lett. **346**: 48–54.

Palmieri, F., Pierri, C.L., De Grassi, A., Nunes-Nesi, A., and Fernie, A.R. (2011). Evolution, structure and function of mitochondrial carriers: A review with new insights. Plant J. **66**: 161–181.

Picault, N., Hodges, M., Palmieri, L., and Palmieri, F. (2004). The growing family of mitochondrial carriers in Arabidopsis. Trends Plant Sci. **9**: 138–146.

Pracharoenwattana, I., Cornah, J.E., and Smith, S.M. (2007). Arabidopsis peroxisomal malate dehydrogenase functions in β-oxidation but not in the glyoxylate cycle. Plant J. **50**: 381–390.

Radin, I., Mansilla, N., Rödel, G., and Steinebrunner, I. (2015). The Arabidopsis COX11 Homolog is Essential for Cytochrome c Oxidase Activity. Front. Plant Sci. **6**: 1–17.

Timm, S., Florian, A., Jahnke, K., Nunes-Nesi, A., Fernie, A.R., and Bauwe, H. (2011). The hydroxypyruvate-reducing system in Arabidopsis: multiple enzymes for the same end. Plant Physiol. **155**: 694–705.

Vest, K.E., Leary, S.C., Winge, D.R., and Cobine, P.A. (2013). Copper import into the mitochondrial matrix in Saccharomyces cerevisiae is mediated by Pic2, a mitochondrial carrier family protein. J. Biol. Chem. **288**: 23884–23892.

III. Introduction

Challenges to improve modern agriculture

Historically, crop breeders were focused on the increase of total yield. Modern agriculture uses fertilizers to overcome environmental disadvantages and to improve yield quantity and quality. But the excessive use of fertilizers today harms the environment and free-living organisms (Wang et al., 2008; Savci, 2012). Additionally, crops are treated with vast amounts of pesticides. Although the use of pesticides does increase crop yield in general, the high level of pesticides used in modern agriculture does not necessarily improve crop quantity anymore (Gaba et al., 2016). Instead, pesticides negatively affect non-target organisms. These organisms are either affected by the consumption of treated crops or through the contamination of the environment. The extend of the negative effect on free-living organisms is not fully understood. Still, non-target vegetation and animals are undeniably harmed (Aktar et al., 2009; Carvalho, 2017). Although farmers and scientists are looking for more environment-friendly alternatives to traditional crop treatments (Chen et al., 2018; Huang et al., 2003), even the optimal yield outcome of present-day agriculture cannot meet the food demands of the following decades. The expansion of the human population is thought to increase to 9.6 billion in 2050. Distribution, pricing and resource competition complicate the availability of food for everyone. Improving crops to meet future food demands while preserving local ecosystems is a major challenge for farmers, breeders and scientists today. First approaches to improve modern agriculture included the modernization of agricultural techniques and machinery, the use of more stable hybrid plants or the identification of beneficial mutations in crop plants (Fedoroff, 2015; Godfray et al., 2010). One major issue of crop cultivation is the handling with abiotic factors.

The limitation of nutrients, especially phosphorus and nitrogen, toxicity of elements like aluminum or boron, soil compaction or stress factors like drought, high temperatures or saline soils have a big impact on the success of crop production. Nutrient availability is usually ensured using an excess of fertilizers. But the production of fertilizers is cost-intensive and partly based on non-renewable resources. But even under nutrient excess conditions crop plants only use 20 - 40 % of nutrients supplied by fertilizers. The surplus of fertilizers reaches ground water and harms the local ecosystem (López-Arredondo et al., 2015; Xu et al., 2012).Drought is countered with local fresh water. But fresh water is a highly limited resource. In some regions up to 90 % of the regional fresh water is used for agriculture. And it is predicted that the water usage will increase by 40 % within the next decade (Bodner et al., 2015). Alternative crop plants or more drought-resistant varieties of established crops could reduce the amount of fresh water for agriculture (Baltzoi et al., 2015). Saline soils are another major challenge for crops. Beneficial microorganisms, especially rhizospheric bacteria were identified to affect soil salinity and promote plant growth. They could hold the potential to face salinity

without the use of chemicals (Gilliham, 2015; Shrivastava and Kumar, 2015). Today, the access to genomes of crop plants, the identification and characterization of metabolic key players and new molecular techniques like CRISPR-based gene editing are the basis of more recent attempts to improve crops in a way that traditional breeding and screening methods could never accomplish (Michael and VanBuren, 2015; Gao, 2018).

Targets of metabolic engineering are transcription factors, enzymes and transporters that are related to nutrient uptake, nutrient usage, stress tolerance or energy turnover in plants (López-Arredondo et al., 2015). Two major metabolic pathways that might improve crop productivity are photosynthesis and photorespiration. Promising approaches regarding photosynthesis include the manipulation of the slow and error-prone CO_2 accepting RuBisCO, enzymes of the Calvin cycle, non-photochemical quenching or the introduction of CO_2 concentrating mechanisms (Orr et al., 2017). The metabolic consequence of oxygen fixation via RuBisCO is photorespiration. Photorespiration is an energy-consuming process with the essential function to reassimilate carbon using a complex metabolic network with a set of enzymes, transporters and associated pathways to convert 2-phosphoglycolate. The energy spent on this process cannot be used for the production of biomass. Hence, the reduction of photorespiration in plants is a major goal of crop improvement. Studies on photorespiratory enzymes did not identify plant mutants with reduced photorespiration rates but normal growth under ambient air conditions (Betti et al., 2016). The reduced activity of photorespiratory enzymes led to loss of biomass and reduced photosynthetic activity, while the overexpression of the mitochondrial enzyme glycine decarboxylase enhanced these factors (Betti et al., 2016; Timm et al., 2015). Additional studies revealed that photorespiration is part of a regulatory network affecting photosynthesis and the Calvin cycle (Timm et al., 2016). To circumvent the photorespiratory pathway, metabolic bypasses were considered and implemented into plants. These bypasses included the plastidic conversion of glycolate into glycerate (Kebeish et al., 2007), the plastidic conversion of 2-phosphoglycolat to CO_2 (Maier et al., 2012) and the peroxisomal conversion of glyoxylate to hydroxypyruvate (Carvalho et al., 2011). Resulting plants were increasing biomass under controlled short-day conditions and optimal nutrient and water supply. The benefit of these bypasses for crops and naturally fluctuating conditions still needs to be proven (Betti et al., 2016). Further attempts have been made to fix the carbon lost during photorespiration in mitochondria. Rice and wheat were found to use an CO_2 assimilation mechanism called photorespiratory CO_2 scavenging. Here, chloroplasts surround the cell periphery and trap the CO_2 before it can leave the plant through the intercellular air space. With this mechanism, CO_2 is available for RuBisCO again (Busch et al., 2013). A more sophisticated approach to improve crops and reduce photorespiration is the introduction of C4 metabolism into C3 crops. Most crops are C3 plants, plants that need photorespiration to survive at ambient air conditions, while maize, sugar cane, millet and sorghum represent few

of the domesticated C4 crops. C4 photosynthesis allows the spatial separation of RuBisCO and oxygen. This enhances the reaction of RuBisCO with CO_2. Basically, CO_2 is assimilated in mesophyll cells, transferred as malic or aspartic acid and released in bundle sheath cells where RuBisCO resides in major amounts (Gowik and Westhoff, 2011). The modification of C3 plants includes structural changes to the C4-specific Kranz anatomy, as well as the introduction of C4 enzymes and transporters (Bräutigam et al., 2014; Sage et al., 2014).

Key targets in many attempts to improve crops via engineering are transport proteins. They play crucial roles in water and nutrient uptake, stress tolerance and metabolite shuttling (Schroeder et al., 2013). Identifying and manipulating these transporters to make crops more tolerant to adverse environments is one of the major challenges in plant engineering and requires a detailed knowledge of intercellular and intracellular metabolic networks and the shuttle of metabolites between subcellular compartments.

Compartmentalization of plant cells

The outstanding characteristic of eukaryotes is the subcellular division into smaller functional diverse compartments. These enclosed compartments are separated from the cytosol via semipermeable double-layered lipid membranes. Specific sets of proteins and structural features define the function of each compartment (Gabaldón and Pittis, 2015; Alberts et al., 2003). While some prokaryotes have developed cell internal membranes like cyanobacterial thylakoids that derive from the plasma membrane (Nickelsen et al., 2011; Santarella-Mellwig et al., 2013), eukaryotes developed the defining separation of transcriptional and translational processes. This separation sets them apart from prokaryotes and archaea and lead to the formation of the nucleus (Devos et al., 2014). Further evolutionary events allowed the formation of other unique organelles.

Plant cell organelles – Structure, function and metabolite exchange

It is widely accepted that cell organelles originate from two sources, either by the modification of preexisting cell-internal structures or by the interaction with cell-external structures, usually other cells. Organelles like the nucleus, the endoplasmic reticulum (ER) or peroxisomes are thought to be a result of cell-internal mechanisms, although endogenous origins for these organelles have been proposed before (discussed in Gabaldón and Pittis, 2015). Similar contradicting hypotheses have been proposed for the evolution of plastids and mitochondria. However, strong evidences like the presence of their own genome support the endogenous origin of these organelles. Today, the evolution of plastids and mitochondria is commonly described by endosymbiotic events (Archibald, 2015). Regardless of their origin, organelles represent functional unique compartments separated from other compartments by at least one lipid bilayer. Despite their separation these organelles are not completely autonomous and are

in fact connected to other compartments through various types of membrane-bound transport proteins. Many metabolic pathways are present in various compartments or are shared between them. Signaling pathways help to coordinate these pathways make subcellular compartments more flexible to inner and outer factors (Alberts et al., 2003, Figure 1). The interaction via transport proteins and the use of certain types of transport proteins varies between the compartments and shall be addressed further by the following selected examples.

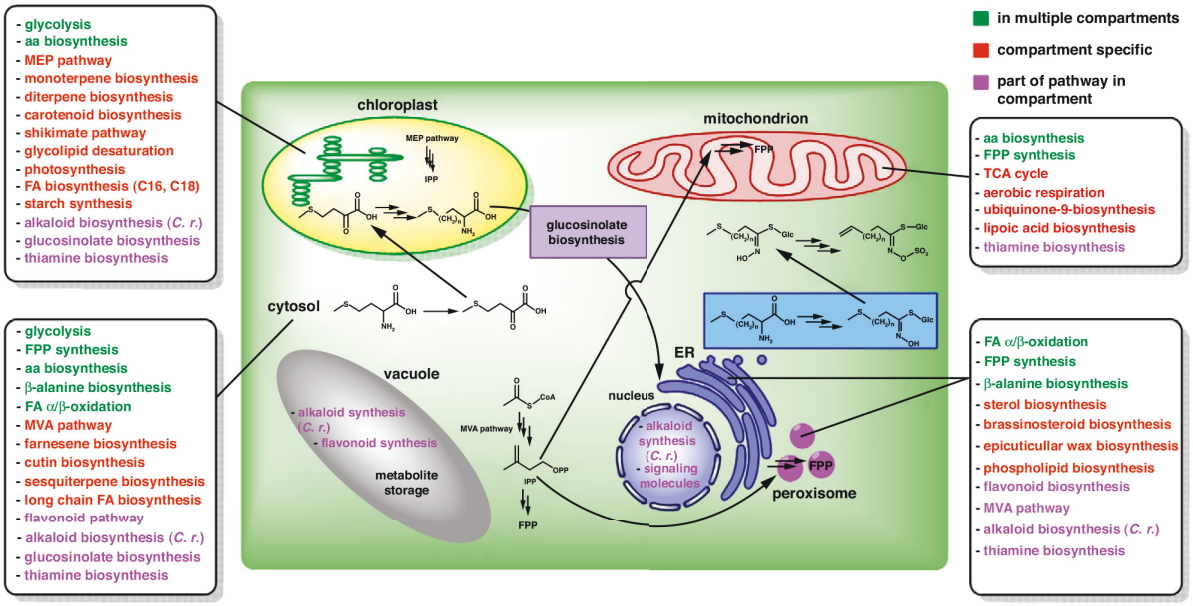

Figure 1. Structural and metabolic compartmentalization of plant cells. Simplified scheme of biosynthetic pathways found in selected organelles of plant cells. Boxes indicate pathways that are exclusive to one compartment (red), present in multiple compartments (green) or spread across multiple compartments (purple). Abbreviations: aa, amino acid; *C. r.*: *Catharanthus roseus*; ER, endoplasmic reticulum; FA, fatty acid; FPP, farnesyl diphosphate; IPP, isopentenyl diphosphate; MEP, 2-C-methylerythritol 4-phosphate; MVA, mevalonic acid. Modified from Heinig et al. (2013).

Plant cell organelles – The nucleus and the ER

The nucleus is separated from the cytosol by the nuclear envelope. It consists of two membranes: the inner and outer membrane. The outer membrane is physically connected to the endoplasmic reticulum (ER). The outer and inner membrane are connected via the nuclear pore complexes (NPC). The NPC allows molecule exchange between the nucleoplasm and the cytosol or the ER. They are highly selective, bidirectional and allow the shuttle of proteins and protein-bound RNA. Smaller solutes and water can freely diffuse (Beck and Hurt, 2017; Wente and Rout, 2010). Several models have been proposed to explain the origin of the nucleus, including the establishment of a nuclear membrane as a protection against reactive oxygen species (ROS) during or after the acquisition of mitochondria (Martin, 2005; Speijer, 2015; Martin et al., 2015).

The ER is the largest organelle in regards of total membrane area (Alberts et al., 2003) and is responsible for the synthesis of proteins, lipid metabolism and calcium storage (Schwarz and Blower, 2016). It closely interacts with the nucleus and consists of the rough and smooth ER. The rough ER is the site of protein biosynthesis. Ribosomes at the cytosol-facing site of the ER allow high rates of translational processes (Voeltz et al., 2002). Although the ER has a large set of transporters responsible for the shuttle of metabolites like sugars, nucleotide-sugars, phosphate, sulfate or various cofactors (Csala et al., 2007), a more striking transport mode of the ER is the formation of lipid vesicles. Specialized domains are responsible for the membrane evagination process. Vesicles transport lipids, proteins and metabolites to compartments like the plasma membrane, Golgi, the vacuole, mitochondria or peroxisomes (Watson and Stephens, 2005).

Plant cell organelles – Chloroplasts

Plastids contain their own genome. It derives from the photosynthetic cyanobacterial cell involved in the primary endosymbiotic event with a heterotrophic eukaryotic host (Archibald, 2015). Although most of the genes were lost or transferred to the nucleus and only 120-130 genes remain in contemporary chloroplasts, the photosynthetic compartment was kept in many lineages (Martin et al., 1998; Moreira and Deschamps, 2014). Secondary endosymbiotic events enclosed plastids in three or more membranes, while other eukaryotes lost the organelle but kept corresponding genes in the nucleus (Gentil et al., 2017; Moreira and Deschamps, 2014). Higher plants contain photosynthetic plastids, called chloroplasts.

Chloroplasts are enclosed within the outer and inner envelope. The outer envelope derives from the former host cell but also contains traces of cyanobacterial origin. The cyanobacterial cell contributed the inner envelope (Jensen and Leister, 2014; Inoue, 2007). Passageways for proteins through the outer envelope is the Tic protein import complex, which corresponds to the inner envelope equivalent, the Toc complex (Jarvis and Soll, 2001). Selective substrate-specific channels for amines, amino acids, carbohydrates, ATP carboxylates, phosphates and sugars have been identified in the outer envelope (Pottosin and Shabala, 2016). The inner envelope contains a variety of selective transporters: phosphate translocators like the triose phosphate/phosphate translocator AtTPT or the glucose-6-phosphate/phosphate translocator AtGPT, ATP:ADP antiporters (Facchinelli and Weber, 2011), members of the mitochondrial carrier family (MCF) like AtSAMC1, AtNDT1 and AtFOLT1 (Palmieri et al., 2006a, 2009; Bedhomme et al., 2005) or dicarboxylate transporters AtDiT1 and AtDiT2 (Renné et al., 2003; Kinoshita et al., 2011) (summarized in Facchinelli and Weber, 2011; Pottosin and Shabala, 2016). The variety of transporters found in chloroplasts corresponds to the manifold functions of this organelle. The most prominent feature of chloroplasts is the conversion of light energy into chemical energy via photosynthesis located

in the plastid-internal thylakoids (Flügge et al., 2016) and photorespiration. Photorespiration is a complex metabolic pathway, which spans three organelles, chloroplasts, peroxisomes and mitochondria, and the cytosol to recycle carbon lost during the Calvin cycle (Bauwe et al., 2010). Photorespiration is regulating and regulated by various other processes of the primary metabolism (Hodges et al., 2016). The synthesis of 12 amino acids is also performed within chloroplasts. This includes the synthesis of tryptophan, phenylalanine, tyrosine, as well as histidine, aspartic acid and their derivatives and most of the arginine synthesis pathway (Pratelli and Pilot, 2014). To maintain cell function in the absence of photosynthesis during the night, chloroplasts synthesize transitory starch during the day using triose phosphates from the Calvin cycle (Pfister and Zeeman, 2016). The subsequent degradation of starch to sucrose makes energy accessible for other cell compartments (Zeeman et al., 2007). All these processes require a constant shuttle of metabolites across both membranes and a complex signaling network with other cell compartments to regulate this shuttle (Marchand et al., 2018; Bobik and Burch-Smith, 2015).

Plant cell organelles – Mitochondria

Mitochondria are thought to be the first stable organelles integrated into an archaebacterial host cell, even before a nucleus had been established. In fact, mitochondria are believed to be the driving force behind eukaryotic cell complexity. Only mitochondria might have been able to generate enough energy to allow the subcellular reconstruction found in eukaryotes today (Martin et al., 2015). Like plastids, mitochondria have retained their own genome from endosymbiotic origin but transferred most of genes to the nucleus (Brandvain and Wade, 2009). Yet, some genes remained in the organelle. These genes are thought to be involved in redox regulation. With this, mitochondria can directly respond to changes of the redox state. The presence of the plastidic genome is also considered to be linked to redox regulation (Allen, 2015; Martin et al., 2015).

Mitochondria are separated from the cytosol by two lipid bilayers: the outer and inner membrane. The outer membrane only contains nuclear encoded proteins. These include the protein import complexes TOM40 and TOB/SAM. Equivalents of the inner membrane are TIM22 and TIM23, as well as Mia40/Tim401-Erv1 (Endo and Yamano, 2010). Ions and small, uncharged molecules can freely pass the outer membrane through voltage-dependent porins (Kühlbrandt, 2015). In contrast to the smooth outer membrane, the inner membrane is known for its folded cristae structure. Cristae morphology can be modified and reacts to the redox state or environmental stress factors (Cogliati et al., 2016). Cristae enlarge the overall surface for oxidative phosphorylation, meaning the electron transport chain (ETC) machinery and ATP production. Oxidative phosphorylation requires a membrane potential using protons pumped into the intermembrane space via the ETC. Hence, the inner membrane is closed to any free

diffusion of metabolites (Kühlbrandt, 2015). The resulting protein gradient is subject o diurnal fluctuations and signals from other compartments. To allow flexibility and the modulation of the mitochondrial membrane and its activity, mitochondria contain a unique set of transport proteins in the inner mitochondrial membrane (Lee and Millar, 2016). Many transporters found here belong to the mitochondrial carrier family (MCF). MCF proteins in plants transport nucleotides, carboxylates and amino acids. The majority of MCF proteins are localized in the inner mitochondrial membrane. Some MCF proteins reside in peroxisomes, plastids, the ER or the plasma membrane (Palmieri et al., 2011; Haferkamp, 2007; Lee and Millar, 2016). In total, 58 MCF members were identified in Arabidopsis. Non-MCF transporters of the inner mitochondrial membrane include the pyruvate importer AtMPC (Wang et al., 2014), the calcium uniporter MCU (Teardo et al., 2017), the molybdenum transporter AtMOT1 (Baxter et al., 2008) and transporters for GABA (Michaeli et al., 2011), glutathione (Schaedler et al., 2014) and magnesium (Li et al., 2008). The main function of mitochondria is energy conversion through oxidative phosphorylation. Sugars are processed to pyruvate in the cytosol and shuttled through pyruvate oxidation and the tricarboxylic acid (TCA) cycle (Araújo et al., 2012). The TCA cycle itself is connected to many metabolic pathways like oxidative defense, detoxification of ROS, photorespiration, amino acid biosynthesis and degradation, gluconeogenesis or the glyoxylate cycle (Mailloux et al., 2007; Araújo et al., 2012). For energy conversion reducing equivalents NADH and $FADH_2$ from the TCA cycle and the ETC are used to generate a proton gradient along the inner mitochondrial membrane. This inward facing proton gradient drives ATP synthesis in the mitochondrial matrix (Millar et al., 2011). Furthermore, mitochondria participate in the photorespiratory conversion of glycine to serine (Schulze et al., 2016), metabolism of amino acids like cysteine, proline, arginine or glutamate (Millar et al., 2008; Hildebrandt et al., 2015), the synthesis of vitamins like folate, biotin or ascorbate (Smith et al., 2007), nucleotides (Witz et al., 2012) or glycerolipids (Michaud et al., 2017). Additionally, mitochondria play a role during ROS defense and programmed cell death (Millar et al., 2008).

Plant cell organelles – Peroxisomes

Peroxisomes are separated from the cytosol by a single lipid bilayer and originate from the ER. While mature peroxisomes can multiply via division, the *de novo* synthesis starts with budding events at the membrane of the ER. Crucial proteins responsible for protein guidance and import (peroxin proteins AtPEX3, AtPEX16 and AtPEX19) are integrated into the membrane of the so called pre-peroxisome to guarantee the subsequent integration of proteins targeted to peroxisomes (Kao et al., 2017). Mature peroxisomes can be degraded via autophagy or divide as a response to cell division, stress factors or environmental cues (Yoshimoto et al., 2014; Sandalio and Romero-Puertas, 2015). Peroxisomal matrix proteins are imported using the AtPEX5 shuttle based on the PTS1 and PTS2 targeting sequences and a complex

PEX5/cargo protein docking, pore assembly and protein translocation process not found in other organelles (Francisco et al., 2017; Meinecke et al., 2016). Knowledge about the transport of metabolites across the peroxisome membrane is limited. Based on the contribution of peroxisomes to crucial metabolic pathways, many metabolites have to be shuttled between the cytosol and the peroxisomal matrix. Yet, only a few transport proteins have been identified to date. Two types of metabolite transport have been proposed: channels for low-molecular weight metabolites and carriers for molecules larger that 300-400 Da (Antonenkov and Hiltunen, 2012). Two non-selective channels have been found: The mammalian Pxmp2 and yeast ScPex11. ScPex11 is thought to play a role during β-oxidation (Rokka et al., 2009; Mindthoff et al., 2016). No channel was identified in plants, yet. Instead, carriers for larger molecules have been identified in Arabidopsis: The NAD^+ transporter PXN, the ATP/ADP transporters AtPNC1 and AtPNC2 and the fatty acyl-CoA transporter COMATOSE or AtPXA1 (van Roermund et al., 2016; Linka et al., 2008; Nyathi et al., 2010). All of these transporters are important for β-oxidation. Non-functional β-oxidation leads to severe impairments of germination and growth of plants. Although most transport proteins still need to be discovered, more is known about the role of peroxisomes in plant cells. Peroxisomes are the site of oxidative reaction, like fatty acid β-oxidation, the detoxification of reactive oxygen species, important enzymatic steps of photorespiration, the glyoxylate cycle, synthesis of signaling hormones jasmonic acid, auxin and salicylic acid or pathogen defense (Kao et al., 2017; Hu et al., 2012).

Modes of metabolite transport at the organellar membrane

All described organelles make use of three basic types of transport, which define how proteins, lipids or metabolites are shuttled between different compartments: 1) gated transport via pores allowing the selected transport of macromolecules and free diffusion of solutes, 2) transmembrane transport via selective protein carriers or channels in the direction or against a concentration gradient and 3) vesicular transport via the evagination of source organellar membranes and fusion of these vesicles with the target organelle membrane (Alberts et al., 2003). The coordination of these transport process is crucial for all cells. Transport proteins can regulate these processes. Various types of transport proteins have been described. Channels catalyze the passive diffusion of molecules based on charge, size or solubility. Voltage-dependent conformational changes or the binding of a certain molecule can trigger the opening or closing of the channel. Pores are constantly open and allow free diffusion of molecules at any time (Takahashi and Tateda, 2013; Jap and Walian, 1996; Kurachi and North, 2004). Primary active transporters, like pumps use energy, e.g. from the hydrolysis of ATP, to transport molecules against a concentration gradient (Yang and Hinner, 2015). These gradients can be used to drive secondary active transporters. They can perform a coupled

transport of substrates (antiport, symport) (Veenhoff et al., 2002). In general, active transporters bind their substrate and guide them through the protein structure by conformational changes, one or only a few molecules at a time. This process allows high selectivity and therefore a precise regulation of metabolite shuttle. Yet, this selectivity comes at the cost of total transport rate. Channels are less selective than active transporters but allow vast amounts of molecules to be transferred in less time (Gadsby, 2009).

The coordination of all these transport processes is crucial for all metabolic pathways in cells. Transport proteins must be expressed and integrated into appropriate compartments. This usually depends on the availability of substrates, diurnal changes or environmental signals. Single metabolic pathways are part of a bigger metabolic network. A system-wide view on this network reveals the tight interaction of these pathways (Sweetlove and Fernie, 2005). A highly dynamic and complex metabolic pathway that is subject to diurnal changes and has to synchronize enzymatic and transporter activity in at least four different compartments is photorespiration.

Photorespiration as prime example for metabolic networks in plant cells

Photorespiration is a complex metabolic network that involves plastids, peroxisomes, mitochondria and the cytosol to recycle carbon lost in the reaction of RuBisCO with oxygen. Furthermore, it reduces the inhibitory effect of the toxic byproduct 2-phosphoglycolate on enzymes of the Calvin cycle (Erb and Zarzycki, 2018). This mechanism evolved with the rise of atmospheric oxygen and is crucial for the survival of most land plants today (Osmond, 1981; Kump, 2008; Eisenhut et al., 2008). The oxygen affinity of RuBisCO increases in hot and dry environments leading to a substantial loss of carbon. Hence, some plants have evolved CO_2 concentrating mechanisms to circumvent oxygen fixation: C4 photosynthesis (Sage, 2017) or CAM photosynthesis (Winter and Holtum, 2014). Other plants depend on photorespiration, a metabolic pathway that requires the input of energy, the expression of genes necessary for enzymatic processing of 2-phosphoglycolate, transport of intermediates, cofactors and substrates for auxiliary enzymatic reactions (Figure 2).

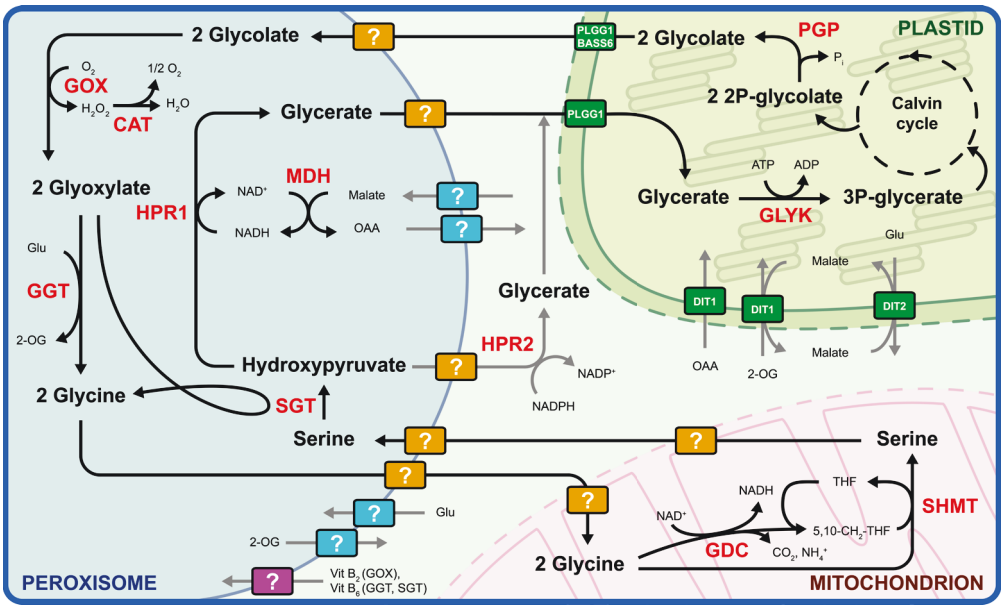

Figure 2. Transport processes of the photorespiratory pathway. Predicted peroxisomal and mitochondrial transport proteins are indicated with "?" and grouped into core metabolites (orange), associated pathways (blue) and co-factors (purple). Enzymes are shown in red. Abbreviations: PGP, 2PG-phosphatase; AtPLGG1, plastidic glycolate/glycerate transporter 1; AtBASS6, Bile Acid Sodium Symporter 6, glycolate exporter; AtGOX, glycolate oxidase; AtCAT, catalase; GGT, glutamate:glyoxylate aminotransferase; AtGDC, glycine decarboxylase; SHMT, serine hydroxymethyltransferase; AtSGT, serine:glyoxylate aminotransferase; AtHPR1, peroxisomal hydroxypyruvate reductase; AtHPR2, cytosolic hydroxypyruvate reductase; AtMDH, malate dehydrogenase; GLYK, glycerate-3-kinase; AtDiT1, dicarboxylate translocator 1; AtDiT2, dicarboxylate translocator 2; Pi, inorganic phosphate; Glu, glutamate; 2-OG, 2-oxoglutarate; OAA, oxaloacetate; THF, tetrahydrofolate; Vit B_6, pyridoxal 5′-phosphate precursor; Vit B_2, flavin mononucleotide precursor.

The core pathway of photorespiration shuttles 2-phosphoglycolate and its intermediates through the chloroplast, peroxisomes and mitochondria before it is returned to the chloroplast, converted to 3-phosphoglycerate and reassimilated by the Calvin cycle. It requires eight enzymes distributed throughout the cell, half of them in peroxisomes, and at least eight transport process across membranes to complete the cycle (Hodges et al., 2016). Enzymes of the core photorespiratory pathway have been identified and their crucial function is apparent in loss-of-function mutants. Small chlorotic leaf structures and lethality under ambient air conditions are characteristic for the impairment of this pathway (Timm and Bauwe, 2013). The knowledge about transport processes of core intermediates is rather limited. Two plastidic transporters have been identified: AtPLGG1 and AtBASS6, both responsible for the export of glycolate, with AtPLGG1 also importing glycerate at the end of the photorespiratory cycle (Pick et al., 2013; South et al., 2017). Peroxisomal and mitochondrial transporters have been proposed but not identified yet. The high flux of metabolites during photorespiration requires a fast shuttle between the different compartments. Non-selective channels have been proposed for peroxisomes (Kunze and Hartig, 2013). Pores might not be likely for mitochondria

considering the membrane potential needed for oxidative phosphorylation. Additionally to the core pathway, numerous associated pathways have to be coordinated. These pathways include the provision of malate and oxaloacetate for the replenishment of the NAD^+/NADH pool of all participating organelles by malate dehydrogenase (AtMDH) (Selinski et al., 2014; Tomaz et al., 2010; Cousins et al., 2008), the plastidic transporters AtDiT1 and AtDiT2 (Renné et al., 2003), bypasses of the peroxisomal AtHPR1 (cytosolic AtHPR2 or plastidic AtHPR3) (Timm et al., 2011), the shuttle of glutamate and 2-oxoglutarate between the plastids and peroxisomes, also by AtDiT1 and AtDiT2, and provision with co-factors, as well as the breakdown of hydrogen peroxide in peroxisomes by the peroxisomal catalase during the conversion of glycolate (Mhamdi et al., 2010), the interplay with the mitochondrial transporter AtBOU (Eisenhut et al., 2013) and the regulating processes of all photorespiratory key players (Timm et al., 2016; Obata et al., 2016).

The photorespiratory core pathway shuttles amino acids and carboxylic acids between the compartments. Members of the MCF are known to shuttle these substrate classes in other pathways. They reside in inner mitochondrial membrane but also in the peroxisomal membrane.

The mitochondrial carrier family

MCF proteins are highly conserved in many species and have been described in plants but more extensively in yeast and mammals. They are localized in non-mitochondrial compartments as well. The majority of the 58 MCF members found in Arabidopsis are predicted to reside in the inner mitochondrial membrane. At least 12 MCF proteins are localized in peroxisomes, plastids, the ER or the plasma membrane (Palmieri et al., 2011; Haferkamp, 2007; Lee and Millar, 2016). Structurally, they share a highly conserved tripartite sequence of 100 repeating amino acids with two α-helices per repeat. Each repeat is separated by a hydrophilic loop and contains a signature PFAM PF00153 motif. Apart from these structural similarities, MCF proteins share only around 11 highly conserved amino acids according to phylogenetic analyses of all 146 MCF proteins found in Arabidopsis, human and yeast (Palmieri et al., 2011; Palmieri, 1994, Figure 3).

MCF proteins are nuclear encoded and appear as homodimers and a molecular mass of 30-35 kDa per subunit (Picault et al., 2004; Haferkamp and Schmitz-Esser, 2012). Based on the high structural and functional similarities between MCF proteins across species, the origin of MCF proteins is predicted to precede the divergence of the three kingdoms. A single ancestral sequence resembling the 100 amino acid repeat was probably duplicated twice, formed the first MCF protein and was the basis of the first set of MCF proteins. This set was further duplicated leading to a variety of MCF proteins. This variety is particularly large in plants

compared to animals and yeast and might indicate a special need for MCF proteins here (Palmieri et al., 2011; Haferkamp and Schmitz-Esser, 2012).

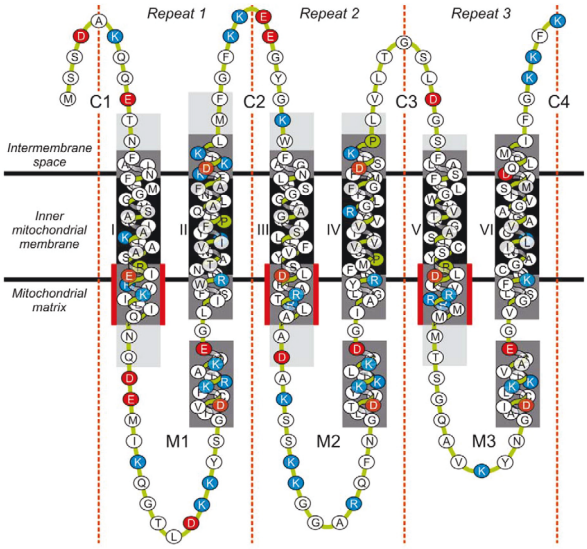

Figure 3. Basic structure of a MCF protein based on the topology model of the yeast ADP/ATP carrier AtAAC3. The tripartite structure of MCF proteins (Repeat 1-3, dotted lines). Each repeat consists of two conserved transmembrane alpha-helices (black bars) and the conserved signature motif PF00153 (red bars). Charged amino acid residues are red (negative), blue (positive), green (proline). Loops are numbered according to the position in the cytosol (C) or the mitochondrial matrix (M). Alpha-helices are numbered with Roman numerals. Modified from Kunji (2004).

The first MCF proteins are assumed to be linked to energy conversion, due to the main function of mitochondria, and transported adenine nucleotides. Based on the broad substrate spectrum of many MCF proteins, the ancestral set of MCF proteins might have been responsible for the shuttle of a variety of substrates (Haferkamp and Schmitz-Esser, 2012). Bioinformatical analyses of protein structures and substrate binding sites predicted three substrate classes for these secondary active MCF proteins: (1) nucleotides, (2) carboxylates and (3) amino acids (Palmieri et al., 2011). This was confirmed in many studies of MCF proteins demonstrating the broad substrate spectrum of this class (Figure 4). The MCF contains nucleotide transporters like AtPNC1 (Linka et al., 2008), AtPM-ANT1 (Rieder and Neuhaus, 2011) or AtAPC1-3 (Lorenz et al., 2015), di-/tri/carboxylate transporters AtUCP1 and AtUCP2 (Monné et al., 2018) or AtDIC1-3 (Palmieri et al., 2008) and amino acid transporters AtBAC1 and AtBAC2 (Palmieri et al., 2006b; Planchais et al., 2014). For some proteins, the transport of phosphate, sulfate and thiosulfate (Monné et al., 2018; Palmieri et al., 2008; Hamel et al., 2004; Monné et al., 2017) or S-adenosyl methionine (SAM) (Bouvier et al., 2006; Palmieri et al., 2006a) was also demonstrated. Most of these transporters are 1:1 antiporters with few exceptions demonstrating uniport or H^+-dependent symport (Palmieri et al., 2011). The large variety of

MCF proteins found in plants indicates the importance of MCF members in plant complexity and diversification.

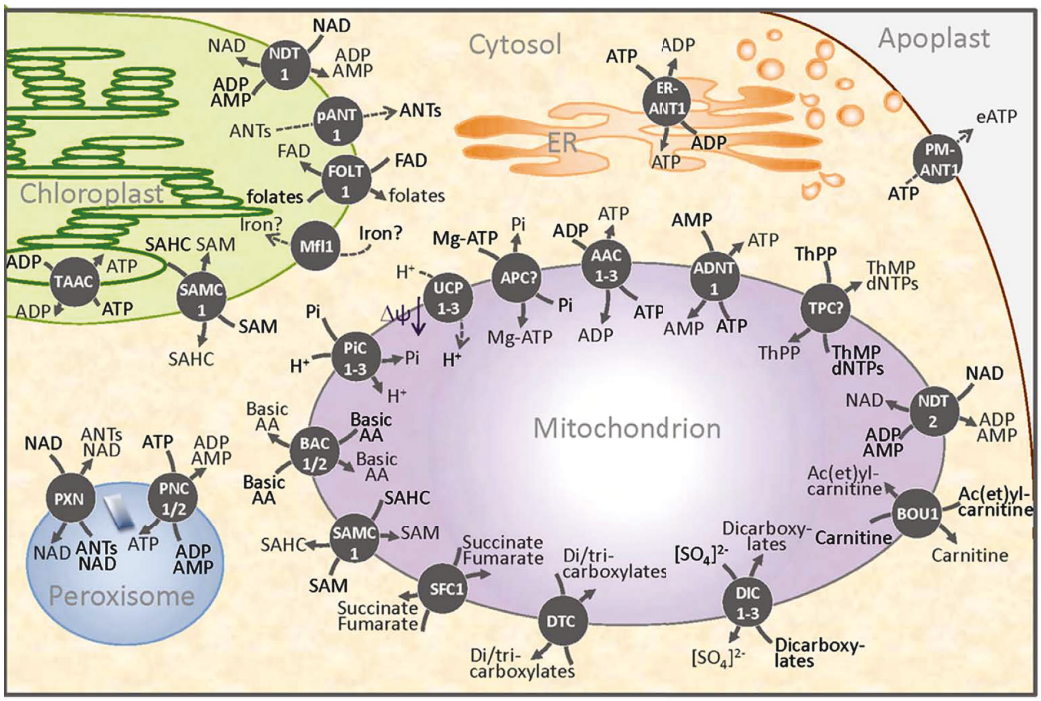

Figure 4. Mitochondrial carrier family proteins in various subcellular compartments of plant cells and their diverse substrate spectrum. MCF proteins in plants have been found in mitochondria, but also peroxisomes, plastids, the ER and the plasma membrane. They transport metabolites from substrate classes like nucleotides, carboxylates and amino acids. Modified from Haferkamp and Schmitz-Esser (2012).

References

Aktar, W., Sengupta, D., and Chowdhury, A. (2009). Impact of pesticides use in agriculture: Their benefits and hazards. Interdiscip. Toxicol. **2**: 1–12.

Alberts, B., Johnson, A., Lewis, J., Raff, M., Roberts, K., and Walter, P. (2003). Molecular biology of the cell (4th ed.):

Allen, J.F. (2015). Why chloroplasts and mitochondria retain their own genomes and genetic systems: Colocation for redox regulation of gene expression. Proc. Natl. Acad. Sci. **112**: 10231–10238.

Antonenkov, V.D. and Hiltunen, J.K. (2012). Transfer of metabolites across the peroxisomal membrane. Biochim. Biophys. Acta - Mol. Basis Dis. **1822**: 1374–1386.

Araújo, W.L., Nunes-Nesi, A., Nikoloski, Z., Sweetlove, L.J., and Fernie, A.R. (2012). Metabolic control and regulation of the tricarboxylic acid cycle in photosynthetic and heterotrophic plant tissues. Plant. Cell Environ. **35**: 1–21.

Archibald, J.M. (2015). Endosymbiosis and eukaryotic cell evolution. Curr. Biol. **25**: R911–R921.

Baltzoi, P., Fotia, K., Kyrkas, D., Nikolaou, K., Paraskevopoulou, A.T., Accogli, A.R., and Karras, G. (2015). Low Water–Demand Plants for Landscaping and Agricultural Cultivations – A Review Regarding Local Species of Epirus/Greece and Apulia/Italy. Agric. Agric. Sci. Procedia **4**: 250–260.

Bauwe, H., Hagemann, M., and Fernie, A.R. (2010). Photorespiration: players, partners and origin. Trends Plant Sci. **15**: 330–336.

Baxter, I., Muthukumar, B., Hyeong, C.P., Buchner, P., Lahner, B., Danku, J., Zhao, K., Lee, J., Hawkesford, M.J., Guerinot, M. Lou, and Salt, D.E. (2008). Variation in molybdenum content across broadly distributed populations of Arabidopsis thaliana is controlled by a mitochondrial molybdenum transporter (MOT1). PLoS Genet. **4**.

Beck, M. and Hurt, E. (2017). The nuclear pore complex: Understanding its function through structural insight. Nat. Rev. Mol. Cell Biol. **18**: 73–89.

Bedhomme, M., Hoffmann, M., McCarthy, E.A., Gambonnet, B., Moran, R.G., Rébeillé, F., and Ravanel, S. (2005). Folate metabolism in plants: An Arabidopsis homolog of the mammalian mitochondrial folate transporter mediates folate import into chloroplasts. J. Biol. Chem. **280**: 34823–34831.

Betti, M., Bauwe, H., Busch, F.A., Fernie, A.R., Keech, O., Levey, M., Ort, D.R., Parry, M.A.J., Sage, R., Timm, S., Walker, B., and Weber, A.P.M. (2016). Manipulating photorespiration to increase plant productivity: Recent advances and perspectives for crop improvement. J. Exp. Bot. **67**: 2977–2988.

Bobik, K. and Burch-Smith, T.M. (2015). Chloroplast signaling within, between and beyond cells. Front. Plant Sci. **6**: 1–26.

Bodner, G., Nakhforoosh, A., and Kaul, H.P. (2015). Management of crop water under drought: a review. Agron. Sustain. Dev. **35**: 401–442.

Bouvier, F., Linka, N., Isner, J.-C., Mutterer, J., Weber, A.P.M., and Camara, B. (2006). Arabidopsis SAMT1 Defines a Plastid Transporter Regulating Plastid Biogenesis and Plant Development. Plant Cell Online **18**: 3088–3105.

Brandvain, Y. and Wade, M.J. (2009). The functional transfer of genes from the mitochondria to the nucleus: The effects of selection, mutation, population size and rate of self-fertilization. Genetics **182**: 1129–1139.

Bräutigam, A., Schliesky, S., Külahoglu, C., Osborne, C.P., and Weber, A.P.M. (2014). Towards an integrative model of C4 photosynthetic subtypes: insights from comparative transcriptome analysis of NAD-ME, NADP-ME, and PEP-CK C4 species. J. Exp. Bot. **65**: 3579–3593.

Busch, F.A., Sage, T.L., Cousins, A.B., and Sage, R.F. (2013). C3 plants enhance rates of photosynthesis by reassimilating photorespired and respired CO2. Plant, Cell Environ. **36**: 200–212.

Carvalho, F.P. (2017). Pesticides, environment, and food safety. Food Energy Secur. **6**: 48–60.

Carvalho, J. de F.C., Madgwick, P.J., Powers, S.J., Keys, A.J., Lea, P.J., and Parry, M.A.J. (2011). An

engineered pathway for glyoxylate metabolism in tobacco plants aimed to avoid the release of ammonia in photorespiration. BMC Biotechnol. **11**: 111.

Chen, J., Lü, S., Zhang, Z., Zhao, X., Li, X., Ning, P., and Liu, M. (2018). Environmentally friendly fertilizers: A review of materials used and their effects on the environment. Sci. Total Environ. **613**–**614**: 829–839.

Cogliati, S., Enriquez, J.A., and Scorrano, L. (2016). Mitochondrial Cristae: Where Beauty Meets Functionality. Trends Biochem. Sci. **41**: 261–273.

Cousins, A.B., Pracharoenwattana, I., Zhou, W., Smith, S.M., and Badger, M.R. (2008). Peroxisomal malate dehydrogenase is not essential for photorespiration in Arabidopsis but its absence causes an increase in the stoichiometry of photorespiratory CO2 release. Plant Physiol. **148**: 786–95.

Csala, M., Marcolongo, P., Lizák, B., Senesi, S., Margittai, É., Fulceri, R., Magyar, J.É., Benedetti, A., and Bánhegyi, G. (2007). Transport and transporters in the endoplasmic reticulum. Biochim. Biophys. Acta - Biomembr. **1768**: 1325–1341.

Devos, D.P., Gräf, R., and Field, M.C. (2014). Evolution of the nucleus. Curr. Opin. Cell Biol. **28**: 8–15.

Eisenhut, M. et al. (2013). Arabidopsis A BOUT de SOUFFLE is a putative mitochondrial transporter involved in photorespiratory metabolism and is required for meristem growth at ambient CO2 levels. Plant J. **73**: 836–849.

Eisenhut, M., Ruth, W., Haimovich, M., Bauwe, H., Kaplan, A., and Hagemann, M. (2008). The photorespiratory glycolate metabolism is essential for cyanobacteria and might have been conveyed endosymbiontically to plants. Proc. Natl. Acad. Sci. **105**: 17199–17204.

Endo, T. and Yamano, K. (2010). Transport of proteins across or into the mitochondrial outer membrane. Biochim. Biophys. Acta - Mol. Cell Res. **1803**: 706–714.

Erb, T.J. and Zarzycki, J. (2018). A short history of RubisCO: the rise and fall (?) of Nature's predominant CO2 fixing enzyme. Curr. Opin. Biotechnol. **49**: 100–107.

Facchinelli, F. and Weber, A.P.M. (2011). The Metabolite Transporters of the Plastid Envelope: An Update. Front. Plant Sci. **2**: 1–18.

Fedoroff, N. V. (2015). Food in a future of 10 billion. Agric. Food Secur. **4**: 1–10.

Flügge, U.-I., Westhoff, P., and Leister, D. (2016). Recent advances in understanding photosynthesis. F1000Research **5**: 2890.

Francisco, T., Rodrigues, T.A., Dias, A.F., Barros-Barbosa, A., Bicho, D., and Azevedo, J.E. (2017). Protein transport into peroxisomes: Knowns and unknowns. BioEssays **39**: 1–8.

Gaba, S., Gabriel, E., Chadœuf, J., Bonneu, F., and Bretagnolle, V. (2016). Herbicides do not ensure for higher wheat yield, but eliminate rare plant species. Sci. Rep. **6**: 1–10.

Gabaldón, T. and Pittis, A.A. (2015). Origin and evolution of metabolic sub-cellular compartmentalization in eukaryotes. Biochimie **119**: 262–268.

Gadsby, D.C. (2009). Ion channels versus ion pumps: the principal difference, in principle. Nat. Rev. Mol. Cell Biol. **10**: 344–352.

Gao, C. (2018). The future of CRISPR technologies in agriculture. Nat. Rev. Mol. Cell Biol. **19**: 275–276.

Gentil, J., Hempel, F., Moog, D., Zauner, S., and Maier, U.G. (2017). Origin of complex algae by secondary endosymbiosis: a journey through time. Protoplasma **254**: 1835–1843.

Gilliham, M. (2015). Salinity tolerance of crops - what is the cost ? Tansley insight Salinity tolerance of crops – what is the cost ? New Phytol. **208**: 668–673.

Godfray, H.C.J., Crute, I.R., Haddad, L., Muir, J.F., Nisbett, N., Lawrence, D., Pretty, J., Robinson, S., Toulmin, C., and Whiteley, R. (2010). The future of the global food system. Philos. Trans. R. Soc. B Biol. Sci. **365**: 2769–2777.

Gowik, U. and Westhoff, P. (2011). The Path from C3 to C4 Photosynthesis. Plant Physiol. **155**: 56–63.

Haferkamp, I. (2007). The diverse members of the mitochondrial carrier family in plants. FEBS Lett. **581**: 2375–

2379.

Haferkamp, I. and Schmitz-Esser, S. (2012). The Plant Mitochondrial Carrier Family: Functional and Evolutionary Aspects. Front. Plant Sci. **3**: 1–19.

Hamel, P., Saint-Georges, Y., De Pinto, B., Lachacinski, N., Altamura, N., and Dujardin, G. (2004). Redundancy in the function of mitochondrial phosphate transport in Saccharomyces cerevisiae and Arabidopsis thaliana. Mol. Microbiol. **51**: 307–317.

Heinig, U., Gutensohn, M., Dudareva, N., and Aharoni, A. (2013). The challenges of cellular compartmentalization in plant metabolic engineering. Curr. Opin. Biotechnol. **24**: 239–246.

Hildebrandt, T.M., Nunes Nesi, A., Araújo, W.L., and Braun, H.P. (2015). Amino Acid Catabolism in Plants. Mol. Plant **8**: 1563–1579.

Hodges, M., Dellero, Y., Keech, O., Betti, M., Raghavendra, A.S., Sage, R., Zhu, X.G., Allen, D.K., and Weber, A.P.M. (2016). Perspectives for a better understanding of the metabolic integration of photorespiration within a complex plant primary metabolism network. J. Exp. Bot. **67**: 3015–3026.

Hu, J., Baker, A., Bartel, B., Linka, N., Mullen, R.T., Reumann, S., and Zolman, B.K. (2012). Plant Peroxisomes: Biogenesis and Function. Plant Cell **24**: 2279–2303.

Huang, J., Hu, R., Pray, C., Qiao, F., and Rozelle, S. (2003). Biotechnology as an alternative to chemical pesticides: A case study of Bt cotton in China. Agric. Econ. **29**: 55–67.

Inoue, K. (2007). The Chloroplast Outer Envelope Membrane: The Edge of Light and Excitement. J. Integr. Plant Biol. **49**: 1100–1111.

Jap, B.K. and Walian, P.J. (1996). Structure and Functional Mechanism of Porins. Physiol. Rev. **76**: 1073–1088.

Jarvis, P. and Soll, J. (2001). Toc, Tic, and chloroplast protein import. Biochim. Biophys. Acta - Mol. Cell Res. **1541**: 64–79.

Jensen, P.E. and Leister, D. (2014). Chloroplast evolution, structure and functions. F1000Prime Rep. **6**: 1–14.

Kao, Y.-T., Gonzalez, K.L., and Bartel, B. (2017). Peroxisome function, biogenesis, and dynamics in plants. Plant Physiol. **176**: pp.01050.2017.

Kebeish, R., Niessen, M., Thiruveedhi, K., Bari, R., Hirsch, H.J., Rosenkranz, R., Stäbler, N., Schönfeld, B., Kreuzaler, F., and Peterhänsel, C. (2007). Chloroplastic photorespiratory bypass increases photosynthesis and biomass production in Arabidopsis thaliana. Nat. Biotechnol. **25**: 593–599.

Kinoshita, H., Nagasaki, J., Yoshikawa, N., Yamamoto, A., Takito, S., Kawasaki, M., Sugiyama, T., Miyake, H., Weber, A.P.M., and Taniguchi, M. (2011). The chloroplastic 2-oxoglutarate/malate transporter has dual function as the malate valve and in carbon/nitrogen metabolism. Plant J. **65**: 15–26.

Kühlbrandt, W. (2015). Structure and function of mitochondrial membrane protein complexes. BMC Biol. **13**: 1–11.

Kump, L.R. (2008). The rise of atmospheric oxygen. Nature **451**: 277–278.

Kunji, E.R.S. (2004). The role and structure of mitochondrial carriers. FEBS Lett. **564**: 239–244.

Kunze, M. and Hartig, A. (2013). Permeability of the peroxisomal membrane: Lessons from the glyoxylate cycle. Front. Physiol. **4 AUG**: 1–12.

Kurachi, Y. and North, A. (2004). Ion channels: their structure, function and control - an overview. J. Physiol. **554**: 245–247.

Lee, C.P. and Millar, A.H. (2016). The Plant Mitochondrial Transportome: Balancing Metabolic Demands with Energetic Constraints. Trends Plant Sci. **21**: 662–676.

Li, L.G., Sokolov, L.N., Yang, Y.H., Li, D.P., Ting, J., Pandy, G.K., and Luan, S. (2008). A mitochondrial magnesium transporter functions in Arabidopsis pollen development. Mol. Plant **1**: 675–685.

Linka, N., Theodoulou, F.L., Haslam, R.P., Linka, M., Napier, J.A., Neuhaus, H.E., and Weber, A.P.M. (2008). Peroxisomal ATP Import Is Essential for Seedling Development in Arabidopsis thaliana. Plant Cell Online **20**: 3241–3257.

López-Arredondo, D., González-Morales, S.I., Bello-Bello, E., Alejo-Jacuinde, G., and Herrera, L. (2015). Engineering food crops to grow in harsh environments. F1000Research **4**.

Lorenz, A., Lorenz, M., Vothknecht, U.C., Niopek-Witz, S., Neuhaus, H.E., and Haferkamp, I. (2015). In vitro analyses of mitochondrial ATP/phosphate carriers from Arabidopsis thaliana revealed unexpected Ca2+-effects. BMC Plant Biol. **15**: 1–16.

Maier, A., Fahnenstich, H., von Caemmerer, S., Engqvist, M.K.M., Weber, A.P.M., Flügge, U.-I., and Maurino, V.G. (2012). Transgenic Introduction of a Glycolate Oxidative Cycle into A. thaliana Chloroplasts Leads to Growth Improvement. Front. Plant Sci. **3**: 1–12.

Mailloux, R.J., Bériault, R., Lemire, J., Singh, R., Chénier, D.R., Hamel, R.D., and Appanna, V.D. (2007). The tricarboxylic acid cycle, an ancient metabolic network with a novel twist. PLoS One **2**.

Marchand, J., Heydarizadeh, P., Schoefs, B., and Spetea, C. (2018). Ion and metabolite transport in the chloroplast of algae: lessons from land plants. Cell. Mol. Life Sci. **75**: 2153–2176.

Martin, W. (2005). Archaebacteria (Archaea) and the origin of the eukaryotic nucleus. Curr. Opin. Microbiol. **8**: 630–637.

Martin, W., Stoebe, B., Goremykin, V., Hansmann, S., Hasegawa, M., and Kowallik, K. V. (1998). Gene transfer to the nucleus and the evolution of chloroplasts. Nature **393**: 162–165.

Martin, W.F., Garg, S., and Zimorski, V. (2015). Endosymbiotic theories for eukaryote origin. Philos. Trans. R. Soc. B Biol. Sci. **370**.

Meinecke, M., Bartsch, P., and Wagner, R. (2016). Peroxisomal protein import pores. Biochim. Biophys. Acta - Mol. Cell Res. **1863**: 821–827.

Mhamdi, A., Queval, G., Chaouch, S., Vanderauwera, S., Van Breusegem, F., and Noctor, G. (2010). Catalase function in plants: A focus on Arabidopsis mutants as stress-mimic models. J. Exp. Bot. **61**: 4197–4220.

Michael, T.P. and VanBuren, R. (2015). Progress, challenges and the future of crop genomes. Curr. Opin. Plant Biol. **24**: 71–81.

Michaeli, S., Fait, A., Lagor, K., Nunes-Nesi, A., Grillich, N., Yellin, A., Bar, D., Khan, M., Fernie, A.R., Turano, F.J., and Fromm, H. (2011). A mitochondrial GABA permease connects the GABA shunt and the TCA cycle, and is essential for normal carbon metabolism. Plant J. **67**: 485–498.

Michaud, M., Prinz, W.A., and Jouhet, J. (2017). Glycerolipid synthesis and lipid trafficking in plant mitochondria. FEBS J. **284**: 376–390.

Millar, A.H., Small, I.D., Day, D.A., and Whelan, J. (2008). Mitochondrial Biogenesis and Function in Arabidopsis †. Arab. B. **6**: e0111.

Millar, A.H., Whelan, J., Soole, K.L., and Day, D.A. (2011). Organization and Regulation of Mitochondrial Respiration in Plants. Annu. Rev. Plant Biol. **62**: 79–104.

Mindthoff, S., Grunau, S., Steinfort, L.L., Girzalsky, W., Hiltunen, J.K., Erdmann, R., and Antonenkov, V.D. (2016). Peroxisomal Pex11 is a pore-forming protein homologous to TRPM channels. Biochim. Biophys. Acta - Mol. Cell Res. **1863**: 271–283.

Monné, M., Daddabbo, L., Gagneul, D., Obata, T., Hielscher, B., Palmieri, L., Miniero, D.V., Fernie, A.R., Weber, A.P.M., and Palmieri, F. (2018). Uncoupling proteins 1 and 2 (UCP1 and UCP2) from Arabidopsis thaliana are mitochondrial transporters of aspartate, glutamate, and dicarboxylates. J. Biol. Chem. **293**: 4213–4227.

Monné, M., Daddabbo, L., Giannossa, L.C., Nicolardi, M.C., Palmieri, L., Miniero, D.V., Mangone, A., and Palmieri, F. (2017). Mitochondrial ATP-Mg/phosphate carriers transport divalent inorganic cations in complex with ATP. J. Bioenerg. Biomembr. **49**: 369–380.

Moreira, D. and Deschamps, P. (2014). What was the real contribution of endosymbionts to the eukaryotic nucleus? Insights from photosynthetic eukaryotes. Cold Spring Harb. Perspect. Biol. **6**: 1–9.

Nickelsen, J., Rengstl, B., Stengel, A., Schottkowski, M., Soll, J., and Ankele, E. (2011). Biogenesis of the cyanobacterial thylakoid membrane system - an update. FEMS Microbiol. Lett. **315**: 1–5.

Nyathi, Y., Lousa, C.D.M., Van Roermund, C.W., Wanders, R.J.A., Johnson, B., Baldwin, S.A., Theodoulou, F.L., and Baker, A. (2010). The Arabidopsis peroxisomal ABC transporter, comatose, complements the Saccharomyces cerevisiae pxa1 pxa2Δ mutant for metabolism of long-chain fatty acids and exhibits fatty Acyl-CoA-stimulated ATpase activity. J. Biol. Chem. **285**: 29892–29902.

Obata, T., Florian, A., Timm, S., Bauwe, H., and Fernie, A.R. (2016). On the metabolic interactions of (photo)respiration. J. Exp. Bot. **67**: 3003–3014.

Orr, D.J., Pereira, A.M., da Fonseca Pereira, P., Pereira-Lima, Í.A., Zsögön, A., and Araújo, W.L. (2017). Engineering photosynthesis: progress and perspectives. F1000Research **6**: 1891.

Osmond, C.B. (1981). Photorespiration and photoinhibition. Some implications for the energetics of photosynthesis. BBA Rev. Bioenerg. **639**: 77–98.

Palmieri, F. (1994). Mitochondrial carrier proteins. FEBS Lett. **346**: 48–54.

Palmieri, F. et al. (2009). Molecular Identification and Functional Characterization of *Arabidopsis thaliana* Mitochondrial and Chloroplastic NAD $^{+}$ Carrier Proteins. J. Biol. Chem. **284**: 31249–31259.

Palmieri, F., Pierri, C.L., De Grassi, A., Nunes-Nesi, A., and Fernie, A.R. (2011). Evolution, structure and function of mitochondrial carriers: A review with new insights. Plant J. **66**: 161–181.

Palmieri, L., Arrigoni, R., Blanco, E., Carrari, F., Zanor, M.I., Studart-Guimaraes, C., Fernie, A.R., and Palmieri, F. (2006a). Molecular Identification of an Arabidopsis S-Adenosylmethionine Transporter. Analysis of Organ Distribution, Bacterial Expression, Reconstitution into Liposomes, and Functional Characterization. Plant Physiol. **142**: 855–865.

Palmieri, L., Picault, N., Arrigoni, R., Besin, E., Palmieri, F., and Hodges, M. (2008). Molecular identification of three Arabidopsis thaliana mitochondrial dicarboxylate carrier isoforms: organ distribution, bacterial expression, reconstitution into liposomes and functional characterization. Biochem. J. **410**: 621–629.

Palmieri, L., Todd, C.D., Arrigoni, R., Hoyos, M.E., Santoro, A., Polacco, J.C., and Palmieri, F. (2006b). Arabidopsis mitochondria have two basic amino acid transporters with partially overlapping specificities and differential expression in seedling development. Biochim. Biophys. Acta - Bioenerg. **1757**: 1277–1283.

Pfister, B. and Zeeman, S.C. (2016). Formation of starch in plant cells. Cell. Mol. Life Sci. **73**: 2781–2807.

Picault, N., Hodges, M., Palmieri, L., and Palmieri, F. (2004). The growing family of mitochondrial carriers in Arabidopsis. Trends Plant Sci. **9**: 138–146.

Pick, T.R., Bräutigam, A., Schulz, M.A., Obata, T., Fernie, A.R., and Weber, A.P.M. (2013). PLGG1, a plastidic glycolate glycerate transporter, is required for photorespiration and defines a unique class of metabolite transporters. Proc. Natl. Acad. Sci. **110**: 3185–3190.

Planchais, S., Cabassa, C., Toka, I., Justin, A.-M., Renou, J.-P., Savouré, A., and Carol, P. (2014). BASIC AMINO ACID CARRIER 2 gene expression modulates arginine and urea content and stress recovery in Arabidopsis leaves. Front Plant Sci **5**: 330.

Pottosin, I. and Shabala, S. (2016). Transport Across Chloroplast Membranes: Optimizing Photosynthesis for Adverse Environmental Conditions. Mol. Plant **9**: 356–370.

Pratelli, R. and Pilot, G. (2014). Regulation of amino acid metabolic enzymes and transporters in plants. J. Exp. Bot. **65**: 5535–5556.

Renné, P., Dreßen, U., Hebbeker, U., Hille, D., Flügge, U.I., Westhoff, P., and Weber, A.P.M. (2003). The Arabidopsis mutant dct is deficient in the plastidic glutamate/malate translocator DiT2. Plant J. **35**: 316–331.

Rieder, B. and Neuhaus, H.E. (2011). Identification of an Arabidopsis Plasma Membrane–Located ATP Transporter Important for Anther Development. Plant Cell **23**: 1932–1944.

van Roermund, C.W.T., Schroers, M.G., Wiese, J., Facchinelli, F., Kurz, S., Wilkinson, S., Charton, L., Wanders, R.J.A., Waterham, H.R., Weber, A.P.M., and Link, N. (2016). The Peroxisomal NAD Carrier

from Arabidopsis Imports NAD in Exchange with AMP. Plant Physiol. **171**: 2127–2139.

Rokka, A., Antonenkov, V.D., Soininen, R., Immonen, H.L., Pirilä, P.L., Bergmann, U., Sormunen, R.T., Weckström, M., Benz, R., and Hiltunen, J.K. (2009). Pxmp2 is a channel-forming protein in mammalian peroxisomal membrane. PLoS One **4**: e5090.

Sage, R.F. (2017). A portrait of the C4 photosynthetic family on the 50th anniversary of its discovery: Species number, evolutionary lineages, and Hall of Fame. J. Exp. Bot. **68**: e11–e28.

Sage, R.F., Khoshravesh, R., and Sage, T.L. (2014). From proto-Kranz to C4 Kranz: building the bridge to C4 photosynthesis. J. Exp. Bot. **65**: 3341–3356.

Sandalio, L.M. and Romero-Puertas, M.C. (2015). Peroxisomes sense and respond to environmental cues by regulating ROS and RNS signalling networks. Ann. Bot. **116**: 475–485.

Santarella-Mellwig, R., Pruggnaller, S., Roos, N., Mattaj, I.W., and Devos, D.P. (2013). Three-Dimensional Reconstruction of Bacteria with a Complex Endomembrane System. PLoS Biol. **11**.

Savci, S. (2012). Investigation of Effect of Chemical Fertilizers on Environment. APCBEE Procedia **1**: 287–292.

Schaedler, T.A., Thornton, J.D., Kruse, I., Schwarzländer, M., Meyer, A.J., Van Veen, H.W., and Balk, J. (2014). A conserved mitochondrial ATP-binding cassette transporter exports glutathione polysulfide for cytosolic metal cofactor assembly. J. Biol. Chem. **289**: 23264–23274.

Schroeder, J.I., Delhaize, E., Frommer, W.B., Guerinot, M. Lou, Harrison, M.J., Herrera-Estrella, L., Horie, T., Kochian, L. V., Munns, R., Nishizawa, N.K., Tsay, Y.-F., and Sanders, D. (2013). Using membrane transporters to improve crops for sustainable food production. Nature **497**: 60–66.

Schulze, S., Westhoff, P., and Gowik, U. (2016). Glycine decarboxylase in C3, C4 and C3-C4 intermediate species. Curr. Opin. Plant Biol. **31**: 29–35.

Schwarz, D.S. and Blower, M.D. (2016). The endoplasmic reticulum: Structure, function and response to cellular signaling. Cell. Mol. Life Sci. **73**: 79–94.

Selinski, J., König, N., Wellmeyer, B., Hanke, G.T., Linke, V., Ekkehard Neuhaus, H., and Scheibe, R. (2014). The plastid-localized NAD-dependent malate dehydrogenase is crucial for energy homeostasis in developing arabidopsis thaliana seeds. Mol. Plant **7**: 170–186.

Shrivastava, P. and Kumar, R. (2015). Soil salinity: A serious environmental issue and plant growth promoting bacteria as one of the tools for its alleviation. Saudi J. Biol. Sci. **22**: 123–131.

Smith, A.G., Croft, M.T., Moulin, M., and Webb, M.E. (2007). Plants need their vitamins too. Curr. Opin. Plant Biol. **10**: 266–275.

South, P.F., Walker, B.J., Cavanagh, A.P., Rolland, V., Badger, M., and Ort, D.R. (2017). Bile Acid Sodium Symporter BASS6 Can Transport Glycolate and Is Involved in Photorespiratory Metabolism in Arabidopsis thaliana. Plant Cell **29**: 808–823.

Speijer, D. (2015). Birth of the eukaryotes by a set of reactive innovations: New insights force us to relinquish gradual models. BioEssays **37**: 1268–1276.

Sweetlove, L.J.L.J. and Fernie, A.R. a. R. (2005). Regulation of Metabolic Networks:Understanding Metabolic Complexity in the Systems Biology Era. New Phytol. **168**: 9–23.

Takahashi, Y. and Tateda, C. (2013). The functions of voltage-dependent anion channels in plants. Apoptosis **18**: 917–924.

Teardo, E. et al. (2017). Physiological Characterization of a Plant Mitochondrial Calcium Uniporter in Vitro and in Vivo. Plant Physiol. **173**: 1355–1370.

Timm, S. and Bauwe, H. (2013). The variety of photorespiratory phenotypes - employing the current status for future research directions on photorespiration. Plant Biol. **15**: 737–747.

Timm, S., Florian, A., Fernie, A.R., and Bauwe, H. (2016). The regulatory interplay between photorespiration and photosynthesis. J. Exp. Bot. **67**: 2923–2929.

Timm, S., Florian, A., Jahnke, K., Nunes-Nesi, A., Fernie, A.R., and Bauwe, H. (2011). The hydroxypyruvate-

reducing system in Arabidopsis: multiple enzymes for the same end. Plant Physiol. **155**: 694–705.

Timm, S., Wittmiß, M., Gamlien, S., Ewald, R., Florian, A., Frank, M., Wirtz, M., Hell, R., Fernie, A.R., and Bauwe, H. (2015). Mitochondrial Dihydrolipoyl Dehydrogenase Activity Shapes Photosynthesis and Photorespiration of *Arabidopsis thaliana*. Plant Cell **27**: 1968–1984.

Tomaz, T., Bagard, M., Pracharoenwattana, I., Linden, P., Lee, C.P., Carroll, A.J., Stroher, E., Smith, S.M., Gardestrom, P., and Millar, A.H. (2010). Mitochondrial Malate Dehydrogenase Lowers Leaf Respiration and Alters Photorespiration and Plant Growth in Arabidopsis. Plant Physiol. **154**: 1143–1157.

Veenhoff, L.M., Heuberger, E.H.M.L., and Poolman, B. (2002). Quaternary structure and function of transport proteins. Trends Biochem. Sci. **27**: 242–249.

Voeltz, G.K., Rolls, M.M., and Rapoport, T.A. (2002). Structural organization of the endoplasmic reticulum. EMBO Rep. **3**: 944–950.

Wang, M., Ma, X., Shen, J., Li, C., and Zhang, W. (2014). The ongoing story: The mitochondria pyruvate carrier 1 in plant stress response in Arabidopsis. Plant Signal. Behav. **9**: 10–12.

Wang, Z.-H., Li, S.-X., and Malhi, S. (2008). Effects of fertilization and other agronomic measures on nutritional quality of crops. J. Sci. Food Agric. **88**: 7–23.

Watson, P. and Stephens, D.J. (2005). ER-to-Golgi transport: Form and formation of vesicular and tubular carriers. Biochim. Biophys. Acta - Mol. Cell Res. **1744**: 304–315.

Wente, S.R. and Rout, M.P. (2010). The nuclear pore complex and nuclear transport. Cold Spring Harb. Perspect. Biol. **2**: 1–19.

Winter, K. and Holtum, J.A.M. (2014). Facultative crassulacean acid metabolism (CAM) plants: Powerful tools for unravelling the functional elements of CAM photosynthesis. J. Exp. Bot. **65**: 3425–3441.

Witz, S., Jung, B., Fürst, S., and Möhlmann, T. (2012). De Novo Pyrimidine Nucleotide Synthesis Mainly Occurs outside of Plastids, but a Previously Undiscovered Nucleobase Importer Provides Substrates for the Essential Salvage Pathway in *Arabidopsis*. Plant Cell **24**: 1549–1559.

Xu, G., Fan, X., and Miller, A.J. (2012). Plant nitrogen assimilation and use efficiency. Annu. Rev. Plant Biol. **63**: 153–182.

Yang, N.J. and Hinner, M.J. (2015). Getting Across the Cell Membrane: An Overview for Small Molecules, Peptides, and Proteins. In Site-Specific Protein Labeling: Methods and Protocols, pp. 29–53.

Yoshimoto, K., Shibata, M., Kondo, M., Oikawa, K., Sato, M., Toyooka, K., Shirasu, K., Nishimura, M., and Ohsumi, Y. (2014). Organ-specific quality control of plant peroxisomes is mediated by autophagy. J. Cell Sci. **127**: 1161–1168.

Zeeman, S.C., Delatte, T., Messerli, G., Umhang, M., Stettler, M., Mettler, T., Streb, S., Reinhold, H., and Kötting, O. (2007). Starch breakdown: Recent discoveries suggest distinct pathways and novel mechanisms. Funct. Plant Biol. **34**: 465–473.

IV. Aim of this thesis

Intra and intercellular metabolic networks highly depend on transport processes. These transport processes connect structurally separated compartments and regulate the shuttle of metabolites. To understand metabolic networks, knowledge about transport proteins and their biochemical and physiological functions are essential. The thesis focuses on the characterization of mitochondrial carrier family (MCF) members found in peroxisomes and mitochondria, their biochemical properties and physiological role in Arabidopsis. Several Arabidopsis MCF members have been described to date. Substrate classes of these proteins are nucleotides, carboxylates and amino acids. Although phylogenetic analyses and structural similarities between MCF proteins hint at certain functions, the biochemical characterization and physiological function is still poorly described for a majority of the MCF. Many *in vitro* studies showed that MCF proteins have a broad substrate spectrum. If this correlates to the *in vivo* function is still unanswered.

This thesis follows two approaches to elucidate the function of MCF proteins in plants. 1) the identification of novel peroxisomal transporters of the MCF, their biochemical properties and function for the peroxisomal metabolism (Manuscript 1) and 2) the physiological analysis of mitochondrial MCF transporter AtPHT3;3 in Arabidopsis (Manuscript 2). Additionally, Manuscript 4 describes the biochemical properties of mitochondrial MCF members AtUCP1 and AtUCP2, two dicarboxylate/amino acid carriers. Manuscript 3 describes the examination of β-oxidation in germinating Arabidopsis seeds via FAME analysis. This method allows the precise observation of peroxisomal activity during an integral part of plant establishment. β-oxidation is involved in many processes and requires the interaction of several transporters, partly found with the MCF. Manuscript 5 describes the characterization of two spermidine hydroxycinnamoyl transferases from *Cichorium intybus* involved in pollen coat composition.

V. Manuscripts

V.1 Manuscript 1

Identification of two novel carriers of the mitochondrial carrier family involved in peroxisomal malate shuttle

Björn Hielscher[1*], Udo Gowik[2], Leonie Wirth[1], Julia Schönknecht[1],
Peter Westhoff[3], Andreas Weber[1] and Nicole Linka[1a]

[1]Heinrich Heine University Düsseldorf, Institute of Plant Biochemistry, Germany
[2]Carl von Ossietzky University of Oldenburg, Plant Evolutionary Genetics, Germany
[3]Heinrich Heine University Düsseldorf,
Institute of Developmental and Molecular Biology of Plants, Germany

[*]First author
[a]Corresponding author

Abstract

Subcellular compartments share a complex metabolic network. This network relies on transport proteins to shuttle metabolites across organellar membranes that are otherwise impermeable for most metabolites. The regulation of metabolite transport is crucial for cells. Transporters can regulate the intracellular metabolite flux. In plants, photorespiration is a prime example of such a complex network that needs to be strictly regulated. This pathway requires three organelles, plastids, peroxisomes and mitochondria, to detoxify cells from 2-phosphoglycerate, a product of the oxygenic reaction of RuBisCO. This energy-demanding process is well described. Most involved enzymes and metabolites have been uncovered. Still, only four plastidic transporters that are involved in this process have been characterized in Arabidopsis. To date no carrier responsible for solute transport across the peroxisomal membrane has been identified although several intermediates of the photorespiratory pathway have to be shuttled between the cytosol and the peroxisomal matrix.

In this study co-expression analysis of closely related C3 and C4 Flaveria species was used to identify genes co-regulated with the expression of typical photorespiratory enzymes using hierarchical clustering and filtering for carriers based on structural traits and phylogenetic relations to known transporter families. This analysis revealed two members of the mitochondrial carrier family (MCF). Members of this protein family are localized in mitochondria, plastids, peroxisomes, the ER, the Golgi and the plasma membrane. The MCF members described here, AtPPR1;1 and AtPPR1;2, show an increased transcript level during ambient air conditions, seed development and in mature seeds. *In vitro* uptake assays revealed the transport of malate for both carriers. With this, AtPPR1;1 and AtPPR1;2 might be involved in the peroxisomal malate/oxaloacetate shuttle required for NAD^+/NADH regeneration. NAD^+ and NADH are crucial for peroxisomal photorespiration as well as for β-oxidation.

Introduction

Photorespiration

Photosynthesis originated in bacteria and manifested in eukaryotes most prominently in land plants and algae but also symbiotic organisms like lichen, corals and molluscs (Björn and Govindjee, 2009). It provides life on earth with energy converted from sun light and oxygen from water and evolved to be most flexible in resource-limited environments (Foyer et al., 2017; Flügge et al., 2016). Photosynthesis is a target for metabolic engineering since plants do not use its full potential (Orr et al., 2017). One factor that limits photosynthesis is RuBisCO.

RuBisCO is the key enzyme of carbon fixation and introduces aerial CO_2 into the food chain (Erb and Zarzycki, 2018). But RuBisCO is a highly error-prone enzyme, which evolved when the atmospheric oxygen concentration was still low (Hagemann et al., 2016; Erb and Zarzycki, 2018). Today, the higher concentration of atmospheric oxygen drives the oxygenic

reaction of RuBisCO producing toxic 2-phosphoglycolate in the process. 2-phosphoglycolate inhibits enzymes of the Calvin cycle. While this inhibition might also represent a control mechanism for photosynthesis (Flügel et al., 2017), 2-phosphoglycolate has to be recycled before it severely impairs this pathway. A more accurate discrimination between carbon dioxide and oxygen by RuBisCO would have lowered the catalytic rate of the enzyme, which is already known to have a rather limiting turnover frequency (Tawfik, 2014; Tcherkez et al., 2006; Erb and Zarzycki, 2018). With an error rate between 20 % and 40 % depending on temperature and intracellular carbon dioxide concentration (Walker et al., 2016), photosynthesis would be a rather unfavorable mechanism. The detoxification of photosynthetic cells and recycling of lost carbon is the objective of photorespiration.

Photorespiration is a highly energy demanding metabolic pathway that is shared between plastids, peroxisomes, mitochondria and the cytosol. The product of photorespiration is 3-phosphoglycerate and can be returned into the Calvin cycle. Whit this, about 70 % of the initially fixed carbon can be recovered (Peterhansel et al., 2010; Bauwe, 2010; Erb and Zarzycki, 2018). Since the evolution of oxygenic photosynthesis, photorespiration is crucial for the survival of land plants (Osmond, 1981; Kump, 2008; Eisenhut et al., 2008). In hot and dry environments when the affinity of RuBisCO for oxygen increases even more, plants reach a critical limit of carbon uptake and have evolved CO_2 concentrating mechanisms to circumvent oxygen fixation and the loss of substantial amounts of energy: C4 photosynthesis (Sage, 2017, 2001). Identifying key players of C4 photosynthesis and photorespiration is essential to counter the energy loss in C3 plants. Understanding photorespiration to improve the energy usage of C3 crops in rather dry environments is the main goal of photorespiration research.

While intermediates and enzymes of the photorespiratory pathway have been well described, the shuttle of metabolites between the different compartments is poorly understood. At least eight transport processes are predicted to shuttle the core metabolites glycolate, glycine, serine and glycerate across all three organellar membranes. But only two plastidic transporters were identified to date: the plastidic glycolate/glycerate transporter AtPLGG1 and the glycolate exporter AtBASS6 (Pick et al., 2013; Dong et al., 2018; South et al., 2017). Two associated transporters involved in photorespiration were found in plastids: the dicarboxylate transporters AtDiT1 and AtDiT2.1 (Renné et al., 2003; Kinoshita et al., 2011).The mitochondrial protein AtBOU is also linked to photorespiration, while its physiological function is still unknown (Eisenhut et al., 2013a). Peroxisomal transporters have not been described.

Photorespiration is a process that combines various compartments, enzymes and transport proteins. During light phases the plastidic RuBisCO performs two reactions: carboxylation and oxygenation. While carboxylation is the preferred reaction, oxygenation leads to the formation of 2-phosphoglycolate (Edwards and Walker, 1983). 2-phosphoglycolate cannot be used in any metabolic pathway in plants and inhibits enzymatic reactions of the

Calvin cycle (Somerville, 2001; Norman and Colman, 1991; Tolbert, 1997). To circumvent this, 2-phosphoglycolate is converted to 3-phosphoglycerate by the photorespiratory pathway and returned into the Calvin cycle (Figure 1).

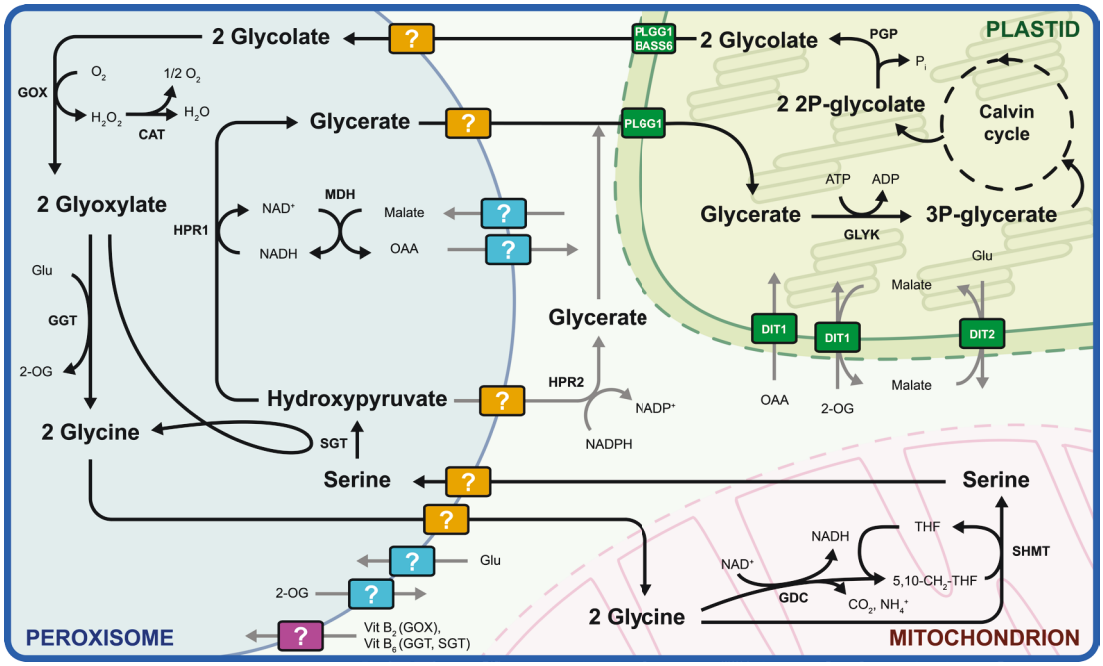

Figure 1. Photorespiration and predicted associated transport processes. Predicted peroxisomal transporters are indicated with "?" and grouped into core metabolites (orange), associated pathways (blue) and co-factors (purple). Abbreviations: AtPGP, 2PG-phosphatase; AtPLGG1, plastidic glycolate/glycerate transporter 1; AtBASS6, Bile Acid Sodium Symporter 6, glycolate exporter; AtGOX, glycolate oxidase; AtCAT, catalase; AtGGT, glutamate:glyoxylate aminotransferase; GDC, glycine decarboxylase; SHMT, serine hydroxymethyltransferase; AtSGT, serine:glyoxylate aminotransferase; AtHPR1, peroxisomal hydroxypyruvate reductase; AtHPR2, cytosolic hydroxypyruvate reductase; AtMDH, malate dehydrogenase; AtGLYK, glycerate-3-kinase; AtDiT1, dicarboxylate translocator 1; AtDiT2, dicarboxylate translocator 2; Pi, inorganic phosphate; Glu, glutamate; 2-OG, 2-oxoglutarate; OAA, oxaloacetate; THF, tetrahydrofolate; Vit B_6, pyridoxal 5′-phosphate precursor; Vit B_2, flavin mononucleotide precursor.

In Arabidopsis, the plastidic 2-phosphoglycolate phosphatase (AtPGP) dephosphorylates 2-phosphoglycolate to glycolate, which is exported to the cytosol via AtPLGG1 and AtBASS6. Glycolate is imported into peroxisomes, where it is oxidized to glyoxylate by the peroxisomal glycolate oxidases AtGOX1 and AtGOX2. The byproduct of the GOX reaction is hydrogen peroxide and needs to be removed by peroxisomal catalase (Esser et al., 2014; Engqvist et al., 2015; Kamada et al., 2003). The glutamate:glyoxylate aminotransferase (AtGGT) transaminates glyoxylate to glycine (Dellero et al., 2015). Glycine is transported to the mitochondrial matrix and converted to serine in two steps: one molecule of glycine is processed by the glycine decarboxylase complex (GDC), producing 5,10-methylene-THF, CO_2 and NH^{4+} (Schulze et al., 2016). The other glycine is converted to serine by the serine

hydroxymethyltransferase (SHMT) using 5,10-methylene-THF (Douce et al., 2001). Serine is transported back to peroxisomes and converted to hydroxypyruvate by the serine:glyoxylate aminotransferase (AtSGT) (Modde et al., 2017). Then, the hydroxypyruvate reductase 1 (AtHPR1) converts hydroxypyruvate to glycerate using NADH as reducing agent (Timm et al., 2008, 2011). NADH is provided by the constant NAD^+/NADH regeneration cycle driven by the peroxisomal malate hydrogenase (AtMDH) (Cousins et al., 2008). Glycerate is transported back to the plastid via AtPLGG1 at the inner plastidic membrane. Finally, glycerate is phosphorylated to 3-phosphoglycerate by the glycerate kinase (AtGLYK) (Boldt et al., 2005). 3-phosphoglycerate is reassimilated by the Calvin cycle (Maurino and Peterhansel, 2010).

The shuttle of photorespiratory metabolites

To allow the high metabolite flux between the compartments, organelles physically interact with each other. Peroxisomes alter their shape to increase the surface area shared with chloroplasts (Oikawa et al., 2015; Reumann and Bartel, 2016). Similar physical interactions between organelles have been described between peroxisomes and the ER, oil bodies and mitochondria (Sinclair et al., 2009; Thazar-Poulot et al., 2015; Jaipargas et al., 2016; Shai et al., 2016; Fransen et al., 2017). For the metabolite transport across membranes channels or transporters are required. In peroxisomes, channels for the passive import of smaller molecules like carboxylic acids have been postulated based on electrophysiological experiments (Reumann et al., 1998). Non have been identified in plants yet (Hu et al., 2012; Antonenkov and Hiltunen, 2006; Vapola et al., 2014; Visser et al., 2007). But non-selective channels were found in mammal and yeast peroxisomes (Pxmp2 and yeast Pex11) (Rokka et al., 2009; Mindthoff et al., 2016). Comparatively big substrates like cofactors or fatty acids are imported by peroxisomal transporters (Linka and Esser, 2012).

The rapid solute flux during photorespiration requires a fast shuttle between the different compartments. While plastids use selective transporters AtPLGG1 and AtBASS6, non-selective channels have been proposed for peroxisomes (Kunze and Hartig, 2013; Linka and Esser, 2012). In contrast to an active transport, channels are less selective but allow vast amounts of molecules to be transferred in less time (Gadsby, 2009).

Identifying photorespiratory transport proteins

Plastidic or mitochondrial proteins are targeted to their corresponding organelles based on N-terminal targeting signals and can be identified on the genomic level (Richardson et al., 2017; Regev-Rudzki et al., 2008). Many peroxisomal matrix proteins can be identified using the conserved C-terminal PTS1 or PTS2 motif, which is a recognition site for the peroxisomal protein import machinery (Brocard and Hartig, 2006; Gould et al., 1989; Meinecke et al., 2016). Some non-PTS1 proteins are associated to PTS1-protein oligomers during the import process

or have internal non-PTS targeting signals, which are not well described. Proteins of the peroxisomal membrane like transporters apparently do not contain the PTS-motif (McNew and Goodman, 1994; van der Klei and Veenhuis, 2006). To identify membrane proteins, enriched organellar membranes have been analyzed by mass spectrometry (Hunt et al., 1986; Barrera and Robinson, 2011; Palms et al., 2009; Newton et al., 2004). Bioinformatical approaches allow the identification based on PEX19-related highly complex targeting signals (Mayerhofer, 2016). Algorithms have been established to screen for these targeting signals in humans and yeast (Schlüter et al., 2007).

This study describes the identification of peroxisomal carriers by comparative transcriptome analyis of Flaveria, Cleomaceae and Arabidopsis and provides evidence for novel peroxisomal carriers with a possible connection to photorespiration and β-oxidation. Co-expression data of closely related C3 and C4 Flaveria species was used to identify genes co-regulated with the expression of known Arabidopsis photorespiratory enzymes. Hierarchical clustering and filtering for structural and phylogenetic protein traits were used to screen for membrane proteins, especially proteins categorized as transporters. Two members of the mitochondrial carrier family (MCF) named peroxisomal photorespiratory carriers 1 and 2 (AtPPR1;1 and AtPPR1;2) were identified and localized in peroxisomes of transiently transformed tobacco protoplasts via confocal laser scanning microscopy of mCherry-tagged proteins. *In vitro* uptake experiments with recombinant protein demonstrated a substrate affinity for the dicarboxylate malate. AtPPR1;1 and AtPPR1;2 could represent the malate/oxaloacetate shuttle that regenerates the peroxisomal NAD^+/NADH pool needed for photorespiration and β-oxidation.

Experimental procedures

Materials

Chemicals, DNA and protein purification kits were purchased from Sigma-Aldrich (sigmaaldrich.com) or Promega (promega.com). Enzymes and molecular reagents were purchased from New England Biolabs (neb.com) or Thermo Fisher Scientific (thermofisher.com), and Qiagen (qiagen.com). Plant growth media was purchased from Duchefa BV (duchefa-biochemie.com).

Transcriptome analysis and bioinformatical procedures

Transcriptomic data of the genus Flaveria mapped against the Arabidopsis genome was used for the identification of putative carriers involved in photorespiration (Mallmann et al., 2014). This data included the transcriptome of the C_3 species *F. robusta* and *F. pringlei*, C3–C4 intermediate species *F. chloraefolia*, *F. pubescens, F. anomala*, *F. ramosissima* and the C4-like species *F*. brownie, as well as the C4 species *F. bidentis* and *F. trinervia*. Mulitple Experiment Viewer (MeV) software (mev.tm4.org) was used for data preparation and hierarchical clustering with Pearson correlation to identify genes co-expressed with photorespiratory enzymes. Photorespiratory reference genes were Flaveria homologues of Arabidopsis genes AT3G14420, AT4G37930, AT1G32470, AT3G14415, AT5G36790, AT5G26780, AT5G04140, AT1G11860, AT1G80380. Resulting candidate genes were screened for the presence of transmembrane domains (Bulk Protein Search, TAIR, arabidopsis.org/tools/bulk/protein/), topology (Aramemnon (aramemnon.uni-koeln.de/), TransportDB (membranetransport.org/transportDB2)) and *in silico* prediction of sub-cellular localization (Aramemnon, SUBA3 (suba3.plantenergy.uwa.edu.au/)).

Transcriptomic data of AtPPR1;1 and AtPPR1;2 homologues found in Cleomaceae *species Gynandropsis gynandra* and *Tarenaya hassleriana* were extracted from Külahoglu et al. (2014). IDs of corresponding photorespiratory reference genes were: T.hassleriana_03290, T.hassleriana_06465, T.hassleriana_06669, T.hassleriana_08434, T.hassleriana_08479, T.hassleriana_09242, T.hassleriana_17256, T.hassleriana_19339, T.hassleriana_25240, T.hassleriana_04208, T.hassleriana_11711. Transcriptomic data of AtPPR1;1 and AtPPR1;2 in Arabidopsis were extracted from the TraVA database (http://travadb.org/), with additional data from Eisenhut et al. (2017) for CO_2-specific experiments. Photorespiratory Arabidopsis reference genes were: AT4G17360, AT5G47435, AT5G36700, AT3G14130, AT3G14150, AT3G14415, AT3G14420, AT4G18360, AT1G70580, AT2G13360, AT2G26080, AT4G33010, AT1G11860, AT1G32470, AT2G35120, AT2G35370, AT4G32520, AT1G12550, AT1G68010, AT1G79870, AT2G45630, AT1G80380. Protein alignments and phylogenetic trees (neighbor joining method) were performed with CLC Sequence viewer (Version 8.0) and protein sequences from Aramemnon, TAIR and UniProt (uniprot.org/).

Plant material and growth conditions

Ecotype Columbia (Col-0) *Arabidopsis thaliana* was purchased from the European Arabidopsis Stock Centre (NASC) at the University of Nottingham (arabidopsis.info). Seeds were surface-sterilized for 10 minutes with 70 % (v/v) ethanol and Triton-X-100, followed by 100 % (v/v) ethanol. Seeds were stratified for at least 3 days and germinated on half-strength MS medium with 0.8 % (w/v) plant agar. Plants were transferred to soil after 14 days and grown under long day conditions (16 h light (100 µmol m^{-2} s^{-1}) / 8 h darkness) at 22 °C (day)/ 18 °C (night) unless stated otherwise. Transgenic plants were selected on half-strength MS medium as described before with appropriate antibiotics.

Bacteria strains and media

For all cloning methods, competent *Escherichia coli* strain mach1 (Invitrogen GmbH, Karlsruhe, Germany) was used. *E. coli* was cultivated in either liquid lysogeny broth (LB, 10 g/L tryptone, 5 g/L yeast extract, 5 g/L NaCl, 15 g/L agar, shaking at 200 rpm) or on solid LB medium (with additional 15 g/L plant agar) with appropriate antibiotics at 37 °C. *Agrobacterium tumefaciens* strain GV3101 was used for stable or transient transformation of Arabidopsis and *Nicotiana benthamiana*. *A. tumefaciens* was cultivated in YPD medium (20 g/L tryptone, 10 g/L yeast extract, 20 g/L glucose) with appropriate antibiotics at 30 °C.

Isolation of genomic DNA, RNA and cDNA from Arabidopsis and Flaveria

Arabidopsis gDNA was isolated according to a modified protocol described by Kasajima et al. (2004). One leave of a at least 4 weeks old plant was pulverized in liquid nitrogen and solubilized in 250 µL extraction buffer (0.2 M Tris-HCl, pH7.5 (HCL), 0.25 M NaCl, 0.025 M EDTA, 0.5 % (w/v) SDS). Insoluble cell material was pelleted via centrifugation for 1 min at 16.000 g at RT. The supernatant was transferred and mixed with 500 µL 100 % (v/v) isopropanol and incubated for 10 min. After centrifugation for 10 min at 16.000 g at RT, the DNA pellet was air-dried and resuspended in 50 µL nuclease free H_2O by mixing the sample for 30 min at 37 °C. Arabidopsis RNA was isolated from leaf material using the GeneMATRIX Universal RNA Purification Kit (Roboklon GmbH). Complementary DNA (cDNA) was synthesized using the SuperScript II Reverse Transcriptase (Promega) with DNAse treated RNA. *F. robusta* cDNA was provided by Dr. Udo Gowik.

Cloning procedures

In silico DNA and mRNA sequences of Arabidopsis genes At1g72820 (AtPPR1;1) and At5g26200 (AtPPR1;2) were received via Aramemnon. The mRNA sequence of FrCUFF.9607 (*Fr*PPR1) from *F. robusta* was provided by Dr. Udo Gowik. Standard cloning methods were performed according to Russel and Sambrook (2001). Gene amplification and insertion into

expression vectors were performed via Gibson assembly (New England Biolabs, (Gibson, 2011)) using primers synthesized by Sigma-Aldrich. Gene sequences were verified via Macrogen (dna.macrogen.com/). Primers and vectors are listed in Supplemental material.

For sub-cellular localization studies AtPPR1;1 and AtPPR1;2 were cloned into the pUB-Dest vector system (Grefen et al., 2010). pUBC-YFP was modified to allow a C-terminal fusion with the fluorescent protein mCherry amplified from mt-rk CD3-991 (Nelson et al., 2007) using primers BH130 (5'-caacCTCGAGATATCCAACTAGTATGGTGAGCAAG-3') and BH131 (5'-caacTTATAATTACTTGTACAGCTCGTCCATGCC-3'). YFP from pUBC-YFP was cut out via restriction digest using SpeI and PsiI. The vector backbone was then fused with mCherry. A multiple cloning site was inserted using primers BH113 (5'-TCGAGAAGCTTCAATTGACTAGTAGGCCTCCATGGC-3') and BH114 (5'-TCGAGCCATGGAGGCCTACTAGTCAATTGAAGCTTC-3') at the XhoI restriction site. This C-terminal mCherry fusion expression vector pBH18 was opened using XhoI and AtPPR1;1 and AtPPR1;2 coding sequences amplified from Arabidopsis ecotype Col-0 leaf cDNA with the following primers: AtPPR1;1 (BH134 5'-GAGTTTTTCTGATTAACACATGAATTTGGGTGCGGCC-3' and BH135 5'-TGCTCACCATACTAGTTGGATATCTTGATTTAGAATAAAACCCGTCATG-3'), AtPPR1;2 (BH136 5'-GAGTTTTTCTGATTAACACATGAGTTTAGGTGCTTTGATG-3' and BH137 5'-TGCTCACCATACTAGTTGGATATCCTTTCTGCTTCTTTGTTGC-3'). The *F. robusta* gene *Fr*PPR1 was amplified from *F. robusta* leaf cDNA with primers BH138 (5'-GAGTTTTTCTGATTAACACATGAGCATGGGACTGGCG-3') and BH139 (5'-TGCTCACCATACTAGTTGGATATCTACTCGAGCAGTGAAGGAAACC-3'). PCR products and expression vector pBH18 were fused via Gibson assembly. Resulting vectors were: pBH20 (AtPPR1;1), pBH21 (AtPPR1;2) and pBH22 (*Fr*PPR1). Expression was driven by an Arabidopsis ubiquitin-10 promoter.

For uptake studies AtPPR1;1 and AtPPR1;2 were cloned into the pIVEX1.3 vector system (Ge and Xu, 2012). pIVEX1.3 was digested with XhoI. AtPPR1;1 and AtPPR1;2 coding sequences were amplified from Arabidopsis ecotype Col-0 leaf cDNA with the following primers: AtPPR1;1 (LW1 5'-ATATGAGCGGCCGCGTCGACACCATGGGGAATTTGGGTG-3' and LW2 5'- AACCCCCCCCGGGAGCTCGCCCTGATTTAGAATAAAACCCGTC-3'), AtPPR1;2 (LW3 5'- ATATGAGCGGCCGCGTCGACACCATGGGGAGTTTAGGTG-3' and LW4 5'- AACCCCCCCCGGGAGCTCGCCCTTTCTGCTTCTTTGTTGC-3'). PCR products and expression vector pIVEX1.3 were fused via Gibson assembly. Resulting vectors were: pLW1 (AtPPR1;1) and pLW2 (AtPPR1;2). Expression was driven by an T7 promoter. Primers and vectors, see Supplemental material.

Transformation of Arabidopsis

Arabidopsis was transformed according to Bernhardt et al. (2012).

Transient transformation of *N. benthamiana*, protoplast isolation and Confocal laser scanning microscopy

Agrobacterium tumefaciens strain GV3101(pMP90) (Koncz and Schell, 1986) was transformed according to Höfgen and Willmitzer (1988). YPD medium was inoculated with *A. tumefaciens* and grown over night at 28 °C. Cells were harvested via centrifugation (10 min, 3000 g) and resuspended in infiltration buffer (10 mM $MgCl_2$, 10 mM MES, pH 5.7, 100 µM acetosyringone) to an OD_{600} of 0.5. *N. benthamiana* leaves were infiltrated with the cell suspension and incubated for two days at long day conditions (16 h light (130 µmol m^{-2} s^{-1}) and 8 h darkness) at 25 °C (day)/ 20 °C (night) (Waadt and Kudla, 2008). Protoplasts were isolated two days after infiltration. *N. benthamiana* leaves were cut into 0.5 x 0.5 cm pieces and incubated in protoplast digestion solution (1.5 % (w/v) cellulase R-10, 0.4 % (w/v) macerozyme R-10, 0.4 M mannitol, 20 mM KCl, 20 mM MES pH 5.6 (KOH), 10 mM CaCl2, 0.1 % (w/v) BSA) for 2 h at 30 °C. Isolated protoplasts were resuspended in W5 solution (154 mM NaCl, 125 mM $CaCl_2$, 5 mM KCl, 2 mM MES pH5.6 (KOH)) and directly used for microscopy (Sheen, 2002). Peroxisomes were stained by adding BODIPY (resuspended in methanol) to a final concentration of 5 µM to the W5 solution (Landrum et al., 2010; Fahy et al., 2017). Protoplasts were directly used for microscopy. Protoplasts were analyzed using a Zeiss LSM 780 Confocal Microscope and Zeiss ZEN software. Excitation/emission settings used in this study: BODIPY (488 nm / 490 to 550 nm), mCherry (561 nm / 580 to 625 nm) and Chlorophyll A (488 nm / 640 to 710 nm). Pictures were processed using Fiji software (fiji.sc) and Adobe Photoshop CS6 (Adobe Systems).

Generation of Arabidopsis mutant lines via the CRISPR/Cas9 system

For phenotyping experiments of knockout or knockdown lines of Arabidopsis plants deficient in protein activity of AtPPR1;1 or AtPPR1;2 mutant lines were generated using the CRISPR/Cas9 system. Target sites were chosen and integrated into the Cas9 expression vector system described in Hahn et al. (2017, 2018). Cas9 constructs containing gene-specific sgRNA were named as followed: pBH25 (AtPPR1;1) with the single target 5'-GGTTTAAGGGGATTGTACAG-3', pBH41 (AtPPR1;2) with the double targets 5'-TTGGCACATGAGACACGAGT-3' and 5'-GTGTAGGTCAAGCAACTGTT-3', pBH42 (AtPPR1;1/ AtPPR1;2) with the double targets 5'-GGTTTAAGGGGATTGTACAG-3' and 5'-TTGGCACATGAGACACGAGT-3', pBH43 (AtPPR1;1/ AtPPR1;2) with the double targets 5'-TTGGCACATGAGACACGAGT-3' and 5'-GTGTAGGTCAAGCAACTGTT-3', pFH186 (AtPPR1;2) with the double targets 5'-TCTTTACACAGATGGACCAA-3' and 5'-

TTGTAGTTCTCAAAACAAGG-3'. sgRNA sequences see also, Table 2. Primers and vectors, see Supplemental material.

Protein expression, reconstitution of liposomes and *in vitro* uptake assay

AtPPR1;1 and AtPPR1;2 were heterologously expressed using expression vector pIVEX1.3 and the RTS Wheat Germ CECF kit (biotechrabbit) in the presence of 1% (w/v) L-a-phosphatidylcholine vesicles and 0.04% (w/v) Brij-35 as described by Bernhardt et al. (2012b). Recombinant proteins were reconstituted into liposomes by freeze-thaw-sonication (Kasahara and Hinkle, 1977). 50 µl of protein extract were added to 950 µl 3 % (w/v) L-a-phosphatidylcholine and frozen in liquid nitrogen. Liposomes were pre-loaded with 30 mM unlabeled malate. The *in vitro* uptake of 200 mM ^{14}C-labelled malate (^{14}C(U), 1.85 GBq/mmol), 2-oxoglutarate (1-^{14}C, 2.04 GBq/mmol) or glutamate (1-^{14}C, 1.85 GBq/mmol) was performed as described by Bernhardt et al. (2012b). The incorporated radiolabeled malate, 2-oxoglutarate or glutamate were analyzed by liquid scintillation counting. Time-dependent uptake kinetics were fitted by non-linear regression based on one-phase exponential association using GraphPad Prism 5.0 software (GraphPad, graphpad.com). The background activities in the absence of recombinant were subtracted. The initial velocity of uptakes were calculated using the equation slope = (plateau – Y0) x k, whereas Y0 was set to 0. The values for the Plateau and k were extracted from the nonlinear regression analyses using a global fit from three technical replicates.

SDS-PAGE and immunoblotting

Protein analysis was performed via SDS-PAGE using standard protocols (Russel and Sambrook, 2001). For immunodetection western blots were treated with Anti-His-HRP. For chemiluminescent detection 'Immobilon Western HRP Substrate' (Millipore GmbH, Schwalbach) and the Luminescence Image Analyzer LAS-4000 Mini (GE Healthcare, Solingen, Deutschland) was used.

Protein quantification

Protein quantification was performed with the Pierce BCA protein assay kit (used for samples with up to 20mM imidazole, high amounts of lipid or detergent; Thermo Fisher Scientific Inc., Rockford, IL, USA) or the Quick Start Bradford Protein Assay (samples with more than 20 mM imidazole, Bio-Rad Laboratories Inc., Hercules, CA, USA).

Results

Identification of genes co-expressed with photorespiratory enzymes in Flaveria

The evolution of C4 photosynthesis introduced Kranz anatomy and the spatial separation of carbon fixation and the Calvin cycle into plants. This favors the carboxylation reaction by RuBisCO (Wang et al., 2017a). It has been shown that the expression level of photorespiratory enzymes reflects the reduction of photorespiratory activity found in C4 plants. On the other hand, genes necessary for the structural changes, transcription factors or transporters were identified to drive C4 anatomy and metabolism. These genes show an increase in transcript abundance in C4 species not seen in C3 relatives, while typical genes assigned to the photorespiratory pathway are down-regulated (Külahoglu et al., 2014; Bräutigam et al., 2011; Mallmann et al., 2014; Gowik et al., 2011).

In general it is assumed that genes involved in the same pathway are co-regulated and expressed simultaneously (Eisen et al., 1998). As a consequence, putative photorespiratory transport proteins should be co-expressed with known photorespiratory enzymes (Bordych et al., 2013). Based on this assumption transcriptomic data of nine different Flaveria species with C3, C4 or transitioning traits (C3 - *F. pringlei*, *F. robusta*; C3-C4 Intermediates - *F. chloraefolia*, *F. pubescens*, *F. anomala*, *F. ramoissima*; C4-like - *F. browni*; C4 - *F. bidentis*, *F. trinervia*, (Mallmann et al., 2014)) were analyzed. Nine typical Arabidopsis homologues of photorespiratory enzymes showing high transcript abundance in C3 compared to C4 Flaveria species were selected as reference: AtGLDT1 (At1g11860), AtPGLP1 (At5g36790), AtFd-GOGAT (At5g04140), AtSHM1 (At4g37930), AtGLYK (At1g80380), AtGOX2 (At3g14415), AtGOX1 (At3g14420), AtSHM2 (At5g26780), AtGLDH3 (At1g32470) (Bauwe, 2010). Additionally, the following known transporters involved in photorespiration were included: AtPLGG1 (At1g32080) (Pick et al., 2013), AtDiT1 (At5g12860), AtDiT2.2 (At5g64280) (Renné et al., 2003) (Figure 2A). AtDiT2.1 (At5g64290) (Renné et al., 2003) and AtBASS6 (At4g22840) (South et al., 2017) did not show up in the original Flaveria data set. All photorespiratory enzymes were down-regulated in both C4 species (*F. bidentis* and *F. trinervia*) and partly in the C4-like species *F. brownie* (Figure 2A).

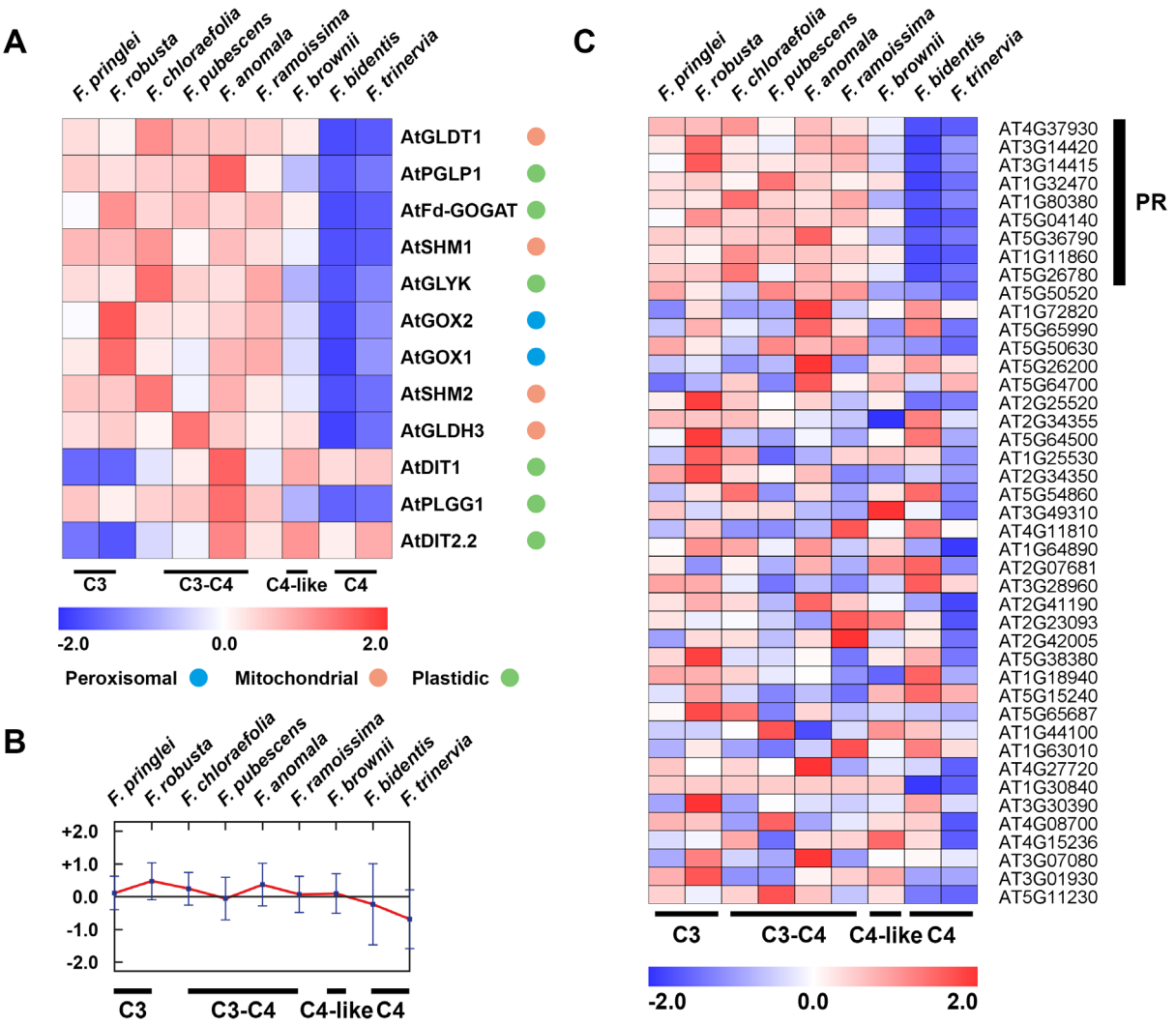

Figure 2. Expression of photorespiratory genes down-regulated in C4 Flaveria species with candidate genes found in co-expression clusters.

(A) Expression pattern of selected photorespiratory marker genes in C3 to C4 Flaveria species (C3 - *F. pringlei*, *F. robusta*; C3-C4 Intermediates - *F. chloraefolia*, *F. pubescens*, *F. anomala*, *F. ramoissima*; C4-like - *F. browni*; C4 - *F. bidentis*, *F. trinervia*). Colored dots indicate subcellular localization (blue: peroxisomal, red: mitochondrial, green: plastidic). Expression levels are indicated with blue (down-regulated relative to normalized expression values) and red (up-regulated relative to normalized expression values). (B) Mean expression of photorespiratory marker genes and selected co-expressed candidate genes. Values represent down (-2.0 to 0) regulation or up regulation (0 to +2.0) relative to normalized expression values. Error bars represent the standard deviation of expression within the cluster of genes for peroxisomal transport proteins. (C) Expression pattern of photorespiratory genes and selected candidate genes. Expression levels are shown as described in (A). All genes resemble best hit homologues found in Arabidopsis. Data is shown as normalized expression values as described for (A).

As expected, photorespiratory enzymes are upregulated in C3 and intermediate species. The same observation was made for the glycolate/glycerate transporter AtPLGG1. Interestingly, AtDiT1 and AtDiT2.2 showed a reversed expression pattern. While the highest expression of both was found in the intermediate species *F. anomala*, the lowest expression was seen in the C3 species *F. pringlei* and *F. robusta* with moderate expression in all C4/C4-like species. Both

are involved in ammonia assimilation while AtDiT1 was recently described to be also involved in redox homeostasis via the malate shuttle from chloroplasts to mitochondria (Zhao et al., 2018). While the overall redox stress due to photorespiration is expected to be reduced in C4 plants, redox homeostasis related genes have shifted in function or spatial expression, which is not covered with the non-tissue-specific data shown here. Indeed, redox homeostasis was altered in the context of C4 photosynthesis as well (Turkan et al., 2018). For the following co-expression analysis AtDiT1 and AtDiT2.2 were omitted as reference genes. Still, it needs to be mentioned that the expression pattern of DiT proteins seen in Flaveria might reflect a pattern for associated photorespiratory proteins not directly involved in the core pathway.

For co-expression analysis, transcriptomic data from Mallmann et al. (2014) was processed via hierarchical clustering with Pearson correlation to identify genes co-expressed with photorespiratory enzymes. Co-expression clusters from a pool of 21973 genes mapped on best hit Arabidopsis genes were generated and selected for the following characteristics: (1) The mean expression of all included genes in C4 species must be under the detected transcript level of all C3 and partly in intermediate species and (2) the cluster must include the pre-selected photorespiratory reference genes as listed above. 2810 genes fulfilled these criteria. Putative membrane proteins must contain hydrophilic alpha-helical transmembrane domains (TMD). Tair Bulk Protein Search was used for TMD prediction leading to the selection of 120 genes with at least 2 predicted TMDs. Already published genes with clear localization in non-peroxisomal cell compartments (e.g. AtPLGG1) were omitted. The list was further narrowed down by using the Transporter Classification Database tcdb (tcdb.org) to reveal protein families favorable for substrates needed for photorespiration. 34 candidate genes were found suitable (Table 1). These genes show a mean overall reduction in expression from C3 to C4 in Flaveria (Figure 2B). A more detailed look at the single expression pattern of those genes reveals that they do not necessarily follow the clear expression pattern observed for photorespiratory core enzymes but rather resemble AtDiT1 and AtDiT2 expression (Figure 2C).

Table 1. List of Arabidopsis homologues co-expressed with photorespiratory enzymes in Flaveria C3, C3-C4 intermediates and C4 species.

Genes were identified using co-expression analysis and filtered for the presence of predicted transmembrane domains, known sub-cellular localization, functional domains and protein family.

Locus	Protein family name	Description
AT1G25530	Amino Acid/Auxin Permease Family	putative LHT-type amino acid transporter
AT1G44100	Amino Acid/Auxin Permease Family	AtAAP5, amino acid transporter
AT2G41190	Amino Acid/Auxin Permease Family	putative unspecified transporter
AT2G42005	Amino Acid/Auxin Permease Family	putative ANT-type amino acid transporter
AT3G28960	Amino Acid/Auxin Permease Family	putative unspecified transporter
AT3G30390	Amino Acid/Auxin Permease Family	putative unspecified transporter
AT5G15240	Amino Acid/Auxin Permease Family	putative unspecified transporter
AT5G65990	Amino Acid/Auxin Permease Family	putative ANT-type amino acid transporter
AT2G07681	ATP-binding Cassette Superfamily	AtABCI4, putative subfamily I ABC protein
AT4G15236	ATP-binding Cassette Superfamily	AtABCG43/AtPDR15, putative subfamily G ABC-type transporter
AT5G38380	Cation Diffusion Facilitator Family	putative EamA-like transporter
AT1G30840	Drug/Metabolite Transporter Superfamily	AtPUP4, putative purine permease
AT2G25520	Drug/Metabolite Transporter Superfamily	putative phosphometabolite transporter
AT3G07080	Drug/Metabolite Transporter Superfamily	putative metabolite transporter
AT4G08700	Drug/Metabolite Transporter Superfamily	AtPUP13, putative purine permease
AT5G11230	Drug/Metabolite Transporter Superfamily	putative phosphometabolite transporter
AT5G64700	Drug/Metabolite Transporter Superfamily	putative unspecified transporter
AT1G64890	Folate-Biopterin Transporter Family	putative BT1-type small solute transporter
AT5G54860	Folate-Biopterin Transporter Family	putative BT1-type small solute transporter
AT1G18940	Major Facilitator Superfamily	putative nodulin-type transporter
AT1G63010	Major Facilitator Superfamily	putative SPX-MFS-type phosphate transporter
AT2G23093	Major Facilitator Superfamily	putative unspecified transporter
AT2G34350	Major Facilitator Superfamily	putative nodulin-type transporter
AT2G34355	Major Facilitator Superfamily	putative nodulin-type transporter
AT3G01930	Major Facilitator Superfamily	putative nodulin-type transporter
AT3G49310	Major Facilitator Superfamily	putative unspecified transporter
AT4G11810	Major Facilitator Superfamily	putative SPX-MFS-type phosphate transporter
AT4G27720	Major Facilitator Superfamily	putative unspecified transporter
AT5G50520	Major Facilitator Superfamily	putative nodulin-type transporter
AT5G50630	Major Facilitator Superfamily	putative nodulin-type transporter
AT5G64500	Major Facilitator Superfamily	putative (yeast AMF1)-like ammonium transporter
AT5G65687	Major Facilitator Superfamily	putative (yeast AMF1)-like ammonium transporter
AT1G72820	Mitochondrial Carrier Family	putative MtcC-type unspecified transporter
AT5G26200	Mitochondrial Carrier Family	putative MtcC-type unspecified transporter

The candidate list includes members of seven transporter families based on tcdb categories: Amino Acid/Auxin Permease Family (AAAP) (8), ATP-binding Cassette Superfamily (ABC) (2), Cation Diffusion Facilitator Family (CDF) (1), Drug/Metabolite

Transporter Superfamily (DMT) (6), Folate-Biopterin Transporter Family (FBT) (2), Major Facilitator Superfamily (MFS) (13), Mitochondrial Carrier Family (MCF) (2). The AAAP family includes proteins only found in eukaryotes. Substrates are auxin (Carraro et al., 2012; Balzan et al., 2014) and amino acids with substrate-specific and broad substrate spectrum carriers (Fischer et al., 2002; Tegeder and Hammes, 2018). Amino acid permeases (AAP) are primarily involved in the source to sink transport of nitrogen and are localized in the plasma membrane (Perchlik and Tegeder, 2017; Wang et al., 2017b; Okumoto et al., 2004). The ABC superfamily is a class of primary active transporters with a broad range of substrates (Zheng et al., 2013). Transporters are localized in the plasma and vacuolar membrane, plastids, mitochondria and peroxisomes and shuttle substrates like auxin, abscisic acid, cytokinins or strigolactones (Rea, 2007; Kang et al., 2011; Verrier et al., 2008; Hwang et al., 2016). Peroxisomal ABC-transporters are linked to 2,4-dichlorophenoxybutyric acid, indole-3-butyric acid, fatty acyl CoAs, jasmonic acid and acetate shuttle (Baker et al., 2015). The CDF superfamily is primarily involved in heavy metal homeostasis in vacuoles, while they can be found in the Golgi complex in animals as well (Haney et al., 2005). DMT superfamily members in plants are localized in plastids and transport phosphorylated C3-, C5- and C6-compounds in exchange for inorganic phosphate (Weber et al., 2005; Facchinelli and Weber, 2011; Knappe, 2003). Very few carriers of the FBT family have been described. In cyanobacteria folate is shuttled between the outer medium and the inner matrix, while in Arabidopsis folate is imported into plastids (Eudes et al., 2010; Klaus et al., 2005). The MFS is the largest superfamily of secondary carriers, spanning 74 families and all kingdoms. Substrates are mostly family-specific and include the shuttle of saccharides, amino acids, peptides, vitamins, cofactors, nucleotides, iron chelates, organic and inorganic anions and cations and many more (Reddy et al., 2012; Quistgaard et al., 2016; Law et al., 2008). Members of the MCF shuttle various classes of substrates like nucleotides, carboxylates and amino acids (Palmieri et al., 2011; Haferkamp, 2007). 58 MCF proteins were found in Arabidopsis. They share a highly conserved tripartite sequence of roughly 100 repeating amino acids forming two α-helices per repeat. Each repeat is separated by a hydrophilic loop and contains a signature PFAM PF00153 motif (Palmieri, 1994).

Candidates cluster with amino acid and carboxylate carriers

Arabidopsis MCF candidates AT1G72820 (peroxisomal photorespiratory carrier 1;1, AtPPR1;1) and AT5G26200 (AtPPR1;2) were selected for further analysis. Various MCF members have been characterized to date. Not only do they localize in different sub-cellular compartments but they also transport a wide range of different substrates (Linka and Esser, 2012). Some substrate classes of MCF members are important in the context of photorespiration (Catoni et al., 2003). These members include amino acid and dicarboxylate carriers like AtUCP1 and AtUCP2 (Monné et al., 2018), S-adenosylmethione (SAM) carriers

like AtSAMC1 and AtSAMC2 (Palmieri et al., 2006a; Bouvier et al., 2006), amino acid carriers like AtBAC1 and AtBAC2 (Hoyos et al., 2003; Palmieri et al., 2006b; Planchais et al., 2014) and the dicarboxylate carriers like AtDIC1-3 (Palmieri et al., 2008a). Also ADP/ATP carriers like AtPNC1-2 (Linka et al., 2008) and AtAAC1-3 (Haferkamp et al., 2002) or NAD carrier like AtPXN (Bernhardt et al., 2012b) belong to the diverse group of the MCF (Figure 4). AtPPR1;1 and AtPPR1;2 are closely related within the MCF phylogenetic tree as shown in Figure 4 and share a high sequence identity of 59.0 % on protein level (Figure 3). The *Flaveria robusta* homologue (FrPPR1) shares an identity of 64.50 % with AtPPR1;1 and 59.20 % with AtPPR1;2. The high sequence identity of AtPPR1;1 and AtPPR1;2 might indicate that they share a similar function or substrate specificity in Arabidopsis. Expressing proteins with a redundant function could also hint at a temporal or spatial differentiation on a subcellular or tissue-specific level which is not uncommon for eukaryotic cells (Blanchoin and Staiger, 2010).

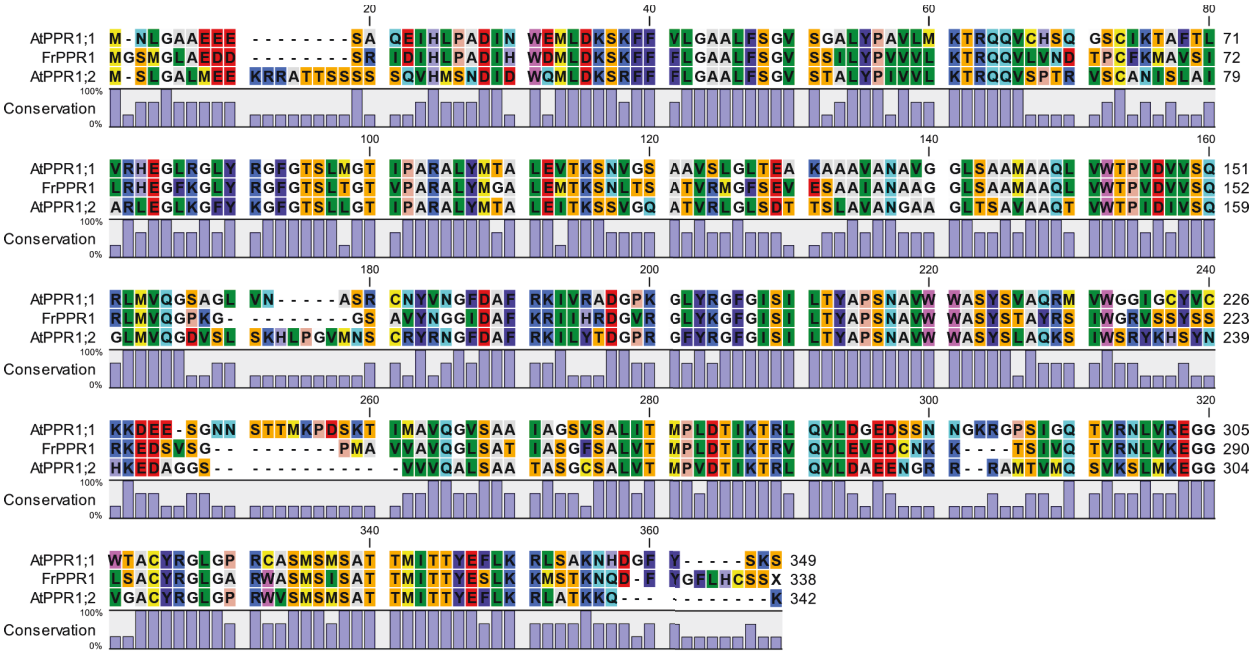

Figure 3. Amino acid sequence alignment of mitochondrial carrier family members *Fr*PPR1, AtPPR1;1 and AtPPR1;2.

Protein alignment of MFC candidates up-regulated in photorespiratory C3 species of Flaveria, Cleome and Arabidopsis (aligned with CLC sequence viewer, gap open cost of 10.0, gap extension cost of 1.0 and end gap cost (as any other)). Bars indicate conservation of amino acids. Colors represent amino acids according to the Rasmol color scheme. Selected PPR carriers share a high sequence identity: AtPPR1;1:AtPPR1;2 (59.0 %), AtPPR1;1:FrPPR1 (64.50 %), AtPPR1;2:FrPPR1 (59.20 %).

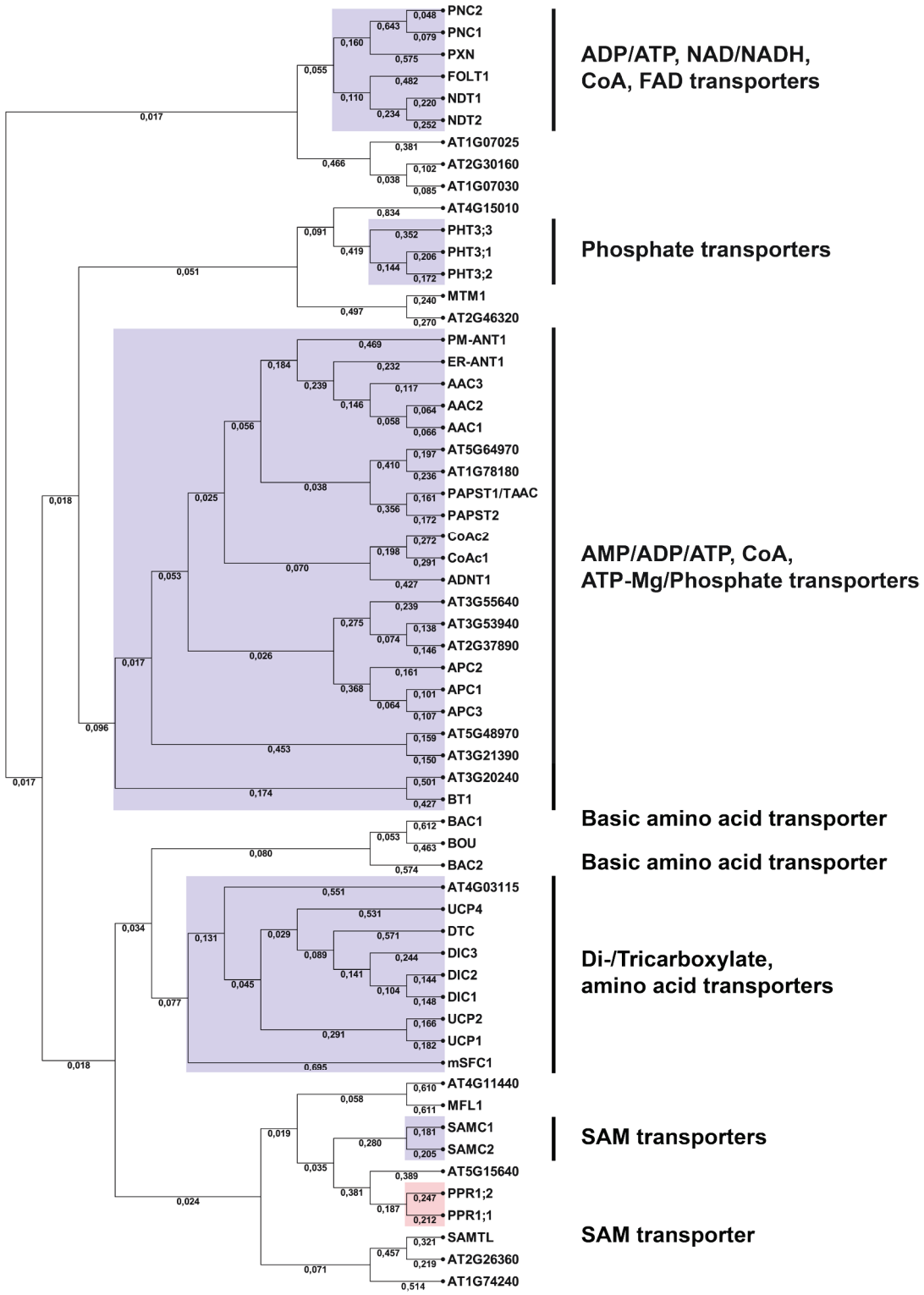

Figure 4. Unrooted phylogenetic tree of all described members of the Arabidopsis mitochondrial carrier family.

The tree was generated using CLC Sequence Viewer (Version 8) based on the neighbor joining method with 1000 replicates for bootstrapping analysis of the phylogenetic tree and gap open cost of 5.0, gap extension cost of 1.0 and end gap cast (cheap) for the alignment. Phylogenetic distances are indicated by numbers based on branch length. Carriers with similar functions (proven and predicted) are highlighted.

PPRs are up-regulated in leaves of *T. hassleriana* and Arabidopsis

Comparison of closely related C3 and C4 species is a powerful tool to reveal key players in photorespiration. The Cleomaceae species *Tarenaya hassleriana* (C3) and *Gynandropsis gynandra* (C4) have been established as an exemplary model to compare typical C4 traits (Külahoglu et al., 2014; Bräutigam et al., 2011). Both are also closely related to Arabidopsis (Brown et al., 2005; Marshall et al., 2007). To verify the expression data of AtPPR1;1 and AtPPR1;2 from Flaveria, PPR homologues were identified in *T. hassleriana* based on the data published by Külahoglu et al. (2014). Two homologues were found for AtPPR1;1 (AtPPR1;1a (Th_17024), AtPPR1;1b (Th_19589)) and one for AtPPR1;2 (Th_09714). PPR expression values from *T. hassleriana* were compared to *G. gynandra* in relation to the mean expression values of known photorespiratory genes (PR) in young to mature leaves (separated into six individual stages of leaf development, Leaf 0-5) (Figure 5A). The mean expression of PR genes slightly increased towards leaf 5 indicating higher photorespiratory activity in mature leaves (Salin and Homann, 1971). Both AtPPR1;1 homologue transcript levels slightly decreased towards leaf 2 but stayed constant in the following developmental stages. The *T. hassleriana* homologue of AtPPR1;2 was reduced (in comparison to *G. gynandra*) in stages 0 and 1 but strongly increased towards leaf 5. AtPPR1;2 showed the comparatively highest increase in mature leaves (Figure 5B).

There is no direct C4 relative species to Arabidopsis. But the expression of photorespiratory genes can be monitored under various aerial carbon dioxide conditions (Eisenhut et al., 2017). Under high CO_2 conditions (1 %) PR genes were-regulated due to the reduced oxygenic reaction. A shift to ambient CO_2 conditions (0.038 %) led to a change of gene expression and increase of photorespiratory metabolites like glycolate, glycine, serine or glycerate. This effect is even more pronounced in mutants of this metabolic pathway (Eisenhut et al., 2017). Both genes, AtPPR1;1 and AtPPR1;2, showed an increase of transcript levels under ambient air conditions compared to high CO_2 conditions (Figure 5C). These results suggest that AtPPR1;1 and AtPPR1;2 correlate with the expression of photorespiratory genes. The induced expression in Arabidopsis under ambient air conditions could also relate to the higher redox stress in photorespiratory tissues (Hossain and Dietz, 2016). Other experiments showed that AtPPR1;2 is up-regulated under biotic and abiotic stresses, including drought (Coolen et al., 2016), high-light conditions (Rasmussen et al., 2013), whereas both candidates are down-regulated under salt stress (Sham et al., 2015) and ROS (Willems et al., 2016).

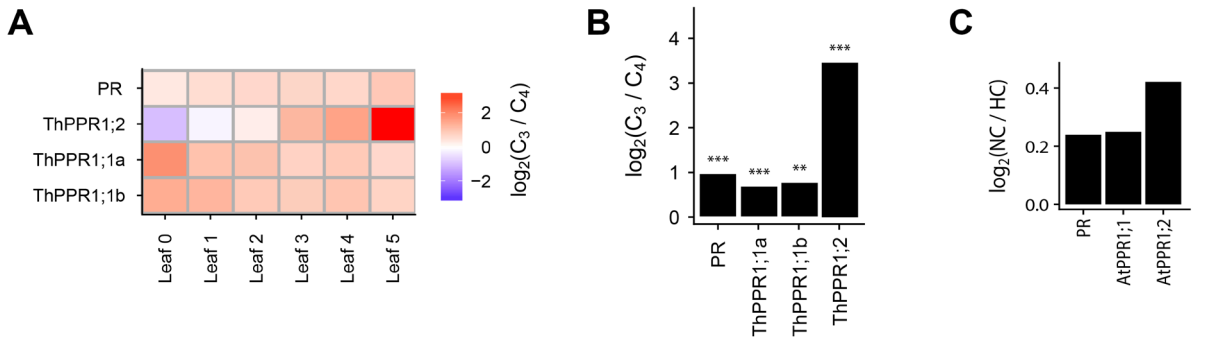

Figure 5. Expression patterns of PPR homologues in *T. hassleriana* and PPRs in Arabidopsis.
(A) Expression pattern of photorespiratory enzymes (mean expression) and PPR homologues in the C3 species *T. hassleriana* in comparison to the C4 species *G. gynandra* in different developmental leaf stages 0 to 5 (Leaf number indicates leaf age: 0 (0-2 days), 1 (2-4 days), 2 (4-6 days), 3 (6-8 days), 4 (8-10 days), 5 (10-12 days)). Expression level is shown in blue (down-regulated relative to normalized expression values in comparison with *G. gynandra*) and red (up-regulated relative to normalized expression values in comparison with *G. gynandra*). Two homologues were found for AtPPR1;1, here shown as AtPPR1;1a and AtPPR1;1b. Expression values are given as log_2 of normalized mean expression values. (B) Expression PR and PPR homologues in leaf 5 of *T. hassleriana* in comparison to *G. gynandra*. Stars indicate significance (p < *0.05, **0.01, ***0.001). Expression values are given as log_2 of normalized mean expression values. (C) Expression levels of PPRs in Arabidopsis under normal CO_2 (ambient (0.038 %)) compared to high CO_2 (1 %) conditions. Expression values are given as log_2 of normalized mean expression values.

PPRs are highly expressed in mature seeds of *T. hassleriana* and Arabidopsis

So far transcriptomic data used in this study resembled genes expression in rosette leaves. Tissue-specific expression data was analyzed for a more detailed insight into the overall expression of AtPPR1;1 and AtPPR1;2. Therefore, data were used from *T. hassleriana* (Külahoglu et al. 2014) and Arabidopsis (TraVA database, Klepikova et al., 2015, 2016). Categories in this analysis were: flower, rosette leaf, root, seed 1 (young seeds), seed 2 (developing seeds), seed 3 (mature seeds), seedling and stem (Figure 6A). In *T. hassleriana*, AtPPR1;1 homologues AtPPR1;1a (Th_17024) and AtPPR1;1b (Th_19589) were ubiquitously expressed. Both showed a remarkable up-regulation in mature seeds. AtPPR1;2 (Th_09714) was ubiquitously low expressed with a slightly transcript level in young seeds. Tissue-specific data from Arabidopsis reflects these observations made for AtPPR1;1 homologues. AtPPR1;1 was ubiquitously expressed, with higher transcript levels in mature seeds (Figure 6B). Additionally, a gradual increase starting in young seeds up to mature seeds was observed. AtPPR1;2 in Arabidopsis was also ubiquitously low expressed. Slightly higher transcript levels appeared in leaves and roots and higher levels in mature seeds. This data indicates that AtPPR1;1 and AtPPR1;2 might be involved in seed development or are stored as long-lived RNA (Sano et al., 2015). Indeed, AtPPR1;1 is expressed during embryogenesis. Higher transcript levels are detectable especially during the first 24 h after pollination just before the globular stage with subsequent comparatively high levels up to the seedling stage (Le et al.,

2010). AtPPR1;2 is rather low expressed during early embryogenesis and contradictory to results described before up-regulated not until the seedling stage (Le et al., 2010).

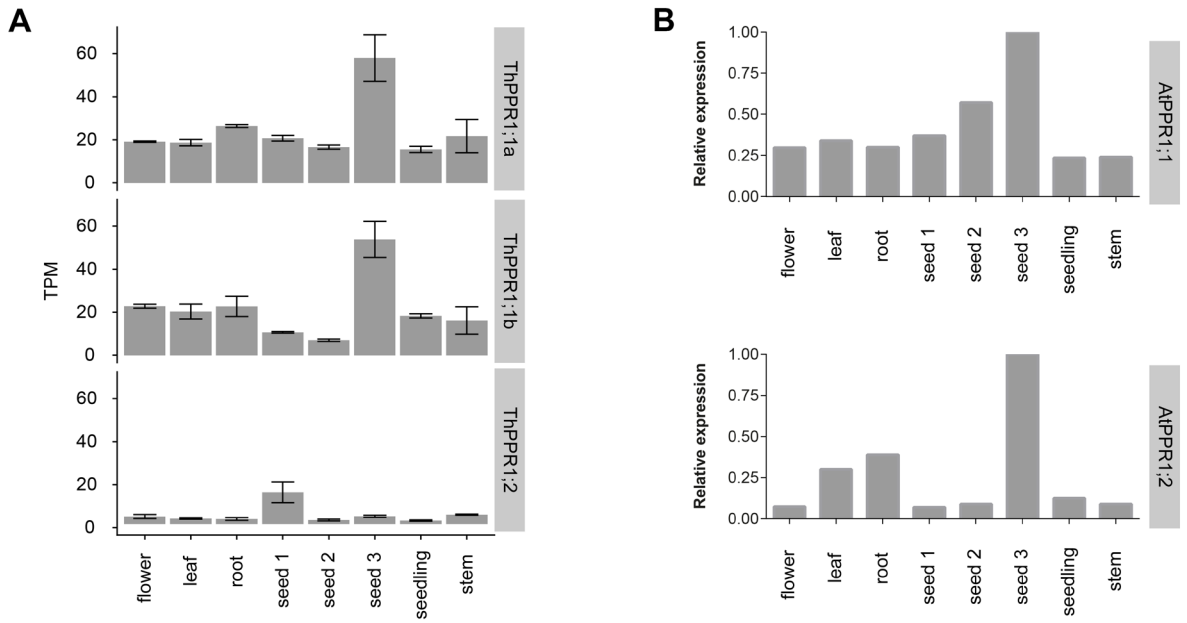

Figure 6. Tissue-specific expression of AtPPR1;1 and AtPPR1;2 homologues in *T. hassleriana* and PPRs in Arabidopsis.

(A) Detailed tissue-specific expression of PPR homologues in *T. hassleriana*. Seed 1 to 3 correspond to young, developing and mature seeds, respectively. Values represent transcripts per million (TPM). Error bars represent standard deviation. (B) Detailed tissue-specific expression of PPRs in Arabidopsis. Seed 1 to 3 correspond to young, developing and mature seeds, respectively. Shown is the relative expression (0.00 to 1.00) based on the highest measured expression value (1.00) found in the dataset for that specific gene transcript.

PPRs are targeted to peroxisomes in transiently transformed tobacco leaf protoplasts

MCF members are not exclusively localized in mitochondria. In Arabidopsis, AtPNC1/PNC2 (Linka et al., 2008) and AtPXN (van Roermund et al., 2016) are localized in peroxisomes. AtNDT1 (Palmieri et al., 2009), AtPAPST1/AtTAAC (Gigolashvili et al., 2012) and AtFOLT1 (Bedhomme et al., 2005) are found in plastids. AtER-ANT1 (Hoffmann et al., 2013) resides in the endoplasmic reticulum and AtPM-ANT1 (Rieder and Neuhaus, 2011) in the plasma membrane. Dicarboxylate carriers AtDIC1-3, AtUCP1-2, AtACC1-3 or ATP-Mg/phosphate carriers AtAPC1-3 (Palmieri et al., 2008a; Picault et al., 2004; Monné et al., 2018, 2017) are mitochondrial carriers. The subcellular localization of Arabidopsis AtPPR1;1 and AtPPR1;2 was not determined yet.

To reveal the subcellular localization C-terminal fusion proteins FrPPR1-mCherry (PPR1 from *Flaveria robusta*), AtPPR1;1-mCherry and AtPPR1;2-mCherry were transiently expressed under the control of an constitutive Arabidopsis ubiquitin-10 promoter in independent *N. benthamiana* leaves. Two days after infiltration protoplasts were isolated and

directly used for confocal laser scanning microscopy. BODIPY (Landrum et al., 2010; Fahy et al., 2017) was used as peroxisomal marker. All observed protoplasts showed a clear co-localization of the mCherry-fusion proteins (shown in magenta) with the peroxisomal marker BODIPY (shown in green) for all three PPR proteins (Figure 7A-C).

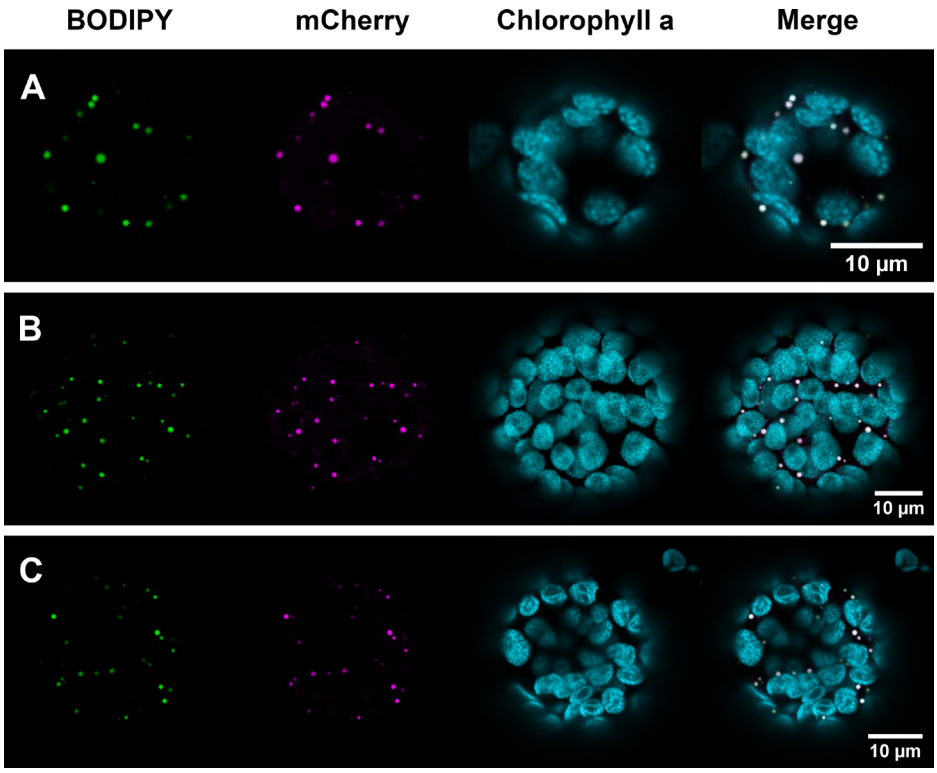

Figure 7. Subcellular localization of PPRs in transiently transformed protoplasts.
Fluorescent signals of C-terminal mCherry fusion proteins (magenta), peroxisomal marker BODIPY (green), chlorophyll a/chloroplasts (cyan) and merge showing the overlap of the fluorescent signals (white) detected via confocal laser scanning microscopy in transiently transformed *N. benthamiana* protoplasts. (A-C) Co-localization of BODIPY with the MCF fusion proteins FrPPR1-mCherry (A), AtPPR1;1-mCherry (B) and AtPPR1;2-mCherry (C), respectively. Scale bar = 10 µM

AtPPR1;1 and AtPPR1;2 show malate transport activity in time-dependent uptake studies and might belong to the group of dicarboxylic acid carriers within the MCF

The MCF is known to shuttle a broad substrate spectrum. Based on sequence alignments and structural analyses of known carriers and their substrate binding sites, it was predicted that they can shuttle (1) nucleotides, (2) carboxylates and (3) amino acids (Robinson and Kunji, 2006; Palmieri et al., 2011). Studies revealed the following substrates: (1) nucleotides: AMP/ADP/ATP (Linka et al., 2008; Arai et al., 2008; Rieder and Neuhaus, 2011; Hoffmann et al., 2013; Haferkamp et al., 2002; Gigolashvili et al., 2012; Palmieri et al., 2008b; Lorenz et al., 2015), NAD/NADH (Bernhardt et al., 2012b; van Roermund et al., 2016; Palmieri et al., 2009), CoA (Zallot et al., 2013) or FAD (Bedhomme et al., 2005). (2) di-/tri/carboxylates: malate, oxaloacetate, 2-oxoglutarate, succinate (Palmieri et al., 2008a; Monné et al., 2018), (3) amino

acids: aspartate, glutamate, cysteine sulfonate, cysteate (Monné et al., 2018), arginine or ornithine (Palmieri et al., 2006b; Planchais et al., 2014). In addition some carriers also transport phosphate, sulfate and thiosulfate (Monné et al., 2018; Palmieri et al., 2008a; Hamel et al., 2004; Monné et al., 2017) or S-adenosyl methionine (SAM) (Bouvier et al., 2006; Palmieri et al., 2006a). The only member of the MCF that was directly linked to photorespiration so far is the mitochondrial carrier AtBOU (Lawand et al., 2002). While glycine concentrations increase in BOU-deficient Arabidopsis mutants, its function is rather linked to glycine decarboxylase activity than glycine shuttle itself. The substrate of this carrier is still unknown (Eisenhut et al., 2013a). AtPPR1;1 and AtPPR1;2 from Arabidopsis have not been biochemically studied yet. Computational predictions of substrate specificity based on recurring sequential amino acid motifs did not reveal a putative substrate (Palmieri et al., 2011).

To test the *in vitro* function of both proteins, liposomes were reconstituted with His-tagged AtPPR1,1 or AtPPR1;2 protein or the empty vector control. Protein was expressed using the cell-free wheat germ expression system in the presence of lipid vesicles and detergents. This expression system has been successfully used for the biochemical characterization of the peroxisomal MCF proteins (Bernhardt et al., 2012b). The presence of protein was verified via immunoblotting with an anti-His antibody (Figure 8A). AtPPR1;1-His has a predicted molecular mass of 40.28 kDa, AtPPR1;2-His a molecular mass of 40.73 kDa. Both proteins were detected at the 40 kDa mark in their respective lane along with smaller degradation products. No protein band was detected in the empty vector control lane.

Cell-free expressed PPR proteins were tested using a liposome uptake system (Bernhardt et al., 2012b; Roell et al., 2017). MCF carriers are known antiporters with few members showing uniport activity (Haferkamp and Schmitz-Esser, 2012). The substrate affinity of PPR proteins for malate (0.2 mM) was tested. Liposomes were preloaded either with 30 mM unlabeled malate or without a counter-exchange substrate as negative control. The time-dependent uptake of radiolabeled [1-^{14}C]-malate was measured (Figure 8B-D). Preloaded liposomes reconstituted with the empty vector control expression did not show any malate uptake compared to liposomes without unlabeled malate as counter-exchange substrate (Figure 8B). Both rates reached a maximum uptake of 3.00 nmol malate/mg protein. Liposomes reconstituted with AtPPR1;1-His did show uptake when malate was used as counter-exchange substrate with a maximum uptake of 28.39 nmol malate/mg protein, while the control did not surpass 2.00 nmol malate/mg protein (Figure 8C). AtPPR1;2-His revealed a maximum malate uptake capacity of 27.98 nmol malate/mg protein (Figure 8C). Both proteins showed a initial velocity of 1.85 nmol malate/ mg total protein.

Since the plastidic transporters AtDiT1 and AtDiT2 (Kinoshita et al., 2011; Renné et al., 2003) accept malate, glutamate and 2-oxoglutarate, these substrates were measured for the

import of radioactive labeled 2-oxoglutarate and glutamate in exchange with the respective metabolite. However, no uptake rate could be confirmed (data not shown).

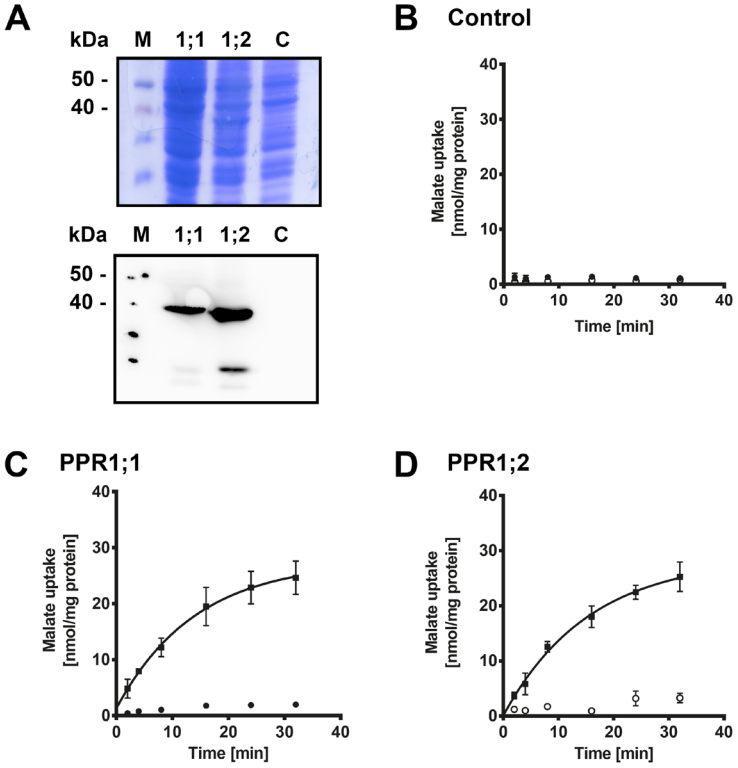

Figure 8. Time-dependent uptake studies of recombinant AtPPR1;1-His and AtPPR1;2-His protein. (A) AtPPR1;1-His (40.28 kDa) and AtPPR1;2-His (40.73 kDa) proteins were expressed using wheat germ cell-free expression system. Proteins were separated by SDS-PAGE and stained using Coomassie (upper panel). The presence of the recombinant PPR protein was verified via immunoblotting using His-tag antibody. Recombinant protein was reconstituted in liposomes pre-loaded with 30 mM malate (closed symbols) or without counter-exchange substrate (open symbols). Uptake of 0.2 mM radioactively labelled [1-^{14}C]-malate mediated by the empty vector control expression (B), AtPPR1;1-His protein (C) and AtPPR1;2-His protein (D). All graphs represent the arithmetic mean ± SE of three technical replicates.

Generation of Arabidopsis PPR knockout lines via the CRISPR/Cas9 system

To elucidate the physiological role of AtPPR1;1 and AtPPR1;2, Arabidopsis knock-out lines are required for further *in planta* experiments. Therefore, T-DNA insertion lines in the publicly available database Signal have been tested first (Alonso et al., 2003). T-DNA insertion are supposed to reduce or nullify the expression of a gene or protein activity (O'Malley et al., 2015). While insertions in the 5'-UTR of genes mostly affect the expression, an insertion in an exon leads to the disruption of the open reading frame (O'Malley and Ecker, 2010; Wang, 2008). T-DNA insertion lines have been used to characterize the physiological state of photorespiratory mutants (Eisenhut et al., 2013a; Pick et al., 2013; South et al., 2017).

Two independent mutant line have been identified for AtPPR1;1: SALK138980 and GABI-Kat119A04 with an insertion in the far 3'-region of the gene. Two AtPPR1;2 mutant lines, SAIL36XA08 and SAIL399B09, have been identified with insertions in the 5'-UTR, probably close to or within the promoter region. However, no lines with a disruption of the exon region was accessible. Homozygous lines AtPPR1;1 SALK_138980 and AtPPR1;2 SAIL_399_B09 were shifted from high to ambient CO_2 conditions to trigger a possible phenotype described for major genes of photorespiration like superficial leaf lesions (Pick et al., 2013), growth inhibition (Eisenhut et al., 2013a) or lethality under ambient CO_2 concentrations (Renné et al., 2003). None of the observed plants did exhibit any of the described visible phenotypes (data not shown). The insertion sites in these lines are located in the 5'-UTR and the far 3'-region of the coding sequence. Based on meta-analyses T-DNA insertions like this have been shown to be less likely to be affected by the insertion (Wang, 2008).

Arabidopsis AtPPR1;1 and AtPPR1;2 loss-of-function mutants the CRISPR/Cas9 system was chosen. Based on the approach published by Hahn et al. (2017, 2018) sgRNA recognition sites within an exon were selected. The endonuclease Cas9 from *Streptococcus pyogenes* requires 20 nucleotides with the subsequent protospacer adjacent motif (PAM) NGG (Jinek et al., 2012). Cas9 from *Staphylococcus aureus* requires the motif NNGGGT (Steinert et al., 2015). Cas9 from *S. pyogenes* has been used successfully for many studies (Ma et al., 2016). The Cas9 orthologue from *S.aureus* was optimized for the disruption of multiple genes and is assumed to be more specific in terms of target recognition (Steinert et al., 2015). Expression vectors with gene-specific sgRNAs using one of the describes endonucleases have been created (Table 2). AtPPR1;1 and AtPPR1;2 share a high sequence identity on protein level. If both share a similar function physiological experiments should be carried out with double-knockouts as well. Therefore, Cas9-constructs were designed to target AtPPR1;1 and AtPPR1;2 genes individually and simultaneously. Arabidopsis ecotype Col-0 plants were transformed with CRISPR constructs and subsequent generations grown under high CO_2 conditions to circumvent any photorespiratory impairment during the selection process.

Table 2. List of constructs and corresponding sgRNA recognition sites for the CRISPR/Cas9 approach. Bold characters in sgRNA recognition site indicate PAM sites (NGG for Cas9 from *S. pyogenes*, NNGGGT for Cas9 from *S. aureus*).

Construct	Gene	sgRNA recognition site	Target	Cleavage site
pBH25 pFH1, SpCas9, UBQ10 promotor	***ppr1;1***	GGTTTAAGGGGATTGTACAG**AGG**	**1**	bps 242/243
pBH26 pFH1, SpCas9, UBQ10 promoter	***ppr1;2***	GCTAGACTTGAAGGTCTTAA**AGG**	**1**	bps 254/255
pBH41 pFH1, SpCas9, UBQ10 promoter	***ppr1;2***	**CCG**ACTCGTGTCTCATGTGCCAA	**2**	bps 204/205
	ppr1;2	GTGTAGGTCAAGCAACTGTT**AGG**	**3**	bps 363/364
pBH42 pFH1, SpCas9, UBQ10 promoter	***ppr1;1***	GGTTTAAGGGGATTGTACAG**AGG**	**1**	bps 242/243
	ppr1;2	**CCG**ACTCGTGTCTCATGTGCCAA	**2**	bps 204/205
pBH43 pFH1, SpCas9, UBQ10 promoter	***ppr1;1***	GGTTTAAGGGGATTGTACAG**AGG**	**1**	bps 242/243
	ppr1;2	GTGTAGGTCAAGCAACTGTT**AGG**	**3**	bps 363/364
pFH186 pFH1, SaCas9, UBQ10 promoter	***ppr1;2***	TCTTTACACAGATGGACCAA**GAGGGT**	**4**	bps 592/293
	ppr1;2	**ACCCTA**TTGTAGTTCTCAAAACAAGG	**5**	bps 169/170

AtPPR1;1 target 1 (construct pBH25)

Positive transformants from the T1 generation were identified via antibiotic selection. A functional Cas9 is usually indicated by chimeric gene sequences starting at the Cas9 cleavage site chosen by the sgRNA. Chimeric sequences originate in different mutations generated by Cas9 in single cells of leaf tissue samples. Stable mutations can only be preserved by Cas9 activity within the germline (Ma et al., 2016). Therefore, rosette leaf gene material from the T2 generation was sequenced. Three individual plants with sequence changes were transferred into the T3 generation without the use of antibiotics to allow the survival of individual plants that have lost the Cas9 expression cassette via crossing over events. With this, possible off-targets cannot be affected by Cas9. Plants were screened via PCR for the absence of Cas9 and sequenced at the sgRNA recognition site. Four different mutations have been confirmed in individual AtPPR1;1 mutant plants (Table 3, Figure 9B). Sequencing chromatograms show only one prominent sequence for all samples indicating that the mutation affected both alleles and is therefore homozygous. All generated mutant genes now contain a premature stop codon

leading to a predicted translational stop between amino acids 80 and 105 according to sequence alignments based on the mutated nucleotide sequence (Figure 10).

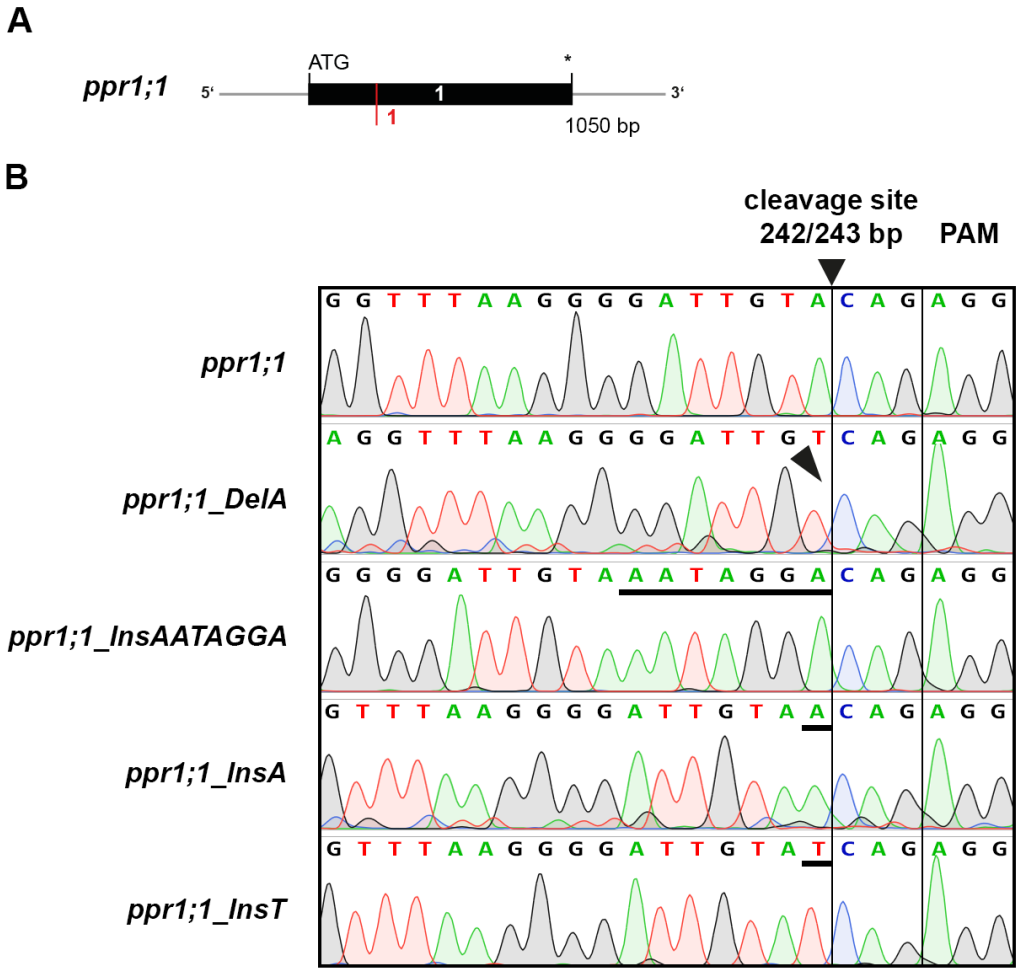

Figure 9. Sequencing data of AtPPR1;1 Arabidopsis mutants created via the CRISPR/Cas9 system. (A) Simplified model of the 1050 bp AtPPR1;1 gene containing only one exon (black box). The relative position of sgRNA recognition site (target 1) is indicated in red (position at bps 242/243). (B) Sequencing chromatograms of T3 generation plants with stable mutations. Black bars indicate inserted sequences, arrowhead indicates deletion.

Table 3. List of mutations in AtPPR1;1 T3 Arabidopsis plants generated via the CRISPR/Cas9 system.

Bold characters indicate PAM sites; red characters indicate mutation.

Line		*Sequence*	*Mutation*	*Sequence*
ppr1;1	WT	GGTTTAAGGGGATTGTACAG**AGG**	-	-
ppr1;1_DelA	Mutant	GGTTTAAGGGGATTGT_CAG**AGG**	Deletion	A
ppr1;1_InsAATAGGA	Mutant	GGTTTAAGGGGATTGTA**AATAGGA**CAG**AGG**	Insertion	AATAGGA
ppr1;1_InsA	Mutant	GGTTTAAGGGGATTGTA**A**CAG**AGG**	Insertion	A
ppr1;1_InsT	Mutant	GGTTTAAGGGGATTGTA**T**CAG**AGG**	Insertion	T

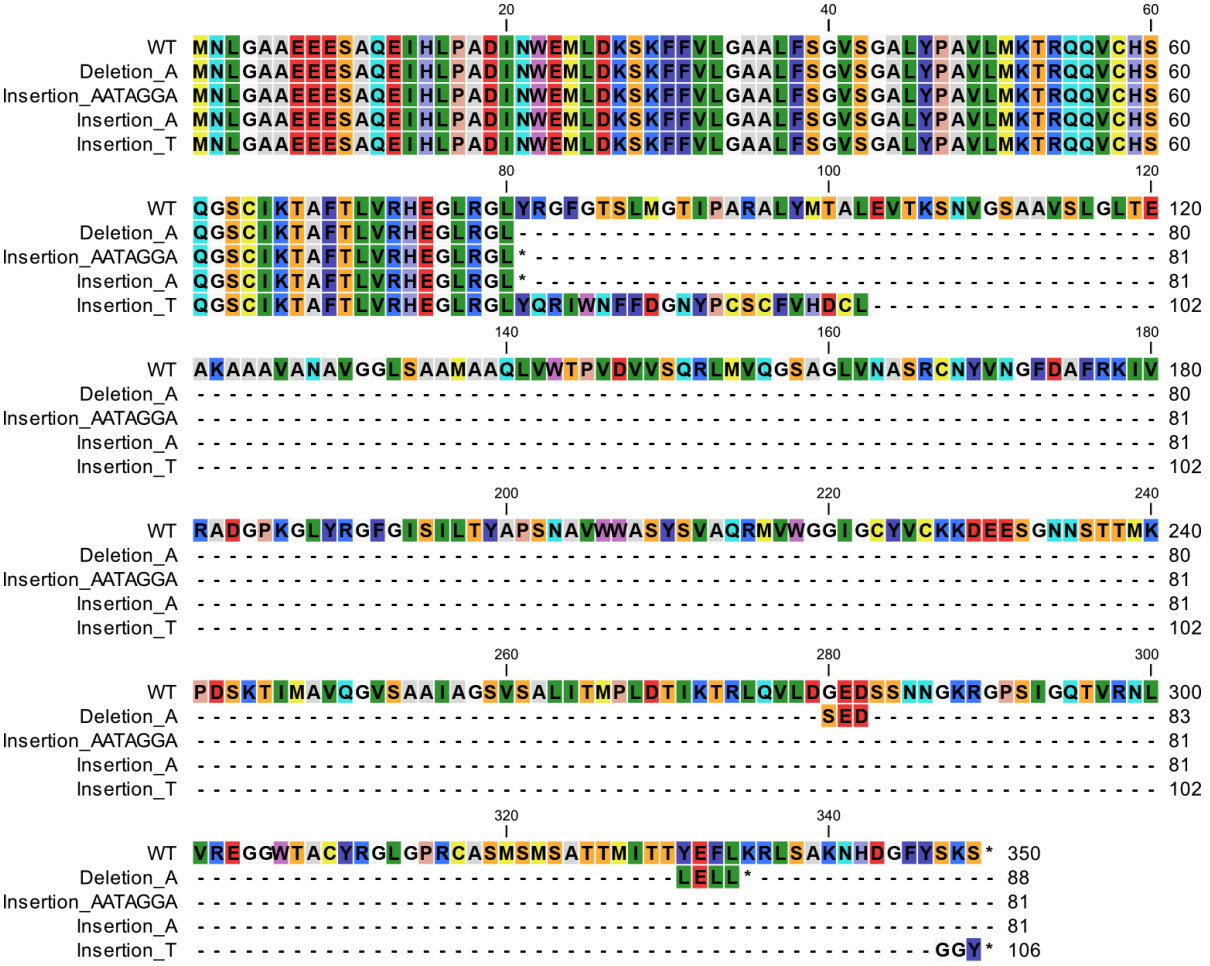

Figure 10. Amino acid sequence alignment of predicted gene products of disrupted AtPPR1;1 in Arabidopsis mutants generated via the CRISPR/Cas9 system.

Mutations at target site 1 in *ppr1;1* (see Table 3) found in isolated Arabidopsis mutants lead to a premature stop in the amino acid sequence after position 80, 87 and 105. Colors represent amino acids according to the Rasmol color scheme.

AtPPR1;2 targets 1-5 (constructs pBH26, pBH41, pFH186)

To target AtPPR1;2, Arabidopsis was transformed and analyzed as described before. For target 1 (construct pBH26) no mutation no was detectable (data not shown). Targets 2 and 3 (construct pBH41) and targets 4 and 5 (construct pFH186) were designed to cut the gene twice to increase mutation probability and transformed separately. Six plants of the T1 generation (construct pBH41) revealed chimeric sequences in target 2 indicating a functional Cas9 (exemplary shown in Figure 11B, lower box). Target 3 was wild-type-like and apparently not affected by Cas9 (data not shown). T2 generation seeds were collected and selected via antibiotics to preserve Cas9 and screen for stable mutations. None of the seedlings survived the selection. Assuming that the Cas9 construct is transmitted according to the Mendelian ratio, 75 % of all plants should have survived the selection process. Cas9 is supposed to only target one allele in the germline creating heterozygous mutants in the process. Theoretically,

plants can be homozygous for this mutation in the T1 generation if Cas9 is successful in targeting both alleles in the germline. The complete loss of a gene product that is important for plant development, especially during early germination, might cause the result observed here (Steinebrunner et al., 2011; Jia et al., 2015).

Only one plant survived the selection process of T1 generation seeds transformed with construct pFH186 (targets 4 and 5). Sequencing revealed no mutation at target site 5 but a three nucleotide (CAA) deletion, apparently in both alleles 4 (Figure 11C, lower box). This indicated that homozygous mutants can be created within one generation. The out of frame mutation successfully deleted amino acid 198 proline. However, with the subsequent two nucleotides the following amino acid 199 arginine is restored (Figure 11C, lower box, black characters). Except for the deletion of one amino acid the overall sequence is not affected and no premature stop codon was established. If the loss of amino acid 198 proline severely affects AtPPR1;2 activity is questionable.

AtPPR1;1 target 1 and AtPPR1;2 targets 2 and 3 (constructs pBH42 and 43)

As mentioned before, AtPPR1;1 and AtPPR1;2 might share the same function. Constructs pBH42 and pBH43 were used to target both exons. Plants were transformed and screens as described before. The sgRNA targets used here correspond to target 1 for AtPPR1;1 and target 2 and 3 for AtPPR1;2 used for single knockouts. The AtPPR1;1 genes was successfully mutated with both constructs resulting in mutations as seen for construct pBH25 (data not shown). No stable non-chimeric mutation was found for the AtPPR1;2 gene after T1 generation.

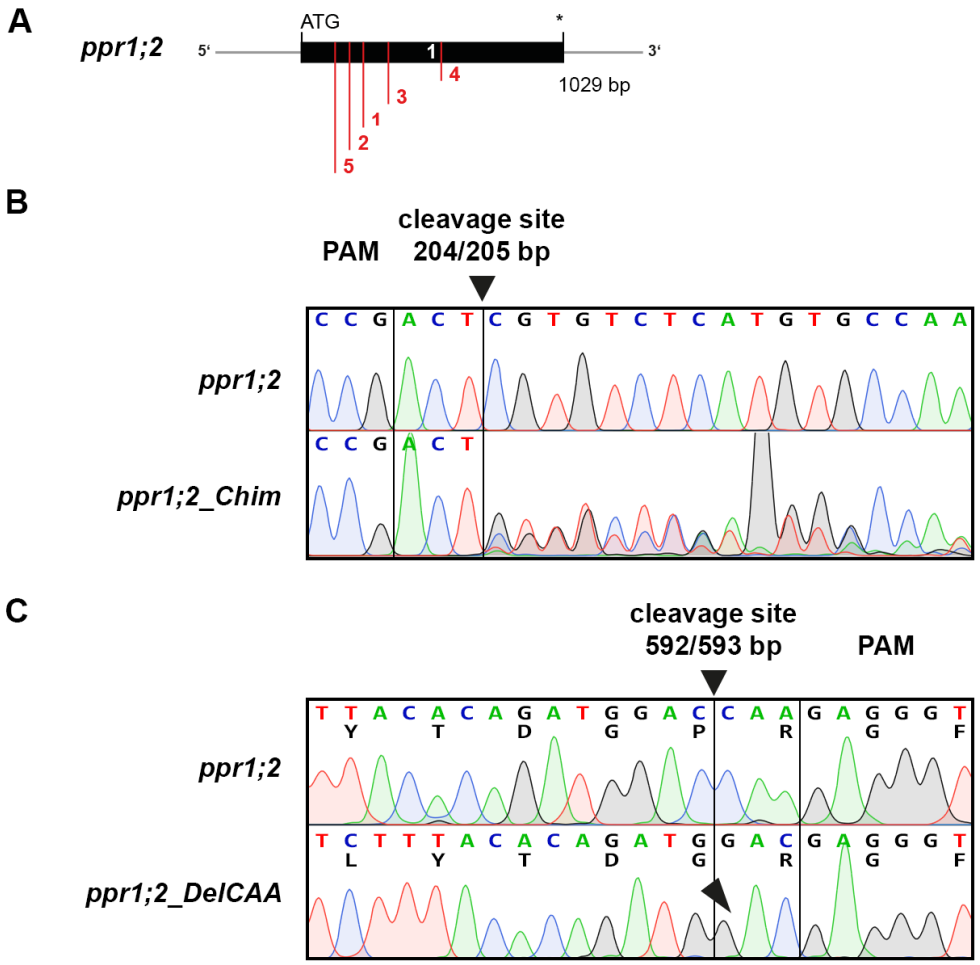

Figure 11. Sequencing data of AtPPR1;2 Arabidopsis mutants created via the CRISPR/Cas9 system. (A) Simplified model of the 1029 bp AtPPR1;2 gene containing only one exon (black box). The relative position of sgRNA recognition sites (targets 1 to 5) are indicated in red. (B) Exemplary sequencing chromatogram of a T1 generation plant with chimeric sequences at target 2. (C) Sequencing chromatogram of only survivor of T1 generation plant mutated at target site 4. Three nucleotides were deleted. Black characters indicate amino acids. Arrowhead indicates deletion. Cas9 is still present in all shown plants.

Discussion

The goal of this study was to identify putative transporters involved in photorespiration. Transport proteins catalyzing the shuttle of intermediates of the photorespiratory pathway across the peroxisomal membrane, channels or carriers, have been proposed but not identified on the molecular level yet.

AtPPR1;1 and AtPPR1;2 belong to the MCF and are up-regulated under photorespiratory conditions and in mature seeds

This study identified putative photorespiratory carriers via co-expression analysis of closely related C3 and C4 Flaveria species. Gene expression of typical photorespiratory enzymes are highly upregulated in C3 species. The evolution of C4 photosynthesis led to the reduction of the photorespiratory pathway, metabolite flux and transcript abundance. This study lists 34 Arabidopsis candidate genes, which cluster with photorespiratory enzymes, represent putative membrane proteins, have not been localized and belong to protein families that shuttle substrates important for photorespiration. Two candidates from the MCF were chosen for a more in-depth analysis.

Peroxisomal AtPPR1;1 (AT1G72820) and AtPPR1;2 (AT5G26200) share a high sequence identity (Figure 3) and cluster with MCF proteins shuttling SAM, carboxylates and amino acids (Figure 4). AtPPR1;1 and AtPPR1;2 are ubiquitously expressed in *T. hassleriana* and Arabidopsis (Figure 6) at relatively low levels as most members of the MCF (Millar and Heazlewood, 2015). Transcript levels of PPR proteins increase under ambient CO_2 conditions in Arabidopsis leaves and in developing and mature seeds of *T. hassleriana* and Arabidopsis. In the latter, AtPPR1;1 expression is also elevated during seed germination until the radicle emerges, whereas AtPPR1;2 mRNA amounts increases only during the first 6 hours after imbibition (Silva et al., 2016). Photorespiration-linked transporter AtDiT1 highly expressed in cotyledons and mature leaves, similar to AtDiT2.1, while AtDiT2.2 is also prominent in developing silique pods and mature seeds. The glycolate exporter AtBASS6 is ubiquitously expressed but predominantly in green tissues, developing seeds and young silique pods, while the glycolate/glycerate transporter AtPLGG1 is almost exclusively expressed in leaves, sepals and silique pods (Klepikova et al., 2016, 2015). The high amount of PPR transcripts in seeds could be linked to storage mechanisms during seed development. It was shown that not only carbohydrates, lipids or proteins are stored in developing seeds but also long-lived mRNA that is needed for germination and seedling growth. Transcription inhibitor studies revealed that germination does not entirely rely on *de novo* transcription but rather uses long-lived mRNA for immediate protein synthesis right after the end of the dormant seed stage (Sano et al., 2012, 2015). The establishment of seedlings is commonly divided into three phases that can be distinguished by prominent metabolic processes including repair mechanisms, antioxidant

mechanisms, the initiation of germination and corresponding energy conversion, lipid and protein turnover. Between 8 h and 24 h after hydration most of the stored mRNA in Arabidopsis is translated into proteins (Galland et al., 2014). Among the proteins found even before this period are enzymes involved in the glyoxylate cycle, glycolysis, the tricarboxylic acid (TCA) cycle and β-oxidation (Galland et al., 2014; Kimura and Nambara, 2010). Since photosynthesis is still absent and cannot provide carbons, energy reserves within the seeds are made accessible for the metabolism, especially respiration (Weitbrecht et al., 2011). In case of Arabidopsis seeds, energy is mainly stored as triacylglyceroles (TAGs) in cytosolic oil bodies. The breakdown of these TAGs via peroxisomal β-oxidation and the subsequent processing of β-oxidation products via the glyoxylate cycle are essential to fuel all metabolic pathways until seedlings become photoautotrophic (Poirier et al., 2006; Weitbrecht et al., 2011). Other peroxisomal MCF members involved in seedling establishment are the peroxisomal adenine nucleotide carriers AtPNC1/2. Inducible knockout mutants were shown to be impaired in β-oxidation and thus unable to break down fatty acids (Linka et al., 2008). The peroxisomal NAD-carrier PXN also stores transcripts in mature seeds. This is crucial for early seed germination and seedling growth (Nakabayashi et al., 2005; Linka and Esser, 2012). The physiological role of AtPPR1;1 and AtPPR1;2 might be important during germination and seedling development.

Based on the expression pattern observed for AtPPR1;1 and AtPPR1;2 under photorespiratory conditions both candidates might be involved in photorespiration. The high transcript abundance of both genes in mature seeds predicts a role during seed germination.

AtPPR1;1 and AtPPR1;2 transport malate *in vitro*

Most characterized MCF carriers are antiporters. PPR proteins are phylogenetically related to di/tri/carboxylic acid carriers of the MCF. Substrates tested in this study were malate, glutamate and 2-oxoglutarate. These substrates shuttled by several MCF members (Palmieri et al., 2008a; Monné et al., 2018) and are involved in photorespiratory processes in plastids and mitochondria as well. Here, they fuel the photorespiratory core pathway with co-factors (Zhao et al., 2018; Weber and Flügge, 2002; Schulze et al., 2016).

Time-dependent uptake studies with His-AtPPR1;1 and His-AtPPR1;2 revealed a malate/malate homo-exchange in reconstituted liposomes with cell-free expressed proteins (Figure 8). The transport of 2-oxoglutarate and glutamate could not be confirmed. In peroxisomes malate is predominantly used for NAD^+/NADH regeneration (Pracharoenwattana et al., 2007). NAD^+ and NADH are not able to diffuse through membranes (Cantó et al., 2015). Hence, plastids, mitochondria and peroxisomes make use of an indirect shuttle via malate/oxaloacetate to fuel photorespiration (Foyer et al., 2011; Al-Saryi et al., 2017). In peroxisomes, malate is converted to oxaloacetate (OAA) by the peroxisomal malate dehydrogenase (MDH). NAD^+ is converted to NADH in the process. The reversed reaction is

used for β-oxidation, producing malate and providing NAD^+ for fatty acid degradation (Figure 12). AtMDH mediates a reversible reaction (Pracharoenwattana et al., 2010) that might be driven according to the physiological state of the organelle and substrate concentrations (Wang et al., 2015).

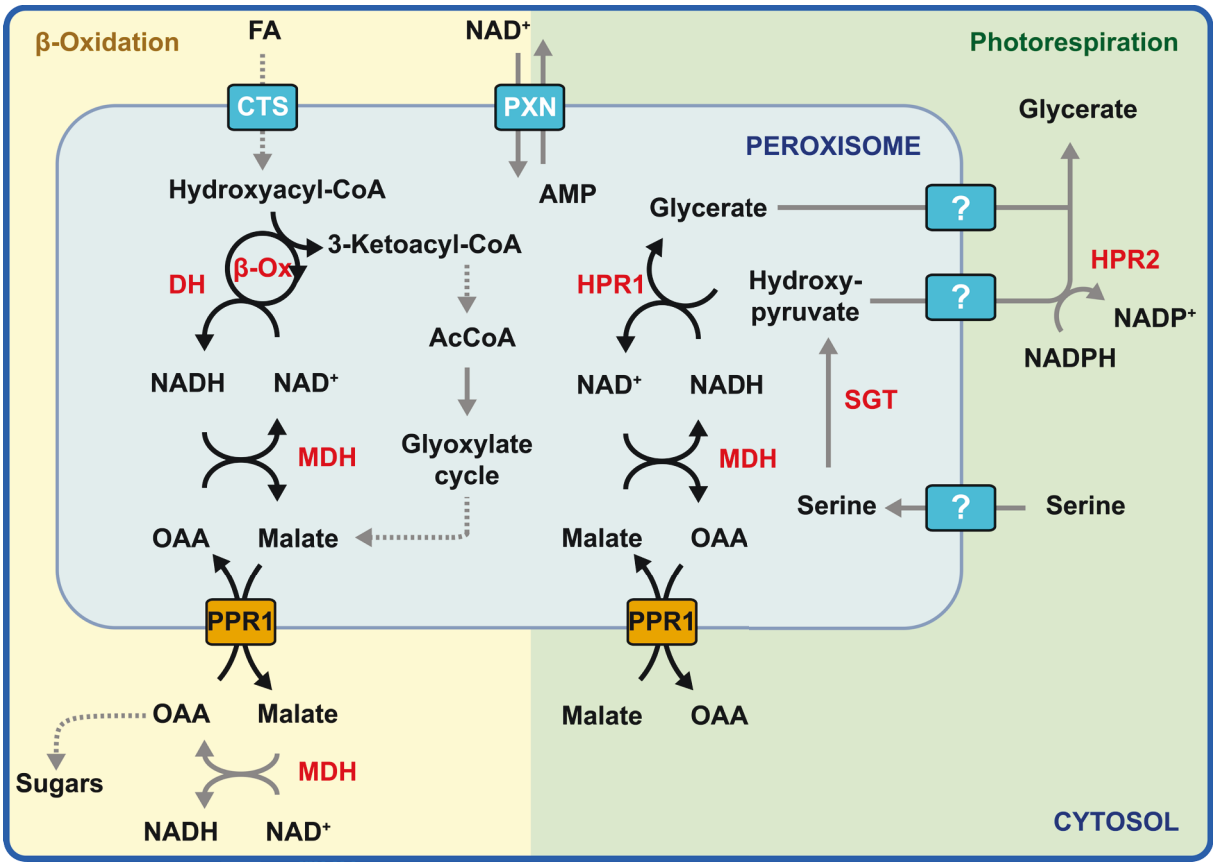

Figure 12. Putative function of AtPPR1;1 and AtPPR1;2 in the peroxisomal malate/OAA shuttle and NAD^+/NADH regeneration needed for β-oxidation and photorespiration.

Left side (yellow): NAD^+-dependent conversion of hydroxyacyl-CoA into 3-ketoacyl-CoA by the hydroxyacyl-CoA dehydrogenase as part of the peroxisomal β-Oxidation with AcCoA as product for the glyoxylate cycle. Right side (green): NADH-dependent conversion of hydroxypyruvate into glycerate by the peroxisomal hydroxypyruvate reductase 1 in the peroxisomal part of photorespiration. Dotted arrows indicate enzymatic reactions omitted in this model. Boxes indicate proven and predicted peroxisomal carriers. Orange boxes indicate peroxisomal carriers predicted for the malate/OAA shuttle. Unknown peroxisomal carriers are marked with "?". Enzymes are shown in red. Abbreviations: AcCoA, acetyl coenzyme A; AMP, adenosine monophosphate; AtCTS, ATP-binding cassette transporter COMATOSE; AtDH, hydroxyacyl-CoA dehydrogenase; FA, fatty acids, AtHPR1, peroxisomal hydroxypyruvate reductase 1; AtHPR2, cytosolic hydroxypyruvate reductase 1; AtMDH, malate dehydrogenase; NAD+, oxidized nicotinamide adenine dinucleotide; NADH, reduced nicotinamide adenine dinucleotide, OAA, oxaloacetate; PPR1; peroxisomal photorespiratory carriers AtPPR1;1 and AtPPR1;2; AtPXN, peroxisomal NAD carrier; AtSGT, serine-glyoxylate aminotransferase; β-Ox, β-oxidation.

The necessity for NAD^+/NADH regeneration is reflected by multiple bypasses probably to be flexible under varying metabolic conditions as found in yeast (Al-Saryi et al., 2017). But the

import of the corresponding substrates malate/oxaloacetate in plants is still not understood. A porin has been investigated in spinach leaf peroxisomes showing the diffusion of dicarboxylic acids including malate but also oxaloacetate, succinate, and 2-oxoglutarate (Reumann et al., 1998). The active transport of malate into organelles has been described for plastids and mitochondria. In the inner envelope of chloroplasts AtDiT1 and AtDiT2.1 shuttle malate across the membrane, with AtDiT1 also mediating the transport of oxaloacetate and AtDiT2.1 the transport of glutamate (Kinoshita et al., 2011; Taniguchi et al., 2002). In mammals, the mitochondrial 2-oxoglutarate/malate carrier is able to import malate as part of the malate-aspartate shuttle allowing the conversion of malate to oxaloacetate by the mitochondrial MDH (Kane, 2014). The mitochondrial malate importer for plants is still unknown but assumed to be involved in NAD^+/NADH regeneration, ROS and programmed cell death and might be represented by MCF members AtDIC1-3. AtDIC3 shows a high affinity for oxaloacetate and could be responsible for the malate/oxaloacetate shuttle *in vivo* (Zhao et al., 2018; Palmieri et al., 2008a). Also MCF members AtUCP1 and AtUCP2 transport malate and oxaloacetate *in vitro* (Monné et al., 2018).

It is important to test if the PPR proteins are also able to transport oxaloacetate into liposomes. Additionally, the antiport of malate/oxaloacetate needs to be tested since most of the characterized MCF members are strict antiporters (Haferkamp and Schmitz-Esser, 2012). This would also reflect the physiological function of plastidic and mitochondrial transport mechanisms of malate transporters as described before. An alternative to active transporters have been studied via electrophysiological experiments on isolated peroxisomes. The presence of peroxisomal channels for smaller molecules like carboxylic acids in plants was revealed (Hu et al., 2012; Reumann et al., 1998). In mammals and yeast Pxmp2 and Pex11 have been identified (Rokka et al., 2009; Mindthoff et al., 2016). In general,channels can shuttle vast amounts of various molecules in less time (Gadsby, 2009). This would benefit the high flux of metabolites needed for photorespiration and associated processes. Still, only active photorespiratory transporters have been found in plastids shuttle core metabolites like glycerate and glycolate, and malate, glutamate and oxaloacetate for NAD^+/NADH regeneration and nitrogen re-assimilation (Eisenhut et al., 2013b). In peroxisomes active transporters shuttle comparatively big substrates like cofactors or fatty acids (Linka and Esser, 2012). Transporters are usually highly selective or have a substrate spectrum of molecules that are structurally related as shown in the MCF protein family (Lee and Millar, 2016). While this selectivity comes at the cost of total transport rate, only photorespiratory transporters have been identified so far. It can be assumed that a highly complex metabolic pathway like photorespiration needs to be tightly regulated, especially in coordination with photosynthesis (Timm et al., 2016). The importance of transporters in regulatory processes and the shuttling of specific metabolites

cannot be stated enough in terms of flexible metabolic networks (Metallo and Vander Heiden, 2014; Pratelli and Pilot, 2014)

AtPPR1;1 and AtPPR1;2 might represent the peroxisomal malate carriers fueling β-oxidation and photorespiration via NAD^+/NADH regeneration

As stated before, the peroxisomal regeneration of NAD^+/NADH requires a shuttle of malate/oxaloacetate across the membrane. Photorespiration requires NADH for the conversion of hydroxypyruvate to glycerate via the peroxisomal hydroxypyruvate reductase 1 (AtHPR1). β-oxidation needs NAD^+ for the conversion of hydroxyacyl-CoA into 3-ketoacyl-CoA via the hydroxyacyl-CoA dehydrogenase (AtDH) or multifunctional protein 2 (AtMFP2) (Rylott et al., 2006).

Both NAD^+/NADH-related reactions do seem to rely on MDH activity. But it was shown that the photorespiratory AtHPR1 can provide reducing power for β-oxidation in *pmdh1pmdh2* mutants. Fatty acid degradation is slowed down in these mutants but seeds are able to germinate (Pracharoenwattana et al., 2010). Photosynthesis should also be affected in *mdh1mdh2* plants. But only a mild reduction of photosynthesis rate was detected although the NADH-dependent conversion of hydroxypyruvate to glycerate should be impaired (Cousins et al., 2008, 2011). The apparent absence of a strong phenotype in *pmdh1pmdh2* plants indicated another source of NADH for HRP1 or a bypass of this reaction. Indeed, the cytosolic NADPH-dependent AtHPR2 is thought to convert hydroxypyruvate to glycerate, although the export of hydroxypyruvate is not yet proven. Still, a knockout of both HRP enzymes leads to more a severe but not lethal phenotype (Timm et al., 2011, 2008). A triple-knockout with the plastidic AtHPR3 pronounces the observed phenotype. This indicates that each of these enzymes might be involved in photorespiration and is able to be used as a bypass (Yu et al., 2008; Timm et al., 2011; Timm and Bauwe, 2013).

β-oxidation requires the malate/oxaloacetate shuttle for NAD^+/NADH regeneration to fuel the conversion of hydroxyacyl-CoA into 3-ketoacyl-CoA by AtDH/MFP2 (Arent et al., 2010). Arabidopsis AtDH/MFP2 mutants are sucrose-dependent during germination, show enlarged peroxisomes and a reduced fatty acid degradation rate but are not resistant to 2,4-dichlorophenoxybutyric acid indicating that β-oxidation is strongly inhibited but functional (Rylott et al., 2006; Germain et al., 2001; Graham, 2008). The glyoxylate cycle itself is independent from the peroxisomal MDH (Pracharoenwattana et al., 2007). But malate, which is a product of glyoxylate and acetyl coenzyme A (AcCoA) in this cycle, is thought to be transported to the cytosol, converted to oxaloacetate by the cytosolic MDH and used for gluconeogenesis. This step is also crucial for seed germination (Kunze et al., 2006; Pracharoenwattana et al., 2007).

If AtPPR1;1/AtPPR1;2 represent the peroxisomal malate/oxaloacetate shuttle, the regeneration of NAD^+/NADH by MDH should be impaired in knockout mutants of these proteins. According to the mild phenotypic effect observed in Arabidopsis *pmdh1pmdh2* mutants due to several bypasses (Cousins et al., 2008, 2011), the effect of PPR loss-of-function mutants might be rather subtle as well. The stronger phenotypic effect seen for AtDH/MFP2 mutants implies a less effective bypass for β-oxidation compared to the knockout of photorespiratory AtHPR1. With this, the knockout of AtPPR1;1/AtPPR1;2 might have a stronger influence on β-oxidation than photorespiration.

Functional redundancy seems to be common in the MCF. With members like AtPNC1/2 (Linka et al., 2008), AtPHT3;1-3 (Hamel et al., 2004), AtDIC1-3 (Palmieri et al., 2008a) or AtUCP1/2 (Monné et al., 2018) this protein family has multiple closely related carriers sharing a similar substrate spectrum or expression pattern (spatial or temporal). For instance, AtDIC1-3 show a very broad substrate spectrum including malate, oxaloacetate, succinate, maleate, malonate, phosphate, sulfate and thiosulfate. But in-depth *in vitro* uptake studies have shown that the substrate specificity differs. AtDIC1/2 are more efficient dicarboxylate and phosphate carriers and AtDIC3 a more efficient oxaloacetate and thiosulfate carrier. Additionally, it was shown that the response to various stress factors induces only single DICs but not all at the same time and not in all tissues (Palmieri et al., 2008a). This illustrates that functional redundancy does not necessarily reflect the function of a single carrier *in vivo*. Redundant carriers are probably part of different metabolic pathways, expressed under different physiological conditions, are tissue-specific or are used as a back-up system. AtPPR1;1 and AtPPR1;2 show a high sequence identity of 59 % which is slightly less compared to AtDIC1/2 (70 % sequence identity (Palmieri et al., 2008a)) or AtUCP1/2 (72 % (Monné et al., 2018)). The shared sequence of the PPRs rather resembles AtDIC1/2 and AtDIC3 (55 to 60 % sequence identity (Palmieri et al., 2008a)). Still, these carriers share a substrate spectrum. It can be assumed that AtPPR1;1 and AtPPR1;2 transport a similar group of substrates as well. The expression data described in this study suggests that both carriers are involved in seed development (Figure 6). AtPPR1;2 seems to be more specifically expressed in mature seeds than AtPPR1;1 which in turn shows a more ubiquitous expression in all observed tissues with higher expression levels in mature seeds as well. Transcriptomic leaf data of *T. hassleriana* suggests that AtPPR1;2 expression increases with leaf age compared to *G. gynandra* while AtPPR1;1 does not (Figure 5). If AtPPR1;1 and AtPPR1;2 are functional in either photorespiration or β-oxidation (or another peroxisomal metabolic pathway) cannot be concluded here. But is seems plausible that, similar to other redundant MCF carriers, AtPPR1;1 and AtPPR1;2 share a similar transport function but have different physiological roles.

Establishing AtPPR1;1 and AtPPR1;2 Arabidopsis mutants

To investigate the physiological role of PPR proteins, the CRISPR/Cas9 system was used to establish mutant lines, since accessible T-DNA insertion lines do not provide the disruption of an exon. Multiple mutations have been introduced into the coding sequence of AtPPR1;1 (Figure 9B). These mutations lead to a putative premature translational stop (Figure 10). Various approaches to mutate the AtPPR1;2 gene led to chimeric sequences in leaf cells with (Figure 11B) and one three nucleotide deletion (Figure 11C). This implies that the chosen sgRNA sites are successfully targeted by Cas9 but the mutations cannot be stabilized in the next generation. To establish a homozygous mutant, the Cas9-induced mutation must occur within the developing embryo to introduce the mutation into the germline (Hahn et al., 2017). But no stable mutation was found in following generations.

Since the chosen sgRNA sites seem to be sufficient to guide Cas9 to the AtPPR1;2 gene, there are two possible explanations for the missing stable mutation. Either, Cas9 cannot establish a mutation in the embryo or the gene is essential and leads to a severe defect during early seed germination. The former scenario seems unlikely using different sgRNA sites and Cas9 proteins as described in this study. Additionally, all approaches are successful in regards of the introduction of chimeric mutations in leaves. The latter scenario would imply that the mutation does take place in embryos but is lethal for the seed. Since heterozygous T-DNA insertion lines of otherwise homozygous embryo-lethal T-DNA insertion plants are usually viable (Steinebrunner et al., 2011; Radin et al., 2015), the mutation here must have affected both alleles right after the transformation of wild type Arabidopsis plants with the CRISPR/Cas9 constructs. A homozygous mutation in the next generation was also observed for AtPPR1;1 (Figure 9) and the three nucleotide deletion mutant of AtPPR1;2 (Figure 11C). If AtPPR1;2 is essential for seed germination and wild type alleles absent in mutant plants, viable homozygous AtPPR1;2 mutants might not be detectable.

Outlook

Biochemical analysis of AtPPR1;1 and AtPPR1;2

Uptake studies of recombinant AtPPR1;1 and AtPRP1;2 protein revealed malate transport activity (Figure 8). Other dicarboxylate carriers are known to transport a variety of other substrates *in vitro*. Mitochondrial dicarboxylate carriers AtDIC1-3 were found to shuttle malate, oxaloacetate, succinate but also phosphate, sulfate and thiosulfate (Palmieri et al., 2008a). These carriers have slightly different substrate specificities but they are supposed to import dicarboxylates for the TCA cycle in exchange for sulfate or phosphate. It is also proposed that AtDIC1-3 represent the mitochondrial malate/oxaloacetate shuttle needed for the regeneration of NAD^+ by the mitochondrial isoform of MDH, which is in turn involved in the photorespiratory conversion of glycine to serine by GDC (Palmieri et al., 2008a; Wang et al., 2015). With malate

as possible substrate for related MCF members AtPPR1;1 and AtPPR1;2, it is likely that other substrates can be transported as well. Therefore, it is important to perform additional uptake studies with other dicarboxylates like oxaloacetate, 2-oxoglutarate and amino acids. Carriers like AtUCP1-2 (Monné et al., 2018) revealed transport capacities for both substrate classes, dicarboxylates and amino acids. The malate carriers identified in this thesis might belong to the malate shuttle network involved in photorespiration together with AtDiT1-2 (Kinoshita et al., 2011; Renné et al., 2003) in plastids and DIC1-3 in mitochondria (Palmieri et al., 2008a).

The uptake of malate in *in vitro* studies as shown in this study does not necessarily reflect the in *vivo* function. With the broad substrate spectrum of the MCF protein family, it is important to test a variety of possible substrates including carboxylates and amino acids of the photorespiratory core pathway (glycerate, glycolate, serine, glycine). Counter-exchange studies using the liposome system with malate and selected substrates in preloaded liposomes will be performed as well as inhibition studies to investigate the effect of competing substrates on malate uptake (Bernhardt et al., 2012b).

Phenotypical analysis of AtPPR1;1 and AtPPR1;2

The shuttle of malate/oxaloacetate is tightly bound to MDH activity in the cytosol and in organellar matrices of peroxisomes, mitochondria and plastids. Therefore, phenotyping experiments need to consider MDH activity as well. If AtPPR1;1/AtPPR1;2 represent the peroxisomal malate/oxaloacetate shuttle, the regeneration of NAD^+/NADH by MDH should be impaired. Arabidopsis *pmdh1pmdh2* mutants only show a mild photosynthetic phenotype: they are viable at ambient CO_2 conditions and photosynthesis rate was only slightly reduced (Cousins et al., 2008, 2011). A stronger β-oxidation phenotype was observed in *pmdh1pmdh2* mutants (Pracharoenwattana et al., 2007). It was shown that AtHPR1 can provide reducing agents for β-oxidation in *pmdh1pmdh2* mutants. Although fatty acid degradation is slowed down in the process the mutants are still viable (Pracharoenwattana et al., 2010). Additionally, the loss of AtHPR1 can be circumvented by cytosolic or plastidic HPR isoforms. A minor growth phenotype and no change in photosynthesis rate was observed. Only *hpr1hpr2* mutants exhibited reduced growth and photosynthetic rate. This effect was accelerated by the additional knockout of the plastidic AtHPR3 (Timm et al., 2008, 2011). The *pmdh1pmdh2hpr1* triple mutant shows reduced growth compared to *pmdh1pmdh2* or *hpr1* mutants (Pracharoenwattana et al., 2010).

Double loss-of-function mutants for either AtHPR1-2 or MDH1-2 would be an excellent tool for phenotypic analysis of NAD^+/NADH regeneration with an easy to measure visual phenotype in combination with the loss of AtPPR1;1/AtPPR1;2. The most interesting question would be if the knockout of AtPPR1;1 or AtPPR1;2 (single or double knockouts) can enhance the effect on the phenotype observed during seed germination or growth at photorespiratory

conditions for *hpr1* and *mdh* mutants. This would clarify if AtPPR1;1 and AtPPR1;2 are both involved in photorespiration and β-oxidation or if they act in different metabolic pathways. First experiments should focus on β-oxidation measuring root and hypocotyl growth on sugar-deficient medium or additional 2,4-DB to measure the activity of β-oxidation in *ppr1;1* or *ppr1;2* mutants compared to *pmdh1pmdh2hpr1*. FAME analysis to measure fatty acid degradation would also give a more detailed insight into this process. If AtPPR1;1/AtPPR1;2 are involved in NAD^+/NADH regeneration and β-oxidation, the degradation of TAGs should be inhibited. As described before, the recipient of NAD^+ in β-oxidation is AtDH/MFP2. The loss of AtDH/MFP2 inhibits TAG degradation but an unknown bypass allows a functional β-oxidation process (Arent et al., 2010). The loss of AtPPR1;1/AtPPR1;2 might show a similar phenotype.

Growth and gas exchange measurements should follow to elucidate the effect on photosynthesis and photorespiration under ambient and high CO_2 conditions. The detection of carbon assimilation, including RuBisCO carboxylation and the electron transport rate would show the effect on photosynthesis (South et al., 2017; Long and Bernacchi, 2003). Changes on the metabolite level, especially of core photorespiratory metabolites like glycerate, glycolate, serine and glycine as well as hydroxypyruvate should be monitored to reveal the impact on photorespiration. Previous studies of AtPLGG1 and AtBASS6 loss-of-function mutants have shown that the increase of these core metabolites can hint at the position of the missing protein within the photorespiratory pathway (Pick et al., 2013; South et al., 2017). As with MDH and HPR, a double knockout mutant for both PPRs is desirable. Due to the high sequence identity and basic transport function PPRs might as a backup system for eachother under experimental conditions.

Mutagenesis of AtPPR1;2

The approach to create stable homozygous AtPPR1;2 mutant lines was not successful (Figure 11). Only a deletion of one amino acid in the T1 generation was confirmed (sgRNA target site 4). Previous chimeric mutations were not stabilized after the T1 generation. This might indicate that homozygous mutants with severe mutations in AtPPR1;2 are embryo-lethal. Another evidence might be that no exon-internal T-DNA insertions are available. Although such a radical phenotype might be unlikely with so many bypasses for NAD^+/NADH regeneration as described above, it cannot be ruled out that AtPPR1;2 is involved in another process during germination and might be more essential than expected.

CRISPR/Cas9 constructs targeting sgRNA target sites 2 and 4 as shown in Figure 11 are functional. Three nucleotides have been deleted at target site 4, probably a mutation that is not affecting protein activity. Target site 2 revealed chimeric sequences at the Cas9 cleavage site in multiple plants. These mutations did not stabilize or were too severe in the subsequent generation. To test if AtPPR1;2 is essential for plant establishment, the described

CRISPR/Cas9 constructs need to be used in combination with an embryo rescue construct. This construct would allow the expression of an AtPPR1;2 during germination. Silent mutations would hid this gene copy from Cas9 detection. The ABI3 promotor has been established to be embryo and seedling specific (Parcy et al., 1994; Devic et al., 1996). Experiments with embryo-lethal *hcc1* lines showed that the promoter is active for 21 days after germination (Steinebrunner et al., 2014). With this strategy, homozygous AtPPR1;2-deficient mutants could be identified in the background of a functional AtPPR1;2 during early plant establishment. Positively tested mutants could be analyzed for various putative phenotypes, like vegetative growth, photosynthesis rate or metabolic state. A subsequent backcross with wild type Arabidopsis would remove the partial rescue construct to determine if homozygous AtPPR1;2-deficient plants are still viable. Another approach would be to transform chimeric mutants with the partial rescue construct. This would allow the identification of homozygous mutants in the next generation but also simplify the removal of the heterozygous rescue construct via selfing. A simple segregation analysis in the subsequent generation would resolve the question if AtPPR1;2-deficient plants are viable.

Conclusion

This study demonstrated the identification of two peroxisomal carriers via co-expression analysis. AtPPR1;1 and AtPPR1;2, were shown to shuttle malate in an *in vitro* assay. Transcript levels are increased under photorespiratory conditions and in mature seeds. Based on this and other studies, it could be hypothesized that these members of the MCF might be involved in the peroxisomal malate/oxaloacetate shuttle and NAD^+/NADH regeneration during β-oxidation and photorespiration.

Author contribution and acknowledgements

Björn Hielscher wrote the manuscript and performed all experiments and analyses unless stated otherwise. Udo Gowik supervised bioinformatic analysis of Flaveria. Nicole Linka, Leonie Wirth and Julia Schönknecht performed uptake experiments. Florian Hahn participated in the generation of CRISPR/Cas9 Arabidopsis mutant lines. Alisandra Denton participated in *T. hassleriana* and Arabidopsis transcriptome analysis. Nicole Linka, Peter Westhoff, Michael Feldbrügge and Andreas Weber participated in scientific discussions. Nicole Linka assisted in drafting this manuscript. Nicole Linka and Björn Hielscher designed the experiments.

Supplemental material

Primer list

Primer	Sequence 5'-3'	Target, used for vector
BH130	CAACCTCGAGATATCCAACTAGTATGGTGAGCAAG	mCherry, pBH18
BH131	CAACTTATAATTACTTGTACAGCTCGTCCATGCC	
BH113	TCGAGAAGCTTCAATTGACTAGTAGGCCTCCATGGC	MCS, pBH18
BH114	TCGAGCCATGGAGGCCTACTAGTCAATTGAAGCTTC	
BH134	GAGTTTTTCTGATTAACACATGAATTTGGGTGCGGCC	At1g72820, pBH20
BH135	TGCTCACCATACTAGTTGGATATCTTGATTTAGAATAAAACCCGTCATG	
BH136	GAGTTTTTCTGATTAACACATGAGTTTAGGTGCTTTGATG	At5g26200, pBH21
BH137	TGCTCACCATACTAGTTGGATATCCTTTCTGCTTCTTTGTTGC	
BH138	GAGTTTTTCTGATTAACACATGAGCATGGGACTGGCG	CUFF.9607 (FrPPR1),
BH139	TGCTCACCATACTAGTTGGATATCTACTCGAGCAGTGAAGGAAACC	pBH22
BH140	TTCGGGTTTAAGGGGATTGTACAG	At1g72820 sgRNA
BH141	AAACCTGTACAATCCCCTTAAACC	target site 1, pBH25
BH227	ATTGTTGGCACATGAGACACGAGT	At5g26200 sgRNA
BH228	AAACACTCGTGTCTCATGTGCCAA	target site 2, pBH41, 42
BH229	ATTGGTGTAGGTCAAGCAACTGTT	At5g26200 sgRNA
BH230	AAACAACAGTTGCTTGACCTACAC	target site 3, pBH41, 43
FH334	ATTGCCTTGTTTTGAGAACTACAA	At5g26200 sgRNA
FH335	AAACTTGTAGTTCTCAAAACAAGG	target site 4, pFH186
FH336	ATTGTCTTTACACAGATGGACCAA	At5g26200 sgRNA
FH337	AAACTTGGTCCATCTGTGTAAAGA	target site 5, pFH186
LW1	ATATGAGCGGCCGCGTCGACACCATGGGGAATTTGGGTG	At1g72820, pLW1
LW2	AACCCCCCCCGGGAGCTCGCCCTGATTTAGAATAAAACCCGTC	
LW3	ATATGAGCGGCCGCGTCGACACCATGGGGAGTTTAGGTG	At5g26200, pLW2
LW4	AACCCCCCCCGGGAGCTCGCCCTTTCTGCTTCTTTGTTGC	

Vector list

Primer	Insert	Backbone, purpose
pBH20	At1g72820, c-terminal mCherry	pBH18, Localization
pBH21	At5g26200, c-terminal mCherry	pBH18, Localization
pBH22	CUFF.9607 (FrPPR1), c-terminal mCherry	pBH18, Localization
pBH25	At1g72820 sgRNA target 1	pFH1, CRISPR/Cas9
pBH41	At5g26200 sgRNA target 2&3	pFH1, CRISPR/Cas9
pBH42	At1g72820 sgRNA target 1, At5g26200 sgRNA target 2	pFH1, CRISPR/Cas9
pBH43	At1g72820 sgRNA target 1, At5g26200 sgRNA target 3	pFH1, CRISPR/Cas9
pFH186	At5g26200, sgRNA target 4&5	pFH1, CRISPR/Cas9
pLW1	At1g72820, c-terminal His	pIVEX1.3 Ge and Xu, 2012), Uptakes
pLW2	At5g26200, c-terminal His	pIVEX1.3 Ge and Xu, 2012), Uptakes
pFH1	-	(Hahn et al., 2017), CRISPR/Cas9
pBH18	-	Modified, (Grefen et al., 2010), Localization

PPR coding sequences

>At1g72820.1 (AtPPR1;1)
ATGAATTTGGGTGCGGCCGAGGAAGAATCGGCTCAGGAGATTCATTTACCAGCTGATATCAATTGGGAGATGCTTGATAAATC
CAAGTTTTTCGTTTTAGGCGCTGCTTTGTTTTCAGGGGTATCTGGAGCTCTTTATCCTGCGGTTTTGATGAAAACTCGGCAAC
AAGTGTGTCATTCGCAAGGTTCTTGTATTAAAACTGCGTTTACTCTTGTGAGACATGAAGGTTTAAGGGGATTGTACAGAGGA
TTTGGAACTTCTTTGATGGGAACTATCCCTGCTCGTGCTTTGTACATGACTGCCTTGGAGGTTACTAAGAGTAACGTAGGCTC
TGCTGCTGTCAGCTTGGGGTTGACAGAGGCTAAAGCTGCTGCTGTTGCTAATGCGGTTGGAGGTTTGAGTGCTGCGATGGCTG
CACAGCTTGTTTGGACTCCTGTTGATGTGGTTAGCCAAAGGCTTATGGTTCAAGGAAGTGCTGGTCTTGTTAATGCATCAAGG
TGTAATTATGTTAACGGGTTTGATGCATTTAGAAAGATCGTTCGCGCTGATGGACCGAAGGGGTTATACAGAGGGTTTGGGAT
ATCGATTCTGACTTATGCGCCGTCTAATGCTGTTTGGTGGGCGTCTTACTCTGTTGCACAGCGGATGGTTTGGGGTGGAATTG
GGTGTTATGTCTGTAAGAAAGACGAAGAAAGCGGGAACAATAGTACCACGATGAAACCAGATTCTAAAACGATAATGGCTGTT
CAAGGAGTTAGTGCTGCGATTGCTGGAAGTGTTTCTGCTTTGATTACAATGCCACTCGACACAATCAAGACGAGATTGCAGGT
TCTTGATGGGGAAGATAGTAGTAACAACGGGAAGCGTGGACCGAGTATTGGACAGACTGTAAGAAACTTGGTTAGAGAAGGTG
GATGGACGGCTTGTTATAGAGGATTGGGACCAAGATGTGCTTCAATGTCAATGTCTGCAACAACTATGATCACTACCTACGAG
TTCTTGAAACGGCTTTCTGCTAAGAACCATGACGGGTTTTATTCTAAATCATAG

>At5g26200.1 (AtPPR1;2)
ATGAGTTTAGGTGCTTTGATGGAAGAGAAGAGAAGAGCAACAACTTCATCTTCTTCTTCTCAGGTACATATGTCAAATGATAT
AGATTGGCAAATGCTTGATAAATCGAGGTTTTTCTTCCTCGGTGCTGCTCTTTTCTCCGGTGTATCCACTGCTCTTTACCCTA
TTGTAGTTCTCAAAACAAGGCAACAAGTCTCTCCGACTCGTGTCTCATGTGCCAACATTTCTCTGGCTATTGCTAGACTTGAA
GGTCTTAAAGGGTTTTACAAGGGTTTTGGAACATCTTTGCTTGGAACCATCCCGGCTCGTGCTCTCTATATGACTGCTCTAGA
GATTACAAAGAGTAGTGTAGGTCAAGCAACTGTTAGGTTAGGATTGTCTGATACTACGTCTTTGGCTGTTGCTAATGGTGCAG
CTGGTTTGACCTCGGCTGTGGCTGCCCAGACTGTCTGGACTCCGATTGATATTGTGAGTCAAGGGCTTATGGTTCAAGGCGAT
GTCTCCTTGAGTAAGCATCTTCCTGGAGTGATGAACTCTTGCAGATACAGAAATGGGTTTGATGCTTTTAGAAAGATTCTTTA
CACAGATGGACCAAGAGGGTTCTACAGAGGATTTGGGATCTCGATCTTGACTTACGCACCTTCCAACGCGGTTTGGTGGGCGT
CTTATTCTTTGGCTCAAAAATCAATTTGGTCTCGATACAAGCACTCCTACAACCACAAGGAAGATGCTGGTGGCTCAGTGGTG
GTTCAAGCGTTGAGTGCAGCTACAGCAAGCGGTTGCTCGGCTTTAGTAACTATGCCAGTAGACACAATCAAGACGCGGTTGCA
AGTCTTAGACGCAGAAGAGAACGGGAGGAGACGAGCAATGACAGTGATGCAGTCAGTGAAGAGCTTGATGAAGGAAGGAGGAG
TTGGTGCTTGTTACAGAGGATTAGGACCAAGATGGGTCTCAATGTCGATGTCCGCAACAACGATGATCACAACCTACGAGTTC
TTGAAGCGCCTAGCAACAAAGAAGCAGAAATGA

>F.robustaCUFF.9607 (FrPPR1)
ATGAGCATGGGACTGGCGGAGGATGACTCAAGGATCGATATACATCTTCCCGCTGACATTCACTGGGACATGCTTGATAAATC
CAAGTTTTTCTTCCTTGGTGCCGCTTTGTTTTCCGGTGTTTCCAGCATCTTATATCCTGTTGTCGTGTTGAAAACACGACAAC
AAGTACTAGTAAACGACACGCCATGCTTTAAGATGGCTGTGTCGATTCTACGACACGAGGGCTTCAAAGGTTTGTATAGAGGG
TTTGGGACATCTCTAACGGGTACTGTCCCGGCTAGAGCTCTTTACATGGGAGCTCTAGAAATGACCAAGAGTAATCTAACGAG
TGCAACGGTGAGAATGGGGTTTTCAGAGGTCGAATCGGCTGCAATCGCGAATGCAGCAGGTGGGTTAAGTGCAGCCATGGCTG
CACAGCTGGTGTGGACACCGGTTGATGTAGTTAGCCAGAGGTTAATGGTCCAAGGTCCAAAAGGTGGTTCGGCTGTTTACAAT
GGAGGCATTGATGCATTCAAGAGAATTATTCATAGAGATGGTGTTAGGGGATTGTACAAGGGGTTTGGTATTTCGATCTTGAC
ATATGCTCCTTCAAATGCTGTTTGGTGGGCTTCTTACTCCACCGCTTATCGATCTATTTGGGGTCGTGTTAGTTCTTACAGTT
CGAGGAAAGAGGACTCCGTTAGTGGCCCGATGGCGGTTGTGGCGGTCCAAGGGCTAAGTGCCACAATAGCGAGCGGGTTTTCG
GCGTTGGTTACAATGCCATTGGATACGATCAAGACAAGAGTGCAAGTTTTAGAAGTTGAAGATTGTAATAAGAAAACAAGTAT
TGTGCAGACTGTTAGAAATTTGGTAAAAGAAGGTGGTTTGAGTGCTTGTTATAGAGGATTGGGAGCAAGATGGGCTTCAATGT
CTATTTCAGCAACTACTATGATCACCACTTATGAGTCACTCAAGAAGATGTCTACTAAGAATCAAGATTTCTATGGTTTCCTT
CACTGCTCGAGTTGA

PPR protein sequences

>At1g72820.1 (AtPPR1;1)
MNLGAAEEESAQEIHLPADINWEMLDKSKFFVLGAALFSGVSGALYPAVLMKTRQQVCHSQGSCIKTAFTLVRHEGLRGLYRG
FGTSLMGTIPARALYMTALEVTKSNVGSAAVSLGLTEAKAAAVANAVGGLSAAMAAQLVWTPVDVVSQRLMVQGSAGLVNASR
CNYVNGFDAFRKIVRADGPKGLYRGFGISILTYAPSNAVWWASYSVAQRMVWGGIGCYVCKKDEESGNNSTTMKPDSKTIMAV
QGVSAAIAGSVSALITMPLDTIKTRLQVLDGEDSSNNGKRGPSIGQTVRNLVREGGWTACYRGLGPRCASMSMSATTMITTYE
FLKRLSAKNHDGFYSKS

>At5g26200.1 (AtPPR1;2)
MSLGALMEEKRRATTSSSSSQVHMSNDIDWQMLDKSRFFFLGAALFSGVSTALYPIVVLKTRQQVSPTRVSCANISLAIARLE
GLKGFYKGFGTSLLGTIPARALYMTALEITKSSVGQATVRLGLSDTTSLAVANGAAGLTSAVAAQTVWTPIDIVSQGLMVQGD
VSLSKHLPGVMNSCRYRNGFDAFRKILYTDGPRGFYRGFGISILTYAPSNAVWWASYSLAQKSIWSRYKHSYNHKEDAGGSVV
VQALSAATASGCSALVTMPVDTIKTRLQVLDAEENGRRRAMTVMQSVKSLMKEGGVGACYRGLGPRWVSMSMSATTMITTYEF
LKRLATKKQK

>F.robustaCUFF.9607 (FrPPR1)
MGSMGLAEDDSRIDIHLPADIHWDMLDKSKFFFLGAALFSGVSSILYPVVVLKTRQQVLVNDTPCFKMAVSILRHEGFKGLYR
GFGTSLTGTVPARALYMGALEMTKSNLTSATVRMGFSEVESAAIANAAGGLSAAMAAQLVWTPVDVVSQRLMVQGPKGGSAVY
NGGIDAFKRIIHRDGVRGLYKGFGISILTYAPSNAVWWASYSTAYRSIWGRVSSYSSRKEDSVSGPMAVVAVQGLSATIASGF
SALVTMPLDTIKTRVQVLEVEDCNKKTSIVQTVRNLVKEGGLSACYRGLGARWASMSISATTMITTYESLKKMSTKNQDFYGF
LHCSSX

References

Al-Saryi, N.A., Al-Hejjaj, M.Y., Van Roermund, C.W.T., Hulmes, G.E., Ekal, L., Payton, C., Wanders, R.J.A., and Hettema, E.H. (2017). Two NAD-linked redox shuttles maintain the peroxisomal redox balance in Saccharomyces cerevisiae. Sci. Rep. **7**: 1–9.

Alonso, J.M. et al. (2003). Genome-Wide Insertional Mutagenesis of Arabidopsis thaliana. Science (80-.). **301**: 653 LP-657.

Antonenkov, V.D. and Hiltunen, J.K. (2006). Peroxisomal membrane permeability and solute transfer. Biochim. Biophys. Acta - Mol. Cell Res. **1763**: 1697–1706.

Arai, Y., Hayashi, M., and Nishimura, M. (2008). Proteomic identification and characterization of a novel peroxisomal adenine nucleotide transporter supplying ATP for fatty acid beta-oxidation in soybean and Arabidopsis. Plant Cell **20**: 3227–40.

Arent, S., Christensen, C.E., Pye, V.E., Nørgaard, A., and Henriksen, A. (2010). The multifunctional protein in peroxisomal β-oxidation: Structure and substrate specificity of the Arabidopsis thaliana protein MFP2. J. Biol. Chem. **285**: 24066–24077.

Baker, A., Carrier, D.J., Schaedler, T., Waterham, H.R., van Roermund, C.W., and Theodoulou, F.L. (2015). Peroxisomal ABC transporters: functions and mechanism. Biochem. Soc. Trans. **43**: 959–965.

Balzan, S., Johal, G.S., and Carraro, N. (2014). The role of auxin transporters in monocots development. Front. Plant Sci. **5**: 1–12.

Barrera, N.P. and Robinson, C. V. (2011). Advances in the Mass Spectrometry of Membrane Proteins: From Individual Proteins to Intact Complexes. Annu. Rev. Biochem. **80**: 247–271.

Bauwe, H. (2010). Chapter 6 Photorespiration: The bridge to C4 photosynthesis. In C4 Photosynthesis and Related CO2 Concentrating Mechanisms, pp. 81–108.

Bedhomme, M., Hoffmann, M., McCarthy, E.A., Gambonnet, B., Moran, R.G., Rébeillé, F., and Ravanel, S. (2005). Folate metabolism in plants: An Arabidopsis homolog of the mammalian mitochondrial folate transporter mediates folate import into chloroplasts. J. Biol. Chem. **280**: 34823–34831.

Bernhardt, K., Vigelius, S.K., Linka, N., and Andreas, P.M. (2012a). Agrobacterium-mediated Arabidopsis thaliana transformation : an overview of T-DNA binary vectors , floral dip and screening for homozygous lines. Endocytobiosis Cell Res. **22**: 19–28.

Bernhardt, K., Wilkinson, S., Weber, A.P.M., and Linka, N. (2012b). A peroxisomal carrier delivers NAD + and contributes to optimal fatty acid degradation during storage oil mobilization. Plant J. **69**: 1–13.

Björn, L.O. and Govindjee (2009). The Evolution of Photosynthesis. Curr. Sci. **96**: 1466–1474.

Blanchoin, L. and Staiger, C.J. (2010). Plant formins: Diverse isoforms and unique molecular mechanism. Biochim. Biophys. Acta - Mol. Cell Res. **1803**: 201–206.

Boldt, R., Edner, C., Kolukisaoglu, U., Hagemann, M., Weckwerth, W., Wienkoop, S., Morgenthal, K., and Bauwe, H. (2005). D-GLYCERATE 3-KINASE, the last unknown enzyme in the photorespiratory cycle in Arabidopsis, belongs to a novel kinase family. Plant Cell **17**: 2413–20.

Bordych, C., Eisenhut, M., Pick, T.R., Kuelahoglu, C., and Weber, A.P.M. (2013). Co-expression analysis as tool for the discovery of transport proteins in photorespiration. Plant Biol. **15**: 686–693.

Bouvier, F., Linka, N., Isner, J.-C., Mutterer, J., Weber, A.P.M., and Camara, B. (2006). Arabidopsis SAMT1 Defines a Plastid Transporter Regulating Plastid Biogenesis and Plant Development. Plant Cell Online **18**: 3088–3105.

Bräutigam, A. et al. (2011). An mRNA Blueprint for C4 Photosynthesis Derived from Comparative Transcriptomics of Closely Related C3 and C4 Species. Plant Physiol. **155**: 142–156.

Brocard, C. and Hartig, A. (2006). Peroxisome targeting signal 1: Is it really a simple tripeptide? Biochim. Biophys. Acta - Mol. Cell Res. **1763**: 1565–1573.

Brown, N.J., Parsley, K., and Hibberd, J.M. (2005). The future of C4 research - Maize, Flaveria or Cleome?

Trends Plant Sci. **10**: 215–221.

Cantó, C., Menzies, K.J., and Auwerx, J. (2015). NAD+ Metabolism and the Control of Energy Homeostasis: A Balancing Act between Mitochondria and the Nucleus. Cell Metab. **22**: 31–53.

Carraro, N., Tisdale-Orr, T.E., Clouse, R.M., Knöller, A.S., and Spicer, R. (2012). Diversification and Expression of the PIN, AUX/LAX, and ABCB Families of Putative Auxin Transporters in Populus.

Catoni, E., Desimone, M., Hilpert, M., Wipf, D., Kunze, R., Schneider, A., Flügge, U.I., Schumacher, K., and Frommer, W.B. (2003). Expression pattern of a nuclear encoded mitochondrial arginine-ornithine translocator gene from Arabidopsis. BMC Plant Biol. **3**: 1–10.

Coolen, S. et al. (2016). Transcriptome dynamics of Arabidopsis during sequential biotic and abiotic stresses. Plant J. **86**: 249–267.

Cousins, A.B., Pracharoenwattana, I., Zhou, W., Smith, S.M., and Badger, M.R. (2008). Peroxisomal malate dehydrogenase is not essential for photorespiration in Arabidopsis but its absence causes an increase in the stoichiometry of photorespiratory CO2 release. Plant Physiol. **148**: 786–95.

Cousins, A.B., Walker, B.J., Pracharoenwattana, I., Smith, S.M., and Badger, M.R. (2011). Peroxisomal hydroxypyruvate reductase is not essential for photorespiration in Arabidopsis but its absence causes an increase in the stoichiometry of photorespiratory CO2release. Photosynth. Res. **108**: 91–100.

Dellero, Y., Lamothe-Sibold, M., Jossier, M., and Hodges, M. (2015). Arabidopsis thaliana ggt1 photorespiratory mutants maintain leaf carbon/nitrogen balance by reducing RuBisCO content and plant growth. Plant J. **83**: 1005–1018.

Devic, M., Albert, S., and Delseny, M. (1996). Induction and expression of seed-specific promoters in Arabidopsis embryo-defective mutants. Plant J. **9**: 205–15.

Dong, H., Bai, L., Chang, J., and Song, C. peng (2018). Chloroplast protein PLGG1 is involved in abscisic acid-regulated lateral root development and stomatal movement in Arabidopsis. Biochem. Biophys. Res. Commun. **495**: 280–285.

Douce, R., Bourguignon, J., Neuburger, M., and Rébeillé, F. (2001). The glycine decarboxylase system: A fascinating complex. Trends Plant Sci. **6**: 167–176.

Edwards, G. and Walker, D. (1983). Photosynthesis: C3, C4. Mechanisms, and cellular and environmental regulation, of photosynthesis. Science **222**: 1009.

Eisen, M.B., Spellman, P.T., Brown, P.O., and Botstein, D. (1998). Cluster analysis and display of genome-wide expression patterns. Proc Natl Acad Sci USA **95**: 14863–14868.

Eisenhut, M. et al. (2013a). Arabidopsis A BOUT de SOUFFLE is a putative mitochondrial transporter involved in photorespiratory metabolism and is required for meristem growth at ambient CO2 levels. Plant J. **73**: 836–849.

Eisenhut, M., Bräutigam, A., Timm, S., Florian, A., Tohge, T., Fernie, A.R., Bauwe, H., and Weber, A.P.M. (2017). Photorespiration Is Crucial for Dynamic Response of Photosynthetic Metabolism and Stomatal Movement to Altered CO2 Availability. Mol. Plant **10**: 47–61.

Eisenhut, M., Pick, T.R., Bordych, C., and Weber, A.P.M. (2013b). Towards closing the remaining gaps in photorespiration - the essential but unexplored role of transport proteins. Plant Biol. **15**: 676–685.

Eisenhut, M., Ruth, W., Haimovich, M., Bauwe, H., Kaplan, A., and Hagemann, M. (2008). The photorespiratory glycolate metabolism is essential for cyanobacteria and might have been conveyed endosymbiontically to plants. Proc. Natl. Acad. Sci. **105**: 17199–17204.

Engqvist, M.K.M., Schmitz, J., Gertzmann, A., Florian, A., Jaspert, N., Arif, M., Balazadeh, S., Mueller-Roeber, B., Fernie, A.R., and Maurino, V.G. (2015). GLYCOLATE OXIDASE3, a Glycolate Oxidase Homolog of Yeast l-Lactate Cytochrome *c* Oxidoreductase, Supports l-Lactate Oxidation in Roots of Arabidopsis. Plant Physiol. **169**: 1042–1061.

Erb, T.J. and Zarzycki, J. (2018). A short history of RubisCO: the rise and fall (?) of Nature's predominant CO2

fixing enzyme. Curr. Opin. Biotechnol. **49**: 100–107.

Esser, C., Kuhn, A., Groth, G., Lercher, M.J., and Maurino, V.G. (2014). Plant and animal glycolate oxidases have a common eukaryotic ancestor and convergently duplicated to evolve long-chain 2-hydroxy acid oxidases. Mol. Biol. Evol. **31**: 1089–1101.

Eudes, A., Kunji, E.R.S., Noiriel, A., Klaus, S.M.J., Vickers, T.J., Beverley, S.M., Gregory, J.F., and Hanson, A.D. (2010). Identification of transport-critical residues in a folate transporter from the Folate-Biopterin Transporter (FBT) family. J. Biol. Chem. **285**: 2867–2875.

Facchinelli, F. and Weber, A.P.M. (2011). The Metabolite Transporters of the Plastid Envelope: An Update. Front. Plant Sci. **2**: 1–18.

Fahy, D., Sanad, M.N.M.E., Duscha, K., Lyons, M., Liu, F., Bozhkov, P., Kunz, H.-H., Hu, J., Neuhaus, H.E., Steel, P.G., and Smertenko, A. (2017). Impact of salt stress, cell death, and autophagy on peroxisomes: quantitative and morphological analyses using small fluorescent probe N-BODIPY. Sci. Rep. **7**: 39069.

Fischer, W.-N.N., Loo, D.D.F., Koch, W., Ludewig, U., Boorer, K.J., Tegeder, M., Rentsch, D., Wright, E.M., Frommer, W.B., and Fischer, W.-N.N. (2002). Low and high affinity amino acid H+-cotransporters for cellular import of neutral and charged amino acids. Plant J. **29**: 717\r-731.

Flügel, F., Timm, S., Arrivault, S., Florian, A., Stitt, M., Fernie, A.R., and Bauwe, H. (2017). The Photorespiratory Metabolite 2-Phosphoglycolate Regulates Photosynthesis and Starch Accumulation in Arabidopsis. Plant Cell **29**: tpc.00256.2017.

Flügge, U.-I., Westhoff, P., and Leister, D. (2016). Recent advances in understanding photosynthesis. F1000Research **5**: 2890.

Foyer, C.H., Noctor, G., and Hodges, M. (2011). Respiration and nitrogen assimilation: Targeting mitochondria-associated metabolism as a means to enhance nitrogen use efficiency. J. Exp. Bot. **62**: 1467–1482.

Foyer, C.H., Ruban, A. V., and Nixon, P.J. (2017). Photosynthesis solutions to enhance productivity. Philos. Trans. R. Soc. B Biol. Sci. **372**: 3–6.

Fransen, M., Lismont, C., and Walton, P. (2017). The peroxisome-mitochondria connection: How and why? Int. J. Mol. Sci. **18**.

Gadsby, D.C. (2009). Ion channels versus ion pumps: the principal difference, in principle. Nat. Rev. Mol. Cell Biol. **10**: 344–352.

Galland, M., Huguet, R., Arc, E., Cueff, G., Job, D., and Rajjou, L. (2014). Dynamic Proteomics Emphasizes the Importance of Selective mRNA Translation and Protein Turnover during *Arabidopsis* Seed Germination. Mol. Cell. Proteomics **13**: 252–268.

Ge, X. and Xu, J. (2012). Cell-Free Protein Synthesis as a Promising Expression System for Recombinant Proteins. In Recombinant Gene Expression. Methods in Molecular Biology, pp. 565–578.

Germain, V., Rylott, E.L., Larson, T.R., Sherson, S.M., Bechtold, N., Carde, J.P., Bryce, J.H., Graham, I.A., and Smith, S.M. (2001). Requirement for 3-ketoacyl-CoA thiolase-2 in peroxisome development, fatty acid beta-oxidation and breakdown of triacylglycerol in lipid bodies of Arabidopsis seedlings. Plant J. **28**: 1–12.

Gibson, D.G. (2011). Enzymatic assembly of overlapping DNA fragments. Methods Enzymol. **498**: 349–361.

Gigolashvili, T., Geier, M., Ashykhmina, N., Frerigmann, H., Wulfert, S., Krueger, S., Mugford, S.G., Kopriva, S., Haferkamp, I., and Flügge, U.-I. (2012). The *Arabidopsis* Thylakoid ADP/ATP Carrier TAAC Has an Additional Role in Supplying Plastidic Phosphoadenosine 5′-Phosphosulfate to the Cytosol. Plant Cell **24**: 4187–4204.

Gould, S.J., Keller, G.A., Hosken, N., Wilkinson, J., and Subramani, S. (1989). A conserved tripeptide sorts proteins to peroxisomes. J. Cell Biol. **108**: 1657–1664.

Gowik, U., Bräutigam, A., Weber, K.L., Weber, A.P.M., and Westhoff, P. (2011). Evolution of C $_4$ Photosynthesis in the Genus *Flaveria* : How Many and Which Genes Does It Take to Make C $_4$? Plant Cell **23**: 2087–2105.

Graham, I.A. (2008). Seed Storage Oil Mobilization. Annu. Rev. Plant Biol. **59**: 115–142.

Grefen, C., Donald, N., Hashimoto, K., Kudla, J., Schumacher, K., and Blatt, M.R. (2010). A ubiquitin-10 promoter-based vector set for fluorescent protein tagging facilitates temporal stability and native protein distribution in transient and stable expression studies. Plant J. **64**: 355–365.

Haferkamp, I. (2007). The diverse members of the mitochondrial carrier family in plants. FEBS Lett. **581**: 2375–2379.

Haferkamp, I., Hackstein, J.H.P., Voncken, F.G.J., Schmit, G., and Tjaden, J. (2002). Functional integration of mitochondrial and hydrogenosomal ADP/ATP carriers in the Escherichia coli membrane reveals different biochemical characteristics for plants, mammals and anaerobic chytrids. Eur. J. Biochem. **269**: 3172–3181.

Haferkamp, I. and Schmitz-Esser, S. (2012). The Plant Mitochondrial Carrier Family: Functional and Evolutionary Aspects. Front. Plant Sci. **3**: 1–19.

Hagemann, M., Weber, A.P.M., and Eisenhut, M. (2016). Photorespiration: Origins and metabolic integration in interacting compartments. J. Exp. Bot. **67**: 2915–2918.

Hahn, F., Eisenhut, M., Mantegazza, O., and Weber, A.P.M. (2018). Homology-Directed Repair of a Defective Glabrous Gene in Arabidopsis With Cas9-Based Gene Targeting. Front. Plant Sci. **9**: 1–13.

Hahn, F., Mantegazza, O., Greiner, A., Hegemann, P., Eisenhut, M., and Weber, A.P.M. (2017). An Efficient Visual Screen for CRISPR/Cas9 Activity in Arabidopsis thaliana. Front. Plant Sci. **08**: 1–13.

Hamel, P., Saint-Georges, Y., De Pinto, B., Lachacinski, N., Altamura, N., and Dujardin, G. (2004). Redundancy in the function of mitochondrial phosphate transport in Saccharomyces cerevisiae and Arabidopsis thaliana. Mol. Microbiol. **51**: 307–317.

Haney, C.J., Grass, G., Franke, S., and Rensing, C. (2005). New developments in the understanding of the cation diffusion facilitator family. J. Ind. Microbiol. Biotechnol. **32**: 215–226.

Hoffmann, C., Plocharski, B., Haferkamp, I., Leroch, M., Ewald, R., Bauwe, H., Riemer, J., Herrmann, J.M., and Neuhaus, H.E. (2013). From Endoplasmic Reticulum to Mitochondria: Absence of the Arabidopsis ATP Antiporter Endoplasmic Reticulum Adenylate Transporter1 Perturbs Photorespiration. Plant Cell **25**: 2647–2660.

Hofgen, R. and Willmitzer, L. (1988). Storage of competent cells for Agrobacterium transformation. Nucleic Acids Res. **16**: 9877.

Hossain, M.S. and Dietz, K.-J. (2016). Tuning of Redox Regulatory Mechanisms, Reactive Oxygen Species and Redox Homeostasis under Salinity Stress. Front. Plant Sci. **7**.

Hoyos, M.E., Palmieri, L., Wertin, T., Arrigoni, R., Polacco, J.C., and Palmieri, F. (2003). Identification of a mitochondrial transporter for basic amino acids in Arabidopsis thaliana by functional reconstitution into liposomes and complementation in yeast. Plant J. **33**: 1027–1035.

Hu, J., Baker, A., Bartel, B., Linka, N., Mullen, R.T., Reumann, S., and Zolman, B.K. (2012). Plant Peroxisomes: Biogenesis and Function. Plant Cell **24**: 2279–2303.

Hunt, D.F., Yates, J.R., Shabanowitz, J., Winston, S., and Hauer, C.R. (1986). Protein sequencing by tandem mass spectrometry. Proc. Natl. Acad. Sci. **83**: 6233–6237.

Hwang, J.U. et al. (2016). Plant ABC Transporters Enable Many Unique Aspects of a Terrestrial Plant's Lifestyle. Mol. Plant **9**: 338–355.

Jaipargas, E.-A., Mathur, N., Bou Daher, F., Wasteneys, G.O., and Mathur, J. (2016). High Light Intensity Leads to Increased Peroxule-Mitochondria Interactions in Plants. Front. Cell Dev. Biol. **4**: 1–11.

Jia, F., Wan, X., Zhu, W., Sun, D., Zheng, C., Liu, P., and Huang, J. (2015). Overexpression of mitochondrial phosphate transporter 3 severely hampers plant development through regulating mitochondrial function in Arabidopsis. PLoS One **10**: 1–14.

Jinek, M., Chylinski, K., Fonfara, I., Hauer, M., Doudna, J.A., and Charpentier, E. (2012). A Programmable Dual-RNA–Guided DNA Endonuclease in Adaptive Bacterial Immunity. Science (80-.). **337**: 816–822.

Kamada, T., Nito, K., Hayashi, H., Mano, S., and Hayashi, M. (2003). Functional Differentiation of Peroxisomes Revealed by Expression Profiles of peroxisomal gene in arabidopsis thanliana.pdf. Plant Cell Physiol **44**: 1275–1289.

Kane, D.A. (2014). Lactate oxidation at the mitochondria: A lactate-malate-aspartate shuttle at work. Front. Neurosci. **8**: 1–6.

Kang, J., Park, J., Choi, H., Burla, B., Kretzschmar, T., Lee, Y., and Martinoia, E. (2011). Plant ABC Transporters. Arab. B. **9**: e0153.

Kasahara, M. and Hinkle, P.C. (1977). Reconstitution and Purificaton of the {D}-Glucose Transporter from Human Erythrocytes. J. Biol. Chem. **252**: 7384–7390.

Kasajima, I., Ide, Y., Ohkama-Ohtsu, N., Hayashi, H., Yoneyama, T., and Fujiwara, T. (2004). A protocol for rapid DNA extraction fromArabidopsis thaliana for PCR analysis. Plant Mol. Biol. Report. **22**: 49–52.

Kimura, M. and Nambara, E. (2010). Stored and neosynthesized mRNA in Arabidopsis seeds: effects of cycloheximide and controlled deterioration treatment on the resumption of transcription during imbibition. Plant Mol. Biol. **73**: 119–129.

Kinoshita, H., Nagasaki, J., Yoshikawa, N., Yamamoto, A., Takito, S., Kawasaki, M., Sugiyama, T., Miyake, H., Weber, A.P.M., and Taniguchi, M. (2011). The chloroplastic 2-oxoglutarate/malate transporter has dual function as the malate valve and in carbon/nitrogen metabolism. Plant J. **65**: 15–26.

Klaus, S.M.J., Kunji, E.R.S., Bozzo, G.G., Noiriel, A., De La Garza, R.D., Basset, G.J.C., Ravanel, S., Rébeillé, F., Gregory, J.F., and Hanson, A.D. (2005). Higher plant plastids and cyanobacteria have folate carriers related to those of trypanosomatids. J. Biol. Chem. **280**: 38457–38463.

van der Klei, I.J. and Veenhuis, M. (2006). PTS1-independent sorting of peroxisomal matrix proteins by Pex5p. Biochim. Biophys. Acta - Mol. Cell Res. **1763**: 1794–1800.

Klepikova, A. V., Kasianov, A.S., Gerasimov, E.S., Logacheva, M.D., and Penin, A.A. (2016). A high resolution map of the Arabidopsis thaliana developmental transcriptome based on RNA-seq profiling. Plant J. **88**: 1058–1070.

Klepikova, A. V., Logacheva, M.D., Dmitriev, S.E., and Penin, A.A. (2015). RNA-seq analysis of an apical meristem time series reveals a critical point in Arabidopsis thaliana flower initiation. BMC Genomics **16**.

Knappe, S. (2003). Analysis of the Plastidic phosphate translocator Gene Family in Arabidopsis and Identification of New phosphate translocator-Homologous Transporters, Classified by Their Putative Substrate-Binding Site. Plant Physiol. **131**: 1178–1190.

Koncz, C. and Schell, J. (1986). The promoter of TL-DNA gene 5 controls the tissue-specific expression of chimaeric genes carried by a novel type of Agrobacterium binary vector. MGG Mol. Gen. Genet. **204**: 383–396.

Külahoglu, C. et al. (2014). Comparative Transcriptome Atlases Reveal Altered Gene Expression Modules between Two Cleomaceae C3 and C4 Plant Species. Plant Cell **26**: 3243–3260.

Kump, L.R. (2008). The rise of atmospheric oxygen. Nature **451**: 277–278.

Kunze, M. and Hartig, A. (2013). Permeability of the peroxisomal membrane: Lessons from the glyoxylate cycle. Front. Physiol. **4 AUG**: 1–12.

Kunze, M., Pracharoenwattana, I., Smith, S.M., and Hartig, A. (2006). A central role for the peroxisomal membrane in glyoxylate cycle function. Biochim. Biophys. Acta - Mol. Cell Res. **1763**: 1441–1452.

Landrum, M., Smertenko, A., Edwards, R., Hussey, P.J., and Steel, P.G. (2010). BODIPY probes to study peroxisome dynamics in vivo. Plant J. **62**: 529–538.

Law, C.J., Maloney, P.C., and Wang, D. (2008). Ins and Outs of Major Facilitator Superfamily Antiporters. Annu. Rev. Microbiol. **62**: 289–305.

Lawand, S., Dorne, A., Long, D., Coupland, G., and Carol, P. (2002). Arabidopsis A BOUT DE SOUFFLE , Which Is Homologous with Mammalian Carnitine Acyl Carrier, Is Required for Postembryonic Growth in the

Light. Plant Cell **14**: 2161–2173.

Le, B.H. et al. (2010). Global analysis of gene activity during Arabidopsis seed development and identification of seed-specific transcription factors. Proc. Natl. Acad. Sci. **107**: 8063–8070.

Lee, C.P. and Millar, A.H. (2016). The Plant Mitochondrial Transportome: Balancing Metabolic Demands with Energetic Constraints. Trends Plant Sci. **21**: 662–676.

Linka, N. and Esser, C. (2012). Transport Proteins Regulate the Flux of Metabolites and Cofactors Across the Membrane of Plant Peroxisomes. Front. Plant Sci. **3**: 1–13.

Linka, N., Theodoulou, F.L., Haslam, R.P., Linka, M., Napier, J.A., Neuhaus, H.E., and Weber, A.P.M. (2008). Peroxisomal ATP Import Is Essential for Seedling Development in Arabidopsis thaliana. Plant Cell Online **20**: 3241–3257.

Long, S.P. and Bernacchi, C.J. (2003). Gas exchange measurements, what can they tell us about the underlying limitations to photosynthesis? Procedures and sources of error. J. Exp. Bot. **54**: 2393–2401.

Lorenz, A., Lorenz, M., Vothknecht, U.C., Niopek-Witz, S., Neuhaus, H.E., and Haferkamp, I. (2015). In vitro analyses of mitochondrial ATP/phosphate carriers from Arabidopsis thaliana revealed unexpected Ca2+-effects. BMC Plant Biol. **15**: 1–16.

Ma, X., Zhu, Q., Chen, Y., and Liu, Y.G. (2016). CRISPR/Cas9 Platforms for Genome Editing in Plants: Developments and Applications. Mol. Plant **9**: 961–974.

Mallmann, J., Heckmann, D., Bräutigam, A., Lercher, M.J., Weber, A.P.M., Westhoff, P., and Gowik, U. (2014). The role of photorespiration during the evolution of C4photosynthesis in the genus Flaveria. Elife **2014**: 1–23.

Marshall, D.M., Muhaidat, R., Brown, N.J., Liu, Z., Stanley, S., Griffiths, H., Sage, R.F., and Hibberd, J.M. (2007). Cleome, a genus closely related to Arabidopsis, contains species spanning a developmental progression from C3 to C4 photosynthesis. Plant J. **51**: 886–896.

Maurino, V.G. and Peterhansel, C. (2010). Photorespiration: Current status and approaches for metabolic engineering. Curr. Opin. Plant Biol. **13**: 249–256.

Mayerhofer, P.U. (2016). Targeting and insertion of peroxisomal membrane proteins: ER trafficking versus direct delivery to peroxisomes. Biochim. Biophys. Acta - Mol. Cell Res. **1863**: 870–880.

McNew, J.A. and Goodman, J.M. (1994). An oligomeric protein is imported into peroxisomes in vivo. J. Cell Biol. **127**: 1245–1257.

Meinecke, M., Bartsch, P., and Wagner, R. (2016). Peroxisomal protein import pores. Biochim. Biophys. Acta - Mol. Cell Res. **1863**: 821–827.

Metallo, C.M. and Vander Heiden, M.G. (2014). Understanding metabolic regulation and its influence on cell physiology. Mol. Cell **49**: 388–398.

Millar, A.H. and Heazlewood, J.L. (2015). Genomic and Proteomic Analysis of Mitochondrial Carrier Proteins in Arabidopsis 1. Plant Physiol. **131**: 443–453.

Mindthoff, S., Grunau, S., Steinfort, L.L., Girzalsky, W., Hiltunen, J.K., Erdmann, R., and Antonenkov, V.D. (2016). Peroxisomal Pex11 is a pore-forming protein homologous to TRPM channels. Biochim. Biophys. Acta - Mol. Cell Res. **1863**: 271–283.

Modde, K., Timm, S., Florian, A., Michl, K., Fernie, A.R., and Bauwe, H. (2017). High serine:glyoxylate aminotransferase activity lowers leaf daytime serine levels, inducing the phosphoserine pathway in Arabidopsis. J. Exp. Bot. **68**: 643–656.

Monné, M., Daddabbo, L., Gagneul, D., Obata, T., Hielscher, B., Palmieri, L., Miniero, D.V., Fernie, A.R., Weber, A.P.M., and Palmieri, F. (2018). Uncoupling proteins 1 and 2 (UCP1 and UCP2) from Arabidopsis thaliana are mitochondrial transporters of aspartate, glutamate, and dicarboxylates. J. Biol. Chem. **293**: 4213–4227.

Monné, M., Daddabbo, L., Giannossa, L.C., Nicolardi, M.C., Palmieri, L., Miniero, D.V., Mangone, A., and

Palmieri, F. (2017). Mitochondrial ATP-Mg/phosphate carriers transport divalent inorganic cations in complex with ATP. J. Bioenerg. Biomembr. **49**: 369–380.

Nakabayashi, K., Okamoto, M., Koshiba, T., Kamiya, Y., and Nambara, E. (2005). Genome-wide profiling of stored mRNA in Arabidopsis thaliana seed germination: Epigenetic and genetic regulation of transcription in seed. Plant J. **41**: 697–709.

Nelson, B.K., Cai, X., and Nebenführ, A. (2007). A multicolored set of in vivo organelle markers for co-localization studies in Arabidopsis and other plants. Plant J. **51**: 1126–1136.

Newton, R.P., Brenton, A.G., Smith, C.J., and Dudley, E. (2004). Plant proteome analysis by mass spectrometry: Principles, problems, pitfalls and recent developments. Phytochemistry **65**: 1449–1485.

Norman, E.G. and Colman, B. (1991). Purification and Characterization of Phosphoglycolate Phosphatase from the Cyanobacterium Coccochloris peniocystis. Plant Physiol. **95**: 693–698.

O'Malley, R.C., Barragan, C.C., and Ecker, J.R. (2015). A user's guide to the Arabidopsis T-DNA insertion mutant collections. Methods Mol. Biol. **1284**: 323–42.

O'Malley, R.C. and Ecker, J.R. (2010). Linking genotype to phenotype using the Arabidopsis unimutant collection. Plant J. **61**: 928–940.

Oikawa, K. et al. (2015). Physical interaction between peroxisomes and chloroplasts elucidated by in situ laser analysis. Nat. Plants **1**: 1–12.

Okumoto, S., Koch, W., Tegeder, M., Fischer, W.N., Biehl, A., Leister, D., Stierhof, Y.D., and Frommer, W.B. (2004). Root phloem-specific expression of the plasma membrane amino acid proton co-transporter AAP3. J. Exp. Bot. **55**: 2155–2168.

Orr, D.J., Pereira, A.M., da Fonseca Pereira, P., Pereira-Lima, Í.A., Zsögön, A., and Araújo, W.L. (2017). Engineering photosynthesis: progress and perspectives. F1000Research **6**: 1891.

Osmond, C.B. (1981). Photorespiration and photoinhibition. Some implications for the energetics of photosynthesis. BBA Rev. Bioenerg. **639**: 77–98.

Palmieri, F. (1994). Mitochondrial carrier proteins. FEBS Lett. **346**: 48–54.

Palmieri, F. et al. (2009). Molecular Identification and Functional Characterization of *Arabidopsis thaliana* Mitochondrial and Chloroplastic NAD $^+$ Carrier Proteins. J. Biol. Chem. **284**: 31249–31259.

Palmieri, F., Pierri, C.L., De Grassi, A., Nunes-Nesi, A., and Fernie, A.R. (2011). Evolution, structure and function of mitochondrial carriers: A review with new insights. Plant J. **66**: 161–181.

Palmieri, L., Arrigoni, R., Blanco, E., Carrari, F., Zanor, M.I., Studart-Guimaraes, C., Fernie, A.R., and Palmieri, F. (2006a). Molecular Identification of an Arabidopsis S-Adenosylmethionine Transporter. Analysis of Organ Distribution, Bacterial Expression, Reconstitution into Liposomes, and Functional Characterization. Plant Physiol. **142**: 855–865.

Palmieri, L., Picault, N., Arrigoni, R., Besin, E., Palmieri, F., and Hodges, M. (2008a). Molecular identification of three Arabidopsis thaliana mitochondrial dicarboxylate carrier isoforms: organ distribution, bacterial expression, reconstitution into liposomes and functional characterization. Biochem. J. **410**: 621–629.

Palmieri, L., Santoro, A., Carrari, F., Blanco, E., Nunes-Nesi, A., Arrigoni, R., Genchi, F., Fernie, A.R., and Palmieri, F. (2008b). Identification and Characterization of ADNT1, a Novel Mitochondrial Adenine Nucleotide Transporter from Arabidopsis. Plant Physiol. **148**: 1797–1808.

Palmieri, L., Todd, C.D., Arrigoni, R., Hoyos, M.E., Santoro, A., Polacco, J.C., and Palmieri, F. (2006b). Arabidopsis mitochondria have two basic amino acid transporters with partially overlapping specificities and differential expression in seedling development. Biochim. Biophys. Acta - Bioenerg. **1757**: 1277–1283.

Palms, J.M., Corpas, F.J., and Del Río, L.A. (2009). Proteome of plant peroxisomes: New perspectives on the role of these organelles in cell biology. Proteomics **9**: 2301–2312.

Parcy, F., Valon, C., Raynal, M., Gaubier-Comella, P., Delseny, M., and Giraudat, J. (1994). Regulation of Gene Expression Programs during Arabidopsis Seed Development: Roles of the ABI3 Locus and of

Endogenous Abscisic Acid. PLANT CELL ONLINE **6**: 1567–1582.

Perchlik, M. and Tegeder, M. (2017). Improving Plant Nitrogen Use Efficiency through Alteration of Amino Acid Transport Processes. Plant Physiol. **175**: 235–247.

Peterhansel, C., Horst, I., Niessen, M., Blume, C., Kebeish, R., Kürkcüoglu, S., and Kreuzaler, F. (2010). Photorespiration. Arabidopsis Book **8**: e0130.

Picault, N., Hodges, M., Palmieri, L., and Palmieri, F. (2004). The growing family of mitochondrial carriers in Arabidopsis. Trends Plant Sci. **9**: 138–146.

Pick, T.R., Bräutigam, A., Schulz, M.A., Obata, T., Fernie, A.R., and Weber, A.P.M. (2013). PLGG1, a plastidic glycolate glycerate transporter, is required for photorespiration and defines a unique class of metabolite transporters. Proc. Natl. Acad. Sci. **110**: 3185–3190.

Planchais, S., Cabassa, C., Toka, I., Justin, A.-M., Renou, J.-P., Savouré, A., and Carol, P. (2014). BASIC AMINO ACID CARRIER 2 gene expression modulates arginine and urea content and stress recovery in Arabidopsis leaves. Front Plant Sci **5**: 330.

Poirier, Y., Antonenkov, V.D., Glumoff, T., and Hiltunen, J.K. (2006). Peroxisomal β-oxidation-A metabolic pathway with multiple functions. Biochim. Biophys. Acta - Mol. Cell Res. **1763**: 1413–1426.

Pracharoenwattana, I., Cornah, J.E., and Smith, S.M. (2007). Arabidopsis peroxisomal malate dehydrogenase functions in β-oxidation but not in the glyoxylate cycle. Plant J. **50**: 381–390.

Pracharoenwattana, I., Zhou, W., and Smith, S.M. (2010). Fatty acid beta-oxidation in germinating Arabidopsis seeds is supported by peroxisomal hydroxypyruvate reductase when malate dehydrogenase is absent. Plant Mol. Biol. **72**: 101–109.

Pratelli, R. and Pilot, G. (2014). Regulation of amino acid metabolic enzymes and transporters in plants. J. Exp. Bot. **65**: 5535–5556.

Quistgaard, E.M., Löw, C., Guettou, F., and Nordlund, P. (2016). Understanding transport by the major facilitator superfamily (MFS): Structures pave the way. Nat. Rev. Mol. Cell Biol. **17**: 123–132.

Radin, I., Mansilla, N., Rödel, G., and Steinebrunner, I. (2015). The Arabidopsis COX11 Homolog is Essential for Cytochrome c Oxidase Activity. Front. Plant Sci. **6**: 1–17.

Rasmussen, S., Barah, P., Suarez-Rodriguez, M.C., Bressendorff, S., Friis, P., Costantino, P., Bones, A.M., Nielsen, H.B., and Mundy, J. (2013). Transcriptome Responses to Combinations of Stresses in Arabidopsis. Plant Physiol. **161**: 1783–1794.

Rea, P.A. (2007). Plant ATP-Binding Cassette Transporters. Annu. Rev. Plant Biol. **58**: 347–375.

Reddy, V.S., Shlykov, M.A., Castillo, R., Sun, E.I., and Saier, M.H. (2012). The major facilitator superfamily (MFS) revisited. FEBS J. **279**: 2022–2035.

Regev-Rudzki, N., Yogev, O., and Pines, O. (2008). The mitochondrial targeting sequence tilts the balance between mitochondrial and cytosolic dual localization. J. Cell Sci. **121**: 2423–2431.

Renné, P., Dreßen, U., Hebbeker, U., Hille, D., Flügge, U.I., Westhoff, P., and Weber, A.P.M. (2003). The Arabidopsis mutant dct is deficient in the plastidic glutamate/malate translocator DiT2. Plant J. **35**: 316–331.

Reumann, S. and Bartel, B. (2016). Plant peroxisomes: recent discoveries in functional complexity, organelle homeostasis, and morphological dynamics. Curr. Opin. Plant Biol. **34**: 17–26.

Reumann, S., Maier, E., Heldt, H.W., and Benz, R. (1998). Permeability properties of the porin of spinach leaf peroxisomes. Eur. J. Biochem. **251**: 359–366.

Richardson, L.G.L., Singhal, R., and Schnell, D.J. (2017). The integration of chloroplast protein targeting with plant developmental and stress responses. BMC Biol. **15**: 118.

Rieder, B. and Neuhaus, H.E. (2011). Identification of an Arabidopsis Plasma Membrane–Located ATP Transporter Important for Anther Development. Plant Cell **23**: 1932–1944.

Robinson, A.J. and Kunji, E.R.S. (2006). Mitochondrial carriers in the cytoplasmic state have a common substrate binding site. Proc. Natl. Acad. Sci. **103**: 2617–2622.

Roell, M.-S., Kuhnert, F., Zamani-Nour, S., and Weber, A.P.M. (2017). In Vitro Analysis of Metabolite Transport Proteins. In Methods in Molecular Biology, pp. 83–96.

van Roermund, C.W.T., Schroers, M.G., Wiese, J., Facchinelli, F., Kurz, S., Wilkinson, S., Charton, L., Wanders, R.J.A., Waterham, H.R., Weber, A.P.M., and Link, N. (2016). The Peroxisomal NAD Carrier from Arabidopsis Imports NAD in Exchange with AMP. Plant Physiol. **171**: 2127–2139.

Rokka, A., Antonenkov, V.D., Soininen, R., Immonen, H.L., Pirilä, P.L., Bergmann, U., Sormunen, R.T., Weckström, M., Benz, R., and Hiltunen, J.K. (2009). Pxmp2 is a channel-forming protein in mammalian peroxisomal membrane. PLoS One **4**: e5090.

Russel, D.W. and Sambrook, J. (2001). Molecular Cloning: A Laboratory Manual. Q. Rev. Biol. **76**: 348–349.

Rylott, E.L., Eastmond, P.J., Gilday, A.D., Slocombe, S.P., Larson, T.R., Baker, A., and Graham, I.A. (2006). The Arabidopsis thaliana multifunctional protein gene (MFP2) of peroxisomal β-oxidation is essential for seedling establishment. Plant J. **45**: 930–941.

Sage, R. (2001). Environmental and Evolutionary Preconditionsfor the Origin and Diversification of the C4 PhotosyntheticSyndrome. Plant Biol. **3**: 202–213.

Sage, R.F. (2017). A portrait of the C4 photosynthetic family on the 50th anniversary of its discovery: Species number, evolutionary lineages, and Hall of Fame. J. Exp. Bot. **68**: e11–e28.

Salin, M.L. and Homann, P.H. (1971). Changes of photorespiratory activity with leaf age. Plant Physiol. **48**: 193–6.

Sano, N., Ono, H., Murata, K., Yamada, T., Hirasawa, T., and Kanekatsu, M. (2015). Accumulation of long-lived mRNAs associated with germination in embryos during seed development of rice. J. Exp. Bot. **66**: 4035–4046.

Sano, N., Permana, H., Kumada, R., Shinozaki, Y., Tanabata, T., Yamada, T., Hirasawa, T., and Kanekatsu, M. (2012). Proteomic analysis of embryonic proteins synthesized from long-lived mRNAs during germination of rice seeds. Plant Cell Physiol. **53**: 687–698.

Schlüter, A., Fourcade, S., Domènech-Estévez, E., Gabaldón, T., Huerta-Cepas, J., Berthommier, G., Ripp, R., Wanders, R.J.A., Poch, O., and Pujol, A. (2007). PeroxisomeDB: A database for the peroxisomal proteome, functional genomics and disease. Nucleic Acids Res. **35**: 815–822.

Schulze, S., Westhoff, P., and Gowik, U. (2016). Glycine decarboxylase in C3, C4 and C3-C4 intermediate species. Curr. Opin. Plant Biol. **31**: 29–35.

Shai, N., Schuldiner, M., and Zalckvar, E. (2016). No peroxisome is an island - Peroxisome contact sites. Biochim. Biophys. Acta - Mol. Cell Res. **1863**: 1061–1069.

Sham, A., Moustafa, K., Al-Ameri, S., Al-Azzawi, A., Iratni, R., and AbuQamar, S. (2015). Identification of Arabidopsis candidate genes in response to biotic and abiotic stresses using comparative microarrays. PLoS One **10**: 1–21.

Sheen, J. (2002). A transient expression assay using Arabidopsis mesophyll protoplasts. Nat. Nat. Plant Physiol. Nat. PNAS Abel Theol. Plant J. Plant J. Plant Mol Biol **425**: 521–525.

Silva, A.T., Ribone, P.A., Chan, R.L., Ligterink, W., and Hilhorst, H.W.M. (2016). A Predictive Coexpression Network Identifies Novel Genes Controlling the Seed-to-Seedling Phase Transition in *Arabidopsis thaliana*. Plant Physiol. **170**: 2218–2231.

Sinclair, A.M., Trobacher, C.P., Mathur, N., Greenwood, J.S., and Mathur, J. (2009). Peroxule extension over ER-defined paths constitutes a rapid subcellular response to hydroxyl stress. Plant J. **59**: 231–242.

Somerville, C.R. (2001). An early Arabidopsis demonstration resolving a few issues concerning photorespiration. Plant Physiol. **127**: 3.

South, P.F., Walker, B.J., Cavanagh, A.P., Rolland, V., Badger, M., and Ort, D.R. (2017). Bile Acid Sodium Symporter BASS6 Can Transport Glycolate and Is Involved in Photorespiratory Metabolism in Arabidopsis thaliana. Plant Cell **29**: 808–823.

Steinebrunner, I., Gey, U., Andres, M., Garcia, L., and Gonzalez, D.H. (2014). Divergent functions of the Arabidopsis mitochondrial SCO proteins: HCC1 is essential for COX activity while HCC2 is involved in the UV-B stress response. Front. Plant Sci. **5**: 1–17.

Steinebrunner, I., Landschreiber, M., Krause-Buchholz, U., Teichmann, J., and Rödel, G. (2011). HCC1, the Arabidopsis homologue of the yeast mitochondrial copper chaperone SCO1, is essential for embryonic development. J. Exp. Bot. **62**: 319–330.

Steinert, J., Schiml, S., Fauser, F., and Puchta, H. (2015). Highly efficient heritable plant genome engineering using Cas9 orthologues from Streptococcus thermophilus and Staphylococcus aureus. Plant J. **84**: 1295–1305.

Taniguchi, M., Taniguchi, Y., Kawasaki, M., Takeda, S., Kato, T., Tabata, S., Miyake, H., and Sugiyama, T. (2002). Identifying and Characterizing Plastidic 2-Oxoglutarate / Malate and Dicarbo- xylate Transporters in Arabidopsis thaliana. Plant Sci. **43**: 706–717.

Tawfik, D.S. (2014). Accuracy-rate tradeoffs: How do enzymes meet demands of selectivity and catalytic efficiency? Curr. Opin. Chem. Biol. **21**: 73–80.

Tcherkez, G.G.B., Farquhar, G.D., and Andrews, T.J. (2006). Despite slow catalysis and confused substrate specificity, all ribulose bisphosphate carboxylases may be nearly perfectly optimized. Proc. Natl. Acad. Sci. **103**: 7246–7251.

Tegeder, M. and Hammes, U.Z. (2018). The way out and in: phloem loading and unloading of amino acids. Curr. Opin. Plant Biol. **43**: 16–21.

Thazar-Poulot, N., Miquel, M., Fobis-Loisy, I., and Gaude, T. (2015). Peroxisome extensions deliver the *Arabidopsis* SDP1 lipase to oil bodies. Proc. Natl. Acad. Sci. **112**: 4158–4163.

Timm, S. and Bauwe, H. (2013). The variety of photorespiratory phenotypes - employing the current status for future research directions on photorespiration. Plant Biol. **15**: 737–747.

Timm, S., Florian, A., Fernie, A.R., and Bauwe, H. (2016). The regulatory interplay between photorespiration and photosynthesis. J. Exp. Bot. **67**: 2923–2929.

Timm, S., Florian, A., Jahnke, K., Nunes-Nesi, A., Fernie, A.R., and Bauwe, H. (2011). The hydroxypyruvate-reducing system in Arabidopsis: multiple enzymes for the same end. Plant Physiol. **155**: 694–705.

Timm, S., Nunes-Nesi, A., Parnik, T., Morgenthal, K., Wienkoop, S., Keerberg, O., Weckwerth, W., Kleczkowski, L.A., Fernie, A.R., and Bauwe, H. (2008). A Cytosolic Pathway for the Conversion of Hydroxypyruvate to Glycerate during Photorespiration in Arabidopsis. Plant Cell Online **20**: 2848–2859.

Tolbert, N.E. (1997). the C2 Oxidative Photosynthetic Carbon Cycle. Annu. Rev. Plant Physiol. Plant Mol. Biol. **48**: 1–25.

Turkan, I., Uzilday, B., Dietz, K.-J., Bräutigam, A., and Ozgur, R. (2018). Reactive oxygen species and redox regulation in mesophyll and bundle sheath cells of C4 plants. J. Exp. Bot.: 1–11.

Vapola, M.H., Rokka, A., Sormunen, R.T., Alhonen, L., Schmitz, W., Conzelmann, E., Wärri, A., Grunau, S., Antonenkov, V.D., and Hiltunen, J.K. (2014). Peroxisomal membrane channel Pxmp2 in the mammary fat pad is essential for stromal lipid homeostasis and for development of mammary gland epithelium in mice. Dev. Biol. **391**: 66–88.

Verrier, P.J. et al. (2008). Plant ABC proteins - a unified nomenclature and updated inventory. Trends Plant Sci. **13**: 151–159.

Visser, W.F., van Roermund, C.W.T., Ijlst, L., Waterham, H.R., and Wanders, R.J.A. (2007). Metabolite transport across the peroxisomal membrane. Biochem. J. **401**: 365–375.

Waadt, R. and Kudla, J. (2008). In plant visualization of protein interactions using bimolecular fluorescence complementation (BiFC). Cold Spring Harb. Protoc. **3**: 1–8.

Walker, B.J., VanLoocke, A., Bernacchi, C.J., and Ort, D.R. (2016). The Costs of Photorespiration to Food Production Now and in the Future. Annu. Rev. Plant Biol. **67**: 107–129.

Wang, P., Khoshravesh, R., Karki, S., Tapia, R., Balahadia, C.P., Bandyopadhyay, A., Quick, W.P., Furbank, R., Sage, T.L., and Langdale, J.A. (2017a). Re-creation of a Key Step in the Evolutionary Switch from C3 to C4 Leaf Anatomy. Curr. Biol. **27**: 3278–3287.e6.

Wang, T., Chen, Y., Zhang, M., Chen, J., Liu, J., Han, H., and Hua, X. (2017b). Arabidopsis AMINO ACID PERMEASE1 Contributes to Salt Stress-Induced Proline Uptake from Exogenous Sources. Front. Plant Sci. **8**: 1–12.

Wang, Y.H. (2008). How effective is T-DNA insertional mutagenesis in Arabidopsis? J Biochem Tech **1**: 11–20.

Wang, Z.A., Li, Q., Ge, X.Y., Yang, C.L., Luo, X.L., Zhang, A.H., Xiao, J.L., Tian, Y.C., Xia, G.X., Chen, X.Y., Li, F.G., and Wu, J.H. (2015). The mitochondrial malate dehydrogenase 1 gene GhmMDH1 is involved in plant and root growth under phosphorus deficiency conditions in cotton. Sci. Rep. **5**: 1–14.

Weber, A. and Flügge, U. (2002). Interaction of cytosolic and plastidic nitrogen metabolism in plants. J. Exp. Bot. **53**: 865–874.

Weber, A.P.M., Schwacke, R., and Flügge, U.-I. (2005). Solute Transporters of the Plastid Envelope Membrane. Annu. Rev. Plant Biol. **56**: 133–164.

Weitbrecht, K., Müller, K., and Leubner-Metzger, G. (2011). First off the mark: Early seed germination. J. Exp. Bot. **62**: 3289–3309.

Willems, P., Mhamdi, A., Stael, S., Storme, V., Kerchev, P., Noctor, G., Gevaert, K., and Van Breusegem, F. (2016). The ROS Wheel: Refining ROS Transcriptional Footprints. Plant Physiol. **171**: 1720–1733.

Yu, Q.-B. et al. (2008). Construction of a chloroplast protein interaction network and functional mining of photosynthetic proteins in Arabidopsis thaliana. Cell Res. **18**: 1007–1019.

Zallot, R., Agrimi, G., Lerma-Ortiz, C., Teresinski, H.J., Frelin, O., Ellens, K.W., Castegna, A., Russo, A., de Crecy-Lagard, V., Mullen, R.T., Palmieri, F., and Hanson, A.D. (2013). Identification of Mitochondrial Coenzyme A Transporters from Maize and Arabidopsis. Plant Physiol. **162**: 581–588.

Zhao, Y. et al. (2018). Malate transported from chloroplast to mitochondrion triggers production of ROS and PCD in Arabidopsis thaliana. Cell Res.: 1–14.

Zheng, W.H., Västermark, Å., Shlykov, M.A., Reddy, V., Sun, E.I., and Saier, M.H. (2013). Evolutionary relationships of ATP-binding cassette (ABC) uptake porters. BMC Microbiol. **13**.

V.2 Manuscript 2

Physiological role of a mitochondrial transporter in Arabidopsis

Björn Hielscher[1*], Andreas Weber[1] and Nicole Linka[1a]

[1]Heinrich Heine University Düsseldorf, Institute of Plant Biochemistry, Germany

[*]First author

[a]Corresponding author

Abstract

Mitochondria are the site of energy conversion in all eukaryotes. The tricarboxylic acid (TCA) cycle converts acetyl coenzyme A converted from carbohydrates, proteins or fatty acids to provide reducing equivalents for ATP-producing oxidative phosphorylation. The electron transport chain (ETC) uses electrons transferred from NADH and $FADH_2$ to pump protons into the intermembrane space (IMS) generating a proton gradient in the process. This proton gradient allows the conversion of ADP and inorganic phosphate to ATP. The import of phosphate is mediated by members of the phosphate transporter family 3 (PHT3) in the inner mitochondrial membrane (IMM). Many plant species like Arabidopsis, rice, poplar, tomato, or wheat have several isoforms of PHT3 carriers. The Arabidopsis genome codes for three phosphate transporters: AtPHT3;1, AtPHT3;2 and AtPHT3;3. AtPHT3;1 and AtPHT3;2 have been shown to transport phosphate. However, the role of AtPHT3;3 has not been described yet.

This study provides evidence that AtPHT3;3 (1) is distinct from the other two mitochondrial phosphate carriers AtPHT3;1 and AtPHT3;2, (2) more related to copper/phosphate transporters found in yeast and mammals and (3) is specifically involved in embryo development of Arabidopsis seeds. Results presented here suggest that AtPHT3;3 is involved in the mitochondrial import of copper needed for COX/complex IV of the ETC. Defects in this pathway are often embryo-lethal or affect reproductive tissues in Arabidopsis. AtPHT3;3 loss-of-function mutants show an increased number of defect seeds. AtPHT3;3 might represent the mitochondrial copper importer in plants fueling the ETC with copper during embryogenesis.

Introduction

Mitochondria are essential organelles in several metabolic pathways in plant cells: oxidative phosphorylation (Millar et al., 2011), photorespiration (Bauwe et al., 2010), stress response (Jacoby et al., 2012), amino acid metabolism (Hildebrandt et al., 2015), fatty acid metabolism (Gueguen, 2000), vitamin biosynthesis or programmed cell death (Millar et al., 2008). The most prominent function of mitochondria is energy conversion (Figure 1). Pyruvate the product of cytosolic glycolysis is imported via the mitochondrial pyruvate carrier (AtMPC) (Wang et al., 2014). Within the mitochondrial matrix pyruvate is oxidized by the pyruvate dehydrogenase complex to acetyl coenzyme A (AcCoA) (Denton, 2009; McCommis and Finck, 2015). AcCoA is processed in the TCA cycle. The TCA cycle produces reducing equivalents NADH and $FADH_2$, ATP and CO_2 (Araújo et al., 2012). NADH and $FADH_2$ are needed for the ETC to generate an inward facing proton gradient. The first proton pump complex 1 or NADH:ubiquinone oxidoreductase transfers electrons from NADH + H^+ to ubiquinone (Mimaki et al., 2012; Liu and Lu, 2016). Complex II or succinate dehydrogenase accepts electrons from

$FADH_2$ (Cecchini, 2003). The second proton pump complex III or cytochrome c - oxidoreductase transfers electrons coming from complex I and II to cytochrome c (Guo et al., 2018). Complex IV or cytochrome c oxidase accepts electrons from cytochrome c, transfers them to ½ O_2 and converts it with two protons to H_2O while pumping protons into the IMS (Mansilla et al., 2018). The backflow of protons into the mitochondrial matrix catalyzes the ATP production via ATP synthase and produces ATP from ADP and inorganic phosphate (Junge and Nelson, 2015). Inorganic phosphate is imported by phosphate transporters in the IMM (Wang et al., 2017).

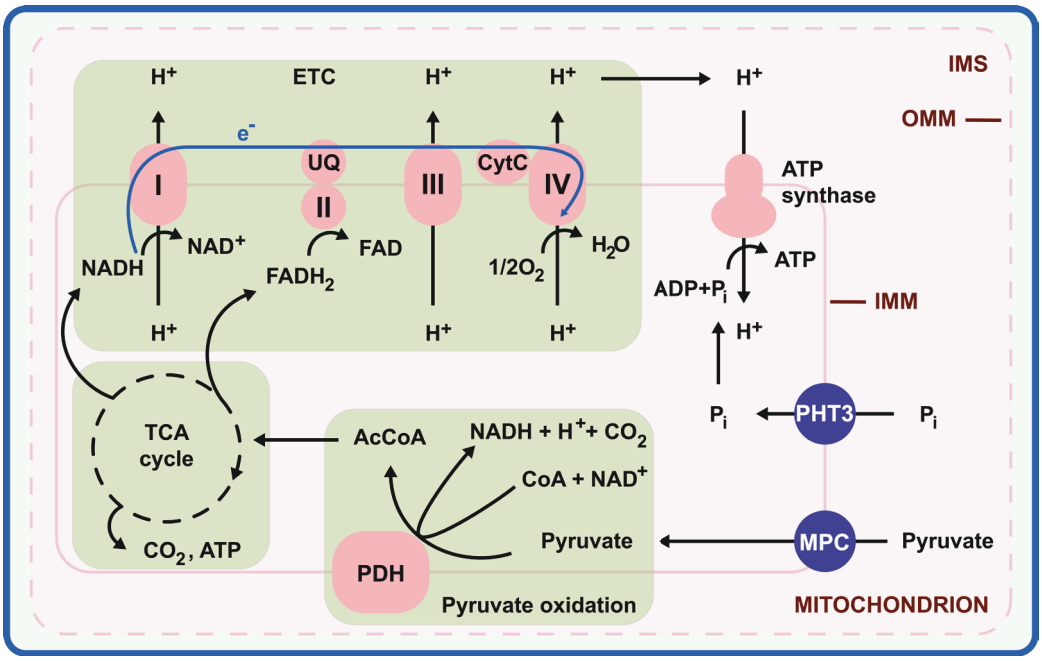

Figure 1. Energy conversion in mitochondria.

Abbreviations: I-IV, complex I to IV of the electron transport chain: I, NADH:ubiquinone oxidoreductase; II, Succinate dehydrogenase; III, cytochrome c – oxidoreductase; IV, cytochrome c oxidase; AcCoA, acetyl coenzyme A; CoA, coenzyme A; CytC, cytochrome C; ETC, electron transport chain; IMM, inner mitochondrial membrane; IMS, intermembrane space; OMM, outer mitochondrial membrane; AtPDH, pyruvate dehydrogenase complex; AtPHT3, phosphate transporter 3 family; Pi, inorganic phosphate; AtMPC, mitochondrial pyruvate transporter; TCA cycle, tricarboxylic acid cycle; UQ, ubiquinone. Green boxes indicate metabolic pathways belonging to pyruvate oxidation, TCA cycle or ETC, respectively.

Metabolic processes require the shuttle of metabolites across the organella membranes. Mitochondria are physically and metabolically connected to other subcellular compartments (Fransen et al., 2017; Kmiecik et al., 2016; Burch-Smith et al., 2011). Non-selective voltage-dependent anion channels in the outer mitochondrial membrane (OMM) allow the free diffusion of solutes into the IMS (Takahashi and Tateda, 2013). Selective transporters facilitate the

import into the mitochondrial matrix. Several of these transporters belong to the mitochondrial carrier family (MCF) (Haferkamp and Schmitz-Esser, 2012).

MCF members were described in plants, yeast and mammals (Palmieri and Monné, 2016; Picault et al., 2004). While most MACF members were localized in mitochondria, some reside in peroxisomes (Bernhardt et al., 2012b; van Roermund et al., 2016; Linka et al., 2008), plastids (Gigolashvili et al., 2012; Bedhomme et al., 2005), the endoplasmic reticulum (ER) (Hoffmann et al., 2013) or the plasma membrane (Rieder and Neuhaus, 2011), 58 MCF proteins were identified in Arabidopsis. They share a highly conserved tripartite sequence of roughly 100 repeating amino acids. Each repeat forms two α-helices separated by a hydrophilic loop and contains the signature PFAM PF00153 motif (Palmieri, 1994). Structural analyses of protein sequences, tertiary structures and substrate binding sites predicted three types of substrates for these transporters: (1) nucleotides, (2) carboxylates and (3) amino acids (Robinson and Kunji, 2006; Palmieri et al., 2011). Most known MCF members can be assigned to these classes: (1) nucleotides: AMP/ADP/ATP (Linka et al., 2008; Arai et al., 2008; Rieder and Neuhaus, 2011; Hoffmann et al., 2013; Haferkamp et al., 2002; Gigolashvili et al., 2012; Palmieri et al., 2008b; Lorenz et al., 2015), NAD/NADH (Bernhardt et al., 2012b; van Roermund et al., 2016; Palmieri et al., 2009), CoA (Zallot et al., 2013) or FAD (Bedhomme et al., 2005). (2) di-/tri/carboxylates: malate, oxaloacetate, 2-oxoglutarate, succinate (Palmieri et al., 2008a; Monné et al., 2018), (3) amino acids: aspartate, glutamate, cysteine sulfonate, cysteate (Monné et al., 2018), arginine or ornithine (Palmieri et al., 2006b; Planchais et al., 2014). Some carriers also transport sulfate and thiosulfate (Monné et al., 2018; Palmieri et al., 2008a; Monné et al., 2017), S-adenosyl methionine (SAM) (Bouvier et al., 2006; Palmieri et al., 2006a) or phosphate (Hamel et al., 2004).

MCF members mediating the import of organic phosphate into mitochondria belong to the phosphate transporter family 3 (PHT3) (Wang et al., 2017). They perform a phosphate/proton symport into the mitochondrial matrix but are thought to work as $H_2PO_4^-/OH^-$ antiporter under physiological conditions as well (Lodish et al., 2001; Igamberdiev and Kleczkowski, 2015).The import of phosphate is essential for mitochondrial ATP synthesis. Two functional redundant members of the MCF have been described to perform phosphate import in yeast, ScMir1 and ScScPic2 (Guérin et al., 1990; Hamel et al., 2004), and one member in mammals (Kolbe et al., 1984). ScMir1/ScPic2-deficient yeast mutants were not viable on non-fermentable carbon sources due to non-functional ATP synthesis and ETC (Zara et al., 1996). But it has been shown in yeast and mammals that some mitochondrial phosphate transporters rather import copper into mitochondria. In the absence of ScMir1, ScPic2 was proposed to ba a redundant phosphate carrier under heat stress conditions (Hamel et al., 2004). Recent studies revealed that ScPic2 imports copper either in form of an yet unidentified low molecular weight non-proteinaceous copper-ligand or phosphate/copper complex (Vest et al., 2013; Mohl

et al., 1990; Mwamba et al., 2016). Another copper carrier was found in the iron import-related ScMrs3 (Vest et al., 2016). The mammalian orthologue of ScPic2 is SLC25A3. SLC25A3 transports phosphate but accepts copper as primary substrate (Kolbe et al., 1984; Boulet et al., 2018). The absence of ScPic2 or SLC25A3 impairs respiration and the activity of the multi-protein complex cytochrome C oxidase (COX or complex IV) (Cobine et al., 2006; Vest et al., 2013; Boulet et al., 2018).

COX is located in the IMM and is the last multi-protein electron acceptor of the ETC (Figure 2). COX reduces oxygen and pumps protons into the IMS to generate the mitochondrial proton gradient. More than 30 proteins were identified to be involved in the biogenesis and assembly of COX, including the delivery of redox-active metal centers and prosthetic groups. The importance of COX is reflected by severe phenotypes in loss-of-function mutants. The impairment of COX assembly or function results in severe growth defects or lethal embryos (Mansilla et al., 2018; Jett and Leary, 2018; Soto et al., 2012; Khalimonchuk and Rödel, 2005). In Arabidopsis, COX contains two copper centers, a di-copper center in COX-subunit AtCOX2 and one copper in subunit AtCOX1. Copper is crucial for the transfer of electrons from cytochrome c to COX and finally to O_2 (Horn and Barrientos, 2008). The assembly of COX and the insertion of copper is highly regulated and involves numerous proteins, which were mostly studied in yeast and mammals. In the IMS of yeast, the copper-binding protein ScCOX17 transfers copper to the IMM proteins ScSco1 and ScCOX11 (Horng et al., 2004). ScSco1 delivers copper to COX subunit ScCOX2, while ScCOX11 transfers it to ScCOX1. The source of copper for ScCOX17 is thought to be an unknown non-proteinaceous copper-ligand originating from the copper storage pool within the mitochondrial matrix (Cobine et al., 2004; McCormick et al., 2015). ScPic2 and ScMrs3 transport copper into the mitochondrial matrix. But COX assembly requires copper in the IMS. A transporter shuttling copper into the IMS allowing the binding by ScCOX17 in unknown (Mansilla et al., 2018). Only few of these yeast proteins important in COX assembly have been identified in plants. The delivery of copper to AtCOX2 is performed by the ScSco1 homologue AtHCC1. AtHCC1 loss-of-function lines were embryo-lethal (Steinebrunner et al., 2011, 2014). The knockdown of the Arabidopsis homologue of ScCOX11 led to reduced COX activity and reduced growth (Radin et al., 2015). Another copper chaperone, AtCOX10, is involved in heme synthesis for AtCOX1. Homozygous mutants were embryo-lethal, heterozygous plants were impaired during embryogenesis and COX activity (Mansilla et al., 2015). Other genes involved with COX assembly have been recently identified in Arabidopsis (Mansilla et al., 2018). This list of genes also includes Arabidopsis homologues for yeast ScPic2 and mammal SLC25A3: the PHT3 family. These results suggest that PHT3 proteins AtPHT3;1-3 might be involved in phosphate and copper import.

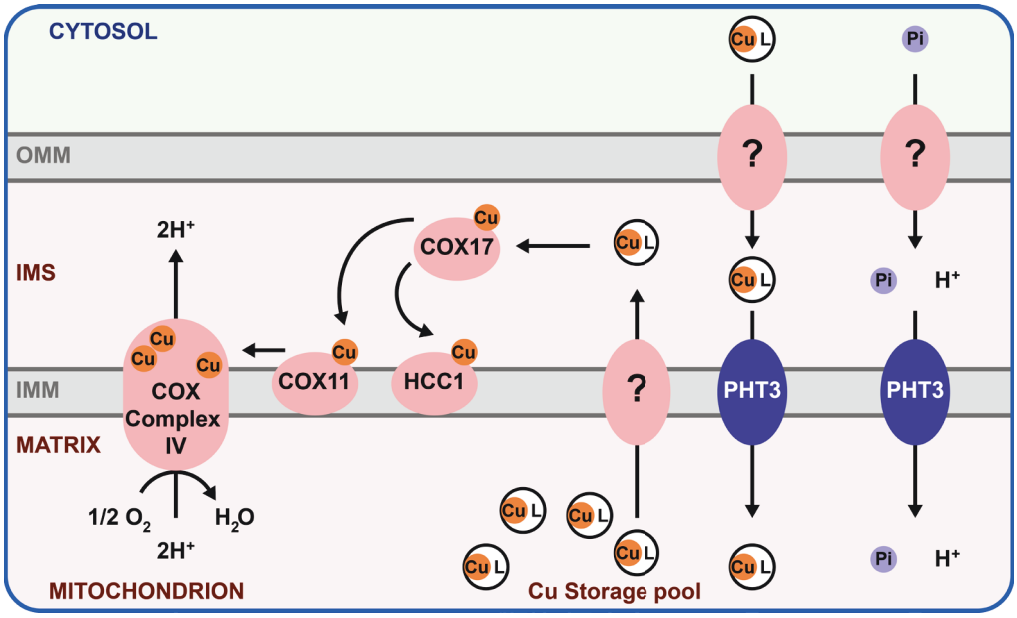

Figure 2. Role of copper in COX/complex IV assembly.

Copper is imported into mitochondria bound to a non-proteinaceous ligand and stored in the mitochondrial matrix copper storage pool. If the ligand is transported or binds to copper before and after the transport process is unknown. Copper is transported back to the IMS and is bound to AtCOX17. AtCOX17 transfers copper to AtCOX11 and AtHCC1. They transfer copper to COX subunit AtCOX1 and AtCOX2, respectively. Abbreviations: COX, cytochrome c oxidase; Cu, copper; CuL, non-proteinaceous copper-ligand; AtHCC1, homologue of copper chaperone ScSco1; IMM, inner mitochondrial membrane; IMS, intermembrane space; OMM, outer mitochondrial membrane; PHT3, members of the phosphate transporter family 3. Predicted transporters are marked with "?".

Arabidopsis, poplar, tomato, maize, rice, soybean or wheat contain various isoforms of the PHT3 family (Wang et al., 2017). Arabidopsis contains three isoforms: At5g14040 (AtPHT3;1), At3g48850 (AtPHT3;2) and At2g17270 (AtPHT3;3). The phosphate uptake by roots is fairly good described (Nussaume et al., 2011). But less is known about the intracellular transport (Versaw and Garcia, 2017). Members of the Arabidopsis PHT3 family are thought to import of phosphate as Pi/H+ symport, Pi/OH- antiport or as Pi homo-exchange between cytosol and mitochondrial matrix (Zhu et al., 2012). AtPHT3;1 and AtPHT3;2 have been indirectly shown to mediate an import of phosphate into mitochondria via phenotype suppression assays with ScMir1/ScPic2-deficient yeast mutants (Hamel et al., 2004). The physiological roles of AtPHT3;1-3 have been assigned to salt stress response, ATP content and gibberellin metabolism during seedling stage (Zhu et al., 2012). AtPHT3;1 was studied in more detail. AtPHT3;1 is a ubiquitous highly expressed MCF member (Millar and Heazlewood, 2015) and essential for seed germination and vegetative growth. AtPHT3;1 overexpression lines accumulate more ATP and reactive oxygen species and have a higher respiration rate. Genes involved in plant development and growth are suppressed, while redox homeostasis and the alternative respiration pathway (alternative oxidase pathway) are upregulated. These observations are thought to be a direct result of mitochondrial dysfunction and represent a

coping mechanism (Jia et al., 2015). Overexpression lines of AtPHT3;2 and AtPHT3;3 did not show any of these phenotypes. Likewise, the biochemical function and physiological role of AtPHT3;3 in Arabidopsis has not been shown yet.

This study provides evidence for the physiological function of AtPHT3;3 in seed development, discusses the shoot apical meristem (SAM) and reproductive tissue-specific expression and the phylogenetically relation to copper transporters. AtPHT3;3 might represent a primary copper transporter expressed in tissues with high energy demand. Under physiological conditions AtPHT3;1 might fuel mitochondria with copper for COX/complex IV of the ETC.

Experimental procedures

Materials

Chemicals and kits were purchased from Sigma-Aldrich (sigmaaldrich.com) or Promega (promega.com). Enzymes and molecular reagents were purchased from New England Biolabs (neb.com) or Thermo Fisher Scientific (thermofisher.com), and Qiagen (qiagen.com). Plant growth media was purchased from Duchefa BV (duchefa-biochemie.com).

Plant material and growth conditions

Ecotype Columbia (Col-0) *Arabidopsis thaliana* was purchased from the European Arabidopsis Stock Centre (NASC) at the University of Nottingham (arabidopsis.info). The heterozygous *pht3;3-1*-T-DNA line (GK-432A12) was purchased from NASC, the homozygous *pht3;3-1*-T-DNA line (GK-432A12) was obtained from Gabi-Kat consortium at the University of Bielefeld (gabi-kat.de). The homozygous *pht3;3-2*-T-DNA line (SAIL_591_H09) was provided by Dr. Ilka Haferkamp, University of Kaiserslautern. Seeds were surface-sterilized for 10 minutes with 70 % ethanol and Triton-X-100, followed by 100 % ethanol. Seeds were stratified for at least 3 days and germinated on half-strength MS medium with 0.8 % (w/v) plant agar. Plants were transferred to soil after 14 days and grown under long day conditions (16 h light (100 µmol m^{-2} s^{-1}) / 8 h darkness) at 22 °C (day)/ 18 °C (night) unless stated otherwise.

Bacteria strains and media

For all cloning methods, competent *Escherichia coli* strain mach1 (Invitrogen GmbH, Karlsruhe, Germany) was used. *E. coli* was cultivated in either liquid lysogeny broth (LB, 10 g/l tryptone, 5 g/L yeast extract, 5 g/L NaCl, 15 g/L agar, shaking at 200 rpm) or on solid LB medium (with additional 15 g/L plant agar) with appropriate antibiotics at 37 °C.

Cloning procedures

In silico DNA and mRNA sequences of all mentioned Arabidopsis genes were received via Aramemnon (aramemnon.uni-koeln.de/). Standard cloning methods were performed according to Russel and Sambrook (2001). Gene amplification and insertion into expression vectors were performed via Gibson assembly (New England Biolabs, (Gibson, 2011)) using primers synthesized by Sigma-Aldrich. Gene sequences were verified via Macrogen (dna.macrogen.com/). Primers and vectors are listed in Supplemental material.

For sub-cellular localization studies AtPHT3;3 was cloned into the pUB-Dest vector system (Grefen et al., 2010). Expression vector pUBC-YFP was opened via restriction digest using PspXI and SpeI. AtPHT3;3 coding sequence (CDS) was amplified from Arabidopsis ecotype Col-0 leaf cDNA with primers BH273 (5'-TAATCTGAGTTTTTCTGATTAACACACCATGGCAAGAGTCAAGAGTAAACTAGACG-3')

and BH274 (5'-CAGCTCCTCGCCCTTGCTCACCATACCGCTACCACCCACTGATAATTTAGCTGCATC-3'). PCR product and expression vector pUBC-YFP were fused via Gibson assembly. Resulting vector pBH61 was used for transient expression in *N. benthamiana* and localization studies. Expression was driven by an Arabidopsis ubiquitin-10 promoter.

Complementation of Arabidopsis *pht3;3-1*-T-DNA insertion lines were generated using the pHygII-UT-c-term-Venus expression vector (Walter et al., 2004). pHygII-UT-c-term-Venus was digested with KpnI and SacI removing the sequence for the fluorescent protein in the process. AtPHT3;3 CDS was amplified via PCR with BH52 (5'-CGACCTCGAGGGTACATGACAAGAGTCAAGAGTAAACTAG-3') and BH53 (5'-TTCATCTTCATGAGCTTTATCACACTGATAATTTAGCTG-3') from Arabidopsis ecotype Col-0 leaf cDNA and fused with the expression vector via Gibson assembly. The resulting vector pBH02 was used for the transformation of homozygous *pht3;3-1*-T-DNA line (GK-432A12) and homozygous *pht3;3-2*-T-DNA line (SAIL_591_H09). Expression was driven by an Arabidopsis ubiquitin-10 promoter.

Transient expression in *N. benthamiana* and confocal laser scanning microscopy

Agrobacterium tumefaciens strain GV3101(pMP90) (Koncz and Schell, 1986) was transformed according to Höfgen and Willmitzer (1988). YPD medium was inoculated with *A. tumefaciens* and grown over night at 28 °C. Cells were harvested via centrifugation (10 min, 3000 g) and resuspended in infiltration buffer (10 mM $MgCl_2$, 10 mM MES, pH 5.7, 100 µM acetosyringone) to an OD_{600} of 0.5. *N. benthamiana* leaves were infiltrated with the cell suspension and incubated for two days at long day conditions (16 h light (130 µmol m^{-2} s^{-1}) and 8 h darkness) at 25 °C (day)/ 20 °C (night) (Waadt and Kudla, 2008). Protoplasts were isolated two days after infiltration. *N. benthamiana* leaves were cut into 0.5 x 0.5 cm pieces and incubated in protoplast digestion solution (1.5 % (w/v) cellulase R-10, 0.4 % (w/v) macerozyme R-10, 0.4 M mannitol, 20 mM KCl, 20 mM MES pH 5.6 (KOH), 10 mM $CaCl_2$, 0.1 % (w/v) BSA) for 2 h at 30 °C. Isolated protoplasts were resuspended in W5 solution (154 mM NaCl, 125 mM $CaCl_2$, 5 mM KCl, 2 mM MES pH5.6 (KOH)) and directly used for microscopy (Sheen, 2002). Protoplasts were examined using a Zeiss LSM 780 Confocal Microscope and Zeiss ZEN software. Mitochondria were visualized using the mitochondrial marker plasmid IVD-eqFP611 (Forner and Binder, 2007). Excitation/emission settings used in this study: YFP (514 nm / 493 to 550 nm), IVD-eqFP611 (561 nm / 580 to 625 nm) and Chlorophyll A (488 nm / 640 to 710 nm). Pictures were processed using Fiji software (fiji.sc) and Adobe Photoshop CS6 (Adobe Systems).

Transcriptome analysis and bioinformatical procedures

Transcriptomic data of At5g14040 (AtPHT3;1) and At2g17270 (AtPHT3;3) in Arabidopsis were extracted from the TraVA database (http://travadb.org/). Protein alignments and phylogenetic trees (neighbor joining method) were performed with CLC Sequence viewer (Version 8.0) using protein sequences from Aramemnon (aramemnon.uni-koeln.de/) and UniProt (uniprot.org/). Complete list of proteins used for sequence analysis, see Supplemental material.

Isolation of genomic DNA from Arabidopsis

Arabidopsis gDNA was isolated according to a modified protocol described by Kasajima et al. (2004). One leave of a at least 4 weeks old plant was pulverized in liquid nitrogen and solubilized in 250 µL extraction buffer (0.2 M Tris, pH7.5 (HCl), 0.25 M NaCl, 0.025 M EDTA, 0.5 % (w/v) SDS). Insoluble cell material was pelleted via centrifugation for 1 min at 16.000 g at RT. The supernatant was transferred and mixed with 500 µL 100 % (v/v) isopropanol and incubated for 10 min. After centrifugation for 10 min at 16.000 g at RT, the DNA pellet was air-dried and resuspended in 50 µL nuclease free H_2O by mixing the sample for 30 min at 37 °C.

Identification of T-DNA insertion lines and quantitative reverse transcriptase-polymerase chain reaction (qRT-PCR)

Phenotyping experiments were performed using the following T-DNA insertion lines: heterozygous *pht3;3-1*-T-DNA line (GK-432A12), homozygous *pht3;3-1*-T-DNA line (GK-432A12), homozygous *pht3;3-2*-T-DNA line (SAIL_591_H09). These lines were tested for the insertion of T-DNA via PCR using leaf gDNA with gene specific primers NL516 (5'-TCATTGGAGAGAAGATGGTGG-3') and NL517 (5'-AAACCGGAAGGAATGCTATTG-3') and T-DNA specific primers P52 (5'-CCCATTTGGACGTGAATGTAGACAC-3') and P49 (5'-CCCATTTGGACGTGAATGTAGACAC-3').

Transcript level of *pht3;3* in T-DNA insertion and complementation lines was tested via quantitative real time PCR (qRT-PCR) with total RNA from respective Arabidopsis lines including ecotype Col-0. RNA was isolated from 3 weeks old seedlings collected from half-strength MS plates using the GeneMATRIX Universal RNA Purification Kit (Roboklon GmbH). Five individual plants were pooled and counted as one biological replicate. Complementary DNA (cDNA) was synthesized using Superscript II RNase H^- Reverse Transcriptase (Thermo Fisher Scientific). The cDNA synthesis was performed according to the manufacturers' instructions. The resulted cDNA pools were used as template for PCR or Real-time PCR with gene-specific primers. Transcript levels in Arabidopsis were determined by qRT-PCR with the MESA-SYBR-Green II Kit without ROX (Eurogentec Germany GmbH) according to the manuals instructions, run with the Standard SYBR-Green protocol of the StepOnePlus™ Real-

Time PCR System (Applied Biosystems, Life technologies Corporation). The BLACK oligonucleotides published by Czechowski et al. (2005) were used as reference primer pair. Five biological replicates per line were collected and tested. All cDNA samples were diluted to a concentration of 35 ng/µL and 1 µL used for transcript measurements using *pht3;3*-3'-UTR specific primers BH84 (5'-GAAGAAACCAGTGGATGCAGCT-3') and BH85 (5'-CTACACAACGCCTCGTATCTACTTG-3'). Transcript level was calculated based on ΔC_T values compared to the wild type (Schmittgen and Livak, 2008; Simon, 2003).

Transformation of Arabidopsis

Arabidopsis was transformed according to Bernhardt et al. (2012). Transgenic lines were selected on half-strength MS medium with appropriate antibiotics.

Analysis of fatty acid degradation in Arabidopsis seeds and seedlings

Degradation of Arabidopsis seed fatty acids used in peroxisomal β-oxidation was analyzed as described in Hielscher et al. (2017). Dried seeds and seedlings from Arabidopsis ecotype Columbia (Col-0), homozygous T-DNA lines *pht3;3-1* and *pht3;3-2* line were examined.

Silique and seed/ seed embryo analysis and chloral hydrate clearing

Arabidopsis siliques or seeds were directly examined or incubated in a chloral hydrate/glycerol/water solution (8:1:2, w/v/v) over night at room temperature to clear the seed tissues for embryo analysis. The chloral hydrate solution was replaced with 70% (v/v) ethanol for microscopy. Seeds and embryos were observed with phase-contrast microscopy (Eclipse Ti, Nikon), siliques via a dissecting microscope (SMZ1500, Nikon).

Pollen analysis and Alexander/DAPI staining

For viability staining of Arabidopsis pollen, primary inflorescences were collected 1 day after flowering and incubated for 5 minutes in 1: 50 Alexander's stain (Stock: 10 ml 96 % ethanol, 1 ml 1 % (w/v) malachite green (in 96 % ethanol), 25 ml glycerol, 5 ml 1 % (w/v) acid fuchsin (in distilled H_2O), 4 ml glacial acetic acid, 100 ml distilled H_2O; Alexander, 1969). Pollen were directly analyzed via phase-contrast microscopy (Eclipse Ti, Nikon).

For pollen nuclei visualization, pollen collected 1 day after flowering were stained with DAPI according to Johnson-Brousseau and McCormick (2004) with a working solution of 1 µg/ml DAPI in distilled water. Pollen were directly analyzed via fluorescence microscopy (Zeiss Axio).

Pollen germination assay

Pollen germination was observed according to Boavida and McCormick (2007). Pollen germination medium (1 mM $CaCl_2$, 1 mM $Ca(No_3)_2$, 1 mM $MgSO_4$, 0.01% (w/v) H_3Bo_3, 18 % (w/v) Sucrose, 0.5 % (w/v) Phyto-agar, pH 7 (NaOH)) was heated up and spread evenly on a microscope slide. Primary inflorescences collected 1 day after flowering were incubated for 30 min at 28 °C in sealed pipette tip box containing filter paper drained in water to hydrate pollen. Flowers were gently brushed on the solidified pollen germination medium to release pollen. Flowers were placed into the corners of the microscope slide on top of the medium after use. Slides were put into the tip box and incubated for 35 min at 37 °C, followed by 4 h at RT (22 °C). Pollen were directly examined via phase-contrast microscopy (Eclipse Ti, Nikon).

Results

AtPHT3;3 is localized in mitochondria in transiently transformed tobacco protoplasts

MCF members have been found in plastids (AtPAPST1/TAAC, Gigolashvili et al., 2012), peroxisomes (AtPNC1/2, Linka et al., 2008; AtPXN, van Roermund et al., 2016), the endoplasmic reticulum (AtER-ANT1, Hoffmann et al., 2013), the plasma membrane (AtPM-ANT1, Rieder and Neuhaus, 2011). Most MCF members reside in the IMM including dicarboxylate carriers AtDIC1-3, AtUCP1-2 or ATP-Mg/phosphate carriers AtAPC1-3 (Palmieri et al., 2008a; Picault et al., 2004; Monné et al., 2018, 2017). The subcellular localization of AtPHT3;3 was not verified so far. *In silico* prediction algorithms (Aramemnon, SUBA3 (http://suba3.plantenergy.uwa.edu.au)) suggest a mitochondrial localization. No evidences via GFP-fusion protein or MS/MS data are publicly available. Fusion protein AtPHT3;3-YFP (C-terminal yellow fluorescent protein, Arabidopsis ubiquitin-10 promoter) was transiently expressed in independent *N. benthamiana* leaves. Mitochondrial marker fusion protein IVD-eqFP611 (cauliflower mosaic virus 35S promoter, Forner and Binder, 2007) was expressed simultaneously. Two days after infiltration protoplasts were isolated and directly used for confocal laser scanning microscopy. All observed protoplasts showed a co-localization of the YFP-fusion protein (shown in yellow) with the mitochondrial marker fusion protein IVD-eqFP611 (shown in red). These results suggest a mitochondrial localization for AtPHT3;3 (Figure 3).

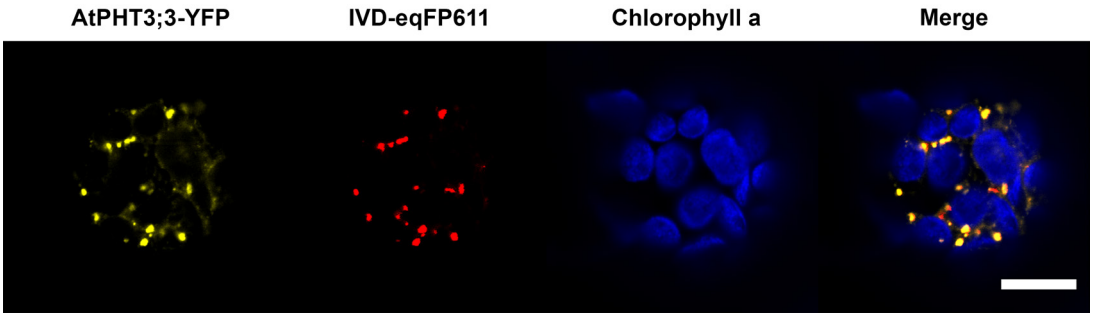

Figure 3. Subcellular localization of AtPHT3;3 in transiently transformed protoplasts.
Fluorescent signals of C-terminal AtPHT3;3-YFP fusion protein (yellow), mitochondrial marker protein IVD-eqFP611 (red), chlorophyll a/chloroplasts (blue). The merged images indicate an overlap of the fluorescent signals (orange) detected via confocal laser scanning microscopy in transiently transformed *N. benthamiana* protoplasts. Co-localization of mitochondrial marker with AtPHT3;3 (Scale bar = 10 µM).

Homologues of AtPHT3;3 in yeast and mammals belong to the COX/complex IV assembly factors in the mitochondrial ETC

AtPHT3;3 belongs to the PHT3 family in Arabidopsis. Only AtPHT3;1 and AtPHT3;2 have been characterized so far. They have been described to transport phosphate in the absence of ScMir1 and ScPic2 in yeast (Hamel et al., 2004). Physiological studies of Arabidopsis suggest AtPHT3;1-3 to be involved in respiration, salt stress response and ATP availability (Zhu et al., 2012; Jia et al., 2015). Homologues in soybean and *Lotus japonicas* have been shown to transport phosphate in reconstituted proteoliposomes (Takabatake et al., 1999; Nakamori et al., 2002). Reports about the transport function of AtPHT3;3 are not available.

Based on homologous copper transporters ScPic2 and SLC25A3 in yeast and mammals, respectively, AtPHT3;3 might transport another primary substrate distinct from phosphate transported by AtPHT3;1 and AtPHT3;2. To assign a putative transport function to AtPHT3;3, PHT3 members from Arabidopsis, copper/phosphate transporters from yeast and mammals and PHT3 homologues from maize (6), rice (7), tomato (4) and poplar (9) were analyzed phylogenetically (Figure 4, gene list used for this alignment, see Supplemental material). As predicted, the copper carrier ScPic2 clusters with the mammalian SLC25A3 from human, bovine, mouse and rat. PHT3 members of Arabidopsis are clearly distinct and form groups with plant homologues. This is in agreement with previous alignments of Arabidopsis PHT3 proteins with rice and poplar homologues (Wang et al., 2017). Interestingly, the AtPHT3;3 cluster with seven genes from maize, rice, tomato and poplar shares a branch with the phosphate/copper cluster including ScPic2, SLC25A3, ScMir1 and ScMrs3 indicating a closer relation to these transporters based on amino acid sequences. However, the AtPHT3;3 cluster has clearly diverged from the phosphate/copper cluster based on the separating branch length indicating amino acid changes since the separation of both clusters. This might indicate some kind of specification for AtPHT3;3 and its homologues.

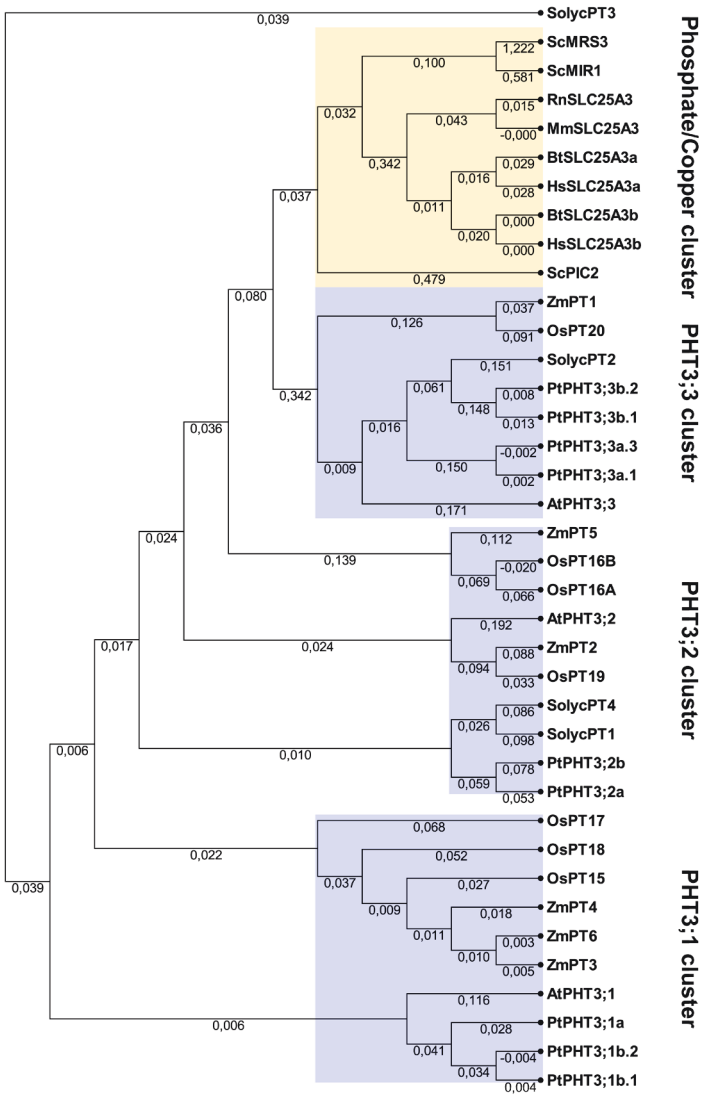

Figure 4. Unrooted phylogenetic tree of phosphate carriers in Arabidopsis, rice, tomato, maize, poplar, yeast and mammals.

The tree was generated using CLC Sequence Viewer (Version 8) based on the neighbor joining method with 1000 replicates for bootstrapping analysis of the phylogenetic tree and gap open cost of 10.0, gap extension cost of 1.0 and end gap cast (cheap) for the alignment. Phylogenetic distances are indicated. Phosphate/copper carriers are highlighted, clusters of either AtPHT3;1, AtPHT3;2 or AtPHT3;3 are highlighted in blue. Numbers indicate branch length.

AtPHT3;3 only shares 53.3 % sequence identity with AtPHT3;1 and 51.5 % with AtPHT3;2, while AtPHT3;1 and AtPHT3;2 share a higher sequence identity of 68.5 % (Figure 5A). To investigate the overlap of sequences within the PHT3;3 cluster (including homologues in additional plant species) six residues have been compared (Figure 5B). These residues were identified to be important for phosphate binding in yeast and mammals (Phelps et al., 1996; Dolce et al., 1994). Five highly conserved residues were shown to be crucial for ScMir1 and an additional one for mammalian SLC25A3 (Phelps et al., 1996; Dolce et al., 1994). These residues are identical in AtPHT3;1 and AtPHT3;2: His(H)-54 (position I), Asp(D)-61 (position II), Cys(C)-65 (position III), Glu(E)-148 (position IV), Glu(E)-159 (position V) and Asp(D)-262

(position VI) (positions correspond to AtPHT3;3 amino acid sequence). Zhu et al.(2012) observed mutations in two of these key residues in AtPHT3;3 (III and IV): Val(V) instead of Cys(C)-65 and Gln(Q) instead of Glu(E)-148. Val(V)-65 (position III) is conserved in the AtPHT3;3 cluster: tomato (SolycPT2), rice (OsPT20, OsPT16B), maize (ZMPT1) and poplar (PtPHT3;3a.1, PtPHT3;3a.3, PtPHT3;3a.1, PtPHT3;3a.2). Gln(Q)-148 (position IV) is conserved in maize (ZMPT1), rice (OsPT20) and poplar (PtPHT3;3a.1, PtPHT3;3a.3).

These results suggest that AtPHT3;3 and its homologues might have another function, probably distinct from phosphate transport.

A

	AtPHT3;1	AtPHT3;2	AtPHT3;3	SolycPT2	OsPT16B	OsPT20	ZmPT1	PtPHT3;3a.1	PtPHT3;3a.3	PtPHT3;3b.1	PtPHT3;3b.2	BtSLC25A3	ScPIC2	ScMIR1
AtPHT3;1	-	68.5	53.3	51.4	69.1	52.0	53.0	52.6	51.9	50.0	49.6	50.5	50.2	41.2
AtPHT3;2	68.5	-	51.5	50.5	66.9	50.7	49.2	52.6	52.6	50.4	50.0	51.2	46.6	40.6
AtPHT3;3	53.3	51.5	-	66.1	45.3	71.2	75.6	74.2	76.2	69.9	70.9	44.9	39.9	34.7

B

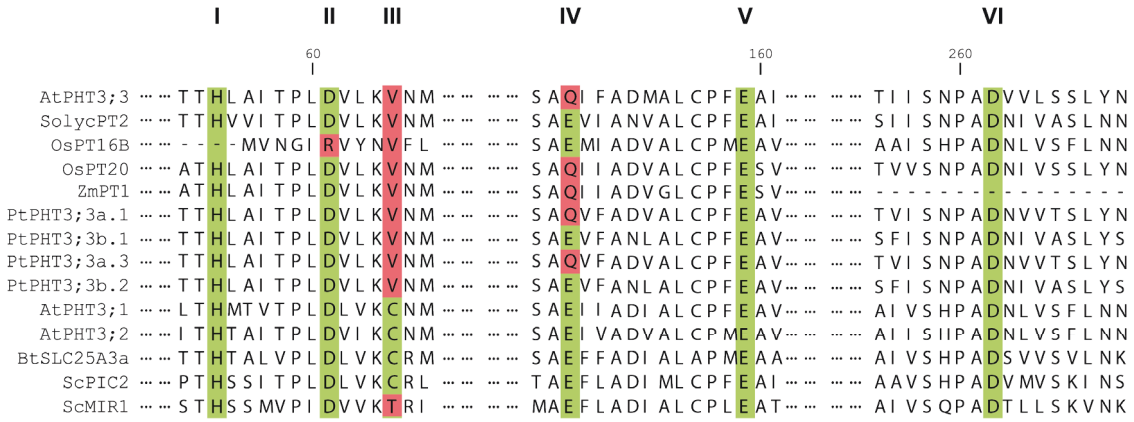

Figure 5. Sequence comparison of AtPHT3;3 with homologues from yeast, mammals, maize, rice, tomato and poplar.

(A) Protein sequence identity [%] of AtPHT3;3 and closest homologs according to phylogenetic analysis (calculated via SIM (expasy.org) (Huang and Miller, 1991). (B) Protein sequence alignment (CLC sequence viewer, aligned with CLC sequence viewer, gap open cost of 10.0, gap extension cost of 1.0 and end gap cost (as any other)) of the same homologs showing conserved regions putatively responsible for phosphate binding according to data from yeast and bovine. Conserved regions are numbered from I to VI and marked green with differing residues in red. Amino acid positions are counted according to AtPHT3;3 amino acid sequence.

AtPHT3;3 is ubiquitously expressed in all tissues of Arabidopsis but shows higher expression in meristems and seeds

COX-related proteins are ubiquitously expressed due to their importance for ATP production. But tissues with high energy demands like meristems or reproductive tissues revealed higher

transcript levels (Mansilla et al., 2018; Liberatore et al., 2016). Loss-of-function mutants impaired in COX assembly show defects during embryogenesis and organogenesis. For instance, homozygous Arabidopsis knockout mutants of the copper-binding AtHCC1 are embryo-lethal. It was shown that seeds were not germinating with most embryos being stuck in heart stage (Steinebrunner et al., 2011; Attallah et al., 2011). Embryonic rescue construct mutants revealed shorter roots, development of only two rosette leaves and lethality after 13 days (Steinebrunner et al., 2014). Heme-transferring AtCOX10-deficient mutants exhibit a similar phenotype during embryogenesis, lower COX activity and accelerated senescence probably due to the lower energy availability (Mansilla et al., 2015). Additionally, mutants of AtCOD1, a protein probably involved in RNA editing of AtCOX2 transcripts, have short roots, bush-like leaf growth and very few flowers with no viable pollen (Dahan et al., 2014). All these phenotypes show that the availability of energy is impaired leading to growth defects.

Arabidopsis tissue-specific transciptomic data was analyzed to reveal the AtPHT3;1 and AtPHT3;3 expression pattern (TraVA database, Klepikova et al., 2015, 2016). Vegetative growth and reproductive tissues including seeds and seed germination were observed: Leaf, internode and root as indicator for vegetative growth and root and shoot meristems, flower tissues and seeds from embryogenesis to germination to screen tissues with relatively high energy demands (Figure 6). AtPHT3;1 is a ubiquitously expressed. High transcript levels were measured compared to other low-expressed MCF members including AtPHT3;3 (Millar and Heazlewood, 2015). Strongest AtPHT3;1expression can be found in anthers and no expression in dry seeds. While AtPHT3;1 is thought to fuel every mitochondrion with phosphates for ATP production, this might indicate a more significant role of AtPHT3;1 during anther or pollen development. Indeed, mitochondria are thought to be the major energy source in these tissues. The extensive production of new pollen and meiotic events in anther tissues might explain the increased need for AtPHT3;1 which correlates with the higher number of mitochondria here (Selinski and Scheibe, 2014; Gómez et al., 2015; Huang et al., 1994). AtPHT3;3 is also ubiquitously expressed. However, AtPHT3;3 is less expressed in photosynthetic active tissues like leaves and sepals, as well as roots. Highest expression can be found in the shoot apical meristem (SAM), the transitioning SAM and inflorescence meristem. These tissues give rise to all flowering parts of the plant including ovaries and pollen inside the stamen. Compared to green tissues, AtPHT3;3 transcript level is also increased during all stages of seed development. Indeed, embryo-specific expression data shows that AtPHT3;3 is up-regulated in unfertilized ovules up to the globular embryo stage and the development of cotyledons and might be predominantly controlled by maternal regulatory pathways (Le et al., 2010; Autran et al., 2011). However, AtPHT3;3 is considerably less expressed in all tissues of Arabidopsis compared to AtPHT3;1. AtPHT3;2 was shown to be leaf-specific via qRT-PCR measurements with no expression in other tissues (Zhu et al., 2012)

and only expressed during senescence and not detectable during embryogenesis (Klepikova et al., 2015; Winter et al., 2007; Le et al., 2010; Nodine and Bartel, 2012).

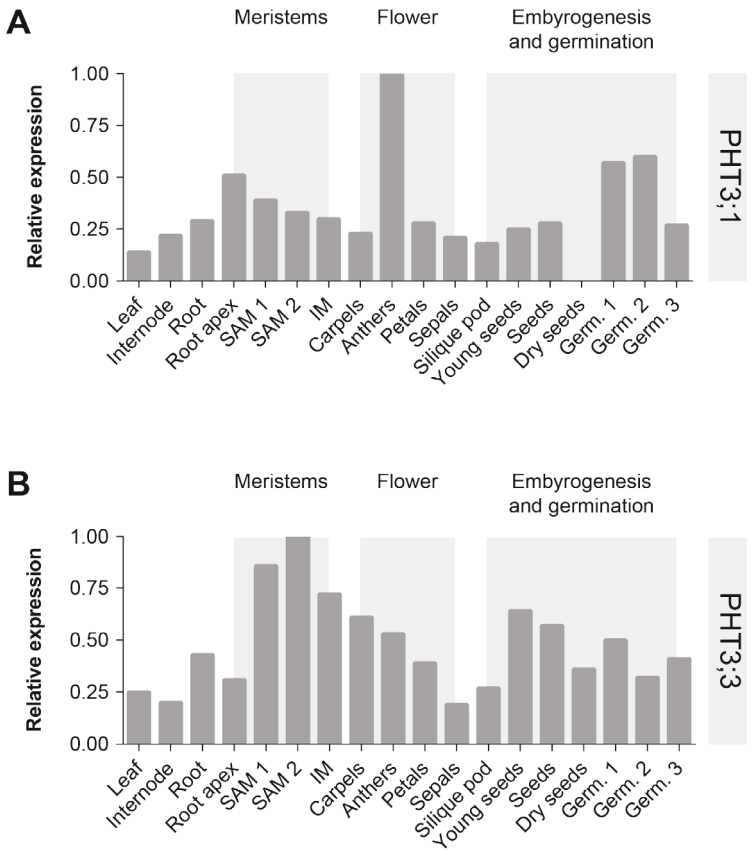

Figure 6. Tissue-specific expression of AtPHT3;1 and AtPHT3;3 in Arabidopsis.

Detailed tissue-specific expression of AtPHT3;1 (A) and AtPHT3;3 (B) in Arabidopsis. Abbreviations and tissue specifications: SAM 1; shoot apical meristem, SAM 2, shoot apical meristem transitioning to inflorescence meristem; IM, Inflorescence meristem; Germ. 1 to 3, germination day 1 to 3 after imbibition. Shown is the relative expression (0.00 to 1.00) based on the highest measured expression value (1.00) found in the dataset for the specific gene transcript of either AtPHT3;1 or AtPHT3;3.

According to these results, AtPHT3;1 might represent the primarily expressed PHT3 member and phosphate transporter in Arabidopsis. The low expressed AtPHT3;2 seems to play a specific role in senescent leaf tissues. AtPHT3;3 is expressed in all tissues, similar to AtPHT3;1 but seems to be more prominent in meristems and reproductive tissues. The impairment of copper supply in reproductive tissues leads to an embryo-lethal phenotype due to the high energy demand in these tissues (Steinebrunner et al., 2011; Radin et al., 2015). A constant expression of two functionally redundant carriers in the same tissue is less plausible. It is likely that AtPHT3;1 and AtPHT3;3 are involved in the transport of different substrates. AtPHT3;1 could act as general phosphate importer while AtPHT3;3 fuels COX with copper to allow the optimal production of ATP via oxidative phosphorylation, especially in reproductive tissues.

AtPHT3;3 deficient T-DNA insertion lines reveal early seed abortion during seed development in Arabidopsis

The impairment of COX or COX-related proteins affects vegetative growth, pollen and seed development in particular. These processes require high amounts of energy, which is provided by mitochondria as ATP (Junge and Nelson, 2015). Homozygous mutants of COX-related genes have been found to be embryo-lethal (Jia et al., 2015; Steinebrunner et al., 2011). AtPHT3;3 is ubiquitously expressed but shows higher expression in seeds during embryogenesis and germination. To investigate the physiological function of AtPHT3;3 as mitochondrial transporter essential for seed development, two Arabidopsis T-DNA insertion lines were established: *pht3;3-1* (GK432A12) and *pht3;3-2* (SAIL591_H09). Mitochondrial ATP production is the major source of energy during extended darkness (Liang et al., 2015). To pronounce a possible COX-related phenotype, plants were grown under short day conditions (8 h light/ 16 h darkness) after an initial phase of long day conditions to induce flowering. Both lines carry the T-DNA insertion in the 5' UTR region (Figure 7A-B). Insertions disrupting the coding sequence were not available within the framework of this study. Both lines show a strong decrease in AtPHT3;3 transcript level, with *pht3;3-1* being a knockout and *pht3;3-2* a strong knockdown mutant, revealed via qRT-PCR (Figure 7C). For complementation analysis and to verify that a putative phenotype is caused by the absence of functional AtPHT3;3, both T-DNA insertion lines were complemented with AtPHT3;3 driven by an Arabidopsis ubiquitin-10 promoter. At least three lines per complementation showed a highly increased AtPHT3;3 transcript above wild type level and were selected for further seed development analysis (Figure 7D).

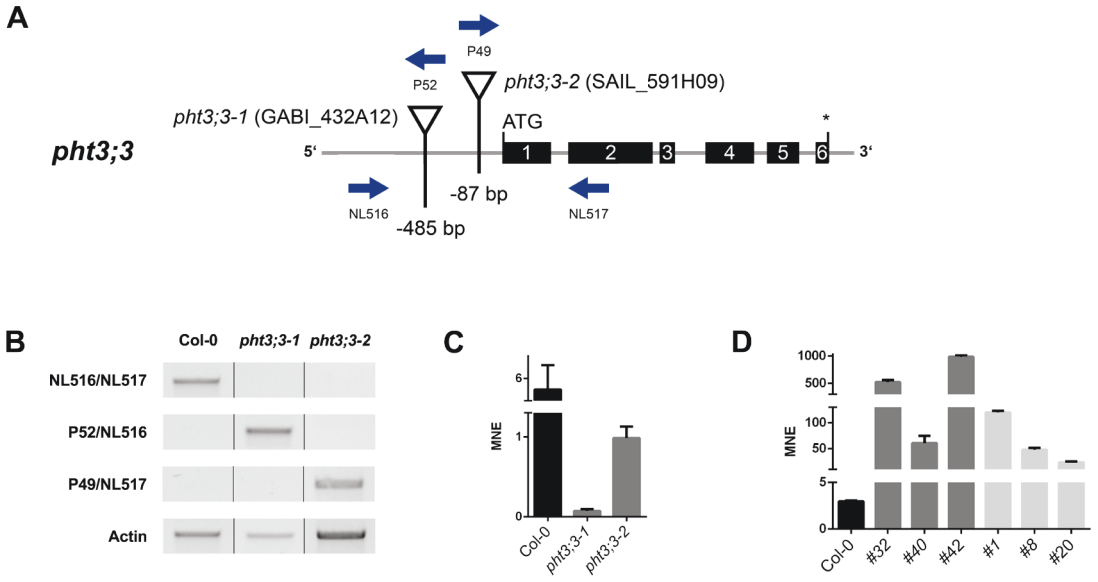

Figure 7. Genotypic analysis of AtPHT3;3 T-DNA insertion and complementation lines.
Homozygous Arabidopsis T-DNA insertion lines *pht3;3-1* and *pht3;3-2* were examined. (A) Schematic representation of T-DNA insertions in lines *pht3;3-1* and *pht3;3-2* in the 5' UTR region of AtPHT3;3 (triangles; base pairs indicate T-DNA insertion in relation to AtPHT3;3 CDS start codon). Black bars indicate exons; blue arrows indicate primers used for T-DNA identification. (B) Identification of T-DNA insertions in respective lines using primers shown in (A) List of primers, see Supplemental material. (C) Transcript level of AtPHT3;3 present in Col-0 and T-DNA insertion lines *pht3;3-1* and *pht3;3-2*. Mean normalized expression (MNE) and standard error, n = 15 technical replicates of five pooled biological samples). (D) Transcript level of AtPHT3;3 present in Col-0 and complemented T-DNA insertion lines as described in Figure 9. Mean normalized expression (MNE) and standard error, n = nine technical replicates of three pooled biological samples).

First, homozygous lines *pht3;3-1* and *pht3;3-2* were analyzed. Siliques of six weeks old plants grown under short day conditions were collected. The visible seed condition (healthy looking green seeds (normal), shrunken and dried seeds (aborted) and empty seed positions (empty)) was examined. Both T-DNA insertion lines showed a decrease in the number of visibly normal seeds (Figure 8A-C). While only 1.25 % of seeds in Col-0 were aborted early during seed maturation, 5.38 % of seeds in *pht3;3-1* and 6.72 % in *pht3;3-2* were aborted (Figure 8B). Although the number of empty positions also increased (1.25 % in Col-0, 4.94 % in *pht3;3-1*, 4.27 % in *pht3;3-2*) this did not vary significantly from Col-0 according to the mathematical test (Figure 8C). Plants grown under optimal conditions contain less than 1% spontaneously aborted seeds (Meinke, 1994). The number of aborted seeds Both independent T-DNA insertion lines were significantly increased, suggesting that the incomplete seed maturation is caused by the mutation of the AtPHT3;3 gene. However, the positions of the defective seeds are randomly distributed.

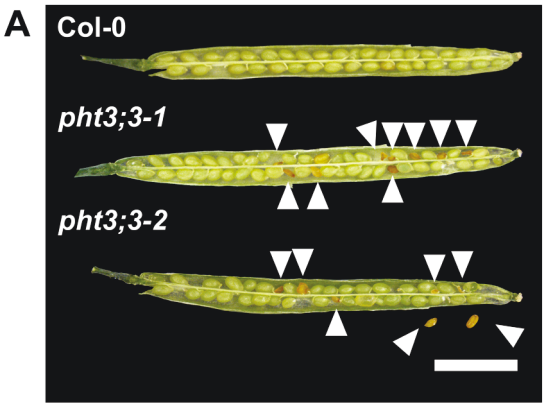

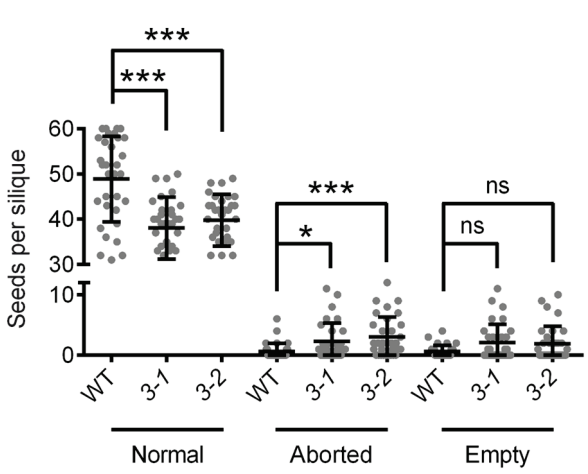

B

Genotype	Seeds Normal (%)	Aborted (%)	Empty (%)
Col-0	97.51	1.25	1.25
pht3;3-1	89.69	5.38	4.94
pht3;3-2	89.02	6.72	4.27

Figure 8. Phenotypic analysis of the homozygous T-DNA insertion lines reveal a defect during seed maturation.

Siliques of the homozygous *A. thaliana* T-DNA insertion lines *pht3;3-1* and *pht3;3-2* were analyzed during seed production within first six weeks. (A) Siliques of six weeks old Col-0 and T-DNA insertion plants were opened and examined via light microscopy. Arrowheads indicate prematurely aborted seeds (Scale bar = 2 mm). (B-C) Analysis of visible seed condition in siliques of Col-0 and T-DNA insertion lines distinguishing between green seeds (normal), prematurely aborted seeds (aborted) and empty positions (empty) (One-way ANOVA with Bonferroni's Multiple Comparison Test, $p<0.05$, n = 32 siliques).

To test if a phenotype already manifests in heterozygous mutants, T-DNA insertion line *pht3;3-1* GK432A12 was isolated and analyzed. Plants were grown under short day conditions (8 h light/ 16 h darkness) after an initial phase of long day conditions to induce flowering. Siliques of six weeks old plants were analyzed (Figure 9A-C). Heterozygous line *pht3;3-1* showed no increase of aborted seeds compared to Col-0. Both lines produce at least 98 % normal sized seeds as previously described for the maturation of wild type seeds (Pan et al., 2014). Transmission of the T-DNA insertion was tested via self-pollination. A change in the Mendelian ratio (3:1 (mutant:wild type) or 1:2:1 (homozygous:heterozygous:wildtype)) in the progeny of self-pollinated heterozygous *pht3;3-1* would hint at an essential role of AtPHT3;3 during germination. No differences were observed between Col-0 and *pht3;3-1* (data not shown). These results suggest that the mutation of AtPHT3;3 is recessive and only homozygous mutants can lead to a mutant phenotype.

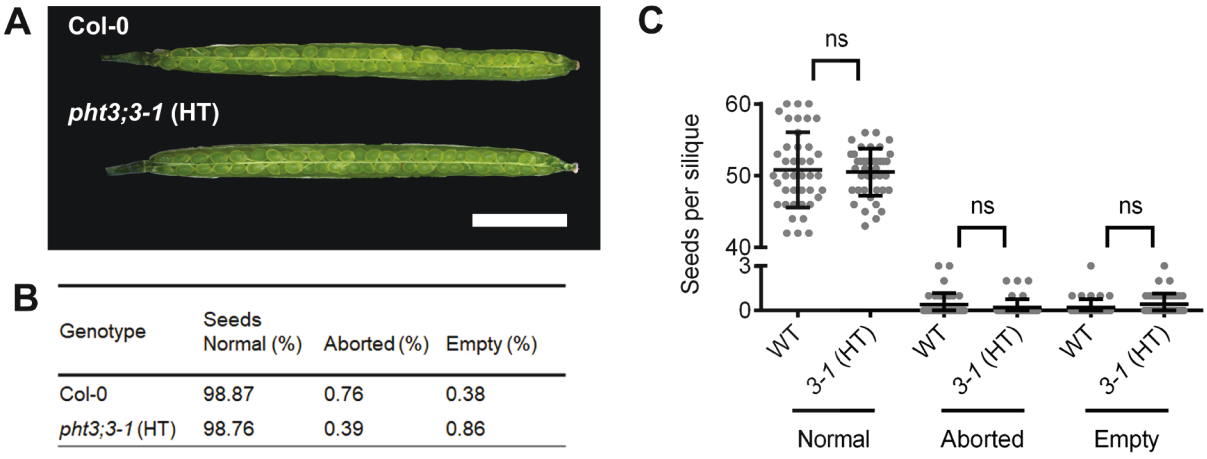

Genotype	Seeds Normal (%)	Aborted (%)	Empty (%)
Col-0	98.87	0.76	0.38
pht3;3-1 (HT)	98.76	0.39	0.86

Figure 9. Phenotypic analysis of the heterozygous T-DNA insertion line shows no visible phenotype during seed production.

The heterozygous *A. thaliana* T-DNA insertion line *pht3;3-1* was examined during seed production in still green siliques. (A) Siliques of six weeks old Col-0 and *pht3;3-1* plants were opened and examined via light microscopy (Scale bar = 2 mm). (B-C) Analysis of visible seed condition in siliques of Col-0 and *pht3;3-1* distinguishing between green seeds (normal), prematurely aborted seeds (aborted) and empty positions (empty) (Unpaired Student's t-Test, $p<0.05$, n = 41 siliques).

To verify that the absence AtPHT3;3 is causing the observed seed phenotype, both T-DNA insertion lines were complemented with AtPHT3;3 driven by an Arabidopsis ubiquitin-10 promoter. Three lines per T-DNA insertion were selected for further seed maturation analysis (Figure 7D, 10A-D). *pht3;3-1* complementation lines #32, #40 and #42, as well as *pht3;3-2* complementation lines #1, #8 and #20 did not reveal the seed phenotype under short day conditions as observed before (Figure 10A). Instead, lines #40, #1, #8 and #20 stored more normal seeds on average than Col-0 (Figure 10C-D). Abnormal seeds or empty seed positions have been sparse in these lines. Only line #32 showed an increase in the number empty seeds positions (Figure 10B-C). Based on this analysis it can be assumed that the absence of AtPHT3;3 is connected to the observed seed maturation phenotype in homozygous T-DNA insertion lines.

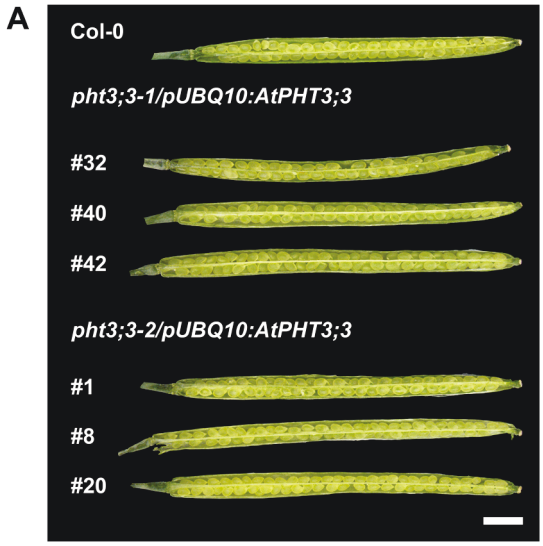

B

Genotype	Seeds Normal (%)	Aborted (%)	Empty (%)
Col-0	96.87	2.03	1.12
#32	87.02	0.1	12.89
#40	97.52	0	2.48
#42	93.47	0.09	6.45
#1	98.73	0.1	1.19
#8	99.74	0	0.27
#20	97.15	0.56	2.31

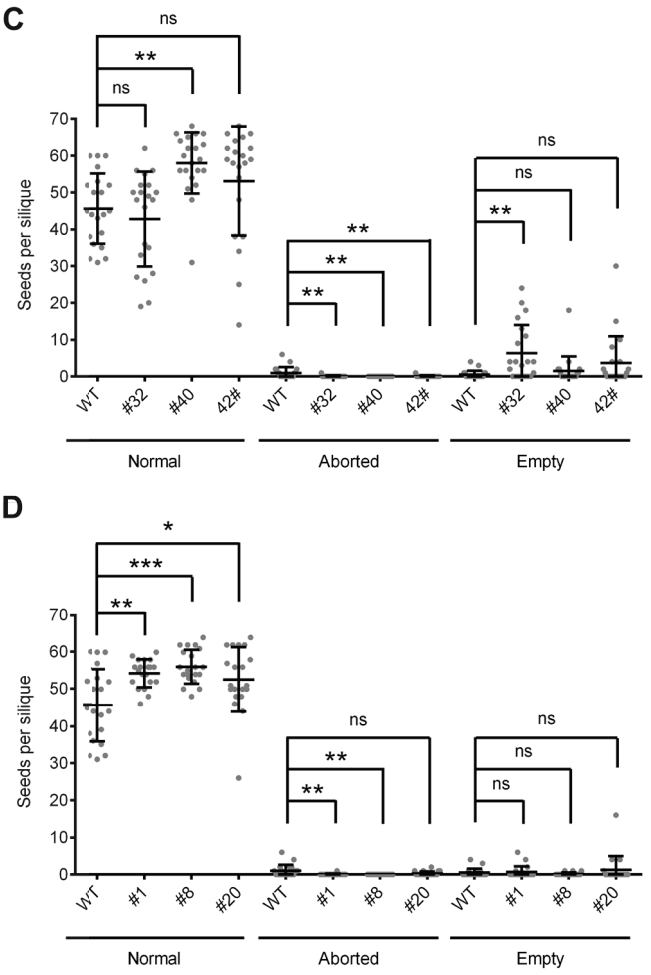

Figure 10. Expression of AtPHT3;3 in T-DNA insertion lines rescues the seed maturation phenotype. Siliques of the complementation lines of homozygous Arabidopsis T-DNA insertion lines *pht3;3-1* and *pht3;3-2* were analyzed during seed maturation within the first six to eight weeks. AtPHT3;3 was expressed under the control of a plant pUBQ10 promotor. (A) Siliques of six to eight weeks old Col-0 and complemented T-DNA insertion plants were opened and examined via light microscopy (Scale bar = 2 mm). (B-D) Analysis of visible seed condition in siliques of Col-0 and T-DNA insertion lines distinguishing between green seeds (normal), prematurely aborted seeds (aborted) and empty positions (empty) (One-way ANOVA with Bonferroni's Multiple Comparison Test, $p<0.05$, n = 21 siliques).

AtPHT3;3 deficient T-DNA insertion lines produce a reduced set of viable seeds and root growth of seedlings is impaired in the absence of AtPHT3;3

The decrease of normal seed number can be the result of various defects during seed maturation. Seed maturation is classically described as a three step mechanism: (1) Early embryogenesis, (2) maturation and (3) late maturation (Baud et al., 2002). Step (1) follows the double fertilization of the future embryo and endosperm and includes the initialization of basic cell structures. Step (2) seed maturation is the phase of extensive accumulation of storage compounds, like carbohydrates, proteins and fatty acids. Main energy storage in the oil-storing seed type Arabidopsis are triacylglyceroles (TAGs), stored in cytosolic oil bodies that account for up to 60 % of the total seed weight and are the target of a massive breakdown during

germination (Theodoulou and Eastmond, 2012). During this stage the embryo and endosperm develop. The last step (3) finalizes the storage of high energetic compounds and prepares the seed to become metabolically dormant. Defects in this process, especially step (2) can lead to a reduced amount of storage compounds, which can have a negative effect on germination. Mutants deficient in oil storage and embryo development show decreased seed filling, impairment of cell division, germination and post germination processes like root growth and hypocotyl elongation due to the limited availability of TAGs and therefore available energy for all metabolic processes (Fatihi et al., 2013; Kong et al., 2017; Ma et al., 2013; Pignocchi et al., 2009; Andre and Benning, 2007).

To test the viability of seeds found in *pht3;3-1* and *pht3;3-2*, normal and aborted seeds were separately spotted on half-strength MS medium. 12 days after imbibition all germinated seeds were counted. Only few of the pre-selected aborted seeds germinated (3.77 % for *pht3;3-1* and *pht3;3-2*). The germination rate of normal seeds decreased about 12.2 % and 4.88 % from *pht3;3-1* and *pht3;3-2* respectively, compared to Col-0 (Figure 11A-B).

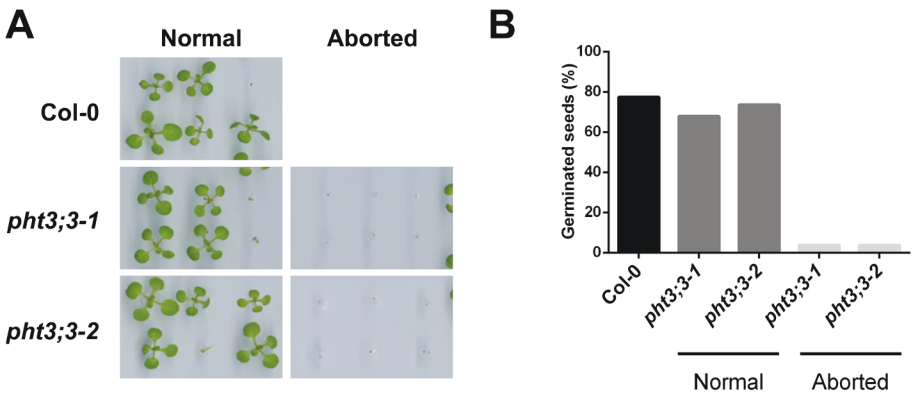

Figure 11. Germination analysis of AtPHT3;3-deficient seeds.

Seeds of the homozygous T-DNA insertion lines *pht3;3-1* and *pht3;3-2* were separated into normal and aborted seeds and analyzed during germination. (A-B) Seeds of Col-0, normal and aborted seeds of *pht3;3* insertion lines were sown on half-strength MS medium and examined 12 days after imbibition. Fully germinated seeds were counted (n = 53 sown seeds per seed type).

Seeds with a defect during embryogenesis or fatty acid biosynthesis are known to differ in shape from wild type seeds. They are smaller due to an overall reduced biomass as a result of disturbed cell division, a reduced amount of storage compounds or impaired suspensor differentiation (Kong et al., 2017; Hotta et al., 2016; Babu et al., 2013). Furthermore, embryo development can be impaired leading to embryo stage arrest (Grini et al., 2002). Fully developed seeds of *pht3;3-1* and *pht3;3-2* did not differ in size or shape from wild type seeds. Aborted seeds appear smaller and wrinkled. A closer look at the embryo via chloral hydrate clearing of the seed coat revealed fully developed mature embryos in normal seeds for both

T-DNA insertion lines. In aborted seeds embryos were not present at all or in rare cases arrested in early stages of embryogenesis like the heart stage (Figure 12).

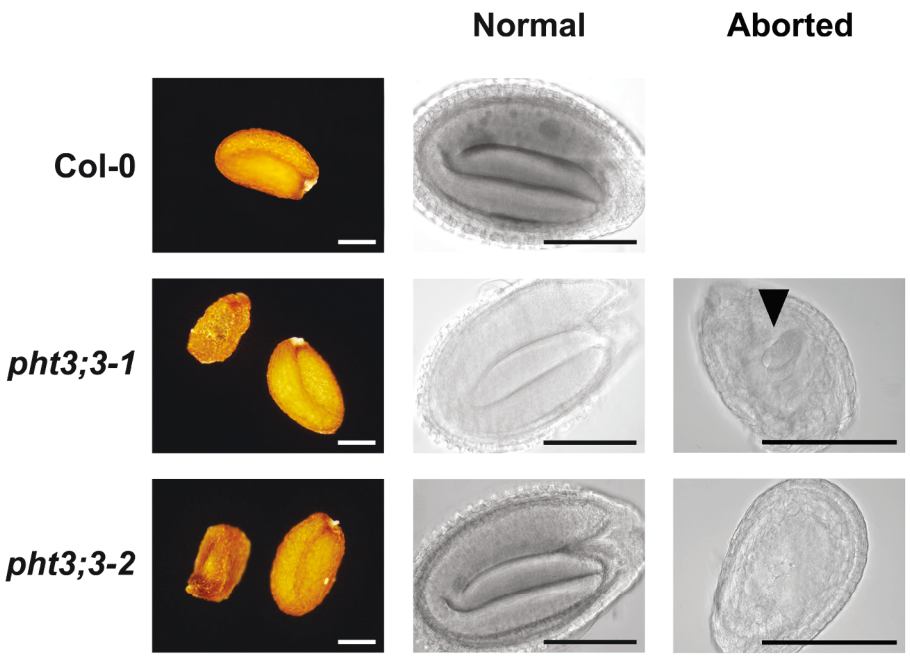

Figure 12. Phenotypic analysis of AtPHT3;3-deficient seeds reveal a defect during seed embryo development.

Seed morphology of normal and aborted seeds. Embryos were examined after chloral hydrate clearing of seed tissues. Arrowhead indicates embryo trapped in the heart stage (Scale bar = 200 µM).

As described before, an impairment of TAG storage can lead to germination or growth defects. To be independent from storage compounds, seedlings form two main structures: Photosynthetic leaves and roots. To monitor a possible effect of reduced seed filling on post-germinative growth, the length of primary roots of seedlings grown from fully developed seeds of Col-0 and AtPHT3;3 insertion lines were measured after 10 days of growth with 12 h light/ 12 h darkness. Indeed, AtPHT3;3 lines showed an overall decrease in root length compared to Col-0 (Figure 13B). Since this could be a direct effect of reduced seed filling and therefore available energy, total fatty acid content of AtPHT3;3 seeds was analyzed via derivatization to fatty acid methyl esters (FAMEs) and detection via GC-MS (Hielscher et al., 2017). The most abundant fatty acid in TAGs of Arabidopsis seeds is eicosenoic acid (C20:1). C20:1 was used as a marker to monitor the breakdown of fatty acids and with this the available energy for seedling establishment (Li et al., 2006). C20:1 content was measured in dry seeds and seedlings 2 days, 4 days and 6 days after imbibition (DAI) (Figure 13A). The seed filling represented by C20:1 content did not differ in *pht3;3-1* and *pht3;3-2* seeds compared to Col-0. The degradation of C20:1 also showed no differences over the course of six days indicating

no impact of the mutation on fatty acid storage or degradation during seed maturation and germination.

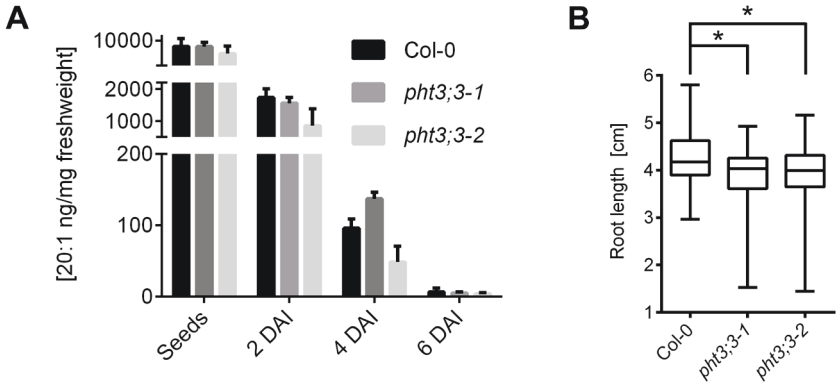

Figure 13. Analysis of fatty acid degradation in AtPHT3;3-deficient seeds and root growth.
TAG degradation and root growth was analyzed in seeds and seedlings of the homozygous T-DNA insertion lines *pht3;3-1* and *pht3;3-2*. (A) Eicosenoic acid (C20:1) degradation during seed germination as a marker for storage oil content and degradation (n = three pooled biological replicates). Analyzed via generation of fatty acid methyl esters (FAMEs) and subsequent gas chromatography coupled to mass spectrometry (GC-MS). (B) Root length of seedlings measured 10 days after germination (12 h light / 12 h darkness) (One-way ANOVA with Bonferroni's Multiple Comparison Test, $p<0.05$, n = 51 seedlings per line).

Pollen are viable and show wild type-like pollen tube growth in the absence of AtPHT3;3

Homozygous AtPHT3;3-deficient mutant lines produce normal and aborted seeds. Since seed production is initialized, At AtPHT3;3 seems to play a role after fertilization. Nevertheless, the fertilization efficiency of T-DNA insertion lines was tested in AtPHT3;3 T-DNA insertion line to explain the slight increase of empty seed positions possibly induced by pollen sterility, pollen abortion, pollen tube growth defects (Zhang et al., 2011; Robertson et al., 2004) or misguided pollen tubes as described with *hapless* mutants not being able to reach the female gametophyte (Johnson et al., 2004; Wang et al., 2016). These pollen phenotypes could lead to empty seed positons with only viable pollen fertilizing the female gametophyte. To investigate the physiological role of AtPHT3;3 in the male gametophyte, pollen of *pht3;3-1* and *pht3;3-2* were examined focusing on morphology and tube growth.

Pollen collected one day after flower opening were treated with Alexander's stain to mark viable pollen with an intact cellular structure and intact cytoplasm (purple) and non-viable pollen without an intact cytoplasm (green) (Figure 14A). All tested pollen from Col-0 and the T-DNA insertion lines did not vary in shape or size and revealed an intact cytoplasm suggesting that pollen development was not impaired. To fertilize the female gametophyte two separate sperm cells are required to initiate endosperm and embryo development. Matured/tricellular pollen carry a vegetative nucleus and two sperm cell nuclei (Twell, 2011). Mutants deficient in nucleus development like GEMINI POLLEN1 mutants show altered cell division and nuclei separation (Park et al., 1998). AtPHT3;3-deficient pollen were treated with DAPI to test the

nuclear constitution in pollen collected one day after flowering. Again *pht3;3-1* and *pht3;3-2* pollen morphology did not differ from wild type pollen as seen in bright field images. Vegetative and sperm nuclei were clearly visible in all observed pollen further indicating that the visible pollen development was not impaired (Figure 14B).

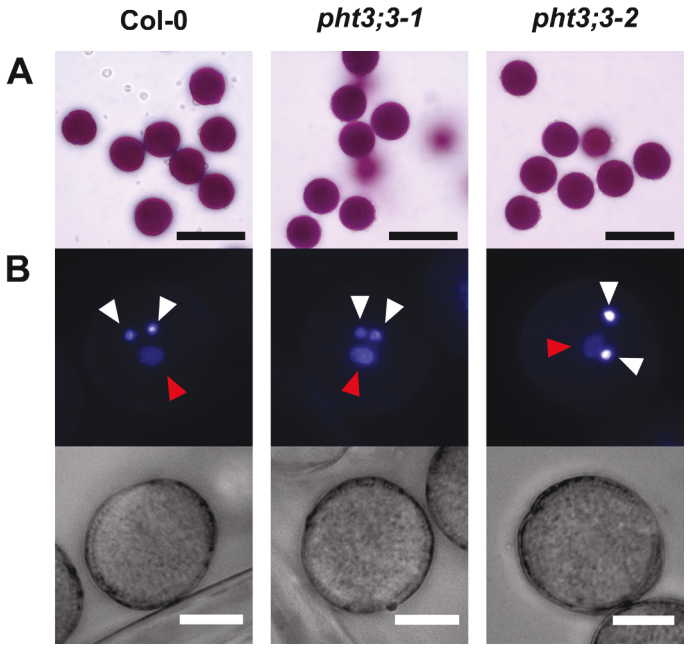

Figure 14. Staining of pollen cytoplasm and nuclei reveals viable pollen in both AtPHT3;3-deficient lines.

Pollen of Col-0, *pht3;3-1* and *pht3;3-2* were stained with Alexander's staining or DAPI to analyze viability of non-germinated pollen grains. (A) Pollen grains treated with Alexander's stain to mark pollen with intact cytoplasm. Examined using a light microscope (Scale bar = 40 µM). (B) Pollen grains stained with DAPI to show vegetative nucleus (red arrowheads) and sperm cell nuclei (white arrowheads) (Scale bar = 5 µM).

Sperm nuclei reach the female gametophyte via pollen tube expansion and chemotropism guided by secreted proteins (Chae and Lord, 2011). Mutants deficient in one of these mechanisms exhibit shortened pollen tubes or slower tube expansion leading to decreased fertilization efficiency (Gebert et al., 2008; Lalanne et al., 2004; Wang et al., 2016). Pollen of Col-0, *pht3;3-1* and *pht3;3-2* were tested via an *in vitro* germination efficiency assay. After 4 hours of incubation in a synthetic pollen germination medium, pollen tube morphology and growth were examined. Col-0 pollen revealed a germination efficiency of 72.07 % similar to *pht3;3-1* with 73.67 %. The germination efficiency of *pht3;3-2* pollen was reduced to 60.59 %. This reduction was the result of the strong decrease in efficiency during the second independent experiment for *pht3;3-2* pollen. Still, none of the T-DNA insertion lines differed significantly in pollen tube germination efficiency indicating healthy pollen tubes (Figure 15A-B). These results suggest that AtPHT3;3 does not play a role in the fertilization process via male gametophytes.

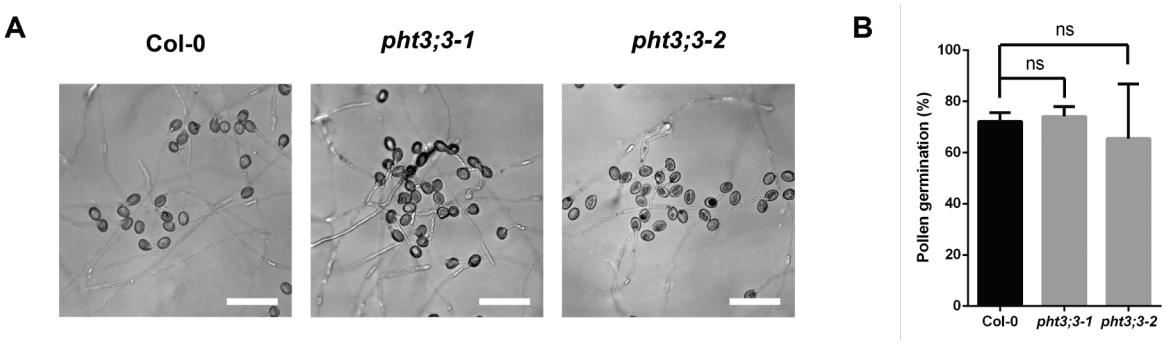

Figure 15. *In vitro* pollen germination.

In vitro germination efficiency in Col-0, *pht3;3-1* and *pht3;3-2* was analyzed after 4 h of incubation. (A) Pollen grains and tube morphology. Examined using a light microscope (Scale bar = 0.1 mm). (B) Germination efficiency analysis in percentage of total pollen count. Experiment was performed twice for each line (t-test, n > 1100 pollen grains, $p < 0.05$).

Discussion

Phosphate, copper and the role of phosphate transporters in plants

In this study the physiological function of AtPHT3;3 from the PHT3 family was examined in reproductive tissues. AtPHT3;1 and AtPHT3;2 were shown to transport phosphate in the absence of related MCF phosphate transporter ScMir1 and copper/ phosphate transporter ScPic2 in yeast (Hamel et al., 2004). Mammal transporter SLC25A3 primarily accepts copper as substrate (Boulet et al., 2018). No transport activity or substrate specificity was reported for AtPHT3;3. The copper transporter in the inner mitochondrial membrane in plants is still unknown.

In plants copper is an essential component of mitochondrial protein complex IV of the ETC. Here, copper transfers electrons across the IMM (Mansilla et al., 2018; Schertl and Braun, 2014). In chloroplasts copper is a crucial for the cupper protein plastocyanin, which transfers electrons from the cytochrome b6f complex to P700 of photosystem I (Johnson, 2018). Furthermore, copper is a co-factor of superoxide dismutase in plastids, peroxisomes and the cytosol (Alscher et al., 2002). Higher copper concentrations can induce reactive oxygen species; lower concentrations can already inhibit photosynthesis or respiration. Copper homeostasis is highly regulated to minimize these negative effects. Copper-chaperones bind copper to make in inaccessible to sensitive structures. Reduced Cu(I) is commonly found in sulfur-compounds, while oxidized Cu(II) rather binds to oxygen or nitrogen-compounds. This makes proteins appropriate targets for copper-binding. Cu(I) preferably binds to cysteine and methionine residues, Cu(II) to histidine (Ravet and Pilon, 2013; Garcia et al., 2014). To detoxify copper or to make it accessible as co-factor, copper is also bound to a range of ligands like pectates or phosphates. In rapeseed copper seems to be predominantly sequestrated by phosphates (Mwamba et al., 2016). In yeast mitochondria store copper bound to a low molecular weight non-proteinaceous ligand (Cobine et al., 2004). How copper is transported into mitochondria was not completely covered yet.

However, various copper transporters have been identified in other compartments like plastids, vacuoles and the plasma membrane. AtPAA1 and AtPAA2 reside in the inner envelope of chloroplasts and the thylakoid membrane. Both are P-type ATPases using ATP to import copper from the cytosol to the stroma and to plastocyanin (Shikanai et al., 2003; Abdel-Ghany et al., 2005). AtCOPT1 is the major importer of copper in root tips and other plant organs and is probably used for long-range transport of copper (Sancenón et al., 2004). AtCOPT2 is expressed in roots, green tissues and reproductive organs of Arabidopsis (Tiwari et al., 2017). Another plasma membrane copper transporter is AtCOPT6, which is thought to me important for copper distribution in aerial parts of the plant (Garcia-Molina et al., 2013). While two other P-type ATPases (AtHMA5, AtHMA7) are responsible for the export of copper into the xylem especially under Cu excess conditions (Peñarrubia et al., 2015), transporters belonging to ZIP

family (AtZIP2, AtZIP4) are also thought to import copper and zinc into roots. But zinc might be the primary substrate under physiological conditions (Printz et al., 2016). Candidates for the import of copper into plant mitochondria have not been studied yet. In yeast, the MCF member ScPic2 transports copper into the mitochondrial matrix with phosphate as secondary substrate (Vest et al., 2013; Hamel et al., 2004). ScPic2 is related to the primary phosphate transporter ScMir1 (Guérin et al., 1990) and mammalian copper transporter SLC25A3, which also accepts phosphate (Boulet et al., 2018). Both, ScPic2 and SLC25A3, were described to transport copper when bound to non-proteinaceous ligand (Vest et al., 2013). Homologues of ScPic2, ScMir1 and SLC25A3 in plants are the phosphate transporters AtPHT3;1-3 (Mansilla et al., 2018). The ability to transport copper and phosphate and the finding that rapeseed predominantly binds copper with phosphates (Mwamba et al., 2016) makes it plausible that a phosphate transporter was recruited to import a copper-phosphate complex into mitochondria.

The PHT3 family is one of five phylogenetically distinct families (PHT1-5) sharing the ability to shuttle phosphate but and are localized in various subcellular compartments. Members of the PHT1 family are well studied and found in virtually all plant species. They are responsible for the uptake of phosphate from soil and arbuscular mycorrhiza, transport from root to shoot and are highly expressed in the plasma membrane of roots (Wang et al., 2017). Only few PHT2 proteins were studied. They were found to reside in the inner envelope of plastids in green tissues regulating the shuttle of phosphate between cytosol and plastids (Versaw and Harrison, 2002; Wang et al., 2017). The PHT3 family is part of the MCF. They are located in the inner mitochondrial membrane and provide mitochondria with phosphate required for ATP synthesis (Hamel et al., 2004; Palmieri et al., 2008a). They are expressed in various tissues and seem to be sensitive to salt and drought stress (Zhu et al., 2012; Zhang et al., 2016). Members of the PHT4 family are localized in various sub-cellular compartments. Carriers have been found in plastids and the Golgi apparatus being involved in leaf development, defense and stress responses but also seed development (Młodzińska and Zboińska, 2016; Wang et al., 2017; Shukla et al., 2016). Few proteins of the PHT5 family have been described. They have been found in the tonoplast and thought to be involved in phosphate signaling and transport in leaves (Liu et al., 2016a; Wang et al., 2015; Młodzińska and Zboińska, 2016). None of these transporters was described to facilitate the transport of copper.

AtPHT3;3 is expressed in tissues with high energy demands

AtPHT3 members respond to salt stress during the seedling stage with higher transcript levels. Seeds and seedlings of overexpressor lines are more sensitive to salt stress and higher levels of ATP was detected (Zhu et al., 2012). Additionally, overexpression of AtPHT3;1 led to growth defects like curly leaves and dwarfism, reduced fertility as a result of misshaped flowers and

non-viable pollen, as well as a higher respiration rate. Overexpression lines of AtPHT3;2 and AtPHT3;3 did not show any visible phenotypes. Heterozygous T-DNA insertions of AtPHT3;1 revealed no visible phenotype. Homozygous lines were embryo-lethal, which might indicate an essential role of this protein during early plant establishment (Jia et al., 2015). PHT3 homologues in wheat have been found to be involved in grain development (Shukla et al., 2016). Phenotype suppression assays in yeast revealed that AtPHT3;1 and AtPHT3;2 are able to import phosphate into mitochondria (Hamel et al., 2004).

A phylogenetic analysis of PHT3 proteins from Arabidopsis, rice, tomato, maize, poplar, yeast and mammals revealed that AtPHT3;3 homologues share high sequence identities about 70 %, while AtPHT3;3 and AtPHT3;1 and AtPHT3;2 share a lower sequence identity of 53.3 % and 51.5 %, respectively (Figure 5A). The AtPHT3;3 cluster shares a branch with primary copper transporters from yeast and mammals (Figure 4). Furthermore, AtPHT3;3 homologues contain conserved amino acid changes in two of six important positions that were shown to be an important factor in the phosphate-binding capacity of transporters in yeast and mammals (Phelps et al., 1996; Dolce et al., 1994). But these residue changes are not present in primary copper transporters ScPic2 and SLC25A3 (Figure 5B). They are identical to AtPHT3;1 and AtPHT3;2. Interestingly, poplar transporter PtPHT3;3a was shown to be upregulated under high phosphate conditions, while homologues of AtPHT3;1 were upregulated under low phosphate conditions. The authors proposed that the former might be a low-affinity transporter in contrast to the latter in regards to phosphate. This might indicate that the AtPHT3;3 transporter in poplar, as suggested for Arabidopsis, is not the predominant phosphate importer (Zhang et al., 2016) Other experiments have shown that AtPHT3;2 responds to phosphate depletion in shoots and roots with higher expression, while AtPHT3;1 and AtPHT3;3 expression do not change(Morcuende et al., 2007).

Tissue-specific expression data revealed a ubiquitous expression of both AtPHT3;1 and AtPHT3;3 (Figure 6). As mentioned before, AtPHT3;1 is one of the few MCF members in Arabidopsis with a general high transcript abundance (Millar and Heazlewood, 2015). As primary phosphate transporter fueling ATP synthesis in mitochondria, AtPHT3;1 should play a crucial role in every tissue, which was confirmed with in non-viable AtPHT3;1 knockout plants (Jia et al., 2015). But mitochondrial activity is particularly important in tissues with high energy demands. These tissues are usually involved in sexual reproduction and are sensitive to mitochondrial defects. These defects often lead to morphological or functional impaired organs (Liberatore et al., 2016). To meet the energy and metabolic requirements of reproductive tissues the number of mitochondria and proteins needed for the ETC are increased (Huang et al., 1994; Warmke and Lee, 1978; Zabaleta et al., 1998). This increase was also observed in Arabidopsis root meristems (Kuroiwa et al., 1992; Fujie et al., 1993) or organs producing male gametophytes (Warmke and Lee, 1978; Lee and Warmke, 1979). In meiotic tissues genes

involved in ETC were highly upregulated (Dukowic-Schulze et al., 2014a, 2014b; Smart et al., 1994). Even after successful fertilization and during seed germination, ETC-related genes are upregulated (Dekkers et al., 2013; Wang et al., 2012; Ehrenshaft and Brambl, 1990). Responding to various abiotic stresses is also affecting mitochondrial activity and leads to expression changes of transcription factors and specific ETC components (Zhang et al., 2008, 2006; Zeller et al., 2009; Garcia et al., 2016; Pu et al., 2015).

AtPHT3;1 shows no specification but in anthers. A slightly higher expression can also been found in germinating seeds but not in dry seeds. Proteins important directly after imbibition are usually translated using long-lived RNA stored during seed development (Sano et al., 2012, 2015). If transcripts of AtPHT3;1 are synthesized not until the start of germination is not known. AtPHT3;2 seems to be senescence-specific and is only found in leaves. An involvement of the ETC during senescence was clearly shown before in plants (Mansilla et al., 2015). AtPHT3;3 is rather ubiquitously low expressed in tissues with high energy demands meaning shoot meristems, seeds and germinating seeds. Although transcript levels do not necessarily correlate with protein abundance (Vogel and Marcotte, 2013; Liu et al., 2016b), these results imply a more general role of AtPHT3;1 and AtPHT3;3, with a certain degree of specialization regarding anthers (AtPHT3;1), shoot meristems (AtPHT3;3), root meristems (AtPHT3;1), seed development (AtPHT3;3), germination (AtPHT3;1, AtPHT3;3) and senescence (AtPHT3;2).

Mutants involved in mitochondrial copper supply in reproductive tissues show an embryo-lethal phenotype due to the high energy demand of these tissues (Steinebrunner et al., 2011; Radin et al., 2015). Two functionally redundant transporters in these tissues are not very likely. Data shown in this study suggests that AtPHT3;1 could act as general phosphate importer while AtPHT3;3 is involved in the copper import of mitochondria. Together they might fuel mitochondrial ATP synthesis via oxidative phosphorylation, especially in reproductive tissues.

AtPHT3;3 is involved in seed development

Two independent homozygous T-DNA insertion lines of AtPHT3;3 have been analyzed and both display a defect during seed development. Siliques contain a significant higher number of aborted seeds during short day conditions compared to wild type plants (Figure 8). The impairment of proteins directly involved in copper transfer (Attallah et al., 2011) or heme synthesis (Mansilla et al., 2015) for COX mostly evoke lethality during early seed germination or embryogenesis and lower COX activity. Here, aborted seeds were smaller and darker as observed in AtPHT3;3-deficient mutants. Human patients with mutations in AtPHT3;3 homologue SLC25A3 presented muscle hypotonia, lactic acidosis and hypertrophic cardiomyopathy based on decreased ATP production (Mayr et al., 2007). Although slightly

higher enzyme activity of the ETC complexes I to IV have been detected (Mayr et al., 2011), these results rather represent hyperproliferation of mitochondria as a coping mechanism to reduced cellular ATP content (Morrow et al., 2017). No copper-specific studies have been performed on these patients yet (Boulet et al., 2018). Another homologue of the Arabidopsis PHT3 family can be found in *Nicotiana alata*. NaSIPP showed reduced phosphate transport activity compared to ScMir1 in yeast phenotype suppression assays (Garcia-Valencia et al., 2017). The transport of copper or the phenotype suppression of ScPic2-deficient yeast has not been investigated.

AtPHT3;3-deficient embryos in abnormal seeds were stuck in the heart stage or devoid of any embryo at all (Figure 12). While the germination of normal AtPHT3;3-deficient seeds does not seem to be impaired (Figure 11) and TAG degradation does not differ from wild type seeds (Figure 13A), root length is slightly reduced (Figure 13B). Pollen development and pollen tube growth is not affected (Figure 15). In general, the defect seen in AtPHT3;3-deficient plants is rather subtle implying that (1) this carrier is not essential, (2) a bypass can suppress the phenotype or (3) AtPHT3;3 is functional redundant. Another transporter in the IMM, probably AtPHT3;1 or AtPHT3;2, might transport the unknown substrate in the absence of AtPHT3;3.

AtPHT3;3 might represent the Arabidopsis counterpart to ScPic2 and SLC25A3

The knowledge about copper transport in plant mitochondria is very limited and is mostly based on comparisons with yeast or mammals. However, more and more plant homologues of yeast metal chaperones/donors have been described. These proteins are supposed to load COX/complex IV of the ETC with copper. The soluble metallochaperone AtCOX17, which is represented by two genes in Arabidopsis, is located in the IMS and transfers copper to yeast AtHCC1 or AtCOX11 (Horng et al., 2004; Balandin and Castresana, 2002; Garcia et al., 2016). These proteins are located in the IMM and transfer copper to COX subunits AtCOX2 and AtCOX1, respectively (Steinebrunner et al., 2011; Radin et al., 2015). But how copper enters mitochondria in the first place, especially how the mitochondrial matrix copper pool is refilled is still unknown in plants. The discovery of copper transporters yeast ScPic2 and SLC25A3 in mammals, which were initially published as phosphate transporters, led to a set of three putative candidates for copper transport in plant mitochondria (Vest et al., 2013; Boulet et al., 2018; Mansilla et al., 2018).

The PHT3 family is thought to import phosphate into mitochondria to fuel ATP synthesis. Retaining several isoforms of a protein with redundant function seems to be common in eukaryotic cells and indicates specific functions under certain conditions (Hamel et al., 2004; Blanchoin and Staiger, 2010). The PHT families are a perfect example for this observation as seen in various sequenced plants (Liu et al., 2011; Sun et al., 2017; Wang et al., 2017). All PHT3 proteins in Arabidopsis were clearly linked to energy content, stress

responses of mitochondria and impairment of the ETC (Garcia et al., 2016; Zhu et al., 2012; Jia et al., 2015; Umbach et al., 2012; Ng et al., 2013; Schwarzländer et al., 2012). The apparent functional redundancy of these proteins might be explained by their tissue-specific expression, the low transcript abundance of AtPHT3;2 and AtPHT3;3 compared to AtPHT3;1 and the diverse impact on plant development in overexpression and knockdown/knockout mutants of the single PHT3s. This might hint at distinct temporal or spatial roles under physiological conditions.

All published data on AtPHT3;1 implies that it might represent the major phosphate transporter in mitochondria and is the most essential member of the PHT3 family during all developmental stages of Arabidopsis (Jia et al., 2015). AtPHT3;3 is rather expressed in tissues with high energy demands, reproductive tissues and meristems. Since AtPHT3;1 is present in virtually all tissues, AtPHT3;2 and AtPHT3;3 might represent isoforms, which support AtPHT3;1 phosphate import when higher amounts of phosphate are required.

Very few members of the PHT3 family in other species have been studied. ScPic2 and SLC25A3 demonstrated the transport of the unknown copper ligand found in the mitochondrial storage pool (Vest et al., 2016; Boulet et al., 2018). This ligand could be phosphate, which would be consistent with the substrate specificity of ScPic2 and SLC25A3 and the finding that copper is bound top phosphate in rapeseed, making the PHT3 family reasonable candidates for the shuttle of copper (Mwamba et al., 2016). Additionally, other MCFs have been shown to transport metals like iron or manganese in yeast (Zhang et al., 2005; Luk et al., 2003; Yang et al., 2006) or iron in rice (Bashir et al., 2011). It is likely, that the ability to transport metals/metal complexes is conserved within the MCF. To date there is no data available regarding the substrate specificity of AtPHT3;3. The phylogenetic proximity to copper transporters and the change in important residues for phosphate binding suggests a functional shift of AtPHT3;3. With this AtPHT3;3 represents a candidate for copper/copper-ligand import into plant mitochondria and might act together with AtPHT3;1 to supply mitochondrial ATP production with phosphate and copper.

Outlook

Biochemical analysis of PHT3 proteins

Phosphate transport by AtPHT3;1 and AtPHT3;2 was indirectly shown via phenotype suppression assays in ScPic2/ScMir1-deficient yeast cells (Hamel et al., 2004). The substrate of AtPHT3;3 was not determined within this study. To investigate the function of AtPHT3;3, these phenotype suppression assays have to be repeated. Direct uptake assays using liposomes reconstituted with heterologously expressed AtPHT3;3 are needed to measure its substrate specificity (Scalise et al., 2013). To test copper uptake the liposome uptake assay has to be coupled to inductively coupled plasma-optical emission spectroscopy (ICP-OES) to

detect the import of metals into liposomes(Vest et al., 2013; Boulet et al., 2018). Additionally, other metals like calcium, zinc, magnesium and iron should be tested to determine the metal substrate specificity of AtPHT3;3. SLC25A3 showed characteristics of an uniporter in uptake studies without preloaded liposomes (Boulet et al., 2018). The transport mode of AtPHT3;3 could be tested with this assay as well. To reveal the role and functional distinction of the PHT3 family in Arabidopsis, all PHT3 members should be tested.

Physiological analysis of AtPHT3;3

Available T-DNA insertion lines of AtPHT3;3 only revealed a subtle phenotype compared to embryo-lethal AtPHT3;1-deficients mutants (Jia et al., 2015). Seedlings showed a slight reduction in root length compared to the wild type (Figure 13B). Viable embryos or young seedlings need to be tested for ATP content, respiration rate and the expression of stress-regulated genes. The observed mutation has seemingly no effect on vegetative growth. This raises the question if another PHT3 protein is used as a bypass and allows most of the seeds to be viable and vegetative growth to function without visible impairments. This functional link might be accessed in mutant plants heterozygous for AtPHT3;1 and homozygous for AtPHT3;3. Furthermore, AtPHT3;3 was highly expressed in shoot apical meristems (SAM) and inflorescence meristems of Arabidopsis. A more in-depth analysis of SAM (Mandel et al., 2016) and floral organs (Su et al., 2013) might reveal further developmental defects.

Insertions in AtPHT3;3-deficient lines are found in the 5'-UTR region of the coding sequence, possibly in the promoter region. Although transcripts were strongly reduced in both lines it cannot be excluded that the remaining transcripts prevent a stronger phenotype. Therefore, new knockout mutants should be established to completely abolish AtPHT3;3 function. Here, more recent methods like the CRISPR/Cas9 system would be most suitable. If homozygous mutants are viable, the response of AtPHT3;3-deficient plants to stress conditions, especially those affecting the ETC, like drought, salt or H_2O_2 should be tested. If AtPHT3;3 resembles ScPic2/SLC25A3 function *in vivo* could be tested by expressing these transporters in AtPHT3;3 mutants or AtPHT3;3 in ScPic2/SLC25A-deficient cell lines. Isolated mitochondria of mutant and wild type plants should be tested for oxygen consumption and ATP level to link AtPHT3;3 to respiration. Based on the lethality of homozygous AtPHT3;1-deficient Arabidopsis knockout mutants (Jia et al., 2015), AtPHT3;2 and AtPHT3;31 are not able to compensate the phenotype during germination or vegetative growth under physiological conditions. This leads to the assumption that they cannot replace AtPHT3;1 function in general (different substrate affinity) or are not present in an adequate amount to fulfill the transport function of AtPHT3;1. It would be interesting to test if the overexpression of AtPHT3;2/AtPHT3;3 can rescue homozygous AtPHT3;3-deficient seeds when inserted into the preceding heterozygous generation.

In SLC25A3-deficient human patients hyperproliferation of mitochondria was hypothesized (Mayr et al., 2011). T-DNA insertion lines should be tested for mitochondria number and morphology using confocal laser scanning microscopy assays with labeled mitochondria (fluorescent dyes or mitochondrial targeted GFP) (Scott and Logan, 2007).

Conclusion

This study covered the physiological role of the mitochondrial transporter of the phosphate transporter family 3 in reproductive tissues of Arabidopsis. The loss of AtPHT3;3 decreases the number viable seeds. The redundancy of PHT3 proteins in mitochondria indicate a distinct function for AtPHT3;3 *in vivo*. AtPHT3;3 is tissue-specifically expressed, induced by salt and drought stress and might represent the Arabidopsis homologue to copper transporters ScPic2 in yeast and SLC25A3 in mammals.

Author contribution and acknowledgements

Björn Hielscher wrote the manuscript and performed all experiments and analyses unless stated otherwise. Nicole Linka, Peter Westhoff, Michael Feldbrügge and Andreas Weber participated in scientific discussions. Nicole Linka assisted in drafting this manuscript. Nicole Linka and Björn Hielscher designed the experiments.

Supplemental material

Primer list

Primer	Sequence 5'-3'	Target, used for vector
BH273	TAATCTGAGTTTTTCTGATTAACACACCATGGCAAGAGTCAAGAGTAAACTAGACG	At2g17270, pBH61
BH274	CAGCTCCTCGCCCTTGCTCACCATACCGCTACCACCCACTGATAATTTAGCTGCATC	
BH52	CGACCTCGAGGGTACATGACAAGAGTCAAGAGTAAACTAG	At2g17270, pBH02
BH53	TTCATCTTCATGAGCTTTATCACACTGATAATTTAGCTG	
P52	TAGCATCTGAATTTCATAACCAATCTCGATACAC	SAIL_591H09
P49	CCCATTTGGACGTGAATGTAGACAC	GABI_432A12
NL516	TCATTGGAGAGAAGATGGTGG	At2g17270 5'-UTR
NL517	AAACCGGAAGGAATGCTATTG	At2g17270 Exon 2
BH84	GAAGAAACCAGTGGATGCAGCT	At2g17270
BH85	CTACACAACGCCTCGTATCTACTTG	At2g17270 3'-UTR

Vector list

Primer	Insert	Backbone, purpose
pBH02	At1g72820	pHyg-Venus (Walter et al., 2004), complementation of T-DNA insertion lines
pBH61	At1g72820, c-terminal YFP	Modified, (Grefen et al., 2010), sub-cellular localization

List of proteins used for phylogenetic tree (Figure 4) and sequence analysis (Figure 5).

Proteins from rice and poplar were named according to (Wang et al., 2017).

Transporter	Organism	Locus/Entry ID Unitprot
AtPHT3;1	*Arabidopsis thaliana*	At5g14040
AtPHT3;2	*Arabidopsis thaliana*	At3g48850
AtPHT3;3	*Arabidopsis thaliana*	At2g17270
BtSLC25A3a	*Bos taurus*	P12234
BtSLC25A3b	*Bos taurus*	P12234
HsSLC25A3a	*Homo sapiens*	Q00325
HsSLC25A3b	*Homo sapiens*	A0A024RBE8
MmSLC25A3	*Mus musculus*	Q8VEM8
OsPT15	*Oryza sativa*	Os02g52860
OsPT16A	*Oryza sativa*	Os03g15690.1
OsPT16B	*Oryza sativa*	Os03g15690.2
OsPT17	*Oryza sativa*	Os04g37600
OsPT18	*Oryza sativa*	Os06g10810
OsPT20	*Oryza sativa*	Os09g38100
OsPT19	*Oryza sativa*	Os09g38100
PtPHT3;3a.1	*Populus trichocarpa*	Potri.004G207200.1
PtPHT3;3a.3	*Populus trichocarpa*	Potri.004G207200.3
PtPHT3;1a	*Populus trichocarpa*	Potri.001G322300.1
PtPHT3;3b.1	*Populus trichocarpa*	Potri.005G098800.1
PtPHT3;3b.2	*Populus trichocarpa*	Potri.005G098800.2
PtPHT3;1b.1	*Populus trichocarpa*	Potri.017G060800.1
PtPHT3;1b.2	*Populus trichocarpa*	Potri.017G060800.2
PtPHT3;2a	*Populus trichocarpa*	Potri.012G105100.1
PtPHT3;2b	*Populus trichocarpa*	Potri.015G104400.2
RnSLC25A3	*Ratus norvegicus*	Q8VEM8
ScPic2	*Saccharomyces cerevisiae*	P40035
ScMir1	*Saccharomyces cerevisiae*	P23641
ScMrs3	*Saccharomyces cerevisiae*	P10566
SolycPT1	*Solanum lycopersicum*	Solyc06g072510
SolycPT2	*Solanum lycopersicum*	Solyc03g032030
SolycPT3	*Solanum lycopersicum*	Solyc02g094470
SolycPT4	*Solanum lycopersicum*	Solyc03g097840
ZmPT1	*Zea mays*	AC233910.1_FGP001
ZmPT2	*Zea mays*	GRMZM2G009045.01
ZmPT3	*Zea mays*	GRMZM2G015401.01
ZmPT4	*Zea mays*	GRMZM2G060630.01
ZmPT5	*Zea mays*	GRMZM2G118208.01
ZmPT6	*Zea mays*	GRMZM2G152827.01

References

Abdel-Ghany, S.E., Müller-Moulé, P., Niyogi, K.K., Pilon, M., and Shikanai, T. (2005). Two P-type ATPases are required for copper delivery in Arabidopsis thaliana chloroplasts. Plant Cell **17**: 1233–51.

Alexander, M.P. (1969). Differential staining of aborted and nonaborted pollen. Biotech. Histochem. **44**: 117–122.

Alscher, R.G., Erturk, N., and Heath, L.S. (2002). Role of superoxide dismutases (SODs) in controlling oxidative stress in plants. J. Exp. Bot. **53**: 1331–1341.

Andre, C. and Benning, C. (2007). Arabidopsis Seedlings Deficient in a Plastidic Pyruvate Kinase Are Unable to Utilize Seed Storage Compounds for Germination and Establishment. Plant Physiol. **145**: 1670–1680.

Arai, Y., Hayashi, M., and Nishimura, M. (2008). Proteomic identification and characterization of a novel peroxisomal adenine nucleotide transporter supplying ATP for fatty acid beta-oxidation in soybean and Arabidopsis. Plant Cell **20**: 3227–40.

Araújo, W.L., Nunes-Nesi, A., Nikoloski, Z., Sweetlove, L.J., and Fernie, A.R. (2012). Metabolic control and regulation of the tricarboxylic acid cycle in photosynthetic and heterotrophic plant tissues. Plant. Cell Environ. **35**: 1–21.

Attallah, C. V., Welchen, E., Martin, A.P., Spinelli, S. V., Bonnard, G., Palatnik, J.F., and Gonzalez, D.H. (2011). Plants contain two SCO proteins that are differentially involved in cytochrome c oxidase function and copper and redox homeostasis. J. Exp. Bot. **62**: 4281–4294.

Autran, D. et al. (2011). Maternal epigenetic pathways control parental contributions to arabidopsis early embryogenesis. Cell **145**: 707–719.

Babu, Y., Musielak, T., Henschen, A., and Bayer, M. (2013). Suspensor Length Determines Developmental Progression of the Embryo in Arabidopsis. Plant Physiol. **162**: 1448–1458.

Balandin, T. and Castresana, C. (2002). AtCOX17, an Arabidopsis homolog of the yeast copper chaperone COX17. Plant Physiol. **129**: 1852–7.

Bashir, K., Ishimaru, Y., and Nishizawa, N.K. (2011). Identification and characterization of the major mitochondrial Fe transporter in rice. Plant Signal. Behav. **6**: 1591–1593.

Baud, S., Baud, S., Boutin, J.-P., Boutin, J.-P., Miquel, M., Miquel, M., Lepiniec, L., Lepiniec, L., Rochat, C., and Rochat, C. (2002). An intergrated overview of seed development in Arabidopsos thaliana ecotype WS. Plant Physiol. Biochem. **40**: 151–160.

Bauwe, H., Hagemann, M., and Fernie, A.R. (2010). Photorespiration: players, partners and origin. Trends Plant Sci. **15**: 330–336.

Bedhomme, M., Hoffmann, M., McCarthy, E.A., Gambonnet, B., Moran, R.G., Rébeillé, F., and Ravanel, S. (2005). Folate metabolism in plants: An Arabidopsis homolog of the mammalian mitochondrial folate transporter mediates folate import into chloroplasts. J. Biol. Chem. **280**: 34823–34831.

Bernhardt, K., Vigelius, S.K., Linka, N., and Andreas, P.M. (2012a). Agrobacterium-mediated Arabidopsis thaliana transformation : an overview of T-DNA binary vectors , floral dip and screening for homozygous lines. Endocytobiosis Cell Res. **22**: 19–28.

Bernhardt, K., Wilkinson, S., Weber, A.P.M., and Linka, N. (2012b). A peroxisomal carrier delivers NAD + and contributes to optimal fatty acid degradation during storage oil mobilization. Plant J. **69**: 1–13.

Blanchoin, L. and Staiger, C.J. (2010). Plant formins: Diverse isoforms and unique molecular mechanism. Biochim. Biophys. Acta - Mol. Cell Res. **1803**: 201–206.

Boavida, L.C. and McCormick, S. (2007). Temperature as a determinant factor for increased and reproducible in vitro pollen germination in Arabidopsis thaliana. Plant J. **52**: 570–582.

Boulet, A. et al. (2018). The mammalian phosphate carrier SLC25A3 is a mitochondrial copper transporter required for cytochrome c oxidase biogenesis. J. Biol. Chem. **293**: 1887–1896.

Bouvier, F., Linka, N., Isner, J.-C., Mutterer, J., Weber, A.P.M., and Camara, B. (2006). Arabidopsis SAMT1 Defines a Plastid Transporter Regulating Plastid Biogenesis and Plant Development. Plant Cell Online **18**:

3088–3105.

Burch-Smith, T.M., Brunkard, J.O., Choi, Y.G., and Zambryski, P.C. (2011). Organelle-nucleus cross-talk regulates plant intercellular communication via plasmodesmata. Proc. Natl. Acad. Sci. **108**: E1451–E1460.

Cecchini, G. (2003). Function and Structure of Complex II of the Respiratory Chain. Annu. Rev. Biochem. **72**: 77–109.

Chae, K. and Lord, E.M. (2011). Pollen tube growth and guidance: Roles of small, secreted proteins. Ann. Bot. **108**: 627–636.

Cobine, P.A., Ojeda, L.D., Rigby, K.M., and Winge, D.R. (2004). Yeast Contain A Non-proteinaceous Pool of Copper in the Mitochondrial Matrix. J. Biol. Chem. **279**: 14447–14455.

Cobine, P.A., Pierrel, F., Bestwick, M.L., and Winge, D.R. (2006). Mitochondrial matrix copper complex used in metallation of cytochrome oxidase and superoxide dismutase. J. Biol. Chem. **281**: 36552–36559.

Czechowski, T. (2005). Genome-Wide Identification and Testing of Superior Reference Genes for Transcript Normalization in Arabidopsis. Plant Physiol. **139**: 5–17.

Dahan, J., Tcherkez, G., Macherel, D., Benamar, A., Belcram, K., Quadrado, M., Arnal, N., and Mireau, H. (2014). Disruption of the CYTOCHROME C OXIDASE DEFICIENT1 Gene Leads to Cytochrome c Oxidase Depletion and Reorchestrated Respiratory Metabolism in Arabidopsis. Plant Physiol. **166**: 1788–1802.

Dekkers, B.J.W. et al. (2013). Transcriptional Dynamics of Two Seed Compartments with Opposing Roles in Arabidopsis Seed Germination. Plant Physiol. **163**: 205–215.

Denton, R.M. (2009). Regulation of mitochondrial dehydrogenases by calcium ions. Biochim. Biophys. Acta - Bioenerg. **1787**: 1309–1316.

Dolce, V., Iacobazzi, V., Palmieri, F., and Walker, J.E. (1994). The sequences of human and bovine genes of the phosphate carrier from mitochondria contain evidence of alternatively spliced forms. J. Biol. Chem. **269**: 10451–10460.

Dukowic-Schulze, S., Harris, A., Li, J., Sundararajan, A., Mudge, J., Retzel, E.F., Pawlowski, W.P., and Chen, C. (2014a). Comparative Transcriptomics of Early Meiosis in Arabidopsis and Maize. J. Genet. Genomics **41**: 139–152.

Dukowic-Schulze, S., Sundararajan, A., Mudge, J., Ramaraj, T., Farmer, A.D., Wang, M., Sun, Q., Pillardy, J., Kianian, S., Retzel, E.F., Pawlowski, W.P., and Chen, C. (2014b). The transcriptome landscape of early maize meiosis. BMC Plant Biol. **14**.

Ehrenshaft, M. and Brambl, R. (1990). Respiration and Mitochondrial Biogenesis in Germinating Embryos of Maize. Plant Physiol. **93**: 295–304.

Fatihi, A., Zbierzak, A.M., and Dormann, P. (2013). Alterations in Seed Development Gene Expression Affect Size and Oil Content of Arabidopsis Seeds. Plant Physiol. **163**: 973–985.

Forner, J. and Binder, S. (2007). The red fluorescent protein eqFP611: Application in subcellular localization studies in higher plants. BMC Plant Biol. **7**: 28.

Fransen, M., Lismont, C., and Walton, P. (2017). The peroxisome-mitochondria connection: How and why? Int. J. Mol. Sci. **18**.

Fujie, M., Kuroiwa, H., Kawano, S., and Kuroiwa, T. (1993). Studies on the behavior of organelles and their nucleoids in the root apical meristem of Arabidopsis thaliana (L.) Col. Planta **189**: 443–452.

Garcia-Molina, A., Andrés-Colás, N., Perea-García, A., Neumann, U., Dodani, S.C., Huijser, P., Peñarrubia, L., and Puig, S. (2013). The arabidopsis COPT6 transport protein functions in copper distribution under copper-deficient conditions. Plant Cell Physiol. **54**: 1378–1390.

Garcia-Valencia, L.E., Bravo-Alberto, C.E., Wu, H., Rodriguez-Sotres, R., Cheung, A.Y., and Cruz-Garcia, F. (2017). SIPP, a novel mitochondrial phosphate carrier mediates in self-incompatibility. Plant Physiol. **175**: pp.01884.2016.

Garcia, L., Welchen, E., Gey, U., Arce, A.L., Steinebrunner, I., and Gonzalez, D.H. (2016). The cytochrome c

oxidase biogenesis factor AtCOX17 modulates stress responses in Arabidopsis. Plant Cell Environ. **39**: 628–644.

Garcia, L., Welchen, E., and Gonzalez, D.H. (2014). Mitochondria and copper homeostasis in plants. Mitochondrion **19**: 269–274.

Gebert, M., Dresselhaus, T., and Sprunck, S. (2008). F-Actin Organization and Pollen Tube Tip Growth in Arabidopsis Are Dependent on the Gametophyte-Specific Armadillo Repeat Protein ARO1. Plant Cell Online **20**: 2798–2814.

Gibson, D.G. (2011). Enzymatic assembly of overlapping DNA fragments. Methods Enzymol. **498**: 349–361.

Gigolashvili, T., Geier, M., Ashykhmina, N., Frerigmann, H., Wulfert, S., Krueger, S., Mugford, S.G., Kopriva, S., Haferkamp, I., and Flügge, U.-I. (2012). The *Arabidopsis* Thylakoid ADP/ATP Carrier TAAC Has an Additional Role in Supplying Plastidic Phosphoadenosine 5′-Phosphosulfate to the Cytosol. Plant Cell **24**: 4187–4204.

Gómez, J.F., Talle, B., and Wilson, Z.A. (2015). Anther and pollen development: A conserved developmental pathway. J. Integr. Plant Biol. **57**: 876–891.

Grefen, C., Donald, N., Hashimoto, K., Kudla, J., Schumacher, K., and Blatt, M.R. (2010). A ubiquitin-10 promoter-based vector set for fluorescent protein tagging facilitates temporal stability and native protein distribution in transient and stable expression studies. Plant J. **64**: 355–365.

Grini, P.E., Jürgens, G., and Hülskamp, M. (2002). Embryo and endosperm development is disrupted in the female gametophytic capulet mutants of arabidopsis. Genetics **162**: 1911–1925.

Gueguen, V. (2000). Fatty Acid and Lipoic Acid Biosynthesis in Higher Plant Mitochondria. J. Biol. Chem. **275**: 5016–5025.

Guérin, B., Bukusoglu, C., Rakotomanana, F., and Wohlrab, H. (1990). Mitochondrial phosphate transport. N-ethylmaleimide insensitivity correlates with absence of beef heart-like Cys42 from the Saccharomyces cerevisiae phosphate transport protein. J. Biol. Chem. **265**: 19736–41.

Guo, R., Gu, J., Zong, S., Wu, M., and Yang, M. (2018). Structure and mechanism of mitochondrial electron transport chain. Biomed. J. **41**: 9–20.

Haferkamp, I., Hackstein, J.H.P., Voncken, F.G.J., Schmit, G., and Tjaden, J. (2002). Functional integration of mitochondrial and hydrogenosomal ADP/ATP carriers in the Escherichia coli membrane reveals different biochemical characteristics for plants, mammals and anaerobic chytrids. Eur. J. Biochem. **269**: 3172–3181.

Haferkamp, I. and Schmitz-Esser, S. (2012). The Plant Mitochondrial Carrier Family: Functional and Evolutionary Aspects. Front. Plant Sci. **3**: 1–19.

Hamel, P., Saint-Georges, Y., De Pinto, B., Lachacinski, N., Altamura, N., and Dujardin, G. (2004). Redundancy in the function of mitochondrial phosphate transport in Saccharomyces cerevisiae and Arabidopsis thaliana. Mol. Microbiol. **51**: 307–317.

Hielscher, B., Charton, L., Mettler-Altmann, T., and Linka, N. (2017). Analysis of Peroxisomal β-Oxidation During Storage Oil Mobilization in Arabidopsis thaliana Seedlings. Methods Mol. Biol. **1595**: 291–304.

Hildebrandt, T.M., Nunes Nesi, A., Araújo, W.L., and Braun, H.P. (2015). Amino Acid Catabolism in Plants. Mol. Plant **8**: 1563–1579.

Hoffmann, C., Plocharski, B., Haferkamp, I., Leroch, M., Ewald, R., Bauwe, H., Riemer, J., Herrmann, J.M., and Neuhaus, H.E. (2013). From Endoplasmic Reticulum to Mitochondria: Absence of the Arabidopsis ATP Antiporter Endoplasmic Reticulum Adenylate Transporter1 Perturbs Photorespiration. Plant Cell **25**: 2647–2660.

Höfgen, R. and Willmitzer, L. (1988). Storage of competent cells for Agrobacterium transformation. Nucleic Acids Res. **16**: 9877.

Horn, D. and Barrientos, A. (2008). Mitochondrial copper metabolism and delivery to cytochromec oxidase. IUBMB Life **60**: 421–429.

Horng, Y.C., Cobine, P.A., Maxfield, A.B., Carr, H.S., and Winge, D.R. (2004). Specific copper transfer from the Cox17 metallochaperone to both Sco1 and Cox11 in the assembly of yeast cytochrome c oxidase. J. Biol. Chem. **279**: 35334–35340.

Hotta, T., Fujita, S., Uchimura, S., Noguchi, M., Demura, T., Muto, E., and Hashimoto, T. (2016). Affinity purification and characterization of functional tubulin from cell suspension cultures of Arabidopsis and tobacco. Plant Physiol.: pp.01173.2015.

Huang, J., Struck, F., Matzinger, D.F., and Levings, C.S. (1994). Flower-enhanced expression of a nuclear-encoded mitochondrial respiratory protein is associated with changes in mitochondrion number. Plant Cell **6**: 439–448.

Huang, X. and Miller, W. (1991). A time-efficient, linear-space local similarity algorithm. Adv. Appl. Math. **12**: 337–357.

Igamberdiev, A.U. and Kleczkowski, L.A. (2015). Optimization of ATP synthase function in mitochondria and chloroplasts via the adenylate kinase equilibrium. Front. Plant Sci. **6**: 1–8.

Jacoby, R.P., Li, L., Huang, S., Pong Lee, C., Millar, A.H., and Taylor, N.L. (2012). Mitochondrial Composition, Function and Stress Response in Plants. J. Integr. Plant Biol. **54**: 887–906.

Jett, K.A. and Leary, S.C. (2018). Building the CuAsite of cytochrome c oxidase: A complicated, redox-dependent process driven by a surprisingly large complement of accessory proteins. J. Biol. Chem. **293**: 4644–4652.

Jia, F., Wan, X., Zhu, W., Sun, D., Zheng, C., Liu, P., and Huang, J. (2015). Overexpression of mitochondrial phosphate transporter 3 severely hampers plant development through regulating mitochondrial function in Arabidopsis. PLoS One **10**: 1–14.

Johnson-Brousseau, S.A. and McCormick, S. (2004). A compendium of methods useful for characterizing Arabidopsis pollen mutants and gametophytically-expressed genes. Plant J. **39**: 761–775.

Johnson, M.A., Von Besser, K., Zhou, Q., Smith, E., Aux, G., Patton, D., Levin, J.Z., and Preuss, D. (2004). Arabidopsis hapless mutations define essential gametophytic functions. Genetics **168**: 971–982.

Johnson, M.P. (2018). Metabolic regulation of photosynthetic membrane structure tunes electron transfer function . Biochem. J.: 1–10.

Junge, W. and Nelson, N. (2015). ATP Synthase. Annu. Rev. Biochem. **84**: 631–657.

Kasajima, I., Ide, Y., Ohkama-Ohtsu, N., Hayashi, H., Yoneyama, T., and Fujiwara, T. (2004). A protocol for rapid DNA extraction fromArabidopsis thaliana for PCR analysis. Plant Mol. Biol. Report. **22**: 49–52.

Khalimonchuk, O. and Rödel, G. (2005). Biogenesis of cytochrome c oxidase. Mitochondrion **5**: 363–388.

Klepikova, A. V., Logacheva, M.D., Dmitriev, S.E., and Penin, A.A. (2015). RNA-seq analysis of an apical meristem time series reveals a critical point in Arabidopsis thaliana flower initiation. BMC Genomics **16**.

Kmiecik, P., Leonardelli, M., and Teige, M. (2016). Novel connections in plant organellar signalling link different stress responses and signalling pathways. J. Exp. Bot. **67**: 3793–3807.

Kolbe, H. V, Costello, D., Wong, A., Lu, R.C., and Wohlrab, H. (1984). Mitochondrial phosphate transport. Large scale isolation and characterization of the phosphate transport protein from beef heart mitochondria. J. Biol. Chem. **259**: 9115–20.

Koncz, C. and Schell, J. (1986). The promoter of TL-DNA gene 5 controls the tissue-specific expression of chimaeric genes carried by a novel type of Agrobacterium binary vector. MGG Mol. Gen. Genet. **204**: 383–396.

Kong, Q., Ma, W., Yang, H., Ma, G., Mantyla, J.J., and Benning, C. (2017). The Arabidopsis WRINKLED1 transcription factor affects auxin homeostasis in roots. J. Exp. Bot. **68**: 4627–4634.

Kuroiwa, T., Fujie, M., and Kuroiwa, H. (1992). Studies on the behavior of mitochondrial DNA: Synthesis of mitochondrial DNA occurs actively in a specific regions just above the quiescent center in the root meristem of Pelargonium zonale. J Cell Sci **101**: 483–493.

Lalanne, E., Honys, D., Johnson, A., Borner, G.H.H., Lilley, K.S., Dupree, P., Grossniklaus, U., and Twell, D. (2004). Glycosylphosphatidylinositol Anchor Biosynthetic Pathway , Are Required for Pollen Germination and Tube Growth in Arabidopsis. Plant Cell **16**: 229–240.

Le, B.H. et al. (2010). Global analysis of gene activity during Arabidopsis seed development and identification of seed-specific transcription factors. Proc. Natl. Acad. Sci. **107**: 8063–8070.

Lee, S.-L.J. and Warmke, H.E. (1979). Organelle size and number in fertile and t-cytoplasmic male-sterile corn. Am. J. Bot. **66**: 141–148.

Li, Y., Beisson, F., Pollard, M., and Ohlrogge, J. (2006). Oil content of Arabidopsis seeds: The influence of seed anatomy, light and plant-to-plant variation. Phytochemistry **67**: 904–915.

Liang, C., Zhang, Y., Cheng, S., Osorio, S., Sun, Y., Fernie, A.R., Cheung, C.Y.M., and Lim, B.L. (2015). Impacts of high ATP supply from chloroplasts and mitochondria on the leaf metabolism of Arabidopsis thaliana. Front. Plant Sci. **6**: 1–17.

Liberatore, K.L., Dukowic-Schulze, S., Miller, M.E., Chen, C., and Kianian, S.F. (2016). The role of mitochondria in plant development and stress tolerance. Free Radic. Biol. Med. **100**: 238–256.

Linka, N., Theodoulou, F.L., Haslam, R.P., Linka, M., Napier, J.A., Neuhaus, H.E., and Weber, A.P.M. (2008). Peroxisomal ATP Import Is Essential for Seedling Development in Arabidopsis thaliana. Plant Cell Online **20**: 3241–3257.

Liu, F., Chang, X.J., Ye, Y., Xie, W.B., Wu, P., and Lian, X.M. (2011). Comprehensive sequence and whole-life-cycle expression profile analysis of the phosphate transporter gene family in rice. Mol. Plant **4**: 1105–1122.

Liu, M. and Lu, S. (2016). Plastoquinone and Ubiquinone in Plants: Biosynthesis, Physiological Function and Metabolic Engineering. Front. Plant Sci. **7**: 1–18.

Liu, T.Y., Huang, T.K., Yang, S.Y., Hong, Y.T., Huang, S.M., Wang, F.N., Chiang, S.F., Tsai, S.Y., Lu, W.C., and Chiou, T.J. (2016a). Identification of plant vacuolar transporters mediating phosphate storage. Nat. Commun. **7**: 1–11.

Liu, Y., Beyer, A., and Aebersold, R. (2016b). On the Dependency of Cellular Protein Levels on mRNA Abundance. Cell **165**: 535–550.

Lodish, H., Arnold Berk, S., Zipursky, L., Matsudaira, P., Baltimore, D., and Darnell, J. (2001). Section 16.2, Electron Transport and Oxidative Phosphorylation. In Molecular Cell Biology. 4th edition., pp. 126–128.

Lorenz, A., Lorenz, M., Vothknecht, U.C., Niopek-Witz, S., Neuhaus, H.E., and Haferkamp, I. (2015). In vitro analyses of mitochondrial ATP/phosphate carriers from Arabidopsis thaliana revealed unexpected Ca2+-effects. BMC Plant Biol. **15**: 1–16.

Luk, E., Carroll, M., Baker, M., and Culotta, V.C. (2003). Manganese activation of superoxide dismutase 2 in Saccharomyces cerevisiae requires MTM1, a member of the mitochondrial carrier family. Proc. Natl. Acad. Sci. **100**: 10353–10357.

Ma, W., Kong, Q., Arondel, V., Kilaru, A., Bates, P.D., Thrower, N.A., Benning, C., and Ohlrogge, J.B. (2013). WRINKLED1, A Ubiquitous Regulator in Oil Accumulating Tissues from Arabidopsis Embryos to Oil Palm Mesocarp. PLoS One **8**: e68887.

Mandel, T., Candela, H., Landau, U., Asis, L., Zelinger, E., Carles, C.C., and Williams, L.E. (2016). Differential regulation of meristem size, morphology and organization by the ERECTA, CLAVATA and class III HD-ZIP pathways. Development **143**: 1612–1622.

Mansilla, N., Garcia, L., Gonzalez, D.H., and Welchen, E. (2015). AtCOX10, a protein involved in haem o synthesis during cytochrome c oxidase biogenesis, is essential for plant embryogenesis and modulates the progression of senescence. J. Exp. Bot. **66**: 6761–6775.

Mansilla, N., Racca, S., Gras, D.E., Gonzalez, D.H., and Welchen, E. (2018). The complexity of mitochondrial complex iv: An update of cytochrome c oxidase biogenesis in plants. Int. J. Mol. Sci. **19**.

Mayr, J.A., Merkel, O., Kohlwein, S.D., Gebhardt, B.R., Böhles, H., Fötschl, U., Koch, J., Jaksch, M.,

Lochmüller, H., Horváth, R., Freisinger, P., and Sperl, W. (2007). Mitochondrial Phosphate–Carrier Deficiency: A Novel Disorder of Oxidative Phosphorylation. Am. J. Hum. Genet. **80**: 478–484.

Mayr, J.A., Zimmermann, F.A., Horváth, R., Schneider, H.C., Schoser, B., Holinski-Feder, E., Czermin, B., Freisinger, P., and Sperl, W. (2011). Deficiency of the mitochondrial phosphate carrier presenting as myopathy and cardiomyopathy in a family with three affected children. Neuromuscul. Disord. **21**: 803–808.

McCommis, K.S. and Finck, B.N. (2015). Mitochondrial pyruvate transport: a historical perspective and future research directions. Biochem. J. **466**: 443–454.

McCormick, S.P., Moore, M.J., and Lindahl, P.A. (2015). Detection of Labile Low-Molecular-Mass Transition Metal Complexes in Mitochondria. Biochemistry **54**: 3442–3453.

Meinke, D.W. (1994). Seed Development in Arabidopsis thaliana. Cold Spring Harb. Monogr. Arch. **27**: 253–295.

Millar, A.H. and Heazlewood, J.L. (2015). Genomic and Proteomic Analysis of Mitochondrial Carrier Proteins in Arabidopsis 1. Plant Physiol. **131**: 443–453.

Millar, A.H., Small, I.D., Day, D.A., and Whelan, J. (2008). Mitochondrial Biogenesis and Function in Arabidopsis †. Arab. B. **6**: e0111.

Millar, A.H., Whelan, J., Soole, K.L., and Day, D.A. (2011). Organization and Regulation of Mitochondrial Respiration in Plants. Annu. Rev. Plant Biol. **62**: 79–104.

Mimaki, M., Wang, X., McKenzie, M., Thorburn, D.R., and Ryan, M.T. (2012). Understanding mitochondrial complex I assembly in health and disease. Biochim. Biophys. Acta - Bioenerg. **1817**: 851–862.

Młodzińska, E. and Zboińska, M. (2016). Phosphate Uptake and Allocation – A Closer Look at Arabidopsis thaliana L. and Oryza sativa L. Front. Plant Sci. **7**: 1–19.

Mohl, W., Schweiger, A., and Motschi, H. (1990). Modes of Phosphate Binding to Copper(I1): Investigations of the Electron.: 1536–1543.

Monné, M., Daddabbo, L., Gagneul, D., Obata, T., Hielscher, B., Palmieri, L., Miniero, D.V., Fernie, A.R., Weber, A.P.M., and Palmieri, F. (2018). Uncoupling proteins 1 and 2 (UCP1 and UCP2) from Arabidopsis thaliana are mitochondrial transporters of aspartate, glutamate, and dicarboxylates. J. Biol. Chem. **293**: 4213–4227.

Monné, M., Daddabbo, L., Giannossa, L.C., Nicolardi, M.C., Palmieri, L., Miniero, D.V., Mangone, A., and Palmieri, F. (2017). Mitochondrial ATP-Mg/phosphate carriers transport divalent inorganic cations in complex with ATP. J. Bioenerg. Biomembr. **49**: 369–380.

Morcuende, R., Bari, R., Gibon, Y., Zheng, W., Pant, B.D., Bläsing, O., Usadel, B., Czechowski, T., Udvardi, M.K., Stitt, M., and Scheible, W.R. (2007). Genome-wide reprogramming of metabolism and regulatory networks of Arabidopsis in response to phosphorus. Plant, Cell Environ. **30**: 85–112.

Morrow, R.M., Picard, M., Derbeneva, O., Leipzig, J., McManus, M.J., Gouspillou, G., Barbat-Artigas, S., Dos Santos, C., Hepple, R.T., Murdock, D.G., and Wallace, D.C. (2017). Mitochondrial energy deficiency leads to hyperproliferation of skeletal muscle mitochondria and enhanced insulin sensitivity. Proc. Natl. Acad. Sci. **114**: 2705–2710.

Mwamba, T.M., Li, L., Gill, R.A., Islam, F., Nawaz, A., Ali, B., Farooq, M.A., Lwalaba, J.L., and Zhou, W. (2016). Differential subcellular distribution and chemical forms of cadmium and copper in Brassica napus. Ecotoxicol. Environ. Saf. **134**: 239–249.

Nakamori, K., Takabatake, R., Umehara, Y., Kouchi, H., Izui, K., and Hata, S. (2002). Cloning, functional expression, and mutational analysis of a cDNA for Lotus japonicus mitochondrial phosphate transporter. Plant Cell Physiol. **43**: 1250–3.

Ng, S. et al. (2013). A Membrane-Bound NAC Transcription Factor, ANAC017, Mediates Mitochondrial Retrograde Signaling in Arabidopsis. Plant Cell **25**: 3450–3471.

Nodine, M.D. and Bartel, D.P. (2012). Maternal and paternal genomes contribute equally to the transcriptome of early plant embryos. Nature **482**: 94–97.

Nussaume, L., Kanno, S., Javot, H., Marin, E., Pochon, N., Ayadi, A., Nakanishi, T.M., and Thibaud, M.-C. (2011). Phosphate Import in Plants: Focus on the PHT1 Transporters. Front. Plant Sci. **2**: 83.

Palmieri, F. (1994). Mitochondrial carrier proteins. FEBS Lett. **346**: 48–54.

Palmieri, F. et al. (2009). Molecular Identification and Functional Characterization of *Arabidopsis thaliana* Mitochondrial and Chloroplastic NAD + Carrier Proteins. J. Biol. Chem. **284**: 31249–31259.

Palmieri, F. and Monné, M. (2016). Discoveries, metabolic roles and diseases of mitochondrial carriers: A review. Biochim. Biophys. Acta - Mol. Cell Res. **1863**: 2362–2378.

Palmieri, F., Pierri, C.L., De Grassi, A., Nunes-Nesi, A., and Fernie, A.R. (2011). Evolution, structure and function of mitochondrial carriers: A review with new insights. Plant J. **66**: 161–181.

Palmieri, L., Arrigoni, R., Blanco, E., Carrari, F., Zanor, M.I., Studart-Guimaraes, C., Fernie, A.R., and Palmieri, F. (2006a). Molecular Identification of an Arabidopsis S-Adenosylmethionine Transporter. Analysis of Organ Distribution, Bacterial Expression, Reconstitution into Liposomes, and Functional Characterization. Plant Physiol. **142**: 855–865.

Palmieri, L., Picault, N., Arrigoni, R., Besin, E., Palmieri, F., and Hodges, M. (2008a). Molecular identification of three Arabidopsis thaliana mitochondrial dicarboxylate carrier isoforms: organ distribution, bacterial expression, reconstitution into liposomes and functional characterization. Biochem. J. **410**: 621–629.

Palmieri, L., Santoro, A., Carrari, F., Blanco, E., Nunes-Nesi, A., Arrigoni, R., Genchi, F., Fernie, A.R., and Palmieri, F. (2008b). Identification and Characterization of ADNT1, a Novel Mitochondrial Adenine Nucleotide Transporter from Arabidopsis. Plant Physiol. **148**: 1797–1808.

Palmieri, L., Todd, C.D., Arrigoni, R., Hoyos, M.E., Santoro, A., Polacco, J.C., and Palmieri, F. (2006b). Arabidopsis mitochondria have two basic amino acid transporters with partially overlapping specificities and differential expression in seedling development. Biochim. Biophys. Acta - Bioenerg. **1757**: 1277–1283.

Pan, X., Chen, Z., Yang, X., and Liu, G. (2014). Arabidopsis voltage-dependent anion channel 1 (AtVDAC1) is required for female development and maintenance of mitochondrial functions related to energy-transaction. PLoS One **9**: 1–11.

Park, S.K., Howden, R., and Twell, D. (1998). The Arabidopsis thaliana gametophytic mutation gemini pollen1 disrupts microspore polarity, division asymmetry and pollen cell fate. Development **125**: 3789–3799.

Peñarrubia, L., Romero, P., Carrió-Seguí, A., Andrés-Bordería, A., Moreno, J., and Sanz, A. (2015). Temporal aspects of copper homeostasis and its crosstalk with hormones. Front. Plant Sci. **6**: 1–18.

Phelps, A., Briggs, C., Mincone, L., and Wohlrab, H. (1996). Mitochondrial phosphate transport protein. Replacements of glutamic, aspartic, and histidine residues affect transport and protein conformation and point to a coupled proton transport path. Biochemistry **35**: 10757–10762.

Picault, N., Hodges, M., Palmieri, L., and Palmieri, F. (2004). The growing family of mitochondrial carriers in Arabidopsis. Trends Plant Sci. **9**: 138–146.

Pignocchi, C., Minns, G.E., Nesi, N., Koumproglou, R., Kitsios, G., Benning, C., Lloyd, C.W., Doonan, J.H., and Hills, M.J. (2009). ENDOSPERM DEFECTIVE1 Is a Novel Microtubule-Associated Protein Essential for Seed Development in Arabidopsis. Plant Cell Online **21**: 90–105.

Planchais, S., Cabassa, C., Toka, I., Justin, A.-M., Renou, J.-P., Savouré, A., and Carol, P. (2014). BASIC AMINO ACID CARRIER 2 gene expression modulates arginine and urea content and stress recovery in Arabidopsis leaves. Front Plant Sci **5**: 330.

Printz, B., Lutts, S., Hausman, J.-F., and Sergeant, K. (2016). Copper Trafficking in Plants and Its Implication on Cell Wall Dynamics. Front. Plant Sci. **7**: 1–16.

Pu, X., Lv, X., Tan, T., Fu, F., Qin, G., and Lin, H. (2015). Roles of mitochondrial energy dissipation systems in plant development and acclimation to stress. Ann. Bot. **116**: 583–600.

Radin, I., Mansilla, N., Rödel, G., and Steinebrunner, I. (2015). The Arabidopsis COX11 Homolog is Essential for Cytochrome c Oxidase Activity. Front. Plant Sci. **6**: 1–17.

Ravet, K. and Pilon, M. (2013). Copper and Iron Homeostasis in Plants: The Challenges of Oxidative Stress. Antioxid. Redox Signal. **19**: 919–932.

Rieder, B. and Neuhaus, H.E. (2011). Identification of an Arabidopsis Plasma Membrane–Located ATP Transporter Important for Anther Development. Plant Cell **23**: 1932–1944.

Robertson, W.R., Clark, K., Young, J.C., and Sussman, M.R. (2004). An Arabidopsis thaliana plasma membrane proton pump is essential for pollen development. Genetics **168**: 1677–1687.

Robinson, A.J. and Kunji, E.R.S. (2006). Mitochondrial carriers in the cytoplasmic state have a common substrate binding site. Proc. Natl. Acad. Sci. **103**: 2617–2622.

van Roermund, C.W.T., Schroers, M.G., Wiese, J., Facchinelli, F., Kurz, S., Wilkinson, S., Charton, L., Wanders, R.J.A., Waterham, H.R., Weber, A.P.M., and Link, N. (2016). The Peroxisomal NAD Carrier from Arabidopsis Imports NAD in Exchange with AMP. Plant Physiol. **171**: 2127–2139.

Russel, D.W. and Sambrook, J. (2001). Molecular Cloning: A Laboratory Manual. Q. Rev. Biol. **76**: 348–349.

Sancenón, V., Puig, S., Mateu-Andrés, I., Dorcey, E., Thiele, D.J., and Peñarrubia, L. (2004). The Arabidopsis Copper Transporter COPT1 Functions in Root Elongation and Pollen Development. J. Biol. Chem. **279**: 15348–15355.

Sano, N., Ono, H., Murata, K., Yamada, T., Hirasawa, T., and Kanekatsu, M. (2015). Accumulation of long-lived mRNAs associated with germination in embryos during seed development of rice. J. Exp. Bot. **66**: 4035–4046.

Sano, N., Permana, H., Kumada, R., Shinozaki, Y., Tanabata, T., Yamada, T., Hirasawa, T., and Kanekatsu, M. (2012). Proteomic analysis of embryonic proteins synthesized from long-lived mRNAs during germination of rice seeds. Plant Cell Physiol. **53**: 687–698.

Scalise, M., Pochini, L., Giangregorio, N., Tonazzi, A., and Indiveri, C. (2013). Proteoliposomes as tool for assaying membrane transporter functions and interactions with xenobiotics. Pharmaceutics **5**: 472–497.

Schertl, P. and Braun, H.-P. (2014). Respiratory electron transfer pathways in plant mitochondria. Front. Plant Sci. **5**: 1–11.

Schmittgen, T.D. and Livak, K.J. (2008). Analyzing real-time PCR data by the comparative CT method. Nat. Protoc. **3**: 1101–1108.

Schwarzländer, M., König, A.C., Sweetlove, L.J., and Finkemeier, I. (2012). The impact of impaired mitochondrial function on retrograde signalling: A meta-analysis of transcriptomic responses. J. Exp. Bot. **63**: 1735–1750.

Scott, I. and Logan, D.C. (2007). Mitochondrial morphology transition is an early indicator of subsequent cell death in Arabidopsis. New Phytol.: 071106233614001–???

Selinski, J. and Scheibe, R. (2014). Pollen tube growth: where does the energy come from? Plant Signal. Behav. **9**: e977200.

Sheen, J. (2002). A transient expression assay using Arabidopsis mesophyll protoplasts. Nat. Nat. Plant Physiol. Nat. PNAS Abel Theol. Plant J. Plant J. Plant Mol Biol **425**: 521–525.

Shikanai, T., Müller-Moulé, P., Munekage, Y., Niyogi, K.K., and Pilon, M. (2003). PAA1, a P-Type ATPase of Arabidopsis, Functions in Copper Transport in Chloroplasts. Plant Cell Online **15**: 1333–1346.

Shukla, V., Kaur, M., Aggarwal, S., Bhati, K.K., Kaur, J., Mantri, S., and Pandey, A.K. (2016). Tissue specific transcript profiling of wheat phosphate transporter genes and its association with phosphate allocation in grains. Sci. Rep. **6**: 1–12.

Simon, P. (2003). Q-Gene: Processing quantitative real-time RT-PCR data. Bioinformatics **19**: 1439–1440.

Smart, C.J., Monéger, F., and Leaver, C.J. (1994). Cell-specific regulation of gene expression in mitochondria during anther development in sunflower. Plant Cell **6**: 811–825.

Soto, I.C., Fontanesi, F., Liu, J., and Barrientos, A. (2012). Biogenesis and assembly of eukaryotic cytochrome c oxidase catalytic core. Biochim. Biophys. Acta - Bioenerg. **1817**: 883–897.

Steinebrunner, I., Gey, U., Andres, M., Garcia, L., and Gonzalez, D.H. (2014). Divergent functions of the Arabidopsis mitochondrial SCO proteins: HCC1 is essential for COX activity while HCC2 is involved in the UV-B stress response. Front. Plant Sci. **5**: 1–17.

Steinebrunner, I., Landschreiber, M., Krause-Buchholz, U., Teichmann, J., and Rödel, G. (2011). HCC1, the Arabidopsis homologue of the yeast mitochondrial copper chaperone SCO1, is essential for embryonic development. J. Exp. Bot. **62**: 319–330.

Su, Z., Ma, X., Guo, H., Sukiran, N.L., Guo, B., Assmann, S.M., and Ma, H. (2013). Flower Development under Drought Stress: Morphological and Transcriptomic Analyses Reveal Acute Responses and Long-Term Acclimation in Arabidopsis. Plant Cell **25**: 3785–3807.

Sun, T., Li, M., Shao, Y., Yu, L., and Ma, F. (2017). Comprehensive Genomic Identification and Expression Analysis of the Phosphate Transporter (PHT) Gene Family in Apple. Front. Plant Sci. **8**: 426.

Takabatake, R., Hata, S., Taniguchi, M., Kouchi, H., Sugiyama, T., and Izui, K. (1999). Isolation and characterization of cDNAs encoding mitochondrial phosphate transporters in soybean, maize, rice, and Arabidopsis. Plant Mol. Biol. **40**: 479–486.

Takahashi, Y. and Tateda, C. (2013). The functions of voltage-dependent anion channels in plants. Apoptosis **18**: 917–924.

Theodoulou, F.L. and Eastmond, P.J. (2012). Seed storage oil catabolism: A story of give and take. Curr. Opin. Plant Biol. **15**: 322–328.

Tiwari, M., Venkatachalam, P., Penarrubia, L., and Sahi, S. V. (2017). COPT2, a plasma membrane located copper transporter, is involved in the uptake of Au in Arabidopsis. Sci. Rep. **7**: 1–9.

Twell, D. (2011). Male gametogenesis and germline specification in flowering plants. Sex. Plant Reprod. **24**: 149–160.

Umbach, A.L., Zarkovic, J., Yu, J., Ruckle, M.E., McIntosh, L., Hock, J.J., Bingham, S., White, S.J., George, R.M., Subbaiah, C.C., and Rhoads, D.M. (2012). Comparison of Intact Arabidopsis thaliana Leaf Transcript Profiles during Treatment with Inhibitors of Mitochondrial Electron Transport and TCA Cycle. PLoS One **7**.

Versaw, W.K. and Garcia, L.R. (2017). Intracellular transport and compartmentation of phosphate in plants. Curr. Opin. Plant Biol. **39**: 25–30.

Versaw, W.K. and Harrison, M.J. (2002). A chloroplast phosphate transporter, PHT2;1, influences allocation of phosphate within the plant and phosphate-starvation responses. Plant Cell **14**: 1751–66.

Vest, K.E., Leary, S.C., Winge, D.R., and Cobine, P.A. (2013). Copper import into the mitochondrial matrix in Saccharomyces cerevisiae is mediated by Pic2, a mitochondrial carrier family protein. J. Biol. Chem. **288**: 23884–23892.

Vest, K.E., Wang, J., Gammon, M.G., Maynard, M.K., White, O.L., Cobine, J.A., Mahone, W.K., and Cobine, P.A. (2016). Overlap of copper and iron uptake systems in mitochondria in Saccharomyces cerevisiae. Open Biol. **6**: 150223-.

Vogel, C. and Marcotte, E.M. (2013). Insights into regulation of protein abundance from proteomics and transcriptomis analyses. Nat. Rev. Genet. **13**: 227–232.

Waadt, R. and Kudla, J. (2008). In plant visualization of protein interactions using bimolecular fluorescence complementation (BiFC). Cold Spring Harb. Protoc. **3**: 1–8.

Walter, M., Chaban, C., Schütze, K., Batistic, O., Weckermann, K., Näke, C., Blazevic, D., Grafen, C., Schumacher, K., Oecking, C., Harter, K., and Kudla, J. (2004). Visualization of protein interactions in living plant cells using bimolecular fluorescence complementation. Plant J. **40**: 428–438.

Wang, C., Yue, W., Ying, Y., Wang, S., Secco, D., Liu, Y., Whelan, J., Tyerman, S., and Shou, H. (2015). OsSPX-MFS3, a vacuolar phosphate efflux transporter, is involved in maintaining Pi homeostasis in rice. Plant Physiol. **169**: pp.01005.2015.

Wang, D., Lv, S., Jiang, P., and Li, Y. (2017). Roles, Regulation, and Agricultural Application of Plant Phosphate Transporters. Front. Plant Sci. **8**: 1–14.

Wang, J.G., Feng, C., Liu, H.H., Ge, F.R., Li, S., Li, H.J., and Zhang, Y. (2016). HAPLESS13-Mediated Trafficking of STRUBBELIG Is Critical for Ovule Development in Arabidopsis. PLoS Genet. **12**: 1–21.

Wang, M., Ma, X., Shen, J., Li, C., and Zhang, W. (2014). The ongoing story: The mitochondria pyruvate carrier 1 in plant stress response in Arabidopsis. Plant Signal. Behav. **9**: 10–12.

Wang, W.Q., Cheng, H.Y., Møller, I.M., and Song, S.Q. (2012). The role of recovery of mitochondrial structure and function in desiccation tolerance of pea seeds. Physiol. Plant. **144**: 20–34.

Warmke, H.E. and Lee, S.L. (1978). Pollen Abortion in T Cytoplasmic Male-Sterile Corn (Zea mays): A Suggested Mechanism. Science **200**: 561–563.

Winter, D., Vinegar, B., Nahal, H., Ammar, R., Wilson, G. V., and Provart, N.J. (2007). An “electronic fluorescent pictograph” Browser for exploring and analyzing large-scale biological data sets. PLoS One **2**: 1–12.

Yang, M., Cobine, P.A., Molik, S., Naranuntarat, A., Lill, R., Winge, D.R., and Culotta, V.C. (2006). The effects of mitochondrial iron homeostasis on cofactor specificity of superoxide dismutase 2. EMBO J. **25**: 1775–1783.

Zabaleta, E., Heiser, V., Grohmann, L., and Brennicke, A. (1998). Promoters of nuclear-encoded respiratory chain Complex I genes from Arabidopsis thaliana contain a region essential for anther/pollen-specific expression. Plant J. **15**: 49–59.

Zallot, R., Agrimi, G., Lerma-Ortiz, C., Teresinski, H.J., Frelin, O., Ellens, K.W., Castegna, A., Russo, A., de Crecy-Lagard, V., Mullen, R.T., Palmieri, F., and Hanson, A.D. (2013). Identification of Mitochondrial Coenzyme A Transporters from Maize and Arabidopsis. Plant Physiol. **162**: 581–588.

Zara, V., Dietmeier, K., Palmisano, A., Vozza, A., Rassow, J., Palmieri, F., and Pfanner, N. (1996). Yeast mitochondria lacking the phosphate carrier/p32 are blocked in phosphate transport but can import preproteins after regeneration of a membrane potential. Mol. Cell. Biol. **16**: 6524–6531.

Zeller, G., Henz, S.R., Widmer, C.K., Sachsenberg, T., Rätsch, G., Weigel, D., and Laubinger, S. (2009). Stress-induced changes in the Arabidopsis thaliana transcriptome analyzed using whole-genome tiling arrays. Plant J. **58**: 1068–1082.

Zhang, C., Meng, S., Li, M., and Zhao, Z. (2016). Genomic Identification and Expression Analysis of the Phosphate Transporter Gene Family in Poplar. Front. Plant Sci. **7**: 426.

Zhang, X., Liu, S., and Takano, T. (2008). Overexpression of a mitochondrial ATP synthase small subunit gene (AtMtATP6) confers tolerance to several abiotic stresses in Saccharomyces cerevisiae and Arabidopsis thaliana. Biotechnol. Lett. **30**: 1289–1294.

Zhang, X., Takano, T., and Liu, S. (2006). Identification of a mitochondrial ATP synthase small subunit gene (RMtATP6) expressed in response to salts and osmotic stresses in rice (Oryza sativa L.). J. Exp. Bot. **57**: 193–200.

Zhang, Y., Li, S., Zhou, L.Z., Fox, E., Pao, J., Sun, W., Zhou, C., and McCormick, S. (2011). Overexpression of Arabidopsis thaliana PTEN caused accumulation of autophagic bodies in pollen tubes by disrupting phosphatidylinositol 3-phosphate dynamics. Plant J. **68**: 1081–1092.

Zhang, Y., Lyver, E.K., Knight, S.A.B., Lesuisse, E., and Dancis, A. (2005). Frataxin and mitochondrial carrier proteins, Mrs3p and Mrs4p, cooperate in providing iron for heme synthesis. J. Biol. Chem. **280**: 19794–19807.

Zhu, W., Miao, Q., Sun, D., Yang, G., Wu, C., Huang, J., and Zheng, C. (2012). The mitochondrial phosphate transporters modulate plant responses to salt stress via affecting ATP and gibberellin metabolism in Arabidopsis thaliana. PLoS One **7**: e43530.

VI. Concluding remarks

Metabolic networks connect various compartments of the plant cell. Key players of these networks are enzymes and transport proteins. Transport proteins have the potential to regulate and coordinate metabolite fluxes based on exogenous or endogenous signals (Linka and Esser, 2012; Västermark and Saier, 2014). Many transporters have been characterized to date and have been shown to possess a variety of transport modes and substrate specificities. With this, metabolic networks and their regulation are accessible and highly relevant for metabolic engineering and industrial biotechnology (Heinig et al., 2013; Kell et al., 2015).

Traditional crop breeding focused on total yield expansion. The excessive use of fresh water, fertilizers and pesticides to overcome environmental disadvantages found in modern agriculture harms the environment. Agriculture and food distribution as managed today will not meet the food demands of the following decades. Major progress has been made in recent years to target crop metabolism by plant engineering. The idea of plant engineering is the manipulation of the metabolic network of crops to enhance productivity. This includes improved energy and water usage, nutrient uptake, transfer and storage and stress tolerance. Main targets of plant engineering are enzymes, transcription factors and transporters that are involved in the aforementioned processes (López-Arredondo et al., 2015). Two major metabolic pathways are thought to enhance crop productivity: photosynthesis and photorespiration. Promising approaches include the improvement of involved enzymes, CO_2 fixation mechanisms and energy absorption (Orr et al., 2017). The highly energy-consuming photorespiratory pathway is known to be essential as regulatory mechanism. But the complex conversion of 2-phosphoglycolate and shuttle of intermediates circumvented as seen in C4 plants. Different approaches show that bypasses can be successfully implemented (Betti et al., 2016). A more sophisticated approach is to introduce C4 metabolism into C3 plants. In C4 plants CO_2 is assimilated more efficiently by RuBisCO (Gowik and Westhoff, 2011). To modify C3 plants to adopt C4 traits would include the structural and metabolic changes (Hagemann et al., 2016; Sage et al., 2014). To achieve this, a detailed knowledge of all the key players in photorespiration is required, as well as the metabolic connection of photorespiration with other pathways. A key target of this research are transport proteins. Transport proteins play a crucial role in water and nutrient uptake, stress tolerance and metabolite shuttling (Schroeder et al., 2013). Characterizing these transporters is one of the major challenges in plant engineering.

This thesis focused on the role of transport proteins belonging to mitochondrial carrier family (MCF). MCF proteins in plants are involved in many metabolic pathways (Haferkamp and Schmitz-Esser, 2012) and are localized in various subcellular compartments. They transport a variety of substrates including nucleotides, carboxylates and amino acids. These substrates are crucial for plant metabolism, showing the importance of this protein family (Palmieri et al., 2011). Studies described in this thesis enhance the knowledge about MCF

transport proteins involved in peroxisomal β-oxidation, photorespiration and mitochondrial energy conversion.

The analyses of co-expression patterns of C3 to C4 Flaveria species revealed a list of 34 putative transporters related to photorespiration (Manuscript 1). Two closely related peroxisomal MCF proteins, AtPPR1;1 and AtPPR1;2, were selected for further analysis. A phylogenetic analysis clusters both proteins with di/tri/carboxylic, amino acid and SAM carriers. Both are upregulated under photorespiratory conditions in *T. hassleriana* and Arabidopsis. *In vitro* uptake studies revealed a substrate affinity for malate for both proteins. Various MCF proteins were shown to transport malate additional to other carboxylates including oxaloacetate (Monné et al., 2018; Palmieri et al., 2008). Many MCF transporters have a broad substrate spectrum, probably a trait that goes back to the origin of this protein family (Haferkamp and Schmitz-Esser, 2012). Although the substrate spectrum observed via *in vitro* experiments does not necessarily reflect the function under physiological conditions, it would be plausible that AtPPR1;1 and AtPPR1;2 transport other substrates as well.

In peroxisomes, malate is part of the malate/oxaloacetate shuttle across the membrane. The malate/oxaloacetate shuttle fuels malate dehydrogenase (AtMDH) (Al-Saryi et al., 2017). which produces NAD^+ or NADH. NAD^+ is needed for β-oxidation and also imported by another peroxisomal MCF protein, AtPXN (Bernhardt et al., 2012). NADH is needed for the conversion of hydroxypyruvate to glycerate via AtHPR1 (Timm et al., 2011). AtPPR1;1 and AtPPR1;2 could be responsible for the malate/oxaloacetate shuttle and be involved in NAD^+/NADH regeneration of peroxisomes. They might contribute to β-oxidation and photorespiration. Further experiments need to provide data about substrate affinity of AtPPR1;1 and AtPPR1;2 and their physiological role in Arabidopsis.

The PHT3 family is responsible for the import of inorganic phosphate into mitochondria to fuel ATP synthesis (Wang et al., 2017; Kühlbrandt, 2015; Hamel et al., 2004) (Manuscript 2). PHT3 proteins are involved in energy content, stress responses and electron transport chain (ETC) based on experiments with Arabidopsis mutants (Garcia et al., 2016; Zhu et al., 2012; Jia et al., 2015; Umbach et al., 2012; Ng et al., 2013; Schwarzländer et al., 2012). AtPHT3;3 is a low expressed protein mostly found in reproductive tissues. Homozygous AtPHT3;3 T-DNA insertion lines show a defect of embryo development. A higher number of aborted seeds and empty seed positions can be found under short day conditions. Aborted seeds contain arrested embryos or no embryo. Homologues of PHT3 proteins are yeast ScMir1, ScPic2 and mammalian SLC25A3. ScMir1is a phosphate transporter (Guérin et al., 1990), while ScPic2 and SLC25A3 were shown to prefer copper as substrate (Vest et al., 2013; Boulet et al., 2018). The PHT3;3 amino acid sequence shows mutations in positions that are responsible for phosphate binding in yeast and mammals (Phelps et al., 1996; Dolce et al., 1994). AtPHT3;3 homologues found in maize, rice, tomato and poplar show these mutations

as well. This might indicate an early evolutionary divergence of AtPHT3;3 from the other PHT3 members and probably a functional shift. ScPIC2 and SLC25A3 are thought to fuel the mitochondrial copper pool (Boulet et al., 2018; Cobine et al., 2004). Here, copper is a crucial component of COX/Complex IV of the ETC. Impairment of COX assembly leads to non-viable mutants or severe growth defects (Steinebrunner et al., 2014; Radin et al., 2015). AtPHT3;3 does not exhibit this drastic phenotype. If AtPHT3;3 is involved in copper transport, AtPHT3;1 or AtPHT3;2 might be able to compensate for the loss of AtPHT3;3 except for embryo development when mitochondria need to produce high amounts of energy.

References

Al-Saryi, N.A., Al-Hejjaj, M.Y., Van Roermund, C.W.T., Hulmes, G.E., Ekal, L., Payton, C., Wanders, R.J.A., and Hettema, E.H. (2017). Two NAD-linked redox shuttles maintain the peroxisomal redox balance in Saccharomyces cerevisiae. Sci. Rep. **7**: 1–9.

Bernhardt, K., Wilkinson, S., Weber, A.P.M., and Linka, N. (2012). A peroxisomal carrier delivers NAD + and contributes to optimal fatty acid degradation during storage oil mobilization. Plant J. **69**: 1–13.

Betti, M., Bauwe, H., Busch, F.A., Fernie, A.R., Keech, O., Levey, M., Ort, D.R., Parry, M.A.J., Sage, R., Timm, S., Walker, B., and Weber, A.P.M. (2016). Manipulating photorespiration to increase plant productivity: Recent advances and perspectives for crop improvement. J. Exp. Bot. **67**: 2977–2988.

Boulet, A. et al. (2018). The mammalian phosphate carrier SLC25A3 is a mitochondrial copper transporter required for cytochrome c oxidase biogenesis. J. Biol. Chem. **293**: 1887–1896.

Cobine, P.A., Ojeda, L.D., Rigby, K.M., and Winge, D.R. (2004). Yeast Contain A Non-proteinaceous Pool of Copper in the Mitochondrial Matrix. J. Biol. Chem. **279**: 14447–14455.

Dolce, V., Iacobazzi, V., Palmieri, F., and Walker, J.E. (1994). The sequences of human and bovine genes of the phosphate carrier from mitochondria contain evidence of alternatively spliced forms. J. Biol. Chem. **269**: 10451–10460.

Garcia, L., Welchen, E., Gey, U., Arce, A.L., Steinebrunner, I., and Gonzalez, D.H. (2016). The cytochrome c oxidase biogenesis factor AtCOX17 modulates stress responses in Arabidopsis. Plant Cell Environ. **39**: 628–644.

Gowik, U. and Westhoff, P. (2011). The Path from C3 to C4 Photosynthesis. Plant Physiol. **155**: 56–63.

Guérin, B., Bukusoglu, C., Rakotomanana, F., and Wohlrab, H. (1990). Mitochondrial phosphate transport. N-ethylmaleimide insensitivity correlates with absence of beef heart-like Cys42 from the Saccharomyces cerevisiae phosphate transport protein. J. Biol. Chem. **265**: 19736–41.

Haferkamp, I. and Schmitz-Esser, S. (2012). The Plant Mitochondrial Carrier Family: Functional and Evolutionary Aspects. Front. Plant Sci. **3**: 1–19.

Hagemann, M., Weber, A.P.M., and Eisenhut, M. (2016). Photorespiration: Origins and metabolic integration in interacting compartments. J. Exp. Bot. **67**: 2915–2918.

Hamel, P., Saint-Georges, Y., De Pinto, B., Lachacinski, N., Altamura, N., and Dujardin, G. (2004). Redundancy in the function of mitochondrial phosphate transport in Saccharomyces cerevisiae and Arabidopsis thaliana. Mol. Microbiol. **51**: 307–317.

Heinig, U., Gutensohn, M., Dudareva, N., and Aharoni, A. (2013). The challenges of cellular compartmentalization in plant metabolic engineering. Curr. Opin. Biotechnol. **24**: 239–246.

Jia, F., Wan, X., Zhu, W., Sun, D., Zheng, C., Liu, P., and Huang, J. (2015). Overexpression of mitochondrial phosphate transporter 3 severely hampers plant development through regulating mitochondrial function in Arabidopsis. PLoS One **10**: 1–14.

Kell, D.B., Swainston, N., Pir, P., and Oliver, S.G. (2015). Membrane transporter engineering in industrial biotechnology and whole cell biocatalysis. Trends Biotechnol. **33**: 237–246.

Kühlbrandt, W. (2015). Structure and function of mitochondrial membrane protein complexes. BMC Biol. **13**: 1–11.

Linka, N. and Esser, C. (2012). Transport Proteins Regulate the Flux of Metabolites and Cofactors Across the Membrane of Plant Peroxisomes. Front. Plant Sci. **3**: 1–13.

López-Arredondo, D., González-Morales, S.I., Bello-Bello, E., Alejo-Jacuinde, G., and Herrera, L. (2015). Engineering food crops to grow in harsh environments. F1000Research **4**.

Monné, M., Daddabbo, L., Gagneul, D., Obata, T., Hielscher, B., Palmieri, L., Miniero, D.V., Fernie, A.R., Weber, A.P.M., and Palmieri, F. (2018). Uncoupling proteins 1 and 2 (UCP1 and UCP2) from Arabidopsis thaliana are mitochondrial transporters of aspartate, glutamate, and dicarboxylates. J. Biol. Chem. **293**:

4213–4227.

Ng, S. et al. (2013). A Membrane-Bound NAC Transcription Factor, ANAC017, Mediates Mitochondrial Retrograde Signaling in Arabidopsis. Plant Cell **25**: 3450–3471.

Orr, D.J., Pereira, A.M., da Fonseca Pereira, P., Pereira-Lima, Í.A., Zsögön, A., and Araújo, W.L. (2017). Engineering photosynthesis: progress and perspectives. F1000Research **6**: 1891.

Palmieri, F., Pierri, C.L., De Grassi, A., Nunes-Nesi, A., and Fernie, A.R. (2011). Evolution, structure and function of mitochondrial carriers: A review with new insights. Plant J. **66**: 161–181.

Palmieri, L., Picault, N., Arrigoni, R., Besin, E., Palmieri, F., and Hodges, M. (2008). Molecular identification of three Arabidopsis thaliana mitochondrial dicarboxylate carrier isoforms: organ distribution, bacterial expression, reconstitution into liposomes and functional characterization. Biochem. J. **410**: 621–629.

Phelps, A., Briggs, C., Mincone, L., and Wohlrab, H. (1996). Mitochondrial phosphate transport protein. Replacements of glutamic, aspartic, and histidine residues affect transport and protein conformation and point to a coupled proton transport path. Biochemistry **35**: 10757–10762.

Radin, I., Mansilla, N., Rödel, G., and Steinebrunner, I. (2015). The Arabidopsis COX11 Homolog is Essential for Cytochrome c Oxidase Activity. Front. Plant Sci. **6**: 1–17.

Sage, R.F., Khoshravesh, R., and Sage, T.L. (2014). From proto-Kranz to C4 Kranz: building the bridge to C4 photosynthesis. J. Exp. Bot. **65**: 3341–3356.

Schroeder, J.I., Delhaize, E., Frommer, W.B., Guerinot, M. Lou, Harrison, M.J., Herrera-Estrella, L., Horie, T., Kochian, L. V., Munns, R., Nishizawa, N.K., Tsay, Y.-F., and Sanders, D. (2013). Using membrane transporters to improve crops for sustainable food production. Nature **497**: 60–66.

Schwarzländer, M., König, A.C., Sweetlove, L.J., and Finkemeier, I. (2012). The impact of impaired mitochondrial function on retrograde signalling: A meta-analysis of transcriptomic responses. J. Exp. Bot. **63**: 1735–1750.

Steinebrunner, I., Gey, U., Andres, M., Garcia, L., and Gonzalez, D.H. (2014). Divergent functions of the Arabidopsis mitochondrial SCO proteins: HCC1 is essential for COX activity while HCC2 is involved in the UV-B stress response. Front. Plant Sci. **5**: 1–17.

Timm, S., Florian, A., Jahnke, K., Nunes-Nesi, A., Fernie, A.R., and Bauwe, H. (2011). The hydroxypyruvate-reducing system in Arabidopsis: multiple enzymes for the same end. Plant Physiol. **155**: 694–705.

Umbach, A.L., Zarkovic, J., Yu, J., Ruckle, M.E., McIntosh, L., Hock, J.J., Bingham, S., White, S.J., George, R.M., Subbaiah, C.C., and Rhoads, D.M. (2012). Comparison of Intact Arabidopsis thaliana Leaf Transcript Profiles during Treatment with Inhibitors of Mitochondrial Electron Transport and TCA Cycle. PLoS One **7**.

Västermark, Å. and Saier, M.H. (2014). The involvement of transport proteins in transcriptional and metabolic regulation. Curr. Opin. Microbiol. **18**: 8–15.

Vest, K.E., Leary, S.C., Winge, D.R., and Cobine, P.A. (2013). Copper import into the mitochondrial matrix in Saccharomyces cerevisiae is mediated by Pic2, a mitochondrial carrier family protein. J. Biol. Chem. **288**: 23884–23892.

Wang, D., Lv, S., Jiang, P., and Li, Y. (2017). Roles, Regulation, and Agricultural Application of Plant Phosphate Transporters. Front. Plant Sci. **8**: 1–14.

Zhu, W., Miao, Q., Sun, D., Yang, G., Wu, C., Huang, J., and Zheng, C. (2012). The mitochondrial phosphate transporters modulate plant responses to salt stress via affecting ATP and gibberellin metabolism in Arabidopsis thaliana. PLoS One **7**: e43530.

VII. Published manuscripts

VII.1 Manuscript 3

Analysis of peroxisomal β-oxidation during storage oil mobilization in Arabidopsis thaliana seedlings

Björn Hielscher[1,2], Lennart Charton[1,2], Tabea Mettler-Altmann[1], Nicole Linka[1,3]

[1] Institute for Plant Biochemistry and Cluster of Excellence on Plant Sciences (CEPLAS), Heinrich Heine University, Universitätsstrasse 1, 40225 Düsseldorf, Germany.

[2] These authors contributed equally to this work.

[3] To whom correspondence should be addressed. E-mail: Nicole.Linka@hhu.de.

i. Summary

Peroxisomal β-oxidation in plants is essential for mobilization of storage oil in seed-oil storing plants, such as *Arabidopsis thaliana*. In plants, degradation of fatty acids occurs exclusively in peroxisomes via the β-oxidation, driving seedling growth and development upon germination. Thus, the determination of storage oil breakdown rates is a useful approach to investigate defects in peroxisomal β-oxidation. Here we describe an acid catalyzed derivatization process of fatty acids representing a fast and efficient procedure to generate high yields of fatty acid methyl esters (FAMEs). The subsequent analysis by gas-chromatography coupled to mass spectrometry (GC-MS) allows the quantification of total fatty acid content. The results provide detailed information of the complete storage oil breakdown process via peroxisomal β-oxidation during seedling growth.

ii. Key Words

Plant seedling, storage oil mobilization, peroxisomes, fatty acid β-oxidation

1. Introduction

Plants accumulate storage molecules during seed maturation in order to provide energy for post-germinative heterotrophic seedling establishment [1]. Depending on the plant species, these molecules can be divided in three major classes: carbohydrates, oil and proteins. But the storage of oil in the form of triacylglyceroles (TAGs), sequestered in cytosolic oil bodies, is arguable the most widely distributed strategy in nature. In the model oilseed plant *Arabidopsis thaliana* (Arabidopsis) the amount of TAGs can account for up to 60 % of seed weight and their complete oxidation yields more than twice the energy of carbohydrates and proteins [2]. Thus, Arabidopsis has been instrumental in investigating molecular mechanisms involved in lipid metabolism [3]. Storage oil reserves are degraded within the first days after imbibition, providing energy until the seedlings become photoautotrophic [4] (Fig. 1).

In contrast to mammals, peroxisomal β-oxidation is the sole site of fatty acid degradation in plants underlying the essential role of this organelle in early seedling development [5]. The process of storage oil mobilization starts with the hydrolysation of TAGs at the oil/water interface of cytosolic oil bodies. The released free fatty acids are subsequently transported into peroxisomes and degraded via β-oxidation. The produced acetyl CoA is further metabolized within the glyoxylate cycle to succinate and malate. These four-carbon compounds are further converted to sucrose via gluconeogenesis [6]. Sucrose represents the mobile form of reduced carbon transported through the cell and serves as an energy source for developing tissues [7].

Arabidopsis mutants deficient in β-oxidation are associated with compromised storage oil breakdown. These plants are impaired in post-germinative growth, which can be rescued

by the exogenous supply of sucrose [1]. This sucrose-dependent phenotype is a suitable marker to detect mutants deficient in storage oil mobilization. However, some Arabidopsis mutants, such as the one for the peroxisomal NAD carrier PXN, exhibit wild type like growth in the absence of sucrose but analysis of the fatty acid amounts during seedling establishment revealed a reduced storage oil turnover [8]. This indicates that once a certain threshold of degraded fatty acids is achieved, there is no obvious seedling phenotype detectable. Thus, information on the ability to break down fatty acids are required to verify a defect in β-oxidation-associated storage oil breakdown.

The analysis of TAG breakdown products by gas chromatography-mass spectrometry (GC-MS) delivers absolute quantitative values and therefore is a powerful tool to identify Arabidopsis mutants involved in peroxisomal β-oxidation [9]. In addition, the use of GC-MS facilitates the analysis of small amounts of tissue and provides complete information on fatty acid composition [9]. Beyond the broad spectrum of different Arabidopsis fatty acids, eicosenoic acid (C20:1) is found almost exclusively in TAGs and therefore can be used as a convenient marker to monitor storage oil degradation [10]. Fatty acid determination is usually performed after derivatization to the corresponding methyl ester by methylation or transmethylation [11]. Many methods have been described for the preparation of fatty acid methyl esters (FAMEs), but the acid catalyzed esterification using methanolic HCl is the most widely used procedure for the rapid isolation of high amounts of FAMEs [12,13,9]. Further, the addition of an internal standard prior extraction permits absolute quantification of the fatty acid content and allows correcting for technical variation, for example, due to slightly different efficiencies of the derivatization process.

Here we describe a fast and efficient isolation procedure of FAMEs from Arabidopsis ecotype Col-0 seeds and seedlings on sucrose containing medium to monitor not only the initial seed oil content but also the storage oil degradation rate. The chosen light regime was short day (8 h light / 16 h darkness), but other growth conditions, such as long day, continuous light or darkness, did not negatively influence fatty acid catabolism, but the rate of fatty acid turnover is elevated when day length is increased [8]. However, stratification of seeds is mandatory to assure simultaneous and efficient germination [14]. In contrast to that, the growth conditions of the parental generation can affect both seed quantity and quality in terms of germination and developmental efficiency, as well as general fatty acid content [9]. Therefore, the respective control and mutant plants have to be grown under equal conditions to yield comparable results. In consideration of the predominant sucrose dependency, it is favorable to cultivate seedlings for fatty acid analysis on sucrose containing medium to avoid the influence of developmental deficiencies on the fatty acid breakdown rate. It is important to note that storage oil breakdown is decelerated but not inhibited in the presence of sucrose [15].

2. Materials

2.1 Plant growth, seed production and germination

1. Arabidopsis ecotype Col-0 seeds from Nottingham Arabidopsis Stock Center (NASC, http://arabidopsis.info, [16])
2. 1.5 mL reaction tubes
3. Commercial white peat-vermiculite soil mix including a starter nutrient charge
4. Autoclave
5. Ethanol, technical grade (70 %, add Triton-X 100 for seed sterilization; 100 %), Ethanol (p.a. grade)
6. Filter paper (Whatman qualitative paper, Grade 1, 8.5 cm diameter)
7. Laminar flow cabinet
8. Half-strength Murashige and Skoog agar medium (0.5x MS agar) [17]: 2.2 g/L MS salts, 10 mL/L 0.5 M MES/KOH, pH 5.7, 8 g/L plant agar. Add 10 g/L sucrose if necessary for germination of plants impaired in β-oxidation. Autoclave at 121 °C for at least 15 min.
9. Petri dishes (8.5 cm diameter)
10. Programmable growth chamber
11. Surgical tape
12. Vortexer

2.2 Fatty acid extraction

1. 1 % (w/v) sodium chloride
2. Acetone
3. Analytical balance
4. Centrifuge (2.000 *g*, for glass reaction tubes)
5. Deep-freezer (-80 °C)
6. Distilled water, add detergent tablet for the first cleaning step
7. Electric water boiler
8. Freezer (-20 °C)
9. Glass GC vials
10. Glass Pasteur pipettes (New or cleaned with n-hexane; purity ≥ 95 %)
11. Glass pipettes (cleaned with n-hexane; purity ≥ 95 %)
12. Glass reaction tubes with screw-cap (Teflon)
13. Hamilton glass syringe (cleaned with n-hexane; purity ≥ 95 %)
14. Heptadecanoic acid (C17:0; 1 mg/ml in n-hexane; purity ≥ 99 %) as internal standard
15. Incubator (60 - 80 °C)
16. Liquid nitrogen
17. Methanolic HCl (3 N hydrochloric acid in methanol)

18. n-hexane (purity ≥ 99 %) for fatty acid extraction and n-hexane (purity ≥ 95 %) to clean pipets and syringes
19. Spoon or spatula
20. Thermoblock (90 °C, for glass reaction tubes)
21. 7200 GC-QTOF (Agilent Technologies, USA)
22. Mass Hunter Software (Agilent Technologies, USA)

3. Methods

3.1 Seed production and germination

Plant growth conditions and seed production

Photoperiod, temperature and humidity have a direct influence on seed production. Therefore, it is highly recommended to choose the most beneficial growth conditions for plants to produce seeds with comparable quality and quantity. Likewise, it is important to analyze seeds of the same age. To compare the β-oxidation rates of different Arabidopsis seedlings, maternal plants should be grown simultaneously.

1. Sterilize the surface of Arabidopsis seeds to minimize fungi contamination of half strength MS agar medium, especially when sucrose was added to the medium (Note 1). Transfer 2 mg of dried seeds (approx. 100 seeds) into 1.5 mL reaction tubes. Add 0.5 to 1 mL ethanol (70 %) and a droplet of detergent (e.g. Triton-X 100). Shake the tubes for 10 min at room temperature (RT) using a vortexer. Afterwards, remove all liquid with a pipet and add 0.5 to 1 mL ethanol (100 %) and shake again (Note 2). Make sure to thoroughly clean the seed surface with ethanol to remove all residual detergent. Remove all liquid and dry the seeds in a Laminar flow cabinet. Alternatively, seeds can also be sterilized via vapor-phase sterilization with chlorine. (Note 3).
2. Sow the Arabidopsis seeds on petri dishes filled with sterile 0.5x MS agar medium supplemented with 1 % (w/v) sucrose. In case of transgenic plants (e.g. T-DNA insertion lines), include appropriate antibiotics for selection. It is recommended to seal the dishes with surgical tape to allow airflow and high humidity, but prevent further contamination. The absorption of water by the dried seeds, called imbibition, is the first step of seed germination. Keep the plates with seeds in the dark at 4 °C for at least 3 days. This cold treatment (stratification) improves germination rate and synchrony of seed germination (Note 4).
3. Transfer the Arabidopsis seeds to a controlled growth chamber (growth conditions, see below). Keep the seedlings on 0.5x MS agar medium until four leaves are visible (approx. after 2 weeks). Then transfer single seedlings to pots filled with soil mix (Note 5). Regardless of the growth medium, the following conditions should provide you with healthy plants with satisfactory yield.

Temperature: Optimal temperatures for flowering plants are at 22 - 23 °C (Note 6).

Light regime and photoperiod: Light intensities of 120 - 150 µmol * m^{-2} * s^{-1} and long day conditions with 16 h light / 8 h darkness induce flowering with first flower buds after approx. 4 - 5 weeks (Note 7).

Humidity: Higher humidity is beneficial for seedlings especially during germination and after the transfer to soil. Set humidity to 60 - 80 %. Later growth on soil allows a subsequent decrease in humidity to 50 - 60 % and lower when siliques develop (Note 8).

Watering: It is not recommended to overwater Arabidopsis plants. Wait for the top layer of soil to be almost dry until the plants are watered again (Note 9). Stop watering when most of the siliques start to dry (see step 5).

4. 5 weeks after germination plants may need to be stabilized. Use wire or string to bind the shoot stems to a wooden stick.
5. 6 - 8 weeks after germination siliques start to dry and are ready to shatter. Harvest seeds by covering the upper part of the plant with a glassine sleeves for seed collection (Note 10).
6. After complete desiccation cut off the bag and sieve the seeds to remove any residues of siliques or other parts of the plant (Note 11).

Germination

Fatty acid degradation is a rapid process during the first days after germination. Hence, stratification is of great importance to achieve a uniform germination rate of the seeds. For β-oxidation related phenotypes the addition or omission of 1 % (w/v) sucrose to the growth agar medium is essential to detect differences in the capability of TAG breakdown via peroxisomal β-oxidation.

1. Degradation of storage fatty acids by β-oxidation will be observed over a time course of 6 days after imbibition (DAI). Plan your experiment in order to harvest enough material at the following stages (Fig. 1): Seeds (10 mg, approx. 500 seeds), 2 DAI (20 mg, approx. 200 seedlings), 4 DAI (20 mg, approx. 60-70 seedlings) and 6 DAI (20 mg, approx. 40-50 seedlings) (Note 12, 13). Collect a minimum of three biological replicates for each stage. Prepare and sterilize seeds as described before.
2. Prepare petri dishes with 0.5x MS agar medium with and without 1 % (w/v) sucrose. Place an autoclaved 8.5 mm filter paper on top of the agar plates (Note 14). Sow seeds on the soaked filter and seal the dishes with surgical tape. Stratify the seeds by keeping them in the dark at 4 °C for at least 3 days.
3. Transfer the seeds into a growth chamber with controlled growth conditions as listed before (Note 15).
4. Retrieve the seedlings after 2 DAI, 4 DAI and 6 DAI, preferably at the same time of day

to assure good reproducibility between different sets of experiments.

3.2 Preparation of plant material and fatty acid extraction

Collecting plant material

For every step of the following protocol use metal or glassware if not stated otherwise. Wearing gloves is mandatory to avoid contamination with fatty acids from skin.

1. Prepare a small spoon or spatula by cleaning it once with water, ethanol (70 %) and acetone, respectively, to remove any fatty acids.
2. Carefully scratch the seedlings from the filter using the spoon or spatula. Weigh 20 mg of plant material for each sample and transfer the plant material into pre-cooled 1.5 mL reaction tubes (Note 16). Directly freeze the tubes in liquid nitrogen. Record the exact weight of the plant material (Note 17). Store the samples frozen at -80 °C until further use.
3. Seeds can be directly taken from the seed stock. Weigh 10 mg of seed material and keep them at RT in already cleaned glass reaction tubes used for fatty acid extraction until further use (Note 18).

Fatty acid derivatization and extraction

The detection of fatty acids via GC-MS requires derivatization to fatty acid methyl esters (FAMEs). Fatty acids will be extracted and derivatized with cleaned or n-hexane rinsed glassware. Again, wearing gloves is mandatory.

1. Thoroughly clean glass reaction tubes and screw caps to prevent fatty acid contamination. Transfer reaction tubes and screw caps into a heat-resistant glass beaker. Add boiling water (e.g. with an electric water boiler) and detergent (Note 19) to the beaker. Wait until water cooled down entirely. Remove the water and rinse the material with boiling water up to eight times. Air-dry the glassware at 60 to 80 °C in an incubator. Rinse the glass tubes with 1 mL ethanol (puriss. p.a. grade) by vortexing, remove the liquid and dry at 60 - 80 °C. Afterwards, close the tubes.
2. Prepare a thermoblock at 90 °C.
3. Take the seedlings from the deep-freezer and keep them in liquid nitrogen. Still frozen, transfer the seedlings into the cleaned glass reaction tubes with a spatula. Likewise, transfer the seeds.
4. Immediately add 10 µl of the internal standard heptadecanoic acid (C17:0, 1 mg / mL) to all seedling samples and 100 µl to all seed samples with a Hamilton glass syringe (Note 20). Then add 1 mL 3 N methanolic HCl with a glass pipet (Note 21).
5. Close the reaction tubes tightly and incubate the samples in the thermoblock at 90 °C for 1 h (Note 22). Check if the screw caps are tightly closed during derivatization.

6. Cool down the reaction tubes to RT for 5 min.
7. Add 1 mL n-hexane (purity ≥ 99 %, Note 23) with a glass pipet and vortex for 10 s to trap the derivatization products.
8. Add 1 mL 1 % (w/v) sodium chloride and vortex again for 10 s. Sodium chloride will allow complete phase separation.
9. Centrifuge the reaction tubes for 5 min at 2000 *g* at RT for clear phase separation.
10. Transfer the resulting upper hexane phase (approx. 1 mL) with a glass Pasteur pipet into a GC vial without piercing through the lower methanolic HCl / sodium chloride phase or seeds and seedlings.
11. Dilute all seed samples (1:10 in n-hexane; purity ≥ 99 %). Store the samples at -20 °C until further analysis.
12. Store one sample of hexane (n-hexane; purity ≥ 99 %) to be used a blank for the GC-MS analysis.

3.3 GC-MS analysis

FAME extracts are analyzed by GC-MS [17] using a 7200 GC-QTOF. Runs of hexane (blanks) are used to distinguish background from biologically meaningful peaks. The peak area is determined via peak integration using the Mass Hunter Software. Peak areas (hereafter referred to as response) are used for further calculations.

3.4 Viability tests

Calibration curve

The precise quantification of fatty acid content requires a linear dependency of concentration and response as can be seen in Fig. 2. With our equipment, quantities starting from 1 pg / µL up to a concentration on 150 pg / µL can be reliably detected for a variety of fatty acids present in Arabidopsis and for the internal standard C17:0. The slopes of the standard curves of the different tested FAMEs are comparable (less than 20 % SD). This means, together with the fact that C17:0 is not present naturally in plant material (see also below) that the amount of added C17:0 to the biological material can be used for absolute quantification of the different FAME species. The quantities of C20:1 FAMEs in extracts from seeds (using 10 mg, extracted in 1000 µl and 1 µl injected of a 1:10 dilution) and seedlings (using 20 mg, extracted in 1000 µl and 1 µl injected) normally ranges from 1.9 to 92.7 ng / µL and is within the linear range for quantities between 1 and 150 ng / µL (Fig. 2) (Note 24).

Recovery experiment

The quality of this method and the influence of plant material on the detection of FAMEs can be verified with a recovery experiment (Equation A) [18]. This test identifies the recoverable

amount of added fatty acid standards from plant material. Separate aliquots of collected plant material are processed as described before with or without the addition of fatty acid standards.

$$\text{(A)}\quad \%\,Recovery = 100 \cdot \frac{Conc_{Observed} - Conc_{Expected}}{Conc_{Expected}} + 100$$

Here we added 10 µl of heptadecanoic acid (C17:0, 1 mg/mL) and derivatized samples with and without frozen plant material (4 DAI). Our results show a C17:0 recovery of 107 %, SD ± 4.8 (N = 3 biological replicates), meaning that the derivatization is not limited by the presence of plant material. Additionally, plant material without the addition of C17:0 was analyzed and minor amounts of C17:0 was detected (138-fold less) making C17:0 a reliable internal standard.

3.5 Data analysis

Quantitation of fatty acid composition

Eicosenoic acid (C20:1) is a TAG-specific fatty acid in Arabidopsis seeds. It is represented by the 13-eicosenoic (C20:1 Δ^{13}) and 11-eicosenoic (C20:1 Δ^{11}) acid in the FAME mass chromatogram (see Fig. 3). The defined concentration of the internal standard heptadecanoic acid (C17:0) will allow calculating the amount of fatty acids of the seed/seedling extracts.

1. For the following calculations the response of C20:1 ($Response_{FA}$) equals the sum of responses of both detected eicosenoic acid forms. Equation (B) determines the concentration of C20:1 in the transferred hexane phase. For this, use the internal standard C17:0 ($Response_{Standard}$) and its defined concentration ($Conc_{Standard}$).

$$\text{(B)}\quad FA\left[\frac{ng}{\mu L}\right] = \frac{Conc_{Standard}\left[\frac{ng}{\mu L}\right] \cdot Response_{FA}}{Response_{Standard}}$$

2. The total content of C20:1 in the collected plant sample can be calculated with equation (B). It includes the dilution factor (*DF*) of the sample (Seeds: 10, seedlings: 1) and the volume of hexane used for extraction (Vol_{Hexane}). For the content of C20:1 per seed, divide the result of equation (C) by the number of collected seeds/seedlings.

$$\text{(C)}\quad FA\left[\frac{ng}{total\ FW}\right] = FA\left[\frac{ng}{total\ Vol_{Hexane}\ [\mu L]}\right] = FA\left[\frac{ng}{\mu L}\right] \cdot Vol_{Hexane}[\mu L] \cdot DF$$

3. Determine the content of C20:1 per mg fresh weight (*FW*) with equation (D). A typical decrease of C20:1 in Arabidopsis during seedling establishment can be seen in Fig. 4.

$$\text{(D)} \quad FA\left[\frac{ng}{mg\ FW}\right] = \frac{FA\left[\frac{ng}{total\ FW}\right]}{FW\ [mg]}$$

4. Equation (E) determines the percentage of C20:1 compared to the sum of all present fatty acids detected in the plant material. Important: subtract the response of the internal standard C17:0 (*Response*$_{Standard}$) from the sum of all fatty acid responses (*Response*$_{TtotalFA}$).

$$\text{(E)} \quad \%\ FA/Total\ FA = \frac{Response_{FA} \cdot 100}{Response_{TotalFA} - Response_{Standard}}$$

4. Notes

1. 1% (w/v) sucrose is required for Arabidopsis mutants defective in β-oxidation supporting seedling establishment. The addition of sucrose suppresses the mutant growth phenotype but also favors growth of fungi if seeds are not properly sterilized.
2. For more than 2 mg seeds repeat the washing steps with 1 mL ethanol (70 %) and detergent, as well as 1 mL ethanol (100 %).
3. Vapor-phase sterilization with chlorine is an alternative method to sterilize the surface of Arabidopsis seeds [19]. Fill 1 - 2 mg seeds into a 1.5 mL tube. Use a desiccator jar located in a fume hood and place the seeds into the jar. Fill a beaker with approx. 100 mL sodium hypochlorite solution (13 % active chlorite) and put it next to your seeds into the desiccator jar. Partly close the jar and add 3 mL concentrated HCl (37 %) to the beaker. Immediately close the jar and make sure it is sealed tightly. After 2 h of sterilization open the jar and let the chlorine fumes evaporate for 1 - 2 min. Close your seed containing reaction tubes and transfer them to a Laminar flow cabinet for complete evaporation of chlorine for 30 min.
4. Arabidopsis seeds need to be cold treated before they start to germinate (stratification). Physiological experiments require at least 3 days to induce simultaneous germination. This highly improves comparability between biological replicates.
5. Choose only healthy looking seedlings, preferably of equal size. Remove any residual agar sticking to the roots (e.g. by carefully washing the roots in water) to avoid the transfer of fungi contamination. Negative interaction between plant roots can be reduced as much as possible by keeping the plants separately in a pot or allow them to grow at least 5-6 cm apart from each other in one pot.
6. The preferred temperature range of Arabidopsis plants is 16 - 25 °C. Temperatures < 22 °C prolong the vegetative state. Higher temperatures induce heat stress and negatively affect growth and seed maturation.

7. Grown under short day conditions with < 12 h light per day cycle favor vegetative growth. Continuous light can be used when the majority of siliques start to dry (yellowish coat, 6 - 8 weeks after germination).
8. Germination on 0.5x MS agar medium provides enough humidity for seedlings, when they are in a covered petri dish. After the transfer to soil, plants should be covered, preferably with a plastic dome, for at least one week to protect plants from drying out.
9. Fertilize plants with fertilizers containing nitrogen, phosphorus, and potassium source on a weekly basis. Extensive watering promotes pests (e.g. insects, moss or fungi). Additional biological pest management should be considered (e.g. *Chrysoperla carnea, Hypoaspis miles*).
10. Glassine bags are permeable for air (when not entirely closed), light and water. This prevents fungi infection but allows silique maturation and speeds up seed collection.
11. Use a sieve with 450 µm mesh size to remove remnants of siliques and other plant parts.
12. Seeds can be directly used for fatty acid extraction without sterilization and stratification.
13. The total fatty acid content of Arabidopsis seeds largely exceeds the content of seedlings. 10 mg of seeds and 20 mg seedlings are sufficient (see also Note 20).
14. The filter facilitates the collection of seeds after germination without piercing through the agar. Wrap filters into aluminum foil to prevent damaging during autoclaving.
15. Short day (8 h light / 16 h darkness), normal day (12 h light / 12 h darkness), long day (16 h light / 8 h darkness) and continuous light do not influence germination or fatty acid catabolism.
16. Form a bale of seedlings. This facilitates the transfer to glass reaction tubes during fatty acid extraction and prevents loss of the frozen material (see also Note 17).
17. The exact weight of the plant material allows the calculation of the fatty acid content per mg of seedlings or seeds, respectively. If required, count the seedlings or seeds to determine the fatty acid content of single seedlings or seeds, respectively. Quantity of seeds: 1 mg equals approximately 50 Arabidopsis seeds.
18. Alternatively, Arabidopsis seeds can be stored in a thoroughly cleaned glass vial prior to fatty acid extraction. Do not use plastic tubes to avoid loss of material due to electrostatics.
19. Detergent tablets used for dishwashers work perfectly.
20. Heptadecanoic acid is not present in plants and can be used as internal standard for quantification. The tenfold amount of this standard is added for a consistent concentration between seedling and diluted seed extracts as the seed extracts are diluted tenfold prior measurement.
21. Add the internal standard, as well as methanolic HCl at the bottom of the reaction tube to avoid loss of the internal standard prior and during derivatization. Do not vortex.

22. Do not shake or vortex the glass reaction tube containing seeds and seedlings before incubation at 90 °C. The material easily sticks to the side of the tube and will not be processed. Return plant material into methanolic HCl with a thin spatula, thoroughly cleaned before.
23. Higher purity of hexane improves the quality of your samples and data.
24. FAMEs in 6 DAI samples may be below detection limit (see Fig. 4). To measure those samples, FAMEs can be extracted in a smaller hexane volume (< 1 mL). It is recommended to use at least 200 µL to allow an easy phase transfer. Alternatively, the 1 mL hexane phase can be evaporated at temperatures ≤ 50 °C after extraction and the FAMEs can be resuspended in 100 µL n-hexane (purity ≥ 99 %). Note: Differences in concentrations have to be included into further calculations.

5. References

1. Graham IA (2008) Seed storage oil mobilization. Annu Rev Plant Biol 59:115-142.

2. Theodoulou FL, Eastmond PJ (2012) Seed storage oil catabolism: a story of give and take. Curr Opin Plant Biol 15 (3):322-328.

3. Graham IA, Eastmond PJ (2002) Pathways of straight and branched chain fatty acid catabolism in higher plants. Prog Lipid Res 41 (2):156-181.

4. Eastmond PJ, Graham IA (2001) Re-examining the role of the glyoxylate cycle in oilseeds. Trends Plant Sci 6 (2):72-78.

5. Kindl H (1993) Fatty acid degradation in plant peroxisomes: function and biosynthesis of the enzymes involved. Biochimie 75 (3-4):225-230.

6. Pracharoenwattana I, Smith SM (2008) When is a peroxisome not a peroxisome? Trends Plant Sci 13 (10):522-525.

7. Williams LE, Lemoine R, Sauer N (2000) Sugar transporters in higher plants--a diversity of roles and complex regulation. Trends Plant Sci 5 (7):283-290.

8. Bernhardt K, Wilkinson S, Weber AP, Linka N (2012) A peroxisomal carrier delivers NAD and contributes to optimal fatty acid degradation during storage oil mobilization. Plant J 69 (1):1-13.

9. Li Y, Beisson F, Pollard M, Ohlrogge J (2006) Oil content of Arabidopsis seeds: the influence of seed anatomy, light and plant-to-plant variation. Phytochemistry 67 (9):904-915.

10. Lemieux B, Miquel M, Somerville C, Browse J (1990) Mutants of Arabidopsis with alterations in seed lipid fatty acid composition. Theor Appl Genet 80 (2):234-240.

11. Garces R, Mancha M (1993) One-step lipid extraction and fatty acid methyl esters preparation from fresh plant tissues. Anal Biochem 211 (1):139-143.

12. Browse J, McCourt PJ, Somerville CR (1986) Fatty acid composition of leaf lipids determined after combined digestion and fatty acid methyl ester formation from fresh tissue. Anal Biochem 152 (1):141-145.

13. Ichihara K, Fukubayashi Y (2010) Preparation of fatty acid methyl esters for gas-liquid chromatography. J Lipid Res 51 (3):635-640.

14. Munir J, Dorn LA, Donohue K, Schmitt J (2001) The effect of maternal photoperiod on seasonal dormancy in *Arabidopsis thaliana* (Brassicaceae). Am J Bot 88 (7):1240-1249

15. Fulda M, Schnurr J, Abbadi A, Heinz E, Browse J (2004) Peroxisomal Acyl-CoA synthetase activity is essential for seedling development in *Arabidopsis thaliana*. Plant Cell 16 (2):394-405.

16. Scholl RL, May ST, Ware DH (2000) Seed and molecular resources for Arabidopsis. Plant Physiol 124 (4):1477-1480.
17. Murashige T, Skoog F (1962) A Revised Medium for Rapid Growth and Bio Assays with Tobacco Tissue Cultures. Physiol Plantarum 15 (3):473-497.
18. Fiehn O, Kind T (2007) Metabolite profiling in blood plasma. Methods Mol Biol 358:3-17
19. Buhrman DL, Price PI, Rudewiczcor PJ (1996) Quantitation of SR 27417 in human plasma using electrospray liquid chromatography-tandem mass spectrometry: A study of ion suppression. J Am Soc Mass Spectrom 7 (11):1099-1105.
20. Clough SJ, Bent AF (1998) Floral dip: a simplified method for Agrobacterium-mediated transformation of *Arabidopsis thaliana*. Plant J 16 (6):735-743.

Figures and figure legends

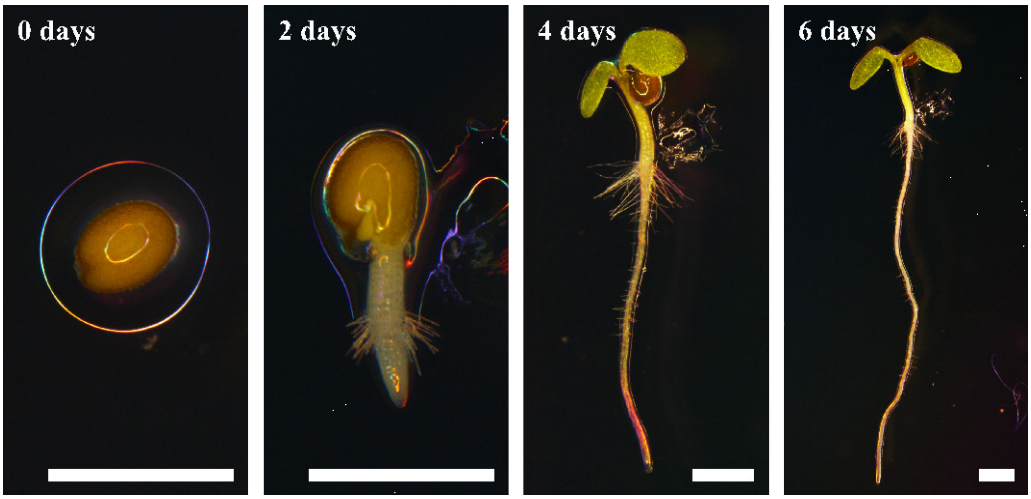

Figure 1. Seedling growth stages of an Arabidopsis Col-0 seed within 6 days after imbibition. Expansion of root and cotyledons solely depends on the breakdown of TAGs until the first photosynthetic active leaves develop. Growth conditions: 8 h light / 16 h darkness. Bars = 1 mm.

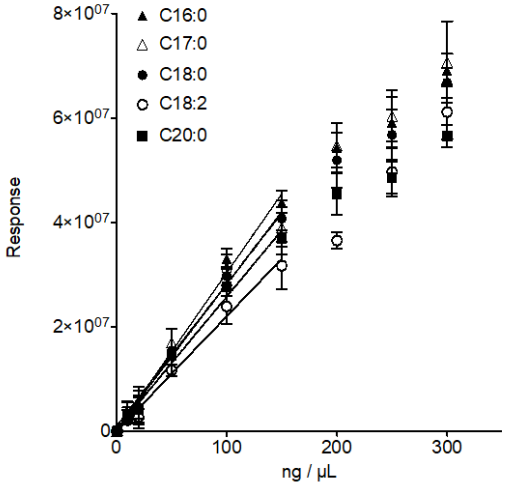

Figure 2. Calibration curve for selected fatty acids in Arabidopsis, palmitic acid (C16:0), stearic acid (C18:0), linoleic acid (C18:2), arachidic acid (C20:0) and the internal standard heptadecanoic acid (C17:0). Final concentrations: 0, 1, 10, 20, 50, 100, 150, 200, 250, 300 ng / µL. Error bars indicate SD (N = 3 replicates; C16:0, slope = 302520 ± 3.5% SD, R^2 = 0.98; C17:0, slope = 272153 ± 4.52% SD, R^2 = 0.96; C18:0, slope = 278161 ± 2.37% SD, R^2 = 0.99; C18:2, slope = 220638 ± 4.23% SD, R^2 = 0.97; C20:0, slope = 254265 ± 2.68% SD, R^2 = 0.99).

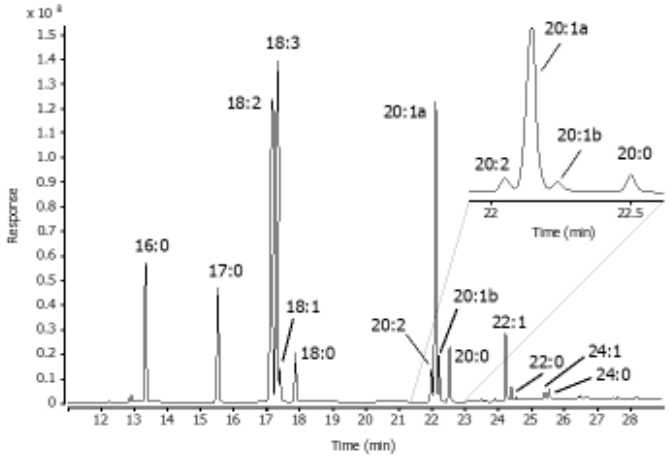

Figure 3. Typical chromatogram of fatty acid methyl esters of Arabidopsis seeds. 13-eicosenoic and 11-eicosenoic acid, two forms of eicosenoic acid in plants, are depicted as two separate peaks (20:1a and C20:1b). For fatty acid content calculation heptadecanoic acid (C17:0), which is not naturally present in Arabidopsis, is added to each sample as internal standard.

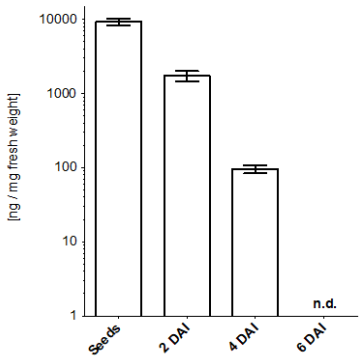

Figure 4. Breakdown of eicosenoic acid (C20:1) within 6 days after imbibition. Eicosenoic acid (C20:1) is used as a marker for TAG breakdown in Arabidopsis. C20:1 is highly abundant in seeds and rapidly degraded (note the logarithmic y-axis). Only approximately 100-fold less of this marker fatty acid is detectable after 4 days of germination. Growth conditions: 8 h light / 16 h darkness. Error bars indicate SD (N = 3 biological replicates). n. d.; not detected.

Acknowledgement

This work was supported by DFG-grant 1781/2-1 and GRK 1525. Authors thank Andreas P.M. Weber for stimulating discussion. We thank Elisabeth Klemp and Katrin Weber for technical assistance and Kirsten Abel for general assistance.

Author contribution

Björn Hielscher and Lennart Charton wrote the manuscript. Björn Hielscher performed all experiments and analyses. Nicole Linka and Tabea Mettler-Altmann participated in scientific discussions. Nicole Linka and Tabea Mettler-Altmann assisted in drafting this manuscript. Nicole Linka and Tabea Mettler-Altmann designed the experiments.

VII.2 Manuscript 4

Uncoupling proteins 1 and 2 (UCP1 and UCP2) from Arabidopsis thaliana are mitochondrial transporters of aspartate, glutamate, and dicarboxylates

Magnus Monné [‡§], Lucia Daddabbo[‡], David Gagneul[¶1], Toshihiro Obata[ǁ],
Björn Hielscher[¶2], Luigi Palmieri[‡**], Daniela Valeria Miniero[‡],
Alisdair R. Fernie[ǁ3], Andreas P. M. Weber[¶4] and Ferdinando Palmieri[‡**5]

From the [‡]Department of Biosciences, Biotechnologies and Biopharmaceutics, Laboratory of Biochemistry and Molecular Biology, University of Bari, via Orabona 4, 70125 Bari, Italy

the [§]Department of Sciences, University of Basilicata, Via Ateneo Lucano 10, 85100 Potenza, Italy

the [¶]Cluster of Excellence on Plant Science (CEPLAS), Institute of Plant Biochemistry, Heinrich-Heine-Universität, Universitätsstrasse 1, 40225 Düsseldorf, Germany

the [ǁ]Department Willmitzer, Max-Planck-Institut fur Molekulare Pflanzenphysiologie, Am Muhlenberg 1, 14476 Potsdam-Golm, Germany

and the [**]Center of Excellence in Comparative Genomics, University of Bari, via Orabona 4, 70125 Bari, Italy

JBC ARTICLE

Uncoupling proteins 1 and 2 (UCP1 and UCP2) from *Arabidopsis thaliana* are mitochondrial transporters of aspartate, glutamate, and dicarboxylates

Received for publication, November 9, 2017, and in revised form, January 15, 2018 Published, Papers in Press, January 25, 2018, DOI 10.1074/jbc.RA117.000771

Magnus Monné[‡§], Lucia Daddabbo[‡], David Gagneul[¶1], Toshihiro Obata[‖], Björn Hielscher[¶2], Luigi Palmieri[‡], Daniela Valeria Miniero[‡], Alisdair R. Fernie[‖3], Andreas P. M. Weber[¶4], and Ferdinando Palmieri[‡**5]**

*From the [‡]Department of Biosciences, Biotechnologies and Biopharmaceutics, Laboratory of Biochemistry and Molecular Biology, University of Bari, via Orabona 4, 70125 Bari, Italy, the [§]Department of Sciences, University of Basilicata, Via Ateneo Lucano 10, 85100 Potenza, Italy, the [¶]Cluster of Excellence on Plant Science (CEPLAS), Institute of Plant Biochemistry, Heinrich-Heine-Universität, Universitätsstrasse 1, 40225 Düsseldorf, Germany, the [‖]Department Willmitzer, Max-Planck-Institut fur Molekulare Pflanzenphysiologie, Am Muhlenberg 1, 14476 Potsdam-Golm, Germany, and the **Center of Excellence in Comparative Genomics, University of Bari, via Orabona 4, 70125 Bari, Italy*

Edited by Joseph M. Jez

The *Arabidopsis thaliana* genome contains 58 members of the solute carrier family SLC25, also called the mitochondrial carrier family, many of which have been shown to transport specific metabolites, nucleotides, and cofactors across the mitochondrial membrane. Here, two *Arabidopsis* members of this family, AtUCP1 and AtUCP2, which were previously thought to be uncoupling proteins and hence named UCP1/PUMP1 and UCP2/PUMP2, respectively, are assigned with a novel function. They were expressed in bacteria, purified, and reconstituted in phospholipid vesicles. Their transport properties demonstrate that they transport amino acids (aspartate, glutamate, cysteine sulfinate, and cysteate), dicarboxylates (malate, oxaloacetate, and 2-oxoglutarate), phosphate, sulfate, and thiosulfate. Transport was saturable and inhibited by mercurials and other mitochondrial carrier inhibitors to various degrees. AtUCP1 and AtUCP2 catalyzed a fast counterexchange transport as well as a low uniport of substrates, with transport rates of AtUCP1 being much higher than those of AtUCP2 in both cases. The aspartate/glutamate heteroexchange mediated by AtUCP1 and AtUCP2 is electroneutral, in contrast to that mediated by the mammalian mitochondrial aspartate glutamate carrier. Furthermore, both carriers were found to be targeted to mitochondria. Metabolite profiling of single and double knockouts shows changes in organic acid and amino acid levels. Notably, AtUCP1 and AtUCP2 are the first reported mitochondrial carriers in *Arabidopsis* to transport aspartate and glutamate. It is proposed that the primary function of AtUCP1 and AtUCP2 is to catalyze an aspartate$_{out}$/glutamate$_{in}$ exchange across the mitochondrial membrane and thereby contribute to the export of reducing equivalents from the mitochondria in photorespiration.

Mitochondrial carriers (MCs)[6] are a large family of membrane proteins that transport nucleotides, amino acids, carboxylic acids, inorganic ions, and cofactors across the mitochondrial inner membrane (1–3). Many metabolic pathways and cellular processes with complete or partial localization in the mitochondrial matrix are dependent on transport steps catalyzed by MCs (*e.g.* oxidative phosphorylation, metabolism of fatty acids and amino acids, gluconeogenesis, thermogenesis, mitochondrial replication, transcription, and translation) (3). The protein sequences of the MC family members have a characteristic three times tandemly repeated 100-residue domain (4), which contains two hydrophobic segments and a signature sequence motif P*X*(D/E)*XX*(K/R)*X*(K/R) (20–30 residues) (D/E)G*XXXX*(W/Y/F)(K/R)G (PROSITE PS50920, PFAM PF00153, and IPR00193) (5). In atomic resolution 3D structures of the only MC family member determined to date (the carboxyatractyloside-inhibited ADP/ATP carrier) (6, 7), the six hydrophobic segments form a bundle of transmembrane α-helices with a central substrate translocation pore, and the three P*X*(D/E)*XX*(K/R) motifs form a gate toward the matrix side. In most cases, the MC signature motif has been used to identify family members in genomic sequences; *Homo sapiens* has 53 members, *Saccharomyces cerevisiae* has 35, and *Arabidopsis thaliana* has 58. About half of these carriers have been identified and characterized in terms of substrate specificity, transport proteins, and kinetic parameters by direct transport assays (1, 8, 9).

This work was supported by grants from the Center of Excellence on Comparative Genomics and Italian Human ProteomeNet Grant RBRN07BMCT_009 (MIUR). The authors declare that they have no conflicts of interest with the contents of this article.

This article contains Tables S1–S4 and Figs. S1–S6.

[1] Present address: Université de Lille, INRA, ISA, Université d' Artois, Université du Littoral Côte d'Opale, EA 7394-ICV-Institut Charles Viollette, F-59000 Lille, France.

[2] Supported by an iGRAD-Plant doctoral fellowship (IRTG 1525).

[3] Work in the laboratory of this author was supported by the Max-Planck-Society.

[4] Supported by the Cluster of Excellence on Plant Science CEPLAS (EXC 1028) and CRC 1208.

[5] To whom correspondence should be addressed: Dept. of Biosciences, Biotechnologies, and Biopharmaceutics, Laboratory of Biochemistry and Molecular Biology, University of Bari, via Orabona 4, 70125 Bari, Italy. Tel.: 39-080-5443323; Fax: 39-080-5442770; E-mail: ferdpalmieri@gmail.com.

[6] The abbreviations used are: MC, mitochondrial carrier; UCP, uncoupling protein; AtUCP1, *A. thaliana* UCP1; AtUCP2, *A. thaliana* UCP2; hUCP2, human UCP2; DIC, dicarboxylate carrier; DTC, di- and tricarboxylate carrier; GDC, glycine decarboxylase; GFP, green fluorescent protein; GS/GOGAT, glutamine synthetase/glutamine oxoglutarate aminotransferase; MAS, malate aspartate shuttle; IVD, isovaleryl-CoA-dehydrogenase; CTD, C-terminal domain.

Transport properties of AtUCP1 and AtUCP2

Studies aiming to biochemically characterize MCs from *A. thaliana* were initiated by comparing selected *Arabidopsis* genes with those of yeast and humans encoding MCs with previously identified substrates (9). *Arabidopsis* has been demonstrated to express MCs for the four main types of substrates (1) (*i.e.* nucleotide carriers for ADP/ATP (AAC1–4, PNC1 and -2, AtBT1, PM-ANT1, and TAAC) (10–16), adenine nucleotides (ADNT1) (17), ATP-Mg/P_i (APC1–3) (18, 19), NAD^+ (NDT1 and -2) (20), NAD^+, NADH, CoA, and adenosine 3′,5′-phosphate (PXN) (21, 22); carboxylate carriers for di- and tricarboxylates (DTC) (23) and dicarboxylates (DIC1–3) (24); amino acid carriers for basic amino acids (BAC1 and -2) (25, 26) and *S*-adenosylmethionine (SAMC1 and -2) (27, 28); and inorganic ion carriers for phosphate and sulfate (29)). It is important to note that some of the carriers characterized from *Arabidopsis* have broader substrate specificities than their human and yeast counterparts, and additionally some of them are localized in compartments other than the mitochondria, such as peroxisomes, chloroplasts, the endoplasmic reticulum, and the plasma membrane (1). It is also noteworthy that the molecular identity of an *Arabidopsis* MC corresponding to the human aspartate/glutamate exchangers (AGC1 and -2) (30) or glutamate uniporters of any type (GC1 and -2) (31) has, to date, not been established.

The mammalian uncoupling protein 1 (UCP1) was demonstrated to transport protons, thereby uncoupling oxidative phosphorylation (32, 33). On the basis of homology with subsequently sequenced MCs, a UCP subfamily was identified containing six members in both humans (hUCP1–6) and *Arabidopsis* (AtUCP1–6). However, AtUCP4–6 were subsequently renamed dicarboxylate carriers (DIC1–3), following the demonstration that they transport malate, oxaloacetate, succinate, P_i, sulfate, thiosulfate, and sulfite (24), and hUCP2 was demonstrated to be a four-carbon metabolite/P_i carrier transporting aspartate, malate, malonate, oxaloacetate, P_i, and sulfate (34).

In the current study, we investigated the potential transport properties of the two closest homologs of hUCP2 in *Arabidopsis*: AtUCP1 and AtUCP2, also known as PUMP1 and PUMP2. Previously, AtUCP1 was shown to be localized to mitochondria and display an uncoupling activity similar to that of hUCP1 (35–37). By contrast, very little is known about AtUCP2; in a proteomic study, it was detected in the Golgi (38), but in another, it was detected at the plasma membrane (39). The results presented here demonstrate that AtUCP1 and the less-studied AtUCP2 are mitochondrially localized isoforms and have a broad substrate specificity, transporting a variety of substrates, including aspartate, glutamate, malate, oxaloacetate, and other metabolites. Characterization of metabolite profiles of T-DNA insertional knockout mutants, including a *ucp1*/*ucp2* double mutant, revealed clear changes in organic acid levels, some of which were exacerbated by the application of salt stress.

Results

Identification of the closest homologs of AtUCP1 and AtUCP2 in various species

The protein sequences of AtUCP1 and AtUCP2 homologs were collected, aligned, and analyzed (Fig. S1). AtUCP1 and AtUCP2 share 72% identical amino acids. Their sequences are much more similar to each other than to any other *Arabidopsis* protein; in *Arabidopsis*, the closest relative to AtUCP1 and AtUCP2 is AtDIC2, which shares 41 and 42% sequence identity with AtUCP1 and AtUCP2, respectively. In humans and *S. cerevisiae*, the closest homologs are hUCP2 (34), having 51 and 44% identical amino acids, and yeast Dic1p (40), exhibiting 30 and 33% sequence identity with AtUCP1 and AtUCP2, respectively. Putative orthologs with high sequence identity with AtUCP1 and AtUCP2 above 75% were found in several plant species. Moreover, from structural sequence alignments using the X-ray structure of the bovine ADP/ATP carrier (6) as a template, it can be deduced that 85 and 54% of the residues lining the surface of the substrate translocation pore are identical between AtUCP1 and AtUCP2 and between AtUCP1, AtUCP2, and hUCP2, respectively. These results suggest that AtUCP1 and AtUCP2 are isoforms, and their closest homolog with identified substrates is hUCP2.

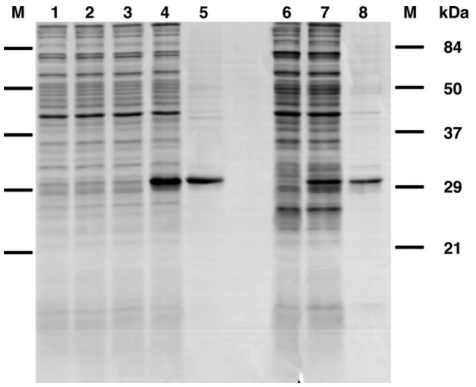

Figure 1. Expression in *Escherichia coli* and purification of AtUCP1 and AtUCP2. Proteins were separated by SDS-PAGE and stained with Coomassie Blue. *Lanes 1–5*, AtUCP1; *lanes 6–8*, AtUCP2. Markers were Bio-Rad prestained SDS-PAGE standards: bovine serum albumin, 84 kDa; ovalbumin, 50 kDa; carbonic anhydrase, 37 kDa; soybean trypsin inhibitor, 29 kDa; lysozyme, 21 kDa). *Lanes 1–4*, *E. coli* BL21(DE3); *lanes 6* and *7*, *E. coli* BL21 CodonPlus(DE3)-RIL containing the expression vector, without (*lanes 1*, *3*, and *6*) and with the coding sequence of AtUCP1 (*lanes 2* and *4*) and the coding sequence of AtUCP2 (*lane 7*). Samples were taken immediately before induction (*lanes 1* and *2*) and 5 h later (*lanes 3*, *4*, *6*, and *7*). The same number of bacteria were analyzed in each sample. *Lanes 5* and *8*, purified AtUCP1 protein (5 μg) and purified AtUCP2 (3 μg) derived from bacteria shown in *lanes 4* and *7*, respectively.

Bacterial expression of AtUCP1 and AtUCP2

AtUCP1 and AtUCP2 were expressed in *Escherichia coli* BL21(DE3) strains (Fig. 1, *lanes 4* and *7*). They accumulated as inclusion bodies and were purified by centrifugation and washing (see "Experimental procedures"). The apparent molecular masses of purified AtUCP1 and AtUCP2 (Fig. 1, *lanes 5* and *8*) were ~31 kDa, which is in good agreement with the calculated value of 33 kDa for both AtUCP1 and AtUCP2. The identities of the recombinant proteins were confirmed by MALDI-TOF mass spectrometry, and the yield of the purified proteins was about 10 and 2 mg/liter of culture for AtUCP1 and AtUCP2, respectively. The proteins were detected neither in non-

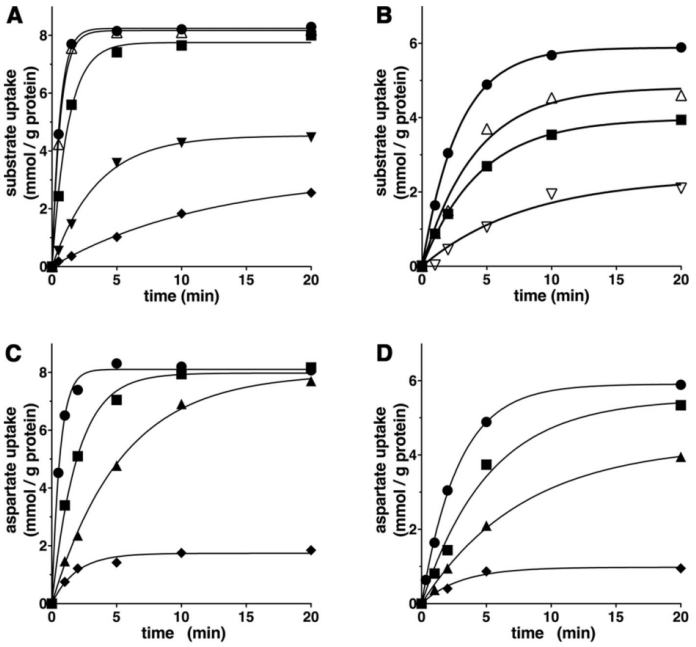

Figure 2. Substrate homo-exchanges in proteoliposomes reconstituted with AtUCP1 (*A* and *C*) and AtUCP2 (*B* and *D*). *A* and *B*, homo-exchanges of aspartate (●), malate (△), glutamate (■), malonate (▼), sulfate (◆), and 2-oxoglutarate (▽) at 25 °C. *C* and *D*, aspartate/aspartate homo-exchange at 4 °C (◆), 8 °C (▲), 16 °C (■), and 25 °C (●). Transport was initiated by adding radioactive substrate (concentration, 1 mM) to proteoliposomes preloaded internally with the same substrate (concentration, 10 mM). The reaction was terminated at the indicated times. Similar results were obtained in at least three independent experiments.

induced cultures nor in cultures with an empty vector (Fig. 1, *lanes 1*, *2*, *3*, and *6*).

Functional characterization of recombinant AtUCP1 and AtUCP2

Recombinant AtUCP1 and AtUCP2 were reconstituted into liposomes, and their transport activities for various radioactive substrates were tested in homo-exchange experiments (*i.e.* with the same external (1 mM) and internal (10 mM) substrate). In a first set of homo-exchange experiments, time-dependent uptake of several radioactive substrates (aspartate, malate, and glutamate for reconstituted AtUCP1 and AtUCP2; malonate and sulfate for AtUCP1; and 2-oxoglutarate for AtUCP2) demonstrated typical curves for carrier-mediated transport (Fig. 2, *A* and *B*). Both AtUCP1- and AtUCP2-mediated homo-exchanges between external [^{14}C]aspartate and internal aspartate were temperature-dependent (Fig. 2, *C* and *D*), as would be expected for protein-catalyzed transport. Furthermore, no [^{14}C]aspartate/aspartate or [^{14}C]malate/malate exchange activity was detected if AtUCP1 and AtUCP2 had been boiled before incorporation into liposomes or if proteoliposomes were reconstituted with lauric acid/sarkosyl-solubilized material from bacterial cells lacking the expression vector for AtUCP1 and AtUCP2 or harvested immediately before induction of expression (data not shown). In all of these experiments, a mixture of pyridoxal-5′-phosphate and bathophenanthroline was used to block the AtUCP1- and AtUCP2-mediated transport reactions at various time points. In addition, AtUCP1 and AtUCP2 were found to catalyze homo-exchanges of glutamate, malonate, malate, succinate, and P_i, whereas no or very low transport was observed with glutamine, arginine, phenylalanine, threonine, valine, proline, γ-aminobutyrate, citrate, ATP, GTP, *S*-adenosylmethionine, or glutathione (Fig. 3).

The substrate specificities of AtUCP1 and AtUCP2 were examined in detail by measuring the initial rate of [^{14}C]aspartate uptake into proteoliposomes that had been preloaded with various potential substrates (Fig. 4). For both AtUCP1 and AtUCP2, the highest activities were observed in the presence of internal aspartate, glutamate, cysteine sulfinate, cysteate, malonate, malate, oxaloacetate, maleate, and (for AtUCP2) 2-oxoglutarate. Both proteins also exchanged, albeit to a lower extent, internal D-aspartate, cysteine, oxalate, succinate, 2-oxoglutarate, α-aminoadipate, P_i, sulfate, and thiosulfate. In addition, AtUCP2 exchanged [^{14}C]aspartate with the internal substrates (Fig. 4*B*) fumarate, glutarate, and nitrate, which were not significantly transported by AtUCP1 (Fig. 4*A*). By contrast, the uptake of labeled aspartate by AtUCP1 and AtUCP2 was negligible with internal asparagine, D-glutamate, glutamine, serine, glycine, homocysteate, adipate, α-ketoadipate, pyrophosphate, citrate, pyruvate, lactate, phosphoenolpyruvate, acetoacetate, β-hydroxybutyrate, *N*-acetylaspartate, ATP, and

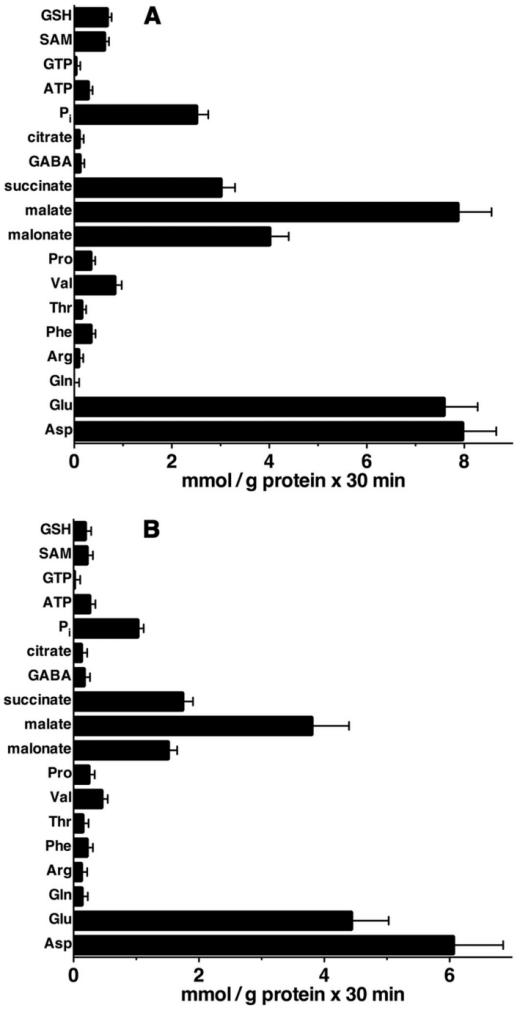

Figure 3. AtUCP1- and AtUCP2-mediated homo-exchanges of various substrates. Proteoliposomes reconstituted with AtUCP1 (*A*) and AtUCP2 (*B*) were preloaded internally with the substrates indicated in the figure (concentration, 10 mM). Transport was initiated by adding radioactive substrate (concentration, 1 mM) to proteoliposomes containing the same substrate. The reaction was terminated after 30 min. The values are means ± S.E. (*error bars*) of at least three independent experiments. *SAM*, *S*-adenosylmethionine.

glutathione (Fig. 4, *A* and *B*). The activity in the presence of these substrates was approximately the same as that observed in the presence of NaCl and no substrate.

The effects of other mitochondrial carrier inhibitors on the [^{14}C]aspartate/aspartate exchange reaction catalyzed by reconstituted AtUCP1 and AtUCP2 were also examined. This transport activity was inhibited strongly by bathophenanthroline, pyridoxal-5′-phosphate, and tannic acid and markedly by mersalyl, $HgCl_2$, and butylmalonate (Fig. 5). Phenylsuccinate and *p*-hydroxymercuribenzoate strongly inhibited AtUCP1 and partially inhibited AtUCP2, whereas bromcresol purple and α-cyano-4-hydroxycinnamate caused partial inhibition of both carriers. By contrast, carboxyatractyloside, bongkrekic acid, and *N*-ethylmaleimide had little or no effect on either AtUCP1 or AtUCP2 activity.

Kinetic characteristics of recombinant AtUCP1 and AtUCP2 proteins

In Fig. 6, the kinetics of 1 mM [^{14}C]aspartate (*A* and *B*) or 1 mM [^{14}C]malate (*C* and *D*) uptake into proteoliposomes catalyzed by recombinant AtUCP1 (*A* and *C*) or AtUCP2 (*B* and *D*) and measured either as uniport (with internal NaCl) or as exchange (in the presence of 10 mM substrates) are compared. The [^{14}C]aspartate/aspartate and [^{14}C]malate/malate exchanges followed first-order kinetics (rate constants 1.6 and 1.4 min^{-1} (AtUCP1) or 0.27 and 0.23 min^{-1} (AtUCP2); initial rates 14 and 11 mmol/min × g of protein (AtUCP1) or 1.9 and 1.3 mmol/min × g of protein (AtUCP2), respectively), isotopic equilibrium being approached exponentially. By contrast, with internal NaCl and no substrate, very low uptake of [^{14}C]aspartate or [^{14}C]malate was observed by liposomes reconstituted either with AtUCP1 or AtUCP2, suggesting that the two proteins catalyze a minor unidirectional transport (uniport) of substrates. In addition, Fig. 6 (*A–D*) illustrates the time courses of several AtUCP1-mediated and AtUCP2-mediated hetero-exchanges between [^{14}C]aspartate or [^{14}C]malate and other transported substrates. The data of Fig. 6 (*A* and *C*) show that AtUCP1 transports cysteate much better than D-aspartate and dicarboxylates with the following order of efficiency: malate > oxaloacetate > malonate > succinate (these substrates better than P_i). Similarly, the data of Fig. 6 (*B* and *D*) demonstrate that cysteate is transported slightly better than D-aspartate and malate more efficiently than oxaloacetate by AtUCP2. The uniport mode of transport was further investigated by measuring the efflux of [^{14}C]aspartate or [^{14}C]malate from preloaded active proteoliposomes because it provides a more convenient assay for unidirectional transport (41). In the absence of external substrate, significant efflux of [^{14}C]aspartate (Fig. 7, *A* and *B*) or [^{14}C]malate (Fig. 7, *C* and *D*) catalyzed by both AtUCP1 and AtUCP2 was observed. However, in the presence of external substrates, the efflux transport rates were at least one order of magnitude higher. These experiments demonstrate that AtUCP1 and AtUCP2 are capable of catalyzing both a rapid antiport of substrates and a slow uniport transport.

The kinetic constants of AtUCP1 and AtUCP2 were determined from the initial transport rates of homo-exchanges at various external labeled substrate concentrations in the presence of a constant saturating internal substrate concentration. The Michaelis constants (K_m) of the two recombinant proteins for aspartate were about 0.8 mM, and for glutamate and malate, they were between 1.9 and 2.5 mM. The maximal activities (V_{max}) for aspartate, glutamate, and malate varied between 24 and 33 mmol/min × g of protein for AtUCP1 and 4.2 and 4.5 mmol/min × g of protein for AtUCP2 (Table 1). Glutamate, malate, cysteine sulfinate, cysteate, oxaloacetate, α-ketoglutarate, and sulfate were competitive inhibitors of the AtUCP1- and AtUCP2-mediated [^{14}C]aspartate/aspartate exchanges, as

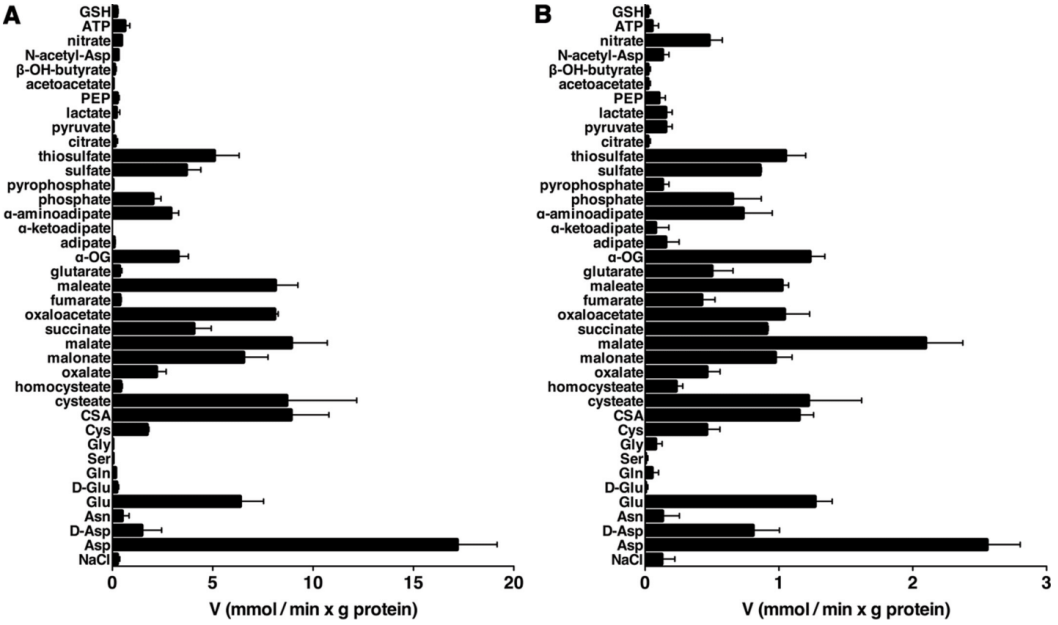

Figure 4. Substrate specificity of AtUCP1 and AtUCP2. Proteoliposomes were preloaded internally with various substrates (concentration, 10 mM). Transport was started by adding 0.8 mM [^{14}C]aspartate and stopped after 7 and 20 s for AtUCP1 (*A*) and AtUCP2 (*B*), respectively. The values are means ± S.E. (*error bars*) of at least three independent experiments. *α-OG*, α-ketoglutarate; *CSA*, cysteinesulfinic acid; *PEP*, phosphoenolpyruvate.

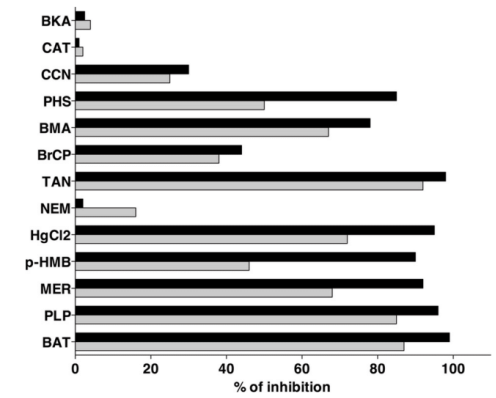

Figure 5. Effect of mitochondrial carrier inhibitors on the rate of AtUCP1- and AtUCP2-mediated [^{14}C]aspartate/aspartate exchange. Proteoliposomes were preloaded internally with 10 mM aspartate, and transport was initiated by adding 1 mM [^{14}C]aspartate. The incubation time was 7 and 20 s for AtUCP1 and AtUCP2, respectively. Thiol reagents and α-cyanocinnamate were added 2 min before the labeled substrate; the other inhibitors were added together with [^{14}C]aspartate. The final concentrations of the inhibitors were as follows: 10 μM for mercuric chloride ($HgCl_2$), carboxyatractyloside (*CAT*), and bongkrekic acid (*BKA*); 0.1 mM for mersalyl (*MER*) and *p*-hydroxymercuribenzoate (*pHMB*); 0.2 mM for bromcresol purple (*BrCP*); 1 mM for *N*-ethylmaleimide (*NEM*) and α-cyanocinnamate (*CCN*); 5 mM for butylmalonate (BMA) and phenylsuccinate (*PHS*); 25 mM for bathophenanthroline (*BAT*); 30 mM for pyridoxal 5′-phosphate (*PLP*); and 0.2% for tannic acid (*TAN*). The extents of inhibition (percentages) for AtUCP1 (*black bars*) and AtUCP2 (*gray bars*) from a representative experiment are given. Similar results were obtained in at least three independent experiments.

they increased the apparent K_m without changing the V_{max} (not shown). The inhibition constants (K_i) of these compounds are listed in Table 2.

Influence of membrane potential and pH gradient on the AtUCP1- and AtUCP2-mediated exchange reactions

Given that the mammalian aspartate glutamate carriers AGC1 and -2 have been shown to catalyze an electrophoretic exchange between aspartate$^-$ and glutamate$^-$ + H^+ (30), we investigated the influence of the membrane potential on the [^{14}C]aspartate/glutamate exchange catalyzed by recombinant AtUCP1 and AtUCP2. A K^+-diffusion potential was generated across the proteoliposomal membranes with valinomycin in the presence of a K^+ gradient of 1:50 (mM/mM, in/out), corresponding to a calculated value of about 100 mV positive inside (Table 3). The rate of the [^{14}C]aspartate$_{out}$/glutamate$_{in}$ heteroexchange was unaffected by valinomycin in the presence of the K^+ gradient. By contrast, the aspartate$_{out}$/glutamate$_{in}$ exchange, mediated by recombinant AGC2 C-terminal domain (AGC2-CTD) (30), was stimulated under the same experimental conditions. These results indicate that the AtUCP1- and AtUCP2-mediated aspartate/glutamate hetero-exchange is not electrophoretic but electroneutral, suggesting that AtUCP1 and AtUCP2 transport either aspartate$^-$ for glutamate$^-$ or both together with a H^+. Also, the AtUCP1- and AtUCP2-mediated aspartate/aspartate, malate/malate, and malate$_{out}$/aspartate$_{in}$ (Table 3) and malate$_{out}$/glutamate$_{in}$ (data not shown) were unaffected by valinomycin in the presence of a K^+ gradient of 1:50. In view of the different charges carried by the amino

Transport properties of AtUCP1 and AtUCP2

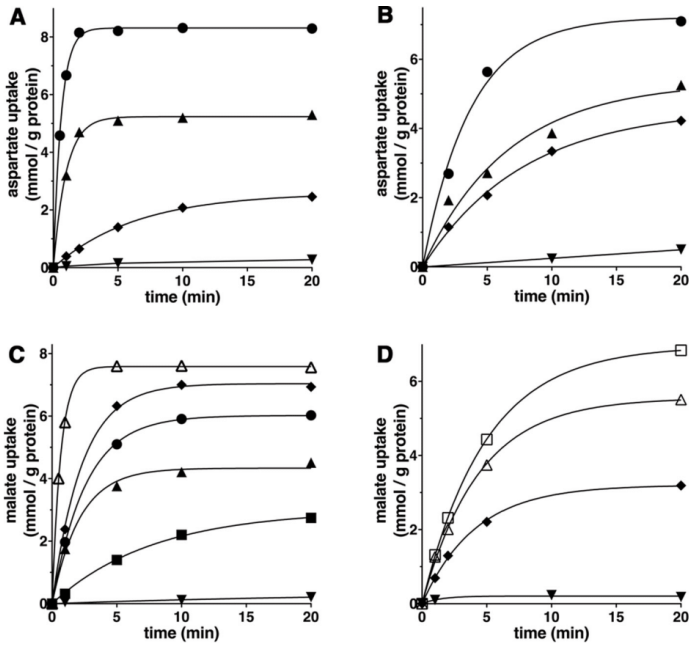

Figure 6. Kinetics of [^{14}C]aspartate or [^{14}C]malate uptake by AtUCP1- and AtUCP2-reconstituted liposomes containing no substrate or various substrates. Proteoliposomes containing AtUCP1 (*A* and *C*) or AtUCP2 (*B* and *D*) were preloaded internally with 10 mM aspartate (●), cysteate (▲), D-aspartate (◆), or 10 mM NaCl and no substrate (▼) (*A* and *B*) and with malate (△), oxaloacetate (◆), malonate (●), succinate (▲), phosphate (■), aspartate (□), or 10 mM NaCl and no substrate (▼) (*C* and *D*). Transport was initiated by adding 1 mM [^{14}C]aspartate (*A* and *B*) or 1 mM [^{14}C]malate (*C* and *D*) and terminated at the indicated times. Similar results were obtained in at least three independent experiments.

acids aspartate and glutamate and dicarboxylates at physiological pH levels, we explored whether the charge imbalance of the malate/aspartate and malate/glutamate hetero-exchanges catalyzed by AtUCP1 and AtUCP2 is compensated by proton movement. A pH difference across the liposomal membranes (basic inside the vesicles) was created by the addition of the K^+/H^+ exchanger nigericin to proteoliposomes in the presence of a K^+ gradient of 1:50 (mM/mM, in/out). Under these conditions, the uptake of [^{14}C]malate in exchange for internal aspartate or glutamate increased (Table 3), whereas the uptake of [^{14}C]malate in exchange for internal malate or 2-oxoglutarate was unaffected (data not shown). Therefore, the charge imbalance of the substrates exchanged by AtUCP1 and AtUCP2 is compensated by the movement of protons.

Subcellular localization of AtUCP1 and AtUCP2 proteins in transiently transformed Nicotiana benthamiana leaf cells

C-terminal fusion proteins of AtUCP1 and AtUCP2 with the green fluorescent protein (GFP) under the control of an *Arabidopsis* ubiquitin-10 promoter were transiently expressed in *N. benthamiana* to investigate the subcellular localization via confocal laser-scanning microscopy. Simultaneously, *N. benthamiana* was co-infiltrated with the mitochondrion-located *Arabidopsis* isovaleryl-CoA-dehydrogenase tagged with a C-terminal eqFP611 (IVD-eqFP611) under the control of the cauliflower mosaic virus 35S promoter. Two days after infiltration, protoplasts were isolated from leaf tissue and directly used for microscopy.

The C-terminal fusion proteins AtUCP1-GFP (Fig. 8*A*) and AtUCP2-GFP (Fig. 8*B*) (shown in *green*) clearly overlap with almost all mitochondrial IVD-eqFP611 fluorescent signals (shown in *red*) in all observed protoplasts, indicating the mitochondrial localization of both proteins. 48 h after infiltration, the mitochondrial marker was generally higher-expressed than the GFP fusion proteins and was also found in the cytosol with more prominent fluorescent signals detected in mitochondria.

Isolation, generation, and metabolic characterization of AtUCP1–2 knockout mutants

After biochemically characterizing the properties of recombinant AtUCP1 and AtUCP2 proteins, we turned our attention to evaluating their physiological role in *Arabidopsis*. For this purpose, we acquired the individual T-DNA insertion mutants and crossed them to obtain the *ucp1*/*ucp2* double mutant (Fig. S2). The *ucp1* line used here was extensively characterized by Sweetlove *et al.* (37), including functional complementation by the *UCP1* genomic sequence. This mutant harbors a T-DNA insertion in the first intron and shows low residual UPC protein amounts in the mitochondria (5% of the wildtype line (37)). Congruent with this previous work, we also detected residual expression of the *UCP1* gene, which was much lower than that of the wildtype (Fig. S3). The expression of the *UCP2* gene was

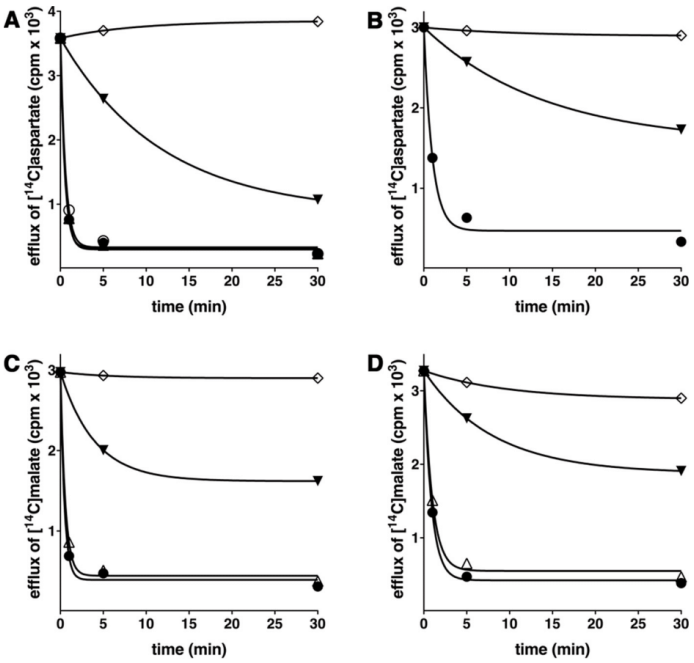

Figure 7. Efflux of [^{14}C]aspartate and [^{14}C]malate from AtUCP1- and AtUCP2-reconstituted liposomes. Proteoliposomes containing AtUCP1 (*A* and *C*) and AtUCP2 (*B* and *D*) with 5 mM aspartate and 5 mM malate internally were loaded with [^{14}C]aspartate and [^{14}C]malate, respectively, by carrier-mediated exchange equilibrium, and external substrate was removed by Sephadex G-75. Efflux of [^{14}C]aspartate (*A* and *B*) and [^{14}C]malate (*C* and *D*) was started by adding 5 mM aspartate (●), malate (△), glutamate (○), 5 mM NaCl and no substrate (▼), and 5 mM aspartate (*A* and *B*) or 5 mM malate (*C* and *D*) together with 20 mM pyridoxal 5′-phosphate and 20 mM bathophenanthroline (◇). The transport was terminated at the indicated times. Similar results were obtained in at least three independent experiments.

Table 1

Kinetic constants of recombinant AtUCP1 and AtUCP2

The values were calculated from linear regression of double reciprocal plots of the initial rates of the indicated homo-exchanges *versus* the external substrate concentration. The exchanges were started by adding appropriate concentrations of labeled substrate to proteoliposomes preloaded internally with the same substrate (10 mM). The reaction time was 7 and 20 s for AtUCP1 and AtUCP2, respectively. The values are means ± S.E. of at least three independent experiments carried out in duplicate.

Carrier and substrate	K_m	V_{max}
	mM	*mmol/min × g protein*
AtUCP1		
[^{14}C]Aspartate/aspartate	0.8 ± 0.1	30 ± 6
[^{14}C]Glutamate/glutamate	1.9 ± 0.2	24 ± 6
[^{14}C]Malate/malate	2.0 ± 0.2	33 ± 6
AtUCP2		
[^{14}C]Aspartate/aspartate	0.8 ± 0.1	4.5 ± 0.5
[^{14}C]Glutamate/glutamate	2.5 ± 0.2	4.2 ± 0.4
[^{14}C]Malate/malate	2.4 ± 0.1	4.3 ± 0.4

Table 2

Competitive inhibition by various substrates of [^{14}C]aspartate uptake into proteoliposomes reconstituted with AtUCP1 or AtUCP2

The inhibition constants (K_i) were calculated from Dixon plots of the inverse rate of [^{14}C]aspartate transport *versus* the competing substrate concentration. The competing substrates at appropriate concentrations were added together with labeled asparate to proteoliposomes containing 10 mM aspartate. The values are means ± S.E. of at least three independent experiments carried out in duplicate.

Inhibitor	K_i	
	AtUCP1	AtUCP2
	mM	
α-Ketoglutarate	3.3 ± 0.2	2.6 ± 0.2
Cysteate	2.2 ± 0.3	2.4 ± 0.2
Cysteinesulfinate	2.7 ± 0.3	2.3 ± 0.2
Glutamate	2.2 ± 0.2	2.3 ± 0.2
Malate	1.7 ± 0.2	2.2 ± 0.2
Oxaloacetate	2.6 ± 0.3	3.2 ± 0.2
Sulfate	3.6 ± 0.3	3.3 ± 0.3

virtually absent in the newly isolated *ucp2* mutant (Fig. S3). Having these genotypes in hand, we next assessed their metabolic phenotypes via GC-MS–based metabolic profiling both in plants grown on normal MS agar and in plants exposed to salt stress. The effects of salt stress were investigated because UCPs have been previously proposed to contribute to the abiotic stress response (36). The clearest metabolic phenotype was that observed in the organic acids; however, changes in phenylalanine, serine, the branched chain amino acids, ornithine, *myo*-inositol, putrescine, and AMP were apparent in one or more of the genotypes (Fig. 9 and Tables S1–S3). These metabolite profiles are thus consistent with the transport assay data suggesting that AtUCP1 and AtUCP2 are important in organic and amino acid metabolism in plants. The metabolic phenotypes of the *ucp1*/*ucp2* double mutant tend to be similar to those of *ucp1*, suggesting a predominant role of UCP1 in *Arabidopsis*, at least in the leaf tissue assayed in the work reported here. Regarding the observed changes, interestingly, for the levels of some of the metabolites, such as malate and fumarate, the imposition of salt stress exacerbated intergenotypic differences. For others, such

Transport properties of AtUCP1 and AtUCP2

Table 3

Influence of membrane potential and pH gradient on the activity of reconstituted AtUCP1 and AtUCP2

The exchanges were started by adding 0.8 mM [^{14}C]aspartate or 0.8 mM [^{14}C]malate to AtUCP1- and AtUCP2-reconstituted proteoliposomes. For the measurements of the aspartate/glutamate carrier activity, 50 μM [^{14}C]aspartate was added to proteoliposomes reconstituted with AGC2-CTD. K^+_{in} was in included as KCl in the reconstitution mixture, whereas K^+_{out} was added as KCl together with the labeled substrate. Valinomycin or nigericin was added in 10 μl ethanol/ml of proteoliposomes, whereas the control samples contained the solvent alone. 20 mM or 2 mM PIPES (pH 7.0) was present inside and outside the proteoliposomes in the experiments with valinomycin or nigericin, respectively. The exchange reactions were stopped after 7, 20, and 30 s for AtUCP1, AtUCP2, and AGC2-CTD, respectively. The values are means ± S.E. of four independent experiments carried out in duplicate.

Uptake of	Internal substrate	K^+_{in}/ K^+_{out}	Transport activity (mmol / min x g protein)					
			AtUCP1		AtUCP2		AGC2-CTD	
			Control	Valinomycin	Control	Valinomycin	Control	Valinomycin
[^{14}C]aspartate	aspartate	1/1	16 ± 2	16 ± 2	2.5 ± 0.4	2.7 ± 0.3	0.19 ± 0.03	0.22 ± 0.02
		1/50	16 ± 2	16 ± 2	2.6 ± 0.3	2.4 ± 0.4	0.20 ± 0.03	0.20 ± 0.04
	glutamate	1/1	6 ± 1	6 ± 1	1.2 ± 0.2	1.3 ± 0.2	0.16 ± 0.03	0.13 ± 0.02
		1/50	7 ± 1	6 ± 1	1.0 ± 0.2	1.2 ± 0.3	0.14 ± 0.02	0.42 ± 0.05
[^{14}C]malate	malate	1/1	10 ± 1	9 ± 1	1.0 ± 0.2	1.1 ± 0.2		
		1/50	10 ± 1	10 ± 1	0.9 ± 0.2	1.1 ± 0.3		
	aspartate	1/1	12 ± 1	12 ± 2	1.1 ± 0.2	1.3 ± 0.2		
		1/50	11 ± 1	11 ± 2	1.3 ± 0.2	1.2 ± 0.2		
			Control	Nigericin	Control	Nigericin		
[^{14}C]malate	aspartate	1/1	9 ± 1	9 ± 1	2.6 ± 0.3	2.1 ± 0.2		
		1/50	9 ± 1	18 ± 1	2.5 ± 0.2	4.2 ± 0.3		
	glutamate	1/1	8 ± 1	7 ± 1	1.5 ± 0.3	1.7 ± 0.2		
		1/50	8 ± 1	19 ± 1	1.8 ± 0.2	3.0 ± 0.2		

as citrate, these differences were ameliorated (Fig. 9). The complexity of these results suggests that further research is warranted into the precise physiological role(s) of these proteins under both optimal and suboptimal conditions and in different plant tissues and developmental stages.

Discussion

A recent report has shown that the MC family member hUCP2, which was thought to have a UCP1-like uncoupling activity (42, 43), transports aspartate, 4-carbon dicarboxylates, phosphate, and sulfate (34). The percentages of identical amino acids between hUCP2 and AtUCP1 (51%) and AtUCP2 (44%) suggest that these proteins are highly related to one another. However, it is not possible to make reliable assumptions about the substrate specificity or about the transport modes on the basis of the amino acid similarity, given that even close MC homologs, such as isoforms 1 and 2 of the human ornithine carrier having 87% identical sequences, exhibit considerable differences in substrate specificity and transport kinetics (44, 45). Therefore, we decided to investigate the transport properties of AtUCP1 and AtUCP2 by recombinant expression, purification, and reconstitution into liposomes (the EPRA method (9)).

The results presented in this study demonstrate that AtUCP1 and AtUCP2 both transport aspartate, glutamate, cysteine sulfinate, cysteate, malonate, malate, oxaloacetate, and 2-oxoglutarate and, to a lesser extent, D-aspartate, cysteine, oxalate, succinate, P_i, sulfate, and thiosulfate (Fig. 4). In addition, AtUCP2 also transports fumarate, glutarate, and nitrate to some extent (Fig. 4*B*). The substrate specificities of AtUCP1 and AtUCP2 are, therefore, (i) similar as expected in light of their high sequence identity (72%) and (ii) broader than those of previously characterized mitochondrial carriers (9), given that their substrates overlap those of hUCP2 and those of the aspar-

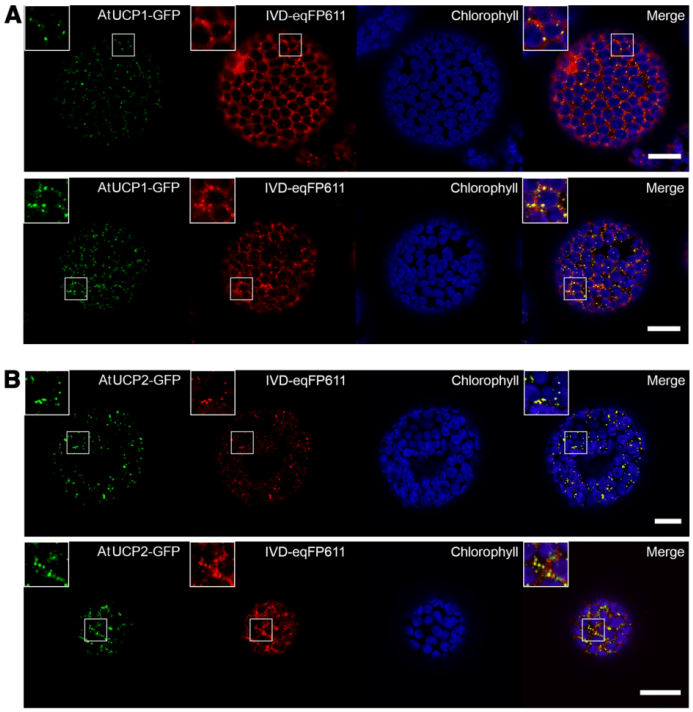

Figure 8. Subcellular localization of AtUCP1-/AtUCP2-GFP fusion proteins in *N. benthamiana* protoplasts. Fluorescent signals of AtUCP1-/AtUCP2-GFP (*green*), mitochondrial marker IVD-eqFP611 (*red*), chlorophyll A/chloroplasts (*blue*), and merge showing the overlap of the fluorescent signals (*yellow*) detected via confocal laser-scanning microscopy. *A*, co-localization of AtUCP1-GFP with the mitochondrial marker. *B*, co-localization of AtUCP2-GFP with the mitochondrial marker. *Scale bar*, 20 μM. Two independently transformed cells are shown in each *panel*.

tate/glutamate and dicarboxylate carriers (24, 30, 40, 46, 47). AtUCP1 and AtUCP2 share a number of similar transport properties; for example, both proteins catalyze a highly efficient counterexchange of substrates; do not transport mono- and tricarboxylates, nucleotides, and other amino acids; respond similarly to the inhibitors tested; and have similar transport affinities (K_i) for aspartate, glutamate, and malate. However, they greatly differ for their specific activities (V_{max}), AtUCP1 being much more active than AtUCP2, although both activities are similar or higher than those exhibited by most mitochondrial carriers characterized to date (1, 9). Furthermore, some substrates (*e.g.* D-aspartate and 2-oxoglutarate) are transported at higher rates by AtUCP2 than AtUCP1 compared with the respective [^{14}C]aspartate/aspartate exchanges.

The results of recombinant protein studies are largely consistent with the *in vivo* evaluation of the function of the proteins that was possible via the isolation and crossing of the respective knockout mutants. Thus, the metabolic phenotype of the mutants was characterized by changes in organic acid and amino acid levels, which are probably due to altered exchanges of these metabolites between the mitochondria and cytosol. However, the differences in metabolite content of the knockouts, which were dependent on salt stress, are difficult to disentangle, and this will probably require considerable further research effort.

Two additional remarks regarding the transport properties of AtUCP1 and AtUCP2 should be made. First, the close biochemical similarities between AtUCP1 and AtUCP2 are understandable, given the commonality of their gene structures; both genes (At3g54110 and At5g58970) share an identical exon/intron structure. We therefore assume that they derive from a common molecular ancestor, accounting for their similarities in biochemical properties. After gene duplication, independent evolution took place allowing the development of individual properties, such as the different specific activity and slightly different substrate preference. Second, our transport measurements, in agreement with the previous data on AtUCP3–6 (24) and hUCP2 (34), are in contrast with the idea that AtUCP1–6 as well as the human UCP1–6 are all "uncoupling proteins" transporting protons and dissipating the proton motive force generated by the respiratory chain. In particular, our findings show that AtUCP1 and AtUCP2 greatly differ from AtUCP4–6 (previously demonstrated to be dicarboxylate carriers) and suggest that they also differ from AtUCP3, which displays only 35 and 37% identical amino acids with AtUCP1 and AtUCP2, respectively. Several protein sequences available in databases

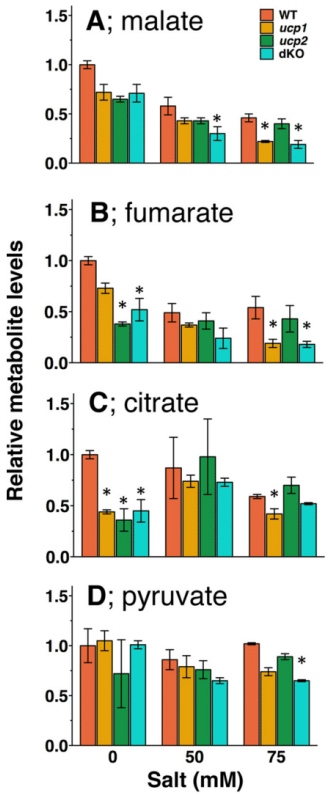

Figure 9. Levels of organic acids in the seedlings of AtUCP knockouts exposed or not to salt stress. Plants were grown on the plates containing 0, 50, and 75 mM NaCl for 12 days, and the relative levels of malate (*A*), fumarate (*B*), citrate (*C*), and pyruvate (*D*) in whole seedlings were determined. The levels of the metabolites were normalized to the mean of those of wildtype plants grown on the plate without salt. The means ± S.E. (*error bars*) from plants grown on three individual plates are shown. *Orange*, wildtype; *brown*, *ucp1*; *green*, *ucp2*; *light green*, *ucp1*/*ucp2* double knockout.

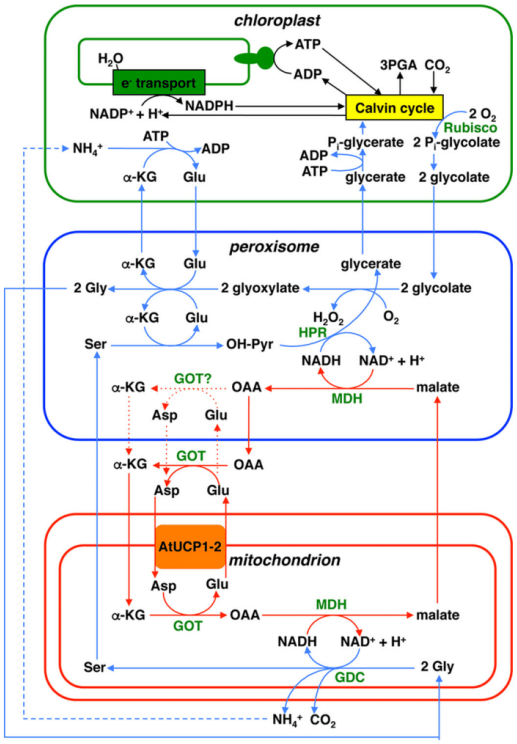

Figure 10. Role of AtUCP1 and AtUCP2 in photorespiration. *Blue* and *red lines* with *arrows* indicate the flow of the glycolate pathway and the transport of reducing equivalents, respectively. *Blue* and *red dashed lines* with *arrows* indicate several transformation steps and alternative paths, respectively. The presence of GOT in the peroxisomes, which is uncertain, has been drawn. Compounds are abbreviated in *black* as follows. α-*KG*, α-ketoglutarate; *OAA*, oxaloacetate; *OH-Pyr*, hydroxypyruvate. Enzymes are abbreviated in *green*. *GDC*, glycine decarboxylate; *GOT*, glutamate oxaloacetate transaminase; *HPR*, hydroxypyruvate reductase; *MDH*, malate dehydrogenase. The figure is modified from Refs. 37 and 51.

are likely to be orthologs of AtUCP1 and AtUCP2 in monocots, dicots, conifers, mosses, and green algae species. These sequences include A9PAU0_POPTR and B9GIV8_POPTR from *Populus trichocarpa* (86 and 79% identity with AtUCP1 and AtUCP2, respectively), A0A077DCK6_TOBAC from *Nicotiana tabacum* (84% identity with AtUCP1), C6T891_SOYBN from *Glycine max* (84% identity), I3ST66_LOTJA from *Lotus japonicus* (83% identity), A9RLI6_PHYP from *Physcomitrella patens* (81% identity), A9P0D2_PICSI from *Picea sitchensis* (79% identity), Q2QZ12_ORYSJ from *Oryza sativa* (77% identity), Q8S4C4_MAIZE from *Zea mays* (76% identity), and A8J1X0_CHLRE from *Chlamydomonas reinhardtii* (76% identity) (Fig. S1). To our knowledge, none of these proteins have been characterized biochemically.

Previous analyses of AtUCP1 knockout mutants revealed impaired photorespiration due to a dramatic decrease in mitochondrial glycine oxidation rate, which led to the suggestion of a physiological role of AtUCP1 in uncoupling the mitochondrial membrane potential for fine-tuning the cell redox state concomitant with photorespiration (37). The substrate specificity and high transport activity of AtUCP1 revealed in this study shed new light on its role in photorespiration. We suggest that AtUCP1 is involved in the glycolate pathway by playing a role in the transfer of reducing equivalents across the mitochondrial inner membrane (Fig. 10). In the glycolate pathway, 2-phosphoglycolate formed from O_2 usage by Rubisco in chloroplasts needs to be transformed in a series of reactions localized in peroxisomes and mitochondria in order to return to the Calvin–Benson cycle as 3-phosphoglycerate. The mitochondrial reaction catalyzed by glycine decarboxylase (GDC), which is the most abundant enzyme in plant mitochondria, reduces NAD^+ to NADH, and peroxisomal hydroxypyruvate reductase oxidizes NADH to NAD^+. This implies that the reducing equivalents of NADH are transported from the mitochondria to the peroxisomes as malate (Fig. 10). In this respect, AtUCP1 (and AtUCP2) would mainly transport aspartate and glutamate

as components of the mitochondrial malate/aspartate shuttle (MAS), which has been suggested to exist in plants in connection to photorespiration (48, 49). More precisely, we propose that the primary function of AtUCP1 (and AtUCP2) is to catalyze an exchange of aspartate$_{out}$ for glutamate$_{in}$ across the inner mitochondrial membrane, thus contributing to the export of reducing equivalents of NADH from mitochondria in conjunction with the other enzymes of MAS. In mammals, MAS transfers the reducing equivalents of NADH from the cytosol to the mitochondria (*i.e.* in the opposite direction of that occurring during photorespiration) because the aspartate glutamate carriers (AGC1 and -2) catalyze an electrophoretic exchange of aspartate$^-$ for glutamate$^-$ + H^+, and hence exit of aspartate and entry of glutamate are greatly favored in active mitochondria with a positive membrane potential outside, making the aspartate/glutamate exchange and the entire MAS unidirectional. By striking contrast, the aspartate/glutamate exchanges mediated by AtUCP1 and AtUCP2 are electroneutral (Table 3) and therefore independent from the proton motive force existing across the mitochondrial membrane. The hypothesis that AtUCP1 and AtUCP2 are involved in the glycolate pathway by catalyzing an aspartate$_{out}$/glutamate$_{in}$ exchange and thereby contributing to the export of reducing equivalents from the mitochondrial matrix is supported by the following considerations: (i) aspartate and glutamate, to the best of our knowledge, are only transported by AtUCP1 (and AtUCP2) in *Arabidopsis* mitochondria; (ii) these metabolites are present in the cytosol at very high concentrations (about 20 mM) (50), which are much higher than those of 2-oxoglutarate, malate, and oxaloacetate; (iii) both mitochondrial glutamate-oxaloacetate transaminase and malate dehydrogenase are involved in the regeneration of NAD^+ by GDC in mitochondria (51), and both mitochondrial and peroxisomal malate dehydrogenases are required for optimal photorespiration rates (52, 53); and (iv) as shown by the BAR *Arabidopsis* eFP Browser 2.0 (http:/bar.utoronto.ca),[7] AtUCP1 and AtUCP2 are expressed in many plant tissues, being more highly expressed in photosynthetic ones (Figs. S4 and S5). Interestingly, the expression of AtUCP1 is co-regulated with enzymes of the citric acid cycle, such as aconitase, isocitrate dehydrogenase, α-ketoglutarate dehydrogenase, and succinyl-CoA ligase, as well as with the peroxisomal transporter for NAD^+ (21, 22) (Fig. S6).

It is noteworthy that AtUCP1 (and AtUCP2) may also catalyze (i) the exchange between malate$_{in}$ and oxoglutarate$_{out}$ (*i.e.* the other mitochondrial membrane reaction of MAS) (Fig. 10) and (ii) an oxaloacetate$_{out}$/malate$_{in}$ exchange, which *per se* would result in export of the reducing equivalents of NADH from the mitochondria. However, these exchanges are also catalyzed by other *Arabidopsis* MCs, such as DTC, DIC1, DIC2, and DIC3 (23, 24), and the affinities of AtUCP1 and AtUCP2 for aspartate are much higher than those for the other substrates.

An additional hypothetical function of AtUCP1 and AtUCP2 in the photorespiratory glycolate pathway concerns the transfer of nitrogen equivalents across the mitochondrial membrane. During oxidative glycine decarboxylation by GDC in mitochondria, ammonia is released and reassimilated by the plastidial glutamine synthetase/glutamine oxoglutarate aminotransferase (GS/GOGAT) reaction. How ammonia released by GDC in mitochondria is shuttled to GS/GOGAT is still unknown, but it has been suggested that shuttling of amino acids across the mitochondrial membrane might be involved in this process (54). One possible route that would involve AtUCP1 and/or AtUCP2 would be incorporation of ammonia into 2-oxoglutarate by mitochondrial glutamate dehydrogenase, yielding glutamate, which is exported to the cytoplasm in counterexchange with external 2-oxoglutarate, thereby providing a new acceptor molecule for the glutamate dehydrogenase reaction. This hypothesis awaits experimental testing in future work.

Due to their broad substrate specificities, AtUCP1 (and AtUCP2) may be multifunctional and play further important physiological roles, depending on the metabolic conditions of the organ/tissue and the light/dark phase. For example, they might be involved in sulfur metabolism by exchanging cysteine sulfinate, cysteate, and cysteine with sulfate. Furthermore, in the dark, AtUCP1 (and AtUCP2) may catalyze the transport of glutamate into the mitochondria and the exit of aspartate to the cytosol, providing (together with the other enzymes of the malate aspartate shuttle) reducing equivalents in the form of NADH + H^+ to the mitochondrial respiratory chain.

Experimental procedures

Sequence analysis

BLAST and reciprocal BLAST were used to search for homologs of AtUCP1 and AtUCP2 (encoded by At3g54110 and At5g58970, respectively) in e!Ensamble and UniProt. Sequences were aligned with ClustalW.

Bacterial expression and purification of AtUCP1 and AtUCP2

PCR using complementary sequence-based primers was used to amplify the coding sequences of AtUCP1 from *A. thaliana* leaf cDNA and AtUCP2 from a custom-made synthetic gene (Invitrogen) with codons optimized for *E. coli*. The forward and reverse oligonucleotide primers contained the restriction sites NdeI and HindIII (AtUCP1) or XhoI and EcoRI (AtUCP2). The amplified gene fragments were cloned into pMW7 (AtUCP1) and pRUN (AtUCP2) vectors and transformed into *E. coli* TG1 cells (Invitrogen). Transformants were selected on LB (10 g/liter tryptone, 5 g/liter yeast extract, 5 g/liter NaCl, pH 7.4) plates containing 100 μg/ml ampicillin. All constructs were verified by DNA sequencing.

AtUCP1 and AtUCP2 were overexpressed as inclusion bodies in the cytosol of *E. coli* BL21(DE3) (AtUCP1) and BL21 CodonPlus(DE3)-RIL (AtUCP2) as described previously (55). Control cultures with the empty vector were processed in parallel. Inclusion bodies were purified on a sucrose density gradient (56) and washed at 4 °C, first with TE buffer (10 mM Tris-HCl, 1 mM EDTA, pH 7.0); once with a buffer containing 3% Triton X-114 (w/v), 1 mM EDTA, 10 mM PIPES (pH 7.0), and 10 mM Na_2SO_4; and finally three times with TE buffer (57). The inclusion body proteins were solubilized in 2% lauric acid, 10 mM PIPES (pH 7.0), and 3% Triton X-114 (AtUCP1) or 1.6% sarkosyl (w/v), 10 mM PIPES, pH 7.0, and 0.6% Triton X-114

[7] Please note that the JBC is not responsible for the long-term archiving and maintenance of this site or any other third party hosted site.

(AtUCP2). Unsolubilized material was removed by centrifugation (15,300 × *g* for 10 min).

Reconstitution of AtUCP1 and AtUCP2 into liposomes and transport measurements

The solubilized recombinant proteins were reconstituted into liposomes by cyclic removal of the detergent with a hydrophobic column of Amberlite beads (Bio-Rad), as described previously (41). The reconstitution mixture contained solubilized proteins (about 6 μg), 1% Triton X-114, 1.4% egg yolk phospholipids as sonicated liposomes, 10 mM substrate, 20 mM PIPES (pH 7.0), 1 mg of cardiolipin, and water to a final volume of 700 μl. These components were mixed thoroughly, and the mixture was recycled 13 times through a Bio-Beads SM-2 column pre-equilibrated with a buffer containing 10 mM PIPES (pH 7.0) and 50 mM NaCl and the substrate at the same concentration used in the starting mixture.

External substrate was removed from proteoliposomes on a Sephadex G-75 column pre-equilibrated with 10 mM PIPES and 50 mM NaCl, pH 7.0. Transport at 25 °C was initiated by adding the indicated radioactive substrates (American Radiolabeled Chemicals Inc. or PerkinElmer Life Sciences) to substrate-loaded (exchange) or empty (uniport) proteoliposomes. Transport was terminated by adding 20 mM pyridoxal 5′-phosphate and 20 mM bathophenanthroline, which in combination inhibit the activity of several MCs completely and rapidly (58–60). In controls, the inhibitors were added at the beginning together with the radioactive substrate according to the "inhibitor-stop" method (41). Finally, the external substrate was removed, and the radioactivity in the proteoliposomes was measured. The experimental values were corrected by subtracting control values. The initial transport rates were calculated from the radioactivity incorporated into proteoliposomes in the initial linear range of substrate transport. The kinetic constants K_m, V_{max}, and K_i were determined from Lineweaver–Burk and Dixon plots. For efflux measurements, proteoliposomes containing 5 mM internal aspartate or malate were loaded with 5 μM [^{14}C] aspartate and [^{14}C]malate, respectively, by carrier-mediated exchange equilibrium (61, 62). The external radioactivity was removed by passing the proteoliposomes through Sephadex G-75 columns pre-equilibrated with 50 mM NaCl. Efflux was started by adding unlabeled external substrate or buffer alone and terminated by adding the inhibitors indicated above.

Cloning and transient expression of GFP fusion constructs

For subcellular localization of AtUCP1 and AtUCP2, the AtUCP1-GFP and the AtUCP2-GFP fusion constructs were prepared. The *AtUCP1* coding sequence was amplified via Phusion High-Fidelity DNA Polymerase (New England Biolabs) using primers BH254 and BH255 (Table S4) and cloned with the Gibson Assembly Cloning Kit (New England Biolabs) into the expression vector pTKan (63) using the restriction sites ApaI and SacII. The GFP coding sequence for C-terminal GFP fusion was inserted via SacII and SpeI into the pTKan vector. The final vector contains AtUCP1 with a C-terminal GFP (AtUCP1-GFP) under the control of an optimized *Arabidopsis* ubiquitin-10 promoter (64) and the terminator of the *nos* gene from *Agrobacterium tumefaciens*. The *AtUCP2* coding sequence was amplified via Phusion High-Fidelity DNA Polymerase (Thermo Fisher Scientific) using primers UCP2_BPF and UCP2_BPR-s (Table S4) and cloned into pDONR207 vector by a BP recombination reaction with BP Clonase II enzyme mix (Invitrogen). The resulting entry clone was used for an LR recombination reaction by LR Clonase II enzyme mix (Invitrogen) with pK7FWG2 destination vector (65) to construct expression vector for the expression of AtUCP2-GFP under the control of the 35S promoter.

A. tumefaciens strain GV3101 (pMP90) (66) was transformed with the localization vectors (AtUCP1-GFP and AtUCP2-GFP) and the mitochondrial marker IVD-eqFP611 expressing the *Arabidopsis* IVD tagged at the C terminus with eqFP611 (67, 68). 5 ml of YPD medium (20 g/liter tryptone, 10 g/liter yeast extract, 20 g/liter glucose) was inoculated with positively transformed cells and grown overnight at 28 °C. Cells were harvested via centrifugation (10 min, 3000 × *g*) and resuspended in infiltration buffer (10 mM $MgCl_2$, 10 mM MES, pH 5.7, 100 μM acetosyringone) to an A_{600} of 0.5. *N. benthamiana* leaves of the same age were co-infiltrated with mitochondrial marker and corresponding AtUCP1 and AtUCP2 fusion proteins (69). Protoplasts were isolated 2 days after infiltration. Therefore, leaves were cut into 0.5 × 0.5-cm pieces and incubated in Protoplast Digestion Solution (1.5% (w/v) cellulase R-10, 0.4% (w/v) macerozyme R-10, 0.4 M mannitol, 20 mM KCl, 20 mM MES, pH 5.6, 10 mM $CaCl_2$, 0.1% (w/v) BSA) for 2 h at 30 °C. Isolated protoplasts were resuspended in W5 solution (154 mM NaCl, 125 mM $CaCl_2$, 5 mM KCl, 2 mM MES, pH 5.6) and directly used for microscopy. Protoplasts were observed using a Zeiss LSM 780 confocal microscope and Zeiss ZEN software. The following excitation/emission wavelength settings were used: GFP (488 nm/490–550 nm), IVD-eqFP611 (561 nm/580–625 nm), and chlorophyll A (488 nm/640–710 nm). Pictures were processed using Fiji software (75) and Adobe Photoshop CS6 (Adobe Systems).

Isolation, generation, and molecular characterization of single- and double-knockout mutants of ucp1 and ucp2

T-DNA insertion lines for At*UCP1* (SAIL_536G01, referred to as *ucp1* (37)) and At*UCP2* (SALK_080188, referred to as *ucp2*) were obtained from the ABRC. To identify homozygous T-DNA insertion lines, genomic DNA was extracted and genotyped using gene-specific primer pairs (DG8/DG9 for *ucp1* and DG6/DG5 for *ucp2*) and a primer pair for T-DNA/gene junction (DG9/SAIL-LBa for *ucp1* and DG6/SALK-LBa1 for *ucp2*) (Table S4). The position of the T-DNA was checked by sequencing. Homozygous *ucp1* and *ucp2* were further propagated. To generate double mutants (referred to as dKO), homozygous *ucp1* and *ucp2* were crossed. Heterozygous plants were selected by PCR in the T1 generation. After self crossing, dKO were selected by PCR and further propagated.

Total RNA was extracted from wildtype, mutant, and transgenic *Arabidopsis* plants using the guanidinium thiocyanate-phenol-chloroform method (70) and subjected after DNase treatment (RQ1 RNase-Free DNase, Promega) to cDNA synthesis (Superscript II Rnase H- reverse transcriptase, Invitrogen). Gene expression of *AtUCP1* and *AtUCP2* were analyzed using gene-specific primer pairs. The following primer sets

were used: DG23/DG24 for At*UCP1* and DG25/DG26 for *AtUCP2* (Table S4). As a control for cDNA quality and quantity, a cDNA fragment of an actin gene (ACT7, At5g09810) was amplified using ML167 and ML168. PCR conditions were as follows: 94 °C for 2 min, followed by cycles of 94 °C for 30 s, 58 °C for 45 s, 72 °C for 60 s, and a final extension for 2 min. Products were visualized on an ethidium bromide–stained 1% agarose gel.

Metabolite profiling

To obtain a broad overview of the major pathways of central metabolism, an established GC-MS–based metabolite profiling method was used to quantify the relative metabolite levels in the *Arabidopsis* rosette (~50 mg fresh weight). The extraction, derivatization, standard addition, and sample injection were performed exactly as described previously (71). This analysis allowed the determination of 46 different compounds, representing the main classes of primary metabolites (*i.e.* amino acids, organic acids, and sugars).

Other methods

Proteins were analyzed by SDS-PAGE and stained with Coomassie Blue dye. The identity of the bacterially expressed, purified AtUCP1 and AtUCP2 was assessed by MALDI-TOF mass spectrometry of trypsin digests of the corresponding band excised from Coomassie-stained gels (25, 72). The amount of purified AtUCP1 and AtUCP2 proteins was estimated by laser densitometry of stained samples using carbonic anhydrase as a protein standard (73). The amount of protein incorporated into liposomes was measured as described (74) and was about 25% of protein added to the reconstitution mixture. K^+-diffusion potentials were generated by adding valinomycin (1.5 μg/mg phospholipid) to proteoliposomes in the presence of K^+ gradients. For the formation of an artificial ΔpH (acidic outside), nigericin (50 ng/mg phospholipid) was added to proteoliposomes in the presence of an inwardly directed K^+ gradient.

Author contributions—M.M., L.P., A.R.F., A.P.W., and F.P. conceptualization; M.M., L.D., D.G., T.O., B.H., L.P., and D.V.M. methodology; A.R.F., A.P.W., and F.P. supervision.

References

1. Palmieri, F., Pierri, C. L., De Grassi, A., Nunes-Nesi, A., and Fernie, A. R. (2011) Evolution, structure and function of mitochondrial carriers: a review with new insights. *Plant J.* **66,** 161–181 CrossRef Medline
2. Palmieri, F. (2013) The mitochondrial transporter family SLC25: identification, properties and physiopathology. *Mol. Aspects Med.* **34,** 465–484 CrossRef Medline
3. Palmieri, F. (2014) Mitochondrial transporters of the SLC25 family and associated diseases: a review. *J. Inherit. Metab. Dis.* **37,** 565–575 CrossRef Medline
4. Saraste, M., and Walker, J. E. (1982) Internal sequence repeats and the path of polypeptide in mitochondrial ADP/ATP translocase. *FEBS Lett.* **144,** 250–254 CrossRef Medline
5. Palmieri, F. (1994) Mitochondrial carrier proteins. *FEBS Lett.* **346,** 48–54 CrossRef Medline
6. Pebay-Peyroula, E., Dahout-Gonzalez, C., Kahn, R., Trézéguet, V., Lauquin, G. J.-M., and Brandolin, G. (2003) Structure of mitochondrial ADP/ATP carrier in complex with carboxyatractyloside. *Nature* **426,** 39–44 CrossRef Medline
7. Ruprecht, J. J., Hellawell, A. M., Harding, M., Crichton, P. G., McCoy, A. J., and Kunji, E. R. S. (2014) Structures of yeast mitochondrial ADP/ATP carriers support a domain-based alternating-access transport mechanism. *Proc. Natl. Acad. Sci. U.S.A.* **111,** E426–E434 CrossRef Medline
8. Palmieri, F., and Pierri, C. L. (2010) Mitochondrial metabolite transport. *Essays Biochem.* **47,** 37–52 CrossRef Medline
9. Palmieri, F., and Monné, M. (2016) Discoveries, metabolic roles and diseases of mitochondrial carriers: a review. *Biochim. Biophys. Acta* **1863,** 2362–2378 CrossRef Medline
10. Haferkamp, I., Hackstein, J. H. P., Voncken, F. G. J., Schmit, G., and Tjaden, J. (2002) Functional integration of mitochondrial and hydrogenosomal ADP/ATP carriers in the *Escherichia coli* membrane reveals different biochemical characteristics for plants, mammals and anaerobic chytrids. *Eur. J. Biochem.* **269,** 3172–3181 CrossRef Medline
11. Leroch, M., Neuhaus, H. E., Kirchberger, S., Zimmermann, S., Melzer, M., Gerhold, J., and Tjaden, J. (2008) Identification of a novel adenine nucleotide transporter in the endoplasmic reticulum of *Arabidopsis*. *Plant Cell* **20,** 438–451 CrossRef Medline
12. Linka, N., Theodoulou, F. L., Haslam, R. P., Linka, M., Napier, J. A., Neuhaus, H. E., and Weber, A. P. M. (2008) Peroxisomal ATP import is essential for seedling development in *Arabidopsis thaliana*. *Plant Cell* **20,** 3241–3257 CrossRef Medline
13. Arai, Y., Hayashi, M., and Nishimura, M. (2008) Proteomic identification and characterization of a novel peroxisomal adenine nucleotide transporter supplying ATP for fatty acid β-oxidation in soybean and *Arabidopsis*. *Plant Cell* **20,** 3227–3240 CrossRef Medline
14. Kirchberger, S., Tjaden, J., and Neuhaus, H. E. (2008) Characterization of the *Arabidopsis* Brittle1 transport protein and impact of reduced activity on plant metabolism. *Plant J.* **56,** 51–63 CrossRef Medline
15. Rieder, B., and Neuhaus, H. E. (2011) Identification of an *Arabidopsis* plasma membrane-located ATP transporter important for anther development. *Plant Cell* **23,** 1932–1944 CrossRef Medline
16. Gigolashvili, T., Geier, M., Ashykhmina, N., Frerigmann, H., Wulfert, S., Krueger, S., Mugford, S. G., Kopriva, S., Haferkamp, I., and Flügge, U.-I. (2012) The *Arabidopsis* thylakoid ADP/ATP carrier TAAC has an additional role in supplying plastidic phosphoadenosine 5′-phosphosulfate to the cytosol. *Plant Cell* **24,** 4187–4204 CrossRef Medline
17. Palmieri, L., Santoro, A., Carrari, F., Blanco, E., Nunes-Nesi, A., Arrigoni, R., Genchi, F., Fernie, A. R., and Palmieri, F. (2008) Identification and characterization of ADNT1, a novel mitochondrial adenine nucleotide transporter from *Arabidopsis*. *Plant Physiol.* **148,** 1797–1808 CrossRef Medline
18. Stael, S., Rocha, A. G., Robinson, A. J., Kmiecik, P., Vothknecht, U. C., and Teige, M. (2011) *Arabidopsis* calcium-binding mitochondrial carrier proteins as potential facilitators of mitochondrial ATP-import and plastid SAM-import. *FEBS Lett.* **585,** 3935–3940 CrossRef Medline
19. Monné, M., Miniero, D. V., Obata, T., Daddabbo, L., Palmieri, L., Vozza, A., Nicolardi, M. C., Fernie, A. R., and Palmieri, F. (2015) Functional characterization and organ distribution of three mitochondrial ATP-Mg/P_i carriers in *Arabidopsis thaliana*. *Biochim. Biophys. Acta* **1847,** 1220–1230 CrossRef Medline
20. Palmieri, F., Rieder, B., Ventrella, A., Blanco, E., Do, P. T., Nunes-Nesi, A., Trauth, A. U., Fiermonte, G., Tjaden, J., Agrimi, G., Kirchberger, S., Paradies, E., Fernie, A. R., and Neuhaus, H. E. (2009) Molecular identification and functional characterization of *Arabidopsis thaliana* mitochondrial and chloroplastic NAD^+ carrier proteins. *J. Biol. Chem.* **284,** 31249–31259 CrossRef Medline
21. Bernhardt, K., Wilkinson, S., Weber, A. P. M., and Linka, N. (2012) A peroxisomal carrier delivers NAD^+ and contributes to optimal fatty acid degradation during storage oil mobilization. *Plant J.* **69,** 1–13 CrossRef Medline
22. Agrimi, G., Russo, A., Pierri, C. L., and Palmieri, F. (2012) The peroxisomal NAD^+ carrier of *Arabidopsis thaliana* transports coenzyme A and its derivatives. *J. Bioenerg. Biomembr.* **44,** 333–340 CrossRef Medline
23. Picault, N., Palmieri, L., Pisano, I., Hodges, M., and Palmieri, F. (2002) Identification of a novel transporter for dicarboxylates and tricarboxylates in plant mitochondria: bacterial expression, reconstitution, functional

characterization, and tissue distribution. *J. Biol. Chem.* **277,** 24204–24211 CrossRef Medline
24. Palmieri, L., Picault, N., Arrigoni, R., Besin, E., Palmieri, F., and Hodges, M. (2008) Molecular identification of three *Arabidopsis thaliana* mitochondrial dicarboxylate carrier isoforms: organ distribution, bacterial expression, reconstitution into liposomes and functional characterization. *Biochem. J.* **410,** 621–629 CrossRef Medline
25. Hoyos, M. E., Palmieri, L., Wertin, T., Arrigoni, R., Polacco, J. C., and Palmieri, F. (2003) Identification of a mitochondrial transporter for basic amino acids in *Arabidopsis thaliana* by functional reconstitution into liposomes and complementation in yeast. *Plant J.* **33,** 1027–1035 CrossRef Medline
26. Palmieri, L., Todd, C. D., Arrigoni, R., Hoyos, M. E., Santoro, A., Polacco, J. C., and Palmieri, F. (2006) *Arabidopsis* mitochondria have two basic amino acid transporters with partially overlapping specificities and differential expression in seedling development. *Biochim. Biophys. Acta* **1757,** 1277–1283 CrossRef Medline
27. Palmieri, L., Arrigoni, R., Blanco, E., Carrari, F., Zanor, M. I., Studart-Guimaraes, C., Fernie, A. R., and Palmieri, F. (2006) Molecular identification of an *Arabidopsis S*-adenosylmethionine transporter: analysis of organ distribution, bacterial expression, reconstitution into liposomes, and functional characterization. *Plant Physiol.* **142,** 855–865 CrossRef Medline
28. Bouvier, F., Linka, N., Isner, J.-C., Mutterer, J., Weber, A. P. M., and Camara, B. (2006) Arabidopsis SAMT1 defines a plastid transporter regulating plastid biogenesis and plant development. *Plant Cell* **18,** 3088–3105 CrossRef Medline
29. Hamel, P., Saint-Georges, Y., de Pinto, B., Lachacinski, N., Altamura, N., and Dujardin, G. (2004) Redundancy in the function of mitochondrial phosphate transport in *Saccharomyces cerevisiae* and *Arabidopsis thaliana*. *Mol. Microbiol.* **51,** 307–317 CrossRef Medline
30. Palmieri, L., Pardo, B., Lasorsa, F. M., del Arco, A., Kobayashi, K., Iijima, M., Runswick, M. J., Walker, J. E., Saheki, T., Satrústegui, J., and Palmieri, F. (2001) Citrin and aralar1 are Ca^{2+}-stimulated aspartate/glutamate transporters in mitochondria. *EMBO J.* **20,** 5060–5069 CrossRef Medline
31. Fiermonte, G., Palmieri, L., Todisco, S., Agrimi, G., Palmieri, F., and Walker, J. E. (2002) Identification of the mitochondrial glutamate transporter: bacterial expression, reconstitution, functional characterization, and tissue distribution of two human isoforms. *J. Biol. Chem.* **277,** 19289–19294 CrossRef Medline
32. Klingenberg, M., and Winkler, E. (1985) The reconstituted isolated uncoupling protein is a membrane potential driven H^+ translocator. *EMBO J.* **4,** 3087–3092 Medline
33. Nicholls, D. G. (2006) The physiological regulation of uncoupling proteins. *Biochim. Biophys. Acta.* **1757,** 459–466 CrossRef Medline
34. Vozza, A., Parisi, G., De Leonardis, F., Lasorsa, F. M., Castegna, A., Amorese, D., Marmo, R., Calcagnile, V. M., Palmieri, L., Ricquier, D., Paradies, E., Scarcia, P., Palmieri, F., Bouillaud, F., and Fiermonte, G. (2014) UCP2 transports C4 metabolites out of mitochondria, regulating glucose and glutamine oxidation. *Proc. Natl. Acad. Sci. U.S.A.* **111,** 960–965 CrossRef Medline
35. Borecký, J., Maia, I. G., Costa, A. D., Jezek, P., Chaimovich, H., de Andrade, P. B., Vercesi, A. E., and Arruda, P. (2001) Functional reconstitution of *Arabidopsis thaliana* plant uncoupling mitochondrial protein (AtPUMP1) expressed in *Escherichia coli*. *FEBS Lett.* **505,** 240–244 CrossRef Medline
36. Vercesi, A. E., Borecký, J., de Godoy Maia, I., Arruda, P., Cuccovia, I. M., and Chaimovich, H. (2006) Plant uncoupling mitochondrial proteins. *Annu. Rev. Plant Biol.* **57,** 383–404 CrossRef Medline
37. Sweetlove, L. J., Lytovchenko, A., Morgan, M., Nunes-Nesi, A., Taylor, N. L., Baxter, C. J., Eickmeier, I., and Fernie, A. R. (2006) Mitochondrial uncoupling protein is required for efficient photosynthesis. *Proc. Natl. Acad. Sci. U.S.A.* **103,** 19587–19592 CrossRef Medline
38. Parsons, H. T., Christiansen, K., Knierim, B., Carroll, A., Ito, J., Batth, T. S., Smith-Moritz, A. M., Morrison, S., McInerney, P., Hadi, M. Z., Auer, M., Mukhopadhyay, A., Petzold, C. J., Scheller, H. V., Loqué, D., and Heazlewood, J. L. (2012) Isolation and proteomic characterization of the *Arabidopsis* Golgi defines functional and novel components involved in plant cell wall biosynthesis. *Plant Physiol.* **159,** 12–26 CrossRef Medline
39. Nikolovski, N., Rubtsov, D., Segura, M. P., Miles, G. P., Stevens, T. J., Dunkley, T. P. J., Munro, S., Lilley, K. S., and Dupree, P. (2012) Putative glycosyltransferases and other plant Golgi apparatus proteins are revealed by LOPIT proteomics. *Plant Physiol.* **160,** 1037–1051 CrossRef Medline
40. Palmieri, L., Palmieri, F., Runswick, M. J., and Walker, J. E. (1996) Identification by bacterial expression and functional reconstitution of the yeast genomic sequence encoding the mitochondrial dicarboxylate carrier protein. *FEBS Lett.* **399,** 299–302 CrossRef Medline
41. Palmieri, F., Indiveri, C., Bisaccia, F., and Iacobazzi, V. (1995) Mitochondrial metabolite carrier proteins: purification, reconstitution, and transport studies. *Methods Enzymol.* **260,** 349–369 CrossRef Medline
42. Brand, M. D., and Esteves, T. C. (2005) Physiological functions of the mitochondrial uncoupling proteins UCP2 and UCP3. *Cell Metab.* **2,** 85–93 CrossRef Medline
43. Jaburek, M., and Garlid, K. D. (2003) Reconstitution of recombinant uncoupling proteins: UCP1, -2, and -3 have similar affinities for ATP and are unaffected by coenzyme Q10. *J. Biol. Chem.* **278,** 25825–25831 CrossRef Medline
44. Fiermonte, G., Dolce, V., David, L., Santorelli, F. M., Dionisi-Vici, C., Palmieri, F., and Walker, J. E. (2003) The mitochondrial ornithine transporter: bacterial expression, reconstitution, functional characterization, and tissue distribution of two human isoforms. *J. Biol. Chem.* **278,** 32778–32783 CrossRef Medline
45. Monné, M., Miniero, D. V., Daddabbo, L., Robinson, A. J., Kunji, E. R. S., and Palmieri, F. (2012) Substrate specificity of the two mitochondrial ornithine carriers can be swapped by single mutation in substrate binding site. *J. Biol. Chem.* **287,** 7925–7934 CrossRef Medline
46. Fiermonte, G., Palmieri, L., Dolce, V., Lasorsa, F. M., Palmieri, F., Runswick, M. J., and Walker, J. E. (1998) The sequence, bacterial expression, and functional reconstitution of the rat mitochondrial dicarboxylate transporter cloned via distant homologs in yeast and *Caenorhabditis elegans*. *J. Biol. Chem.* **273,** 24754–24759 CrossRef Medline
47. Cavero, S., Vozza, A., del Arco, A., Palmieri, L., Villa, A., Blanco, E., Runswick, M. J., Walker, J. E., Cerdán, S., Palmieri, F., and Satrústegui, J. (2003) Identification and metabolic role of the mitochondrial aspartate-glutamate transporter in Saccharomyces cerevisiae. *Mol. Microbiol.* **50,** 1257–1269 CrossRef Medline
48. Dry, I. B., Dimitriadis, E., Ward, A. D., and Wiskich, J. T. (1987) The photorespiratory hydrogen shuttle: synthesis of phthalonic acid and its use in the characterization of the malate/aspartate shuttle in pea (*Pisum sativum*) leaf mitochondria. *Biochem. J.* **245,** 669–675 CrossRef Medline
49. Noguchi, K., and Yoshida, K. (2008) Interaction between photosynthesis and respiration in illuminated leaves. *Mitochondrion* **8,** 87–99 CrossRef Medline
50. Winter, H., Robinson, D. G., and Heldt, H. W. (1994) Subcellular volumes and metabolite concentrations in spinach leaves. *Planta* **193,** 530–535 CrossRef
51. Journet, E. P., Neuburger, M., and Douce, R. (1981) Role of glutamate-oxaloacetate transaminase and malate dehydrogenase in the regeneration of NAD for glycine oxidation by spinach leaf mitochondria. *Plant Physiol.* **67,** 467–469 CrossRef Medline
52. Cousins, A. B., Pracharoenwattana, I., Zhou, W., Smith, S. M., and Badger, M. R. (2008) Peroxisomal malate dehydrogenase is not essential for photorespiration in *Arabidopsis* but its absence causes an increase in the stoichiometry of photorespiratory CO_2 release. *Plant Physiol.* **148,** 786–795 CrossRef Medline
53. Lindén, P., Keech, O., Stenlund, H., Gardeström, P., and Moritz, T. (2016) Reduced mitochondrial malate dehydrogenase activity has a strong effect on photorespiratory metabolism as revealed by ^{13}C labelling. *J. Exp. Bot.* **67,** 3123–3135 CrossRef Medline
54. Linka, M., and Weber, A. P. M. (2005) Shuffling ammonia between mitochondria and plastids during photorespiration. *Trends Plant Sci.* **10,** 461–465 CrossRef Medline
55. Fiermonte, G., Walker, J. E., and Palmieri, F. (1993) Abundant bacterial expression and reconstitution of an intrinsic membrane-transport protein from bovine mitochondria. *Biochem. J.* **294,** 293–299 CrossRef Medline

56. Elia, G., Fiermonte, G., Pratelli, A., Martella, V., Camero, M., Cirone, F., and Buonavoglia, C. (2003) Recombinant M protein-based ELISA test for detection of antibodies to canine coronavirus. *J. Virol. Methods* **109,** 139–142 CrossRef Medline
57. Agrimi, G., Russo, A., Scarcia, P., and Palmieri, F. (2012) The human gene SLC25A17 encodes a peroxisomal transporter of coenzyme A, FAD and NAD^+. *Biochem. J.* **443,** 241–247 CrossRef Medline
58. Palmieri, L., Lasorsa, F. M., Iacobazzi, V., Runswick, M. J., Palmieri, F., and Walker, J. E. (1999) Identification of the mitochondrial carnitine carrier in *Saccharomyces cerevisiae*. *FEBS Lett.* **462,** 472–476 CrossRef Medline
59. Castegna, A., Scarcia, P., Agrimi, G., Palmieri, L., Rottensteiner, H., Spera, I., Germinario, L., and Palmieri, F. (2010) Identification and functional characterization of a novel mitochondrial carrier for citrate and oxoglutarate in *S. cerevisiae*. *J. Biol. Chem.* **285,** 17359–17370 CrossRef Medline
60. Di Noia, M. A., Todisco, S., Cirigliano, A., Rinaldi, T., Agrimi, G., Iacobazzi, V., and Palmieri, F. (2014) The human SLC25A33 and SLC25A36 genes of solute carrier family 25 encode two mitochondrial pyrimidine nucleotide transporters. *J. Biol. Chem.* **289,** 33137–33148 CrossRef Medline
61. Marobbio, C. M. T., Di Noia, M. A., and Palmieri, F. (2006) Identification of a mitochondrial transporter for pyrimidine nucleotides in *Saccharomyces cerevisiae*: bacterial expression, reconstitution and functional characterization. *Biochem. J.* **393,** 441–446 CrossRef Medline
62. Fiermonte, G., Paradies, E., Todisco, S., Marobbio, C. M. T., and Palmieri, F. (2009) A novel member of solute carrier family 25 (SLC25A42) is a transporter of coenzyme A and adenosine 3′,5′-diphosphate in human mitochondria. *J. Biol. Chem.* **284,** 18152–18159 CrossRef Medline
63. Krebs, M., Held, K., Binder, A., Hashimoto, K., Den Herder, G., Parniske, M., Kudla, J., and Schumacher, K. (2012) FRET-based genetically encoded sensors allow high-resolution live cell imaging of Ca^{2+} dynamics. *Plant J. Cell Mol. Biol.* **69,** 181–192 CrossRef
64. Grefen, C., Donald, N., Hashimoto, K., Kudla, J., Schumacher, K., and Blatt, M. R. (2010) A ubiquitin-10 promoter-based vector set for fluorescent protein tagging facilitates temporal stability and native protein distribution in transient and stable expression studies. *Plant J.* **64,** 355–365 CrossRef Medline
65. Karimi, M., Inzé, D., and Depicker, A. (2002) GATEWAY vectors for *Agrobacterium*-mediated plant transformation. *Trends Plant Sci.* **7,** 193–195 CrossRef Medline
66. Koncz, C., and Schell, J. (1986) The promoter of TL-DNA gene 5 controls the tissue-specific expression of chimaeric genes carried by a novel type of *Agrobacterium* binary vector. *Mol. Gen. Genet.* **204,** 383–396 CrossRef
67. Höfgen, R., and Willmitzer, L. (1988) Storage of competent cells for *Agrobacterium* transformation. *Nucleic Acids Res.* **16,** 9877 CrossRef Medline
68. Forner, J., and Binder, S. (2007) The red fluorescent protein eqFP611: application in subcellular localization studies in higher plants. *BMC Plant Biol.* **7,** 28 CrossRef Medline
69. Waadt, R., and Kudla, J. (2008) *In planta* visualization of protein interactions using bimolecular fluorescence complementation (BiFC). *CSH Protoc.* **2008,** pdb.prot4995 CrossRef Medline
70. Chomczynski, P., and Sacchi, N. (1987) Single-step method of RNA isolation by acid guanidinium thiocyanate-phenol-chloroform extraction. *Anal. Biochem.* **162,** 156–159 CrossRef Medline
71. Lisec, J., Schauer, N., Kopka, J., Willmitzer, L., and Fernie, A. R. (2006) Gas chromatography mass spectrometry-based metabolite profiling in plants. *Nat. Protoc.* **1,** 387–396 CrossRef Medline
72. Palmieri, L., Agrimi, G., Runswick, M. J., Fearnley, I. M., Palmieri, F., and Walker, J. E. (2001) Identification in *Saccharomyces cerevisiae* of two isoforms of a novel mitochondrial transporter for 2-oxoadipate and 2-oxoglutarate. *J. Biol. Chem.* **276,** 1916–1922 CrossRef Medline
73. Indiveri, C., Iacobazzi, V., Giangregorio, N., and Palmieri, F. (1998) Bacterial overexpression, purification, and reconstitution of the carnitine/acylcarnitine carrier from rat liver mitochondria. *Biochem. Biophys. Res. Commun.* **249,** 589–594 CrossRef Medline
74. Porcelli, V., Fiermonte, G., Longo, A., and Palmieri, F. (2014) The human gene SLC25A29, of solute carrier family 25, encodes a mitochondrial transporter of basic amino acids. *J. Biol. Chem.* **289,** 13374–13384 CrossRef Medline
75. Schindelin, J., Arganda-Carreras, I., Frise, E., Kaynig, V., Longair, M., Pietzsch, T., Preibisch, S., Rueden, C., Saalfeld, S., Schmid, B., Tinevez, J. Y., White, D. J., Hartenstein, V., Eliceiri, K., Tomancak, P., and Cardona, A. (2012) Fiji: an open-source platform for biological-image analysis. *Nat. Methods* **9,** 676–682 CrossRef Medline

Author contribution

Björn Hielscher performed all sub-cellular localization experiments shown in **Figure 8 Subcellular localization of AtUCP1-/AtUCP2-GFP fusion proteins in N. benthamiana protoplasts**

VII.3 Manuscript 5

A BAHD neofunctionalization promotes tetrahydroxycinnamoyl spermine accumulation in pollen coat of the Asteraceae family

Marianne Delporte[1], Guillaume Bernard[1], Guillaume Legrand[1], Björn Hielscher[2], Arnaud Lanoue[3], Roland Molinié[4], Caroline Rambaud[1], David Mathiron[5], Sébastien Besseau[3], Nicole Linka[2], Jean-Louis Hilbert[1] and David Gagneul[1*]

1. EA 7394, USC INRA 1411, Institut Charles Viollette (ICV), Agro-food and biotechnology research institute, Université de Lille, INRA, ISA, Univ. Artois, Univ. Littoral Côte d'Opale, Cité Scientifique, 59655 Villeneuve d'Ascq, France
2. Institute for Plant Biochemistry and Cluster of Excellence on Plant Sciences (CEPLAS), Heinrich Heine University, Universitätsstrasse 1, Düsseldorf, 40225, Germany.
3. Biomolécules et Biotechnologies Végétales, EA 2106, Université François Rabelais de Tours, 37200 Tours, France
4. Biologie des Plantes & Innovation (EA 3900 BIOPI), Laboratoire de Phytotechnologie et Pharmacognosie, Faculté de Pharmacie, Université de Picardie Jules Verne, 80037 Amiens Cedex 1, France.
5. Plateforme Analytique (PFA), Université de Picardie Jules Verne, 80039 Amiens Cedex 1, France.

*.Corresponding author. Email: david.gagneul@univ-lille1.fr. Phone: +33 (0)3 20 43 40 21

Abstract

In the Eudicotyledons, accumulation of trihydroxycinnamoyl spermidine restricted to the pollen wall constitutes an evolutionary conserved trait. Nevertheless, the role of this compound synthetized by a BAHD enzyme i.e. Spermidine Hydroxycinnamoyl Transferase (SHT) is still a matter of debate. Interestingly, we showed that this particular phenolamide is replaced by tetrahydroxycinnamoyl spermine in the pollen coat of the Asteraceae. Phylogenetic analyses combined with qRT-PCR experiments allowed the identification of two homologous genes from *Cichorium intybus* putatively involved in its metabolism. *In vitro* biochemical characterization of the two enzymes named CiSHT1 and CiSHT2 confirmed the capability of recombinant proteins to synthesize spermine derivatives as well as spermidine derivatives. The Arabidopsis wild-type metabolic phenotype was partially restored in Arabidopsis *sht* mutant expressing *CiSHT2*. Remarkably, the transgenic plants also accumulate spermine derivatives absent in the wild-type. Overexpression of *CiSHT2* in chicory hairy roots also led to the accumulation of spermine derivatives confirming its *in vivo* function. Complementary sequence analyses revealed the presence of an amino-acid motif typical of the SHTs among the BAHD. This work highlights a recent neofunctionalization among the SHTs promoting the emergence of new phenolamides in the Asteraceae that could potentially have contributed to the evolutionary success of this family.

Keywords: Acylated spermine, BAHD Acyltransferases, *Cichorium intybus*, metabolic diversification, pollen coat, phenolamides, SHTs.

Introduction

Evolution within the plant kingdom is highly correlated with the apparition of new metabolic pathways, and notably those leading to the synthesis of the so-called specialized metabolites. They are responsible for the tremendous adaptability of plants to their challenging environment and their number increased constantly since terrestrialization. Enzymes required for their biosynthesis expend consequently during evolution of the green lineage (Weng and Noel, 2013). This is mostly due to gene duplication events that could result either from whole-genome duplications but probably more from local duplications (Chae et al., 2014). The certain substrate flexibility is a common trait for enzymes involved in these pathways that lead to rapid neofunctionalization (Weng et al., 2012; Weng and Noel, 2012). As a result, number of specialized metabolites occur in a lineage-specific manner and participate to plant speciation. Thus, they confer to the host species the ability to adjust to their particular environment. Nevertheless, some of these chemicals such as flavonoids are widely conserved across

species revealing a positive Darwinian selection and so essential functions (Weng and Noel, 2013).

Evolution of the reproductive structures was a key element during the colonization of the land habitat and emergence of pollen was a major event as well as the appearance of pollen coat among Angiosperms. The pollen coat is produced by the anther tapetum (Pacini and Hesse, 2005). This lipidic matrix is then deposited on the surface of the pollen grain filling the exine cavities. Pollen coat assumes a wide range of functions such as protection against biotic or abiotic stresses, stigma-pollen recognition mechanisms or pollinator attraction but nonetheless with a composition that could be variable among species (Quilichini et al., 2015). However, trihydroxycinnamoyl spermidines are phenolamides found in pollen coat of nearly all Eudicots (Elejalde-Palmett et al., 2015). Phenolamides, also referred as hydroxycinnamic acid amides or phenylamides, are specialized metabolites resulting from the conjugation of aliphatic or aromatic amines with phenolic acids. These molecules were largely described for their involvement in floral induction and development or as defense compounds (Bassard et al., 2010). However, fully substituted spermidines (N^1,N^5,N^{10}-trihydroxycinnamoyl spermidines) are often considered distinctly due to their specific location in pollen coat. Still, to date, no clear function was assigned to these compounds albeit a probable function in sporopollenin ultrastructure (Fellenberg and Vogt, 2015; Elejalde-Palmett et al., 2015; Aloisi et al., 2016). Indeed, lack of pollen coat phenolamides in *Arabidopsis thaliana* mutant lead to abnormal formation of the pollen grain but has no consequence on its viability or fertility (Grienenberger et al., 2009). Nevertheless, maintenance since appearance of these particular phenolamides suggests their major significance in evolution of the green lineage.

Appearance of trihydroxycinnamoyl spermidine in pollen coat is linked with the emergence of a new class of enzymes i.e. Spermidine Hydroxycinnamoyl Transferase (SHT) specifically expressed in the tapetum of the anther (Grienenberger et al., 2009). These enzymes belong to the clade Vb of the superfamily of BAHD acyltransferases (St-Pierre and De Luca, 2000; Tuominen et al., 2011). This family, named after the four enzymes firstly characterized, is subdivided in eight clades and encompasses acyltansferases that catalyze either O-acylation or N-acylation in an acyl-CoA dependent manner (D'Auria, 2006). So far, all the enzymes described to promote phenolamide synthesis from aliphatic amine fall within this BAHD family: agmatine coumaroyltransferase (ACT) described in barley and Arabidopsis (Burhenne et al., 2003; Muroi et al., 2009), spermidine disinapoyltransferase (SDT) and spermidine dicoumaroyltransferase (SCT) in Arabidopsis (Luo et al., 2009), hydroxycinnamoyl-CoA: spermidine acyltransferase (DH29) and hydroxycinnamoyl-CoA: putrescine acyltransferase (AT1) in *Nicotiana attenuata* (Onkokesung et al., 2012), putrescine hydroxycinnamoyl transferase (PHT) in potato and rice (Yogendra et al., 2017; Tanabe et al., 2016) and SHT from Arabidopsis and *Malus domestica* (Grienenberger et al., 2009; Elejalde-

Palmett et al., 2015). Up to now, the last two cited enzymes are the sole identified enzymes catalyzing acylation of secondary amino-group to synthetize fully substituted polyamines i.e. trihydroxycinnamoyl spermidines.

Nevertheless, very few studies report another type of fully substituted polyamine i.e. tetrahydroxycinnamoyl spermine. This spermine derived phenolamide was first described in pollen and/or flowers of *Matricaria chamomilla* and four other Asteraceae species (Yamamoto et al., 2002). This compound was more recently found in flowers of *Coreopsis tinctoria* (Asteraceae) (Lam et al., 2016) as well as in few other species belonging to the Asteraceae family (Božičević et al., 2017). Tetracoumaroyl spermine was identified as the first natural tachykinin NK1 receptor antagonist. As such, this amine could be a good drug candidate for the treatment of diseases like depression, anxiety, insomnia or certain cancers (Yamamoto et al., 2002; Park et al., 2017). Another study reports that synthetic tetracoumaroyl spermine has potent inhibitory effects on HIV-1 protease (Ma et al., 2001). This type of spermine derivatives was also mentioned in the composition of bee pollen where they were described as antioxidant of paramount importance (Ohta et al., 2007). Hence, tetrahydroxycinnamoyl spermines emerge as promising natural medicinal compounds.

Tetracoumaroyl spermine accumulation in *M. chamomilla* was evaluated during flower ontogenesis showing that this particular phenolamide is especially concentrated in pollen (Eliašová et al., 2012). Thus, the hypothesis was that tetrahydroxycinnamoyl spermines could replace trihydroxycinnamoyl spermidines in the pollen coat of certain species.

As the only reports we could find about tetrahydroxycinnamoyl spermine were related to species belonging to the Asteraceae, we first decided to screen members of this family for spermine-based phenolamides. Because of the public and in house genomic tools available for chicory (*Cichorium intybus* L.), we first start to examine this species before to broaden analyses to cover the entire family. Then, we used chicory to identify the molecular determinants involved in the metabolic diversification we observed among the Asteraceae. Our starting assumption was that the last step of the biosynthesis of tetrahydroxycinamoyl spermine would be related to that of trihydroxycinnamoyl spermidine. Accordingly, we identified and cloned two genes encoding BAHD acyltransferases phylogenetically close to SHTs previously characterized. Further investigations showed their involvement in tetrahydroxycinnamoyl spermine biosynthesis and suggest that the appearance of these new metabolites in the Asteraceae family results from the neofunctionalization of a duplicated gene.

Material and Methods

Plant material

C. intybus L. line "CC", an auto fertile and rapid cycling line (Habarugira et al., 2015), and the "clone 17" line (Florimond Desprez, Cappelle en Pévèle, France) were used in this study. Arabidopsis ecotype Columbia 0 (Col-0) and the *sht* mutant line SALK_055511, homozygous for T-DNA insertion, were used for complementation and overexpression experiments (Grienenberger et al., 2009). Plants were grown in a greenhouse under a 16h-light/8h-dark cycle.

Floral buds from the other species were collected in the countryside around Lille (France). For species unavailable under our latitudes, samples from the herbarium collection were kindly provided by the French National Museum of Natural History (Paris, France).

Metabolites extraction and analysis

The lyophilized plant material was powdered and resuspended in a methanol/water/acetic acid mixture (75/23/2, v/v/v). The mixtures were then incubated in the dark under agitation for 1h at 4°C. Homogenates were clarified by centrifugation (14000 g, 4°C, 10 min) and passed through a 0.45 µm filter. Methanolic wash of pollen was used to extract phenolics from pollen coat. Metabolite profiles were analyzed by HPLC/DAD and compound identification was performed by UPLC/MS/MS as described in Method S1.

RNA extraction

Total RNA was isolated from *C. intybus* or Arabidopsis using the Nucleospin RNA Kit (Macherey–Nagel) including a DNAse treatment. The yield and purity of total RNA were determined using the Experion Automated Electrophoresis System (Bio-Rad). One µg of DNAse treated total RNA was used for cDNA synthesis with the iScript cDNA synthesis kit (BioRad).

qPCR experiments

For expression pattern determination, two references genes were used to normalize data i.e. *TIP41* and *Clath*. Reference genes evaluation and qPCR experiment were conducted as previously described (Delporte et al., 2015). Gene specific primers are listed in Table S1.

Identification and cloning of SHT-like sequences from chicory

Putative SHT-like sequences from chicory were identified in EST databases. Full-length cDNA of *CiSHT1* or *CiSHT2* including or not the stop codon were amplified from chicory floral bud cDNA by PCR using a proofreading polymerase (PrimeSTAR HS DNA polymerase, Takara). The PCR primers designed for these amplifications are listed in Table

S1. The entry clones (pDONR221_*SHT1*, pDONR221_*SHT2*, pDONR207_*SHT1*, pDONR207_*SHT1*-stop, pDONR207_*SHT2*, pDONR207_*SHT2*-stop) were obtained through recombination of the PCR products with either pDONR207 or pDONR221(Invitrogen). The consensus sequences were established after sequencing of independent clones.

Expression, purification, and in vitro assays of recombinant proteins

Entry clones pDONR221-*SHT1* and pDONR221-*SHT2* were used to introduce open reading frame of *CiSHT1* and *CiSHT2* into pDEST17 expression vector (Invitrogen) by LR recombination to produce pDEST17-*SHT1* or pDEST17-*SHT2*. Recombinant proteins with an N-terminal 6XHis-tag were expressed in *Escherichia coli* BL21-CodonPlus-(DE3)-RIL cells and purified as described in (Legrand et al., 2016).

The standard *in vitro* assay was performed in a total volume of 50µL containing 400µM acyl donor and 2mM acyl acceptor freshly prepared in 50mM phosphate buffer. After incubation at 28°C for 1h, the reaction was stopped by adding 15µL acetonitrile and 1µL 12N HCl. As no production of free acid was observed, diminution of the CoA ester quantified after 1 hour, in the linear phase of the enzymatic reaction, was used to compare acyltransferase activities. pH optima were determined by performing the assay in 50µM phosphate buffer pH 5.0 to 9.0 or in Tris-HCl pH 7.0 to 10.0. Reverse reaction assays were conducted with phenolamides extracted from chicory pollen as substrates. One mM of CoASH and 1µg of protein were added in 50 mM Phosphate buffer, pH 9 in a final volume of 50µL. The production of coumaroylCoA was evaluated after incubation at 28°C for 3 hours. Reaction mixtures were then centrifuged at 14000g for 5min and filtered through a 0.45µm filter before being used for HPLC or HPLC-MS/MS analysis. Hydroxycinnamoyl-CoA were prepared enzymatically as described in (Legrand et al., 2016).

Chicory hairy root generation and growing conditions

pB2GW7 binary expression vector was used. pDONR207_SHT1 and pDONR207_SHT2 were used to generate pB2GW7_SHT1 and pB2GW7_SHT2 by LR recombination. *Agrobacterium rhizogenes* strain 15834 (Kindly provided by Marc Buée, INRA, Nancy, France) was transformed with the expression vectors by electroporation as described in Nagel et al. (1990). Hairy root induction was performed on "clone 17" leaves using *A. rhizogenes* (wild type or transformed with either pB2GW7_*SHT1* or pB2GW7_*SHT2*). Three independent lines were isolated. Hairy roots were maintained in liquid half strength MS (Murashige and Skoog, 1962) media added with sucrose (30 $g.L^{-1}$) in flasks on orbital shaker at an agitation speed of 110 rpm with a light source providing about 5 $W.m^{-2}$ on a 16/8-h light/dark cycle with a temperature of 25°C in the light phase and 20°C in the dark phase. Supplementation experiments were done in triplicates on 20 mL subcultures seeded with about 300 mg of root fragments. Twelve

days later, spermine was added to the medium to reach a final concentration of 1.5 mM. Roots were sampled 6 days after spermine addition and immediately frozen in liquid nitrogen until metabolite extraction. Spermine derivatives production was further quantified using free coumaric acid as standard.

Complementation of Arabidopsis *sht* mutant with *CiSHT1* or *CiSHT2*

For complementation experiments, the expression vector pB2GW7 was modified to replace 35S promoter by the TA29 promoter for specific expression in the anther (Karimi et al., 2002; Koltunow et al., 1990). TA29 promoter was amplified from *Nicotiana tabacum* gDNA using primers listed in Table S1. pB2GW7 was digested with SacI and SpeI restriction enzymes to remove 35S promoter and the TA29 promoter previously amplified was inserted using InFusion Cloning kit (Takara). The resulting expression vector named pB2GW7(TA29) was sequenced to verify the correct insertion of the TA29 promoter. pDONR207_SHT1 and pDONR207_SHT2 were then used to generate pB2GW7(TA29)_SHT1 and pB2GW7(TA29)_SHT2 by LR recombination.

Agrobacterium tumefaciens strain GV220 was transformed by electroporation with either pB2GW7(TA29)_SHT1 or pB2GW7(TA29)_SHT2. The floral-dipping method was then use to transform the Arabidopsis *sht* mutant line SALK_055511 (Clough and Bent, 1998). Phosphinotricin-resistant plants were selected and four independent homozygous lines per construction were further isolated by progeny segregation on selective medium.

Sub-cellular localization experiments

Gateway compatible binary vectors pUBC-Dest and pUBN-Dest (Grefen et al., 2010), allowing YFP fusion in C-terminal or N-terminal of the protein of interest respectively, were used for subcellular localization assays. Vectors pUBC_SHT1, pUBN_SHT1, pUBC_SHT2 and pUBN_SHT2 were obtained by LR recombination with the entry clones pDONR207_SHT1-stop, pDONR207_SHT1, pDONR207_SHT2-stop and pDONR207_SHT2 respectively. *A. tumefaciens* strain GV3101 (pMP90) was transformed *via* heat-shock with the localization vectors (pUBC_SHT1, pUBC_SHT2, pUBN_SHT1 or pUBN_SHT2) (Koncz and Schell, 1986; Höfgen and Willmitzer, 1988). 6-8 weeks old *N. benthamiana* plants were transiently transformed by agroinfiltration of the youngest leaves (Waadt and Kudla, 2008). Protoplasts were isolated two days after infiltration and directly used for microscopy (Sheen, 2002). *A. tumefaciens* strain GV220 were transformed by electroporation with either pUBN_SHT1 or pUBC_SHT1 and used to stably transform Arabidopsis Col-0 using the floral dip method (Clough and Bent, 1998). Transformants were then selected based on their resistance to phosphoinotricine. Seeds collected from the transformants were grown *in vitro* and fluorescence was observed in roots from 7 days old seedlings. For plasmolysis, roots were treated in a 500 mM NaCl solution for 5 min before observation as described in (Hou, 2005).

N. Benthamiana protoplasts or Arabidopsis root cells were observed using a Zeiss LSM 780 Confocal Microscope and Zeiss ZEN software. The following excitation/emission wavelength settings were used: YFP (514 nm / 493 to 550 nm) and Chlorophyll A (488 nm / 640 to 710 nm). Pictures were processed using Fiji software (https://fiji.sc/) and Adobe Photoshop CS6 (Adobe Systems).

Sequences and structure analyses

Sequence data from this article can be found in the GenBank data librarie under accession numbers listed in Table S2. Alignment and phylogenetic tree were generated using CLC Sequence Viewer 7 software (Qiagen). Sequences were aligned with MUSCLE (with default parameters) and phylogenetic tree was constructed using the neighbor-joining method and bootstrap analysis (1000 replications). Conserved motif determination was conducted with the MEME suite (Bailey et al., 2009). Homology models of CiSHT1 and CiSHT2 were built with I-TASSER (Yang et al., 2015) and docking experiments were proceeded with autodock vina (Trott and Olson, 2009). Results were analyzed and images generated with PyMOL (Schrodinger, 2015).

Results

Identification and characterization of pollen coat phenolamides in *C. intybus*

Chicory floral buds were dissected and methanolic extracts were analyzed by HPLC-DAD in order to identify and localize phenolamides accumulated in this species. Results showed the presence of three compounds (C1, C2 and C3) restricted to the androecium that exhibit UV spectra typical of phenolamides (Fig.1A, Fig. S1, S2, S3). These unknown compounds were further investigated by mass spectrometry. In their positive-ion electrospray ionization mass spectra, C1 gave an ion $[M+H]^+$ at a mass-to-charge ratio (m/z) of 787, C2 gave a protonated ion at m/z of 949 and C3 gave a protonated ion at m/z of 584 (Fig.1B). The molecular formula of the major compound C1 was determined to be $C_{46}H_{51}N_4O_8$, and C1 was tentatively identified as N^1,N^5,N^{10},N^{14}-tetracoumaroyl spermine. Fragmentation pattern of compound C1, presented in Fig. 1C, shows the presence of fragment ions at m/z 147 indicating the presence of coumaroyl residues. The ion at m/z 641 could be assigned to loss of a coumaroyl residue whereas ion at m/z 495 could arise from the loss of a second coumaroyl residue. The major ions at m/z 275 and 204 probably result from the cleavage of the N^5-C^6 and N^{10}-C^{11} bonds in the spermine moiety. Similarly C2 and C3 were identified as *N*-coumaroyl(glucose), *N*',*N*'',*N*'''-tricoumaroyl spermine and N^1,N^5,N^{10}-tricoumaroyl spermidine, respectively (Fig. S2 and S3). Position of the glycoside residue on C2 was not further investigated.

Analyses of methanolic wash of pollen grains were then conducted to confirm that these androecium specific compounds are constituents of the pollen coat. Indeed, the pollen coat is extractable by organic solvents without any alteration of the intracellular content of the pollen grain (Piffanelli et al. 1998; Murphy, 2006). Chromatogram presented in Fig. 1A revealed the presence of the three phenolamides previously identified in the androecium as well as their photoisomerization products. Indeed, studies on trihydroxycinnamoyl spermidine have shown the high photosensitivity of this kind of molecules with the apparition of photoisomers readily after the flower opens (Sobolev et al., 2008).

Identification of tetrahydroxycinnamoylspermine as a conserved constituent of Asteraceae pollen coat

Our results on chicory show that trihydroxycinnamoyl spermidine could be replaced by tetrahydroxycinnamoyl spermine as major phenolamide of the pollen coat. Moreover, previously published data on other species belonging to the Asteraceae suggest that this may be specific to this family (Yamamoto et al., 2002; Lam et al., 2016). A targeted metabolic profiling of either floral bud or pollen coat was undertaken among a wide range of Asteraceae and species belonging to related families. In order to reach the greatest possible diversity, freshly collected samples or samples coming from herbarium specimens were analyzed. We first established that time-dependent decomposition of the phenolamides were negligible by comparing the contents of phenolamides of freshly cut flowers immediately frozen in liquid nitrogen and lyophilized (see material and methods) to that of flowers conserved in herbaria for decades (unpublished). Results presented in Fig. 2 show that tetrahydroxycinnamoyl spermine was found in almost all Asteraceae species with spermine amino-groups substituted with either coumaric acid or caffeic acid. Spermine derivatives were most of the time accumulated together with spermidine derivatives as well. In the nearest families investigated i.e. the Calyceraceae, the Argophyllaceae or the Stylidiaceae, no spermine derivatives were identified whereas, except for the Stylidiaceae, spermidine derivatives were found.

Identification of candidate genes for tetracoumaroyl spermine biosynthesis

Considering the structural similarity between trihydroxycinnamoyl spermidine and tetrahydroxycinnamoyl spermine, candidate genes for spermine derivative biosynthesis could be phylogenetically close to genes involved in biosynthesis of spermidine derivatives in the anthers's tapetum i.e. SHT. BLAST searches for SHT-like sequences in the Asteraceae family enable the identification of two sequences in five species: *Helianthus annuus*, *Lactuca sativa*, *C. intybus*, *Carthamus tinctorius* and *Cynara cardunculus*. Phylogenetic analyses of these ten amino-acid sequences among other characterized BAHD belonging to the clade Vb lead to identification of two clusters for the Asteraceae SHT-like sequences identified (Fig. 3).

Subsequently, for each species, one sequence was named SHT1 and the other was named SHT2. The two sequences from *C. intybus*, CiSHT1 and CiSHT2, were selected for further characterization. The associated genes *CiSHT1* and *CiSHT2* are 1356bp and 1359bp long, respectively and share 72.9% nucleotide sequence identity. No intron was identified for both of these genes. The deduced protein sequences of 451 and 452 amino acids for CiSHT1 and CiSHT2, respectively have a calculated molecular mass of 50.2 and 50.4 kDa and harbour the two peptide motives HXXXD and DFGWG conserved among the BAHD family (St-Pierre and De Luca, 2000). In addition, the two proteins share respectively 63% and 66% similarity with AtSHT.

CiSHT1 and CiSHT2 gene expression patterns are correlated with phenolamide accumulation in chicory flowers

The contents of the three phenolamides previously described were measured in roots, leaves and flower buds. Flower buds were sampled at different developmental stages starting from the stage corresponding to the formation of the tetrads of microspores, which corresponds to the stage 9-10, to the stage 16 that is the anthesis (Habarugira et al., 2015).

Tetracoumaroyl spermine was the major phenolamide at every stages of the floral bud development As for the two other phenolamides, accumulation of tetracoumaroyl spermine was restricted to the floral parts of the plant and increased drastically until the flower open and then decreased probably due to petal formation and pollen release as recently observed in *M. chamomilla* (Fig. 4) (Park et al., 2017). In an attempt to assign a function to *CiSHT1* and *CiSHT2*, their expression pattern was examined in the same tissues by quantitative RT-PCR (qRT-PCR). For both genes, these analyses showed a nearly undetectable to weak expression in roots, leaves and in the youngest floral buds (stage 9-10) when the tapetum is not fully formed. Transcripts accumulation was then multiplied by up to 10.000. Transcripts quantity started to diminish between stage 14 and 15 corresponding to the degeneration of the tapetum (Fig. 4). These expression profiles were hence in accordance with tetracoumaroyl spermine accumulation during floral bud development supporting the hypothesis of the involvement of CiSHT1 and/or CiSHT2 in chicory phenolamide biosynthesis. Moreover, *CiSHT1* and *CiSHT2* transcripts accumulation throughout flower development is similar to that already described of *AtSHT* and *MdSHT* (Grienenberger et al., 2009; Elejalde-Palmett et al., 2015).

CiSHT2 shows a net in vitro activity towards the production of tetracoumaroyl spermine

In order to explore catalytic activities of CiSHT1 and CiSHT2, recombinant proteins with an N-terminal 6xHis-tag were produced in *E. coli* and purified by affinity chromatography. Their purity and identity were verified by SDS-PAGE and Western Blot analysis using anti-His antibody. Both purified proteins gave a major band at the expected molecular mass i.e. about 50 kDa (Fig. 5). Activities of the recombinant proteins were firstly assayed against spermidine and

spermine as acyl acceptor and coumaroyl-CoA as acyl donor. Production of tricoumaroyl spermidine and tetracoumaroyl spermine was achieved with both CiSHT1 and CiSHT2. During the time of activity monitoring, the partially substituted polyamines appeared first in the reaction media but diminished over time in favor of the fully substituted products showing the sequential nature of the reaction (Fig. 6). Spermine appeared to be the preferential polyamine substrate of CiSHT2. Its activity measured with spermidine was 56% lower than that measured with spermine. Concerning CiSHT1, its relative activity compared to that of CiSHT2 was much weaker making difficult the determination of substrate preference (Fig. 6). Other acyl acceptors were used. Although the activities were very weak for the two enzymes, positive results were obtained with the diamine putrescine and more surprisingly with quinic and shikimic acids (10mM) and glycerol in extreme conditions of concentration (100 mM). Concerning acyl donors, as already shown for AtSHT (Grienenberger et al., 2009), all the common CoA-esters tested (cinnamoyl-CoA, caffeoylCoA and feruloyl-CoA) were used by both enzymes to produced substituted spermidine or spermine.

The pH optimum for the recombinant enzyme activity was determined over the pH range of 5.0 to 10.0 using spermine or spermidine and coumaroyl-CoA as substrates. The pH optimum was 9.0 and matched values for previously identified BAHD N-acyltransferases (Luo et al., 2009; Schmidt et al., 2015). The ability to catalyze the reverse reaction was also examined. Indeed, numbers of BAHD enzyme have been demonstrated as freely reversible including enzymes from chicory that belong to the same clade Vb (Legrand et al., 2016). Both CiSHT1 and CiSHT2 were tested in presence of CoA-SH and phenolamides extracted from chicory pollen but no production of coumaroyl-CoA was detected in our experimental conditions.

Overexpression of CiSHT2 in chicory hairy roots lead to production of spermine derivatives

In vitro characterization of the studied enzymes highlighted a substrate flexibility often observed in the specialized metabolism. In order to ensure the *in vivo* biochemical function of CiSHT1 and CiSHT2, the corresponding genes were stably overexpressed in chicory hairy roots. Agrobacteria carrying the plant overexpression plasmid pB2GW7 containing either *CiSHT1* or *CiSHT2* downstream from the 35S promoter were used to transform chicory.

Production of phenolamides by hairy roots supplemented with spermine was then evaluated. In hairy roots lines expressing *CiSHT1*, no differences with the control lines were observed in terms of phenolic compound production. However, production of acylated spermines was confirmed by UPLC-MS/MS analysis in lines expressing *CiSHT2*. These spermine derivatives were quantified in three independent lines (Table 1). Dicoumaroyl spermine was the more abundant and accounts for 78% of total phenolamides. These results confirm the ability of CiSHT2 to promote spermine-based phenolamide synthesis *in vivo* but the fully substituted

compound was not detected. The negative results observed with the lines transformed with *CiSHT1* are in accordance with the very weak enzymatic activity observed *in vitro*.

CiSHT2 partly complement the phenolamide deficiency in pollen coat of Arabidopsis *sht* mutant and also lead to production of spermine derivatives

The Arabidopsis *sht* T-DNA insertion mutant already described as lacking trihydroxycinnamoyl spermidine conjugates in pollen coat (Grienenberger et al., 2009; Elejalde-Palmett et al., 2015) was used to overexpressed either *CiSHT1* or *CiSHT2* under control of the TA29 promoter, which allows overexpression in tapetum cells (Koltunow et al., 1990). As previously observed, dihydroxyferuloyl-sinapoyl spermidine was the main phenolamide in wild-type flowers associated with its biosynthetic intermediates (Table 2). The overexpression of *CiSHT1* did not lead to a different chemotype compared to the mutant but a panel of different phenolamides was observed in the lines overexpressing *CiSHT2* (*sht*ê*CiSHT2*). The production of dihydroxyferuloyl-sinapoyl spermidine was weakly restored to 3.8% of the wild-type level. Moreover, the most abundant intermediate was the monoferuloyl spermidine. This shows the difficulty of CiSHT2 to fully acylate spermidine and highlight the difference between this enzyme and the two previously characterized SHTs from Arabidopsis and *M. domestica* (Grienenberger et al., 2009; Elejalde-Palmett et al., 2015). In addition to spermidine derivatives, spermine derivatives were also found in the *sht*ê*CiSHT2* lines. Thus, diferuloyl and triferuloyl spermines were detected but tetrahydroxycinnamoyl spermine, if produced, was under level of detection (Table 2). Still, production of spermine conjugates in Arabidopsis, a species that does not produce these particular phenolamides, demonstrate once more the ability of CiSHT2 to acylate spermine *in vivo*.

CiSHT1 and CiSHT2 are targeted to the nucleo-cytoplasmic compartment

The expression of *CiSHT1* and *CiSHT2* early in the stamen development suggests an expression restricted to tapetum cells as it was demonstrated in Arabidopsis (Grienenberger et al., 2009). The accumulation of phenolamides in the pollen coat thus implied the export of either the final molecules or the enzymes implicated in their synthesis. It is assumed that, as most of the characterized BAHD acyltransferases, SHT-like enzymes should be cytoplasmic but this was never confirmed until now. Consequently, the subcellular localization of CiSHT1 and CiSHT2 was investigated using two constructions. pUB vectors were used to fused yellow fluorescent protein (YFP) at the C-terminus or at the N-terminus of CiSHT1 or CiSHT2. YFP:SHT1, SHT1:YFP, YFP:SHT2 and SHT2:YFP were then transiently expressed in *Nicotiana benthamiana* leaves. Fluorescence was observed in protoplasts obtained from transformed leaves. For the four constructs, the predominant fluorescence was cytoplasmic, as evidenced by the strong signal detected at the periphery of the cells and in cytoplasmic strands (Fig. 7). A fluorescent signal was also observed in the nucleus. Moreover, there was

no signal in the chloroplasts as shown by the merged pictures of YFP fluorescence and chlorophyll auto-fluorescence. This clearly demonstrates that both proteins share a nucleocytoplasmic localization.

This localization was further evidenced in additional experiments conducted with YFP:SHT1 and SHT1:YFP stably expressed in Arabidopsis. Confocal microscopic analyses were conducted on root cells, because this tissue is free of interference by the chlorophyll autofluorescence. Observations made on independent positives lines confirm the nucleocytoplasmic localization of CiSHT1. Indeed, the fluorescent signal was clearly visible at the periphery of the cells and in nucleus-like structures (Fig. S4). Plasmolysis experiments led up to the retraction of the vacuole associated with a strong signal inside the cell corroborating a cytosolic localization (Fig. S4).

Sequence analyses highlight a specific motif shared by members of the SHT subfamily

We have demonstrated that the appearance of spermine-based phenolamides in pollen coat of the species belonging to the Asteraceae family coincidentally with the presence of 2 SHT-like enzymes (Fig. 3). The high sequence identity shared by these 2 SHT-like whatever the species (68% on average) suggest that they could arise from the duplication of an ancestral *SHT* gene. Thereafter the neofunctionnalization of the one named SHT2 would have spearhead the emergence of tetrahydroxycinnamoyl spermine in pollen coat. Sequences of the characterized enzymes from Arabidopsis, *M. domestica* and *C. intybus* as well as the orthologues identified in *L. sativa*, *C. tinctorius*, *C. cardunculus* and *H. annuus* were aligned in an attempt to link the neofunctionalization observed in this SHT-like family with some structural particular features (Grienenberger et al., 2009; Elejalde-Palmett et al., 2015; This work). In terms of sequence, no clear difference that could explain the functional divergence was observed. Similarly, CiSHT1 and CiSHT2 homology based models were constructed and coumaroylCoA was manually docked in the active site (Fig. 8). Docking of either spermine or spermidine was then attempted but this did not allow the identification of residues that could explain the substrate specificity (data not shown).

However, alignment of the SHT-like sequences with other characterized members of the clade Vb highlights the insertion of few amino acid residues slightly upstream of the DFGWG motif conserved in the BAHD family (Fig. 9 A and B). This fragment does not seem to be very conserved and is also present in the Fabaceae sequences TpHCT2 (HydroxycinnamoylCoA:malic acid transferase from *Trifolium pratense*) and PvHHHT (HydroxycinnamoylCoA:tetrahydroxyhexandioic acid transferase from *Phaseolus vulgaris*). Interestingly a 4 amino acid motif i.e. FYGN appear to be characteristic of the SHT-like sequences. Conserved motif search was then conducted using MEME with all the predicted

SHT-like sequences publicly available and resulted in the identification of the same motif (Fig. 9 C). However, as shown by the homology based models of CiSHT1 and CiSHT2 presented in Fig. 8, this motif seems to be located too far from the active site to be directly involved in the catalytic activity of the SHT-like enzyme albeit a structural implication is possible.

Discussion

The wide conservation of pollen coat phenolamides suggests an essential function independently from specific environmental constraints. However, our data underline a metabolic diversification of these particular compounds in the Asteraceae family. Instead of trihydroxycinnamoyl spermidine, tetrahydroxycinnamoyl spermine was shown to be the main phenolamide accumulated in the pollen coat of most of the members of the Asteraceae family analyzed (Fig. 2). This diversification could potentially give an evolutionary advantage to species belonging to the Asteraceae family. With more than 23,500 species, the Asteraceae family represent nearly 10% of the angiosperms and is one of the largest family of flowering plants colonizing most parts of the earth except Antarctica (Panero and Crozier, 2016). The worldwide success of this family is often linked to its secondary metabolism in addition to its flower architecture, complex reproductive biology and habit plasticity (Calabria et al., 2007). The metabolic diversification of the pollen coat could constitute a supplemental feature contributing to its evolutionary success. In Arabidopsis and *M. domestica*, trihydroxycinnamoyl spermidine is synthetized by an enzyme called SHT belonging to the clade Vb of the BAHD acyltransferases (as defined by Tuominen et al., 2011). Notably, HCTs (hydroxycinnamoyl-CoA:shikimate/quintate hydroxycinnamoyl transferases) involved in the synthesis of lignin precursors and thus ubiquitously distributed in higher plants belong to this clade Vb. The other members of this clade probably came from duplication and neofunctionalization of ancestral HCTs as it was suggested for the rosmarinic acid synthase (RAS) but also for the SHTs (Petersen et al., 2009; Elejalde-Palmett et al., 2015). Mining of the genomic data of 5 members of the Asteraceae family reveals the presence of two AtSHT homologues in each species. The presence of two SHTs-like undoubtedly favoured the emergence of new pollen coat phenolamides releasing the selective pressure apparently applied on these compounds. These proteins, named SHT1 and SHT2, group into two distinct groups in a phylogenetic tree (Fig. 3). The biochemical *in vitro* characterization of the recombinant enzymes from chicory confirms that they are both capable of transferring hydroxycinnamoyl moieties from their respective CoA thiolesters to spermidine or spermine acceptors to synthetize phenolamides. In the case of CiSHT2, the tetramine spermine appears to be the preferred substrate. In our experimental conditions, CiSHT1 was shown to have a very weak activity whatever the substrates. The ability of CiSHT1 and CiSHT2 to accept other acyl acceptors than polyamines was tested and the weak but positive results obtained with quinate and shikimate constitute an argument in

favour of their supposed evolutionary origin i.e. the neofunctionalization of an ancestral duplicated HCT as already suggested in a previous report (Elejalde-Palmett et al., 2015).

Expression profiles of *CiSHT1* and *CiSHT2* were also established and pointed out a clear correlation between gene expression and phenolamide accumulation in the androecium. Moreover, if the *in planta* overexpression of CiSHT1 did not give any results in accordance with the weak activity of this enzyme already observed *in vitro*, the overexpression of CiSHT2 in chicory hairy roots and in Arabidopsis *sht* mutant demonstrate the ability of this enzyme to produce *in vivo* hydroxycinnamoyl spermines. However, the fully substituted spermine was not the major phenolamide contrary to the observations made in chicory floral buds and pollen. This may suggest specific conditions of the biosynthetic pathway in the anthers' tapetum of Asteraceae flowers that acts in favor of the accumulation of tetrahydroxycinnamoyl spermine. Polyamine availability could be an element of a specific metabolic environment. Indeed, it is known that spermidine is by far the most abundant polyamine in Arabidopsis flowers (Tassoni et al., 2000, 2008). This could explain why spermine conjugates are not efficiently produced in flowers of the *sht*ê*CiSHT2* transgenic lines. This hypothesis is supported by assays conducted on hairy roots suggesting that spermine concentration is of paramount importance. Indeed, in chicory hairy roots overexpressing CiSHT2, the production of poly acylated spermines is significantly enhanced by exogenous supplementation with spermine (not shown). From that perspective, it would be interesting to quantify the different polyamines in flowers of chicory.

Spatial organization of the metabolic pathway may be another element to explain the sole accumulation of fully substituted spermine in the pollen coat of chicory. Subcellular localization of the two enzymes was hence examined by transient expression in *N. benthamiana* leaves and underlined a nucleo-cytoplasmic localization of the SHTs. The members of the BAHD family are predicted to be localized in the cytosol due to the absence of peptide signal (D'Auria, 2006). Such subcellular localization was previously experimentally confirmed in Arabidopsis for HCT and in *C. cardunculus* for an HQT responsible for chlorogenic acid biosynthesis (Bassard et al., 2012; Moglia et al., 2014). This cytosolic localization excludes the involvement of a macrocompartmentation that could be an element to explain the metabolic fluxes leading to the sole accumulation of fully substituted spermine in the pollen coat. Numbers of proteins involved in the phenylpropanoid pathway are also assembled in so called metabolons (Ralston and Yu, 2006; Laursen et al., 2015). This type of supramolecular complex is the main form of microcompartment and is supposed to improve channeling of compounds between consecutive enzymes. In addition, such organization may increase local concentrations of the enzymes and their substrates. Assembly of metabolons relies on several parameters (availability of the constituents, concentrations of the constituents...). It could be assumed that these conditions were not brought together in hairy roots and in Arabidopsis floral buds. That could explain the differences between phenolamides accumulated in these overexpression

systems and chicory floral buds but this hypothesis still has to be assessed. Subcellular localization results obtained in this study also suggest that, once synthesized, phenolamides have to be exported outside of the tapetal cells to be deposited on the surface of the pollen grains. Thus, it would be interesting to identify the mechanisms involved in this deposition. Most of the pollen coat components are released after programmed cell death of the tapetum. However, a study from Quilichini et al. (2014) suggests the involvement of an ABC transporter in the export of the pollen coat phenolamides. Transport of spermidine derivatives or spermine derivatives could involve different systems and the lack of an efficient transport of the particular spermine based phenolamides produced in our in vivo assays may be an element to explain the weak concentration obtained. Indeed, a retro-inhibition phenomenon could occur explaining in the same time that tetracoumaroyl spermine is not produced more efficiently *in vitro*.

To gain insight into the structural characteristics of these enzymes and try to figure out evolution within the clade Vb, sequence analysis was performed. It evidenced the presence of a specific motif, FYGN, in the amino-acid sequence of the enzymes belonging to the SHT family (Fig. 9). This motif, associated with the insertion of few amino-acid upstream, is located slightly before the DFGWG motif of the BAHD family and may be directly or not involved in the ability of the SHTs to synthetize fully substituted polyamine. However, the lack of crystallographic data makes difficult the confirmation of this hypothesis. Enzymes that clustered close to SHTs i.e. TpHCT2 from *T. pratense* and PvHHHT from *P. vulgaris* also exhibit in their sequence the insertion observed in the SHT family but not the SHT conserved motif (Sullivan, 2009, 2016). These enzymes could arise from the same ancestor than SHTs but would have evolved differently leading to synthesis of new compounds such as phaselic acid in *T. pratense* whereas phenolamides are absent from the pollen coat (Elejalde-Palmett et al., 2015).

Hence, to the best of our knowledge, this study reports for the first time the identification and characterization of an enzyme catalyzing the *N*-acylation of spermine. Acylation of spermine with hydroxycinnamoyl-CoA was previously described in crude protein extract of *Aphelandra tetragona.* Nevertheless, the enzymes were only able to produce monocoumaroyl spermine, a precursor of the alkaloid aphelandrine and no molecular characterization was achieved (Hedberg et al., 1996). Still, complementary experiments are needed in order to achieve a better understanding of the determinants involved in the sole production of fully substituted polyamine observed in floral buds. Indeed, results obtained *in vitro* and *in vivo* suggest that the affinity of CiSHT2 for the different intermediates cannot explain by itself this specific pattern.

Furthermore, the role of trihydroxycinnamoyl spermidine in pollen coat has been questioned in several studies and some assumptions have been posed but not confirmed yet. The

abnormal formation of pollen grains of the *sht* mutant described in Arabidopsis points an apparent involvement in sporopollenin structure. However, the lack of phenolamides do not lead to an alteration of pollen fertility in the tested conditions (Grienenberger et al., 2009). These compounds are also thought to play a role in the protection of pollen against biotic or abiotic stresses or in interactions with pollinators or with stigma (Fellenberg and Vogt, 2015). Appearance of spermine derivatives instead of spermidine derivatives in the pollen coat of the Asteraceae raises questions and knowledge acquisition on these spermine derivatives could give additional clues on the role of pollen coat phenolamides in regard to plant evolution.

Supplementary Data

Figure S1: Proposed fragmentation scheme of compound C1 and its UV spectra
Figure S2: LC/MS/MS fragmentation of C2 and its UV spectra
Figure S3: LC/MS/MS fragmentation of C3 and its UV spectra
Figure S4: Subcellular imaging of YFP-tagged constructs stably expressed in Arabidopsis
Table S1: Sequences of primers used in this study
Table S2: Description of proteins used in phylogenetic analysis
Method S1: Metabolite analysis

Acknowledgments

The authors thank Florian Jabbour (Herbarium of the Muséum national d'Histoire naturelle, Paris, France) for sampling and providing of herbarium samples. MD and GL were supported by a doctoral fellowship from the doctoral school 104 SMRE, while GB was supported by a doctoral fellowship from University of Lille1 and the Région Hauts de France. BH was funded by DFG-grant GRK 1525. Experiments performed at Charles Viollette Institute were supported by Alibiotech grant (2016-2020) obtained from CPER/FEDER program.

References

Aloisi, I., Cai, G., Serafini-Fracassini, D., and Del Duca, S. (2016). Polyamines in Pollen: From Microsporogenesis to Fertilization. Front. Plant Sci. **7**.

Bailey, T.L., Boden, M., Buske, F.A., Frith, M., Grant, C.E., Clementi, L., Ren, J., Li, W.W., and Noble, W.S. (2009). MEME SUITE: tools for motif discovery and searching. Nucleic Acids Res. **37**: W202–W208.

Bassard, J.-E., Mutterer, J., Duval, F., and Werck-Reichhart, D. (2012). A novel method for monitoring the localization of cytochromes P450 and other endoplasmic reticulum membrane associated proteins: a tool for investigating the formation of metabolons.
FEBS J. **279**: 1576–1583.

Bassard, J.E., Ullmann, P., Bernier, F., and Werck-Reichhart, D. (2010). Phenolamides:

Bridging polyamines to the phenolic metabolism. Phytochemistry **71**: 1808–1824.

Božičević, A., De Mieri, M., Nassenstein, C., Wiegand, S., and Hamburger, M. (2017). Secondary Metabolites in Allergic Plant Pollen Samples Modulate Afferent Neurons and Murine Tracheal Rings. J. Nat. Prod. **80**: 2953–2961.

Burhenne, K., Kristensen, B.K., and Rasmussen, S.K. (2003). A New Class of NHydroxycinnamoyltransferases. Purification, cloning, and expression of a barley agmatine coumaroyltransferase (EC 2.3.1.64). J. Biol. Chem. **278**: 13919–13927.

Calabria, L.M., Emerenciano, V.P., Ferreira, M.J.P., Scotti, M.T., and Mabry, T.J. (2007). A phylogenetic analysis of tribes of the Asteraceae based on phytochemical data. Nat. Prod. Commun. **2**: 277–285.

Chae, L., Kim, T., Nilo-Poyanco, R., and Rhee, S.Y. (2014). Genomic signatures of specialized metabolism in plants. Science **344**: 510–3.

Clough, S.J. and Bent, A.F. (1998). Floral dip: a simplified method forAgrobacteriummediated transformation ofArabidopsis thaliana. Plant J. **16**: 735–743.

D'Auria, J.C. (2006). Acyltransferases in plants: a good time to be BAHD. Curr. Opin. Plant Biol. **9**: 331–340.

Delporte, M., Legrand, G., Hilbert, J.-L.J., and Gagneul, D. (2015). Selection and validation of reference genes for quantitative real-time PCR analysis of gene expression in Cichorium intybus. Front. Plant Sci. **6**.

Elejalde-Palmett, C., Dugé De Bernonville, T., Glevarec, G., Pichon, O., Papon, N., Courdavault, V., St-Pierre, B., Giglioli-Guivarc 'h, N., Lanoue, A., and Besseau, S. (2015). Characterization of a spermidine hydroxycinnamoyltransferase in Malus domestica highlights the evolutionary conservation of trihydroxycinnamoyl spermidines in pollen coat of core Eudicotyledons. J. Exp. Bot. **66**: 7271–7285.

Eliašová, A., Poracká, V., Pal'ove-Balang, P., Imrich, J., and Repčák, M. (2012). Accumulation of tetracoumaroyl spermine in Matricaria chamomilla during Floral development and nitrogen deficiency. Zeitschrift fur Naturforsch. - Sect. C J. Biosci. **67**: 58–64.

Fellenberg, C. and Vogt, T. (2015). Evolutionarily conserved phenylpropanoid pattern on angiosperm pollen. Trends Plant Sci. **20**: 212–218.

Grefen, C., Donald, N., Hashimoto, K., Kudla, J., Schumacher, K., and Blatt, M.R. (2010). A ubiquitin-10 promoter-based vector set for fluorescent protein tagging facilitates temporal stability and native protein distribution in transient and stable expression studies. Plant J. **64**: 355–365.

Grienenberger, E., Besseau, S., Geoffroy, P., Debayle, D., Heintz, D., Lapierre, C., Pollet, B., Heitz, T., and Legrand, M. (2009). A BAHD acyltransferase is expressed in the tapetum of Arabidopsis anthers and is involved in the synthesis of hydroxycinnamoyl spermidines. Plant J. **58**: 246–59.

Habarugira, I., Hendriks, T., Quillet, M.C., Hilbert, J.L., and Rambaud, C. (2015). Effects of nuclear genomes on anther development in cytoplasmic male sterile chicories (Cichorium intybus L.): Morphological analysis. Sci. World J. **2015**: 529521.

Hedberg, C., Hesse, M., and Werner, C. (1996). Spermine and spermidine hydroxycinnamoyl transferases in Aphelandra tetragona. Plant Sci. **113**: 149–156.

Höfgen, R. and Willmitzer, L. (1988). Storage of competent cells for Agrobacterium. Nucleic Acids Res. **16**: 9877.

Hou, X. (2005). Involvement of a Cell Wall-Associated Kinase, WAKL4, in Arabidopsis Mineral Responses. Plant Physiol. **139**: 1704–1716.

Karimi, M., Inzé, D., and Depicker, A. (2002). Gateway vectors for Agrobacteriummediated plant transformation. Trends Plant Sci. **7**: 193–195.

Koltunow, A.M., Truettner, J., Cox, K.H., Wallroth, M., and Goldberg, R.B. (1990). Different Temporal and Spatial Gene-Expression Patterns Occur During Anther Development. Plant Cell **2**: 1201–1224.

Koncz, C. and Schell, J. (1986). The promoter of TL-DNA gene 5 controls the tissuespecific expression of chimaeric genes carried by a novel type of Agrobacterium binary vector. MGG Mol. Gen. Genet. **204**: 383–396.

Lam, S.-C., Liu, X., Chen, X.-Q., Hu, D.-J., Zhao, J., Long, Z.-R., Fan, B., and Li, S.-P. (2016). Chemical characteristics of different parts of *Coreopsis tinctoria* in China using microwave-assisted extraction and high-performance liquid chromatography followed by chemometric analysis. J. Sep. Sci. **39**: 2919–2927.

Laursen, T., Møller, B.L., and Bassard, J.E. (2015). Plasticity of specialized metabolism as mediated by dynamic metabolons. Trends Plant Sci. **20**: 20–32.

Legrand, G., Delporte, M., Khelifi, C., Harant, A., Vuylsteker, C., Mörchen, M., Hance, P., Hilbert, J.-L.J.-L., and Gagneul, D. (2016). Identification and characterization of five BAHD acyltransferases involved in hydroxycinnamoyl ester metabolism in chicory. Front. Plant Sci. **7**.

Luo, J., Fuell, C., Parr, A., Hill, L., Bailey, P., Elliott, K., Fairhurst, S. a, Martin, C., and Michael, A.J. (2009). A novel polyamine acyltransferase responsible for the accumulation of spermidine conjugates in Arabidopsis seed. Plant Cell **21**: 318–33.

Ma, C.-M., Nakamura, N., and Hattori, M. (2001). Inhibitory Effects on HIV-1 Protease of Tri-p-coumaroylspermidine from Artemisia caruifolia and Related Amides. Chem. Pharm. Bull **49**: 915–917.

Moglia, A., Lanteri, S., Comino, C., Hill, L., Knevitt, D., Cagliero, C., Rubiolo, P., Bornemann, S., and Martin, C. (2014). Dual catalytic activity of hydroxycinnamoylCoA quinate transferase from tomato allows it to moonlight in the synthesis of both mono- and dicaffeoylquinic acids. Plant Physiol. **166**: 1777–87.

Murashige, T. and Skoog, F. (1962). A revised medium for rapid growth and bio assays with tobacco tissue cultures. Physiol. Plant. **15**: 473–497.

Muroi, A., Ishihara, A., Tanaka, C., Ishizuka, A., Takabayashi, J., Miyoshi, H., and Nishioka, T. (2009). Accumulation of hydroxycinnamic acid amides induced by pathogen infection and identification of agmatine coumaroyltransferase in Arabidopsis thaliana. Planta **230**: 517–527.

Ohta, S., Fujimaki, T., Uy, M.M., Yanai, M., Yukiyoshi, A., and Hirata, T. (2007). Antioxidant hydroxycinnamic acid derivatives isolated from Brazilian bee pollen. Nat Prod Res **21**: 726–732.

Onkokesung, N., Gaquerel, E., Kotkar, H., Kaur, H., Baldwin, I.T., and Galis, I. (2012). MYB8 Controls Inducible Phenolamide Levels by Activating Three Novel Hydroxycinnamoyl-Coenzyme A:Polyamine Transferases in Nicotiana attenuata. Plant Physiol. **158**: 389–407.

Pacini, E. and Hesse, M. (2005). Pollenkitt – its composition, forms and functions. Flora - Morphol. Distrib. Funct. Ecol. Plants **200**: 399–415.

Panero, J.L. and Crozier, B.S. (2016). Macroevolutionary dynamics in the early diversification of Asteraceae. Mol. Phylogenet. Evol. **99**: 116–132.

Park, S.B., Song, K., and Kim, Y.S. (2017). Tetra- cis / trans -Coumaroyl Polyamines as NK 1 Receptor Antagonists from Matricaria chamomilla. Planta Medica Int. **4**: 43–51.

Petersen, M., Abdullah, Y., Benner, J., Eberle, D., Gehlen, K., Hücherig, S., Janiak, V., Kim, K.H., Sander, M., Weitzel, C., and Wolters, S. (2009). Evolution of rosmarinic acid biosynthesis. Phytochemistry **70**: 1663–1679.

Quilichini, T.D., Grienenberger, E., and Douglas, C.J. (2015). The biosynthesis, composition and assembly of the outer pollen wall: A tough case to crack. Phytochemistry **113**: 170–82.

Quilichini, T.D., Samuels, a L., and Douglas, C.J. (2014). ABCG26-Mediated Polyketide Trafficking and Hydroxycinnamoyl Spermidines Contribute to Pollen Wall Exine Formation in Arabidopsis. Plant Cell **26**: 4483–4498.

Ralston, L. and Yu, O. (2006). Metabolons involving plant cytochrome P450s. Phytochem. Rev. **5**: 459–472.

Varesio, E., Hopfgartner, G., Gershenzon, J., and D'Auria, J.C. (2015). The Last Step in Cocaine Biosynthesis Is Catalyzed by a BAHD Acyltransferase. Plant Physiol. **167**: 89–101.

Schrodinger, L. (2015). The PyMOL Molecular Graphics System, Version 1.8.

Sheen, J. (2002). A transient expression assay using Arabidopsis mesophyll protoplasts. Nat. Nat. Plant Physiol. Nat. PNAS Abel Theol. Plant J. Plant J. Plant Mol Biol **425**: 521– 525.

Shen, H. et al. (2013). A genomics approach to deciphering lignin biosynthesis in switchgrass. Plant Cell **25**: 4342–61.

Sobolev, V.S., Sy, A.A., and Gloer, J.B. (2008). Spermidine and flavonoid conjugates from peanut (Arachis hypogaea) flowers. J. Agric. Food Chem. **56**: 2960–2969.

St-Pierre, B. and De Luca, V. (2000). Evolution of acyltransferase genes: Origin and diversification of the BAHD superfamily of acyltransferases involved in secondary metabolism. Recent Adv. Phytochem. **34**: 285–315.

Sullivan, M. (2009). A novel red clover hydroxycinnamoyl transferase has enzymatic activities consistent with a role in phaselic acid biosynthesis. Plant Physiol. **150**: 1866– 1879.

Sullivan, M.L. (2016). Identification of bean hydroxycinnamoylCoA:tetrahydroxyhexanedioate hydroxycinnamoyl transferase (HHHT): use of transgenic alfalfa to determine acceptor substrate specificity. Planta: 1–12.

Tanabe, K., Hojo, Y., Shinya, T., and Galis, I. (2016). Molecular evidence for biochemical diversification of phenolamide biosynthesis in rice plants. J. Integr. Plant Biol.: n/a-n/a.

Tassoni, A., Van Buuren, M., Franceschetti, M., Fornalè, S., and Bagni, N. (2000). Polyamine content and metabolism in Arabidopsis thaliana and effect of spermidine on plant development. Plant Physiol. Biochem. **38**: 383–393.

Tassoni, A., Franceschetti, M., and Bagni, N. (2008). Polyamines and salt stress response and tolerance in Arabidopsis thaliana flowers. Plant Physiol. Biochem. **46**: 607–613.

Trott, O. and Olson, A.J. (2009). AutoDock Vina: Improving the speed and accuracy of docking with a new scoring function, efficient optimization, and multithreading. J. Comput. Chem. **31**: NA-NA.

Tuominen, L.K., Johnson, V.E., and Tsai, C.-J. (2011). Differential phylogenetic expansions in BAHD acyltransferases across five angiosperm taxa and evidence of divergent expression among Populus paralogues. BMC Genomics **12**: 236.

Waadt, R. and Kudla, J. (2008). In plant visualization of protein interactions using bimolecular fluorescence complementation (BiFC). Cold Spring Harb. Protoc. **3**: 1–8.

Weng, J.-K. and Noel, J.P. (2013). Chemodiversity in Selaginella: a reference system for parallel and convergent metabolic evolution in terrestrial plants. Front. Plant Sci. **4**: 119.

Weng, J.-K., Philippe, R.N., and Noel, J.P. (2012). The rise of chemodiversity in plants. Science **336**: 1667–70.

Weng, J.K. and Noel, J.P. (2012). The remarkable pliability and promiscuity of specialized metabolism. Cold Spring Harb. Symp. Quant. Biol. **77**: 309–320.

Yamamoto, A., Nakamura, K., Furukawa, K., Konishi, Y., Ogino, T., Higashiura, K., Yago, H., Okamoto, K., and Otsuka, M. (2002). A new nonpeptide tachykinin NK1 receptor antagonist isolated from the plants of Compositae. Chem. Pharm. Bull. (Tokyo). **50**: 47–52.

Yang, J., Yan, R., Roy, A., Xu, D., Poisson, J., and Zhang, Y. (2015). The I-TASSER Suite: protein structure and function prediction. Nat. Methods **812**.

Yogendra, K.N., Sarkar, K., Kage, U., and Kushalappa, A.C. (2017). Potato NAC43 and MYB8 Mediated Transcriptional Regulation of Secondary Cell Wall Biosynthesis to Contain Phytophthora infestans Infection. Plant Mol. Biol. Report.: 1–15.

Table 1. Spermine derivative contents in chicory hairy roots overexpressing *CiSHT2*.

Hairy root line	phenolamides content (nmol.mg^{-1} DW)			
	monocoumaroyl spermine	dicoumaroyl spermine	tricoumaroyl spermine	tetracoumaroyl spermine
Line 1	1.15 ± 0.08	6.12 ± 0.80	0.31 ± 0.02	nd
Line 2	1.08 ± 0.19	6.40 ± 0.26	0.33 ± 0.03	nd
Line 3	1.54 ± 0.14	6.51 ± 0.44	0.27 ± 0.01	nd
mean	1.26 ± 0.25	6.35 ± 0.21	0.30 ± 0.03	nd

Media were supplemented with spermine 1.5 mM for 6 days. No spermine conjugates were detected in control lines. Values are means of 3 independent biological replicates ± SD. nd: not detected.

Table 2. Identification and relative quantification of phenolamides in Arabidopsis floral buds (WT, *sht*, *sht*/*CiSHT2*) by LC/MS.

Rt (min)	m/z ES(-)	m/z ES(+)	Compounds	Relative quantity (%)		
				WT	*sht*	*sht*/*CiSHT2*
2.31	320 [M-H]-	322 $[M+H]^+$ 177 $[M+H\text{-}Spd]^+$ 146 $[M+H\text{-}Fer]^+$	Feruloyl spermidine	4.2	nd	92.5
5.89	553 [M-H]-	555 $[M+H]^+$ 379 $[M+H\text{-}Fer]^+$ 305 $[M+H\text{-}Fer\text{-}C3\ chain]^+$ 234 $[M+H\text{-}Fer\text{-}C3NC4\ chain]^+$ 177 $[M+H\text{-}Fer\text{-}Spm]^-$	Diferuloyl spermine	nd	nd	9
8.84	496 [M-H]-	498 $[M+H]^+$ 322 $[M+H\text{-}Fer]^+$ 177 $[M+H\text{-}Fer\text{-}Spd]^+$	Diferuloyl spermidine	14.2	nd	2.4
10.73	729 [M-H]-	731 $[M+H]^+$ 555 $[M+H\text{-}Fer]^+$ 234 $[M+H\text{-}Fer\text{-}C3NC4\ chain]^+$ 177 $[M+H\text{-}Fer\text{-}Fer\text{-}Spm]^+$	Triferuloyl spermine	nd	nd	11
10.86	720 [M-H]-	722 $[M+H]^+$ 530 $[M+H\text{-}OHfer]^+$ 338 $[M+H\text{-}OHfer\text{-}OHfer]^+$ 193 $[M+H\text{-}OHfer\text{-}OHfer\text{-}Spd]^+$	Trihydroxyferuloyl spermidine	13.9	nd	nd
11.78	734 [M-H]-	736 $[M+H]^+$ 544 $[M+H\text{-}OHfer]^+$ 338 $[M+H\text{-}OHfer\text{-}Sin]^+$ 278 $[M+H\text{-}OHfer\text{-}OHfer\text{-}C3\ chain]^+$ 264 $[M+H\text{-}OHfer\text{-}OHfer\text{-}C4\ chain]^+$ 250 $[M+H\text{-}OHfer\text{-}Sin\text{-}C4\ chain]^+$ 207 $[M+H\text{-}OHfer\text{-}OHfer\text{-}Spd]^+$ 193 $[M+H\text{-}OHfer\text{-}Sin\text{-}Spd]^+$	Dihydroxyferuloyl sinapoyl spermidine	100	nd	3.8

For relative quantification, phenolamide signals were normalized to the dihydroxyferuloyl sinapoyl spermidine signal. Values presented for one line per construct are representatives of four independent lines.

Figure legends

Fig. 1: Identification of phenolamides present in chicory floral buds. A: Stacked HPLC chromatograms of methanolic extract obtained from different parts of floral buds and of methanol pollen wash. B: Structures of C1 (N^1,N^5,N^{10},N^{14}-tetracoumaroyl spermine), C2 (*N*coumaroyl(glucose)-N',N'',N'''-tricoumaroyl spermine) and C3 (N^1,N^5,N^{10}-tricoumaroyl spermidine) identified in chicory pollen cell wall. The hexose position in C2 was not confirmed. C: LC/MS/MS fragmentation of C1.

Fig. 2: Occurrence of tetrahydroxycinnamoyl spermine in floral buds among Asteraceae and close families. Methanolic extracts of flowers from various species (at least one by represented genus) were screened for tetrahydroxycinnamoyl spermine using HPLC/DAD or UPLC/MS/MS. Tetra-HCSpm: tetrahydroxycinnamoyl spermine. nd: not detected.

Fig. 3: Phylogenetic analysis of the ten SHT-like amino-acid sequences identified in five species of the Asteraceae family and other biochemically characterized members of the BAHD family clade Vb. Two clusters of SHT-like sequences are highlighted for the Asteraceae sequences. See Table S2 for protein name details and accession numbers.

Fig. 4: Expression profiles of *CiSHT1* and *CiSHT2* and tetracoumaroyl spermine contents in roots, leaves and in floral buds at different development stages. Gene expression was determined by qRT-PCR. After reference genes determination, expression levels were normalized to the expression of TIP41 and Clath and presented relative to that of roots. The accumulation of tetracoumaroyl spermine during floral bud development is represented with plain line. Tetracoumaroyl spermine was not detected in roots and leaves. Error bars indicate SD from three independent biological replicates. Numbers for floral bud developmental stages are as in Habarugia et al. (2015).

Fig. 5: Expression and purification of recombinant CiSHT1 and CiSHT2. A: SDS-PAGE separation of recombinant proteins. The gel was stained with Coomassie blue. B: Immunoblot analysis confirming the expression of the recombinant proteins. The proteins were detected with anti-His antibody. L: Ladder.

Fig. 6: HPLC chromatograms of *in vitro* assays of recombinant CiSHT2 (A) and CiSHT1 (B) in presence of coumaroylCoA and spermine (grey line) or spermidine (black line) or without acyl acceptor (dotted line). Identity of the numbered peaks was confirmed by mass spectrometry. (1): monocoumaroylspemine, (2): dicoumaroylspermine, (3): tricoumaroyl spermine, (4): tetracoumaroylspermine, (5): monocoumaroylspermidine,

(6): dicoumaroylspermidine, (7): tricoumaroylspermidine, (8): coumaroylCoA.

Fig. 7: Subcellular imaging of YFP-tagged constructs transiently expressed in *N. benthamiana* leaves. Confocal microscopy observations of leaf cell protoplasts show the fluorescence pattern for YFP:SHT1 (A), SHT1:YFP (B), YFP:SHT2 (C) and SHT2:YFP (D). bars = 20µm

Fig. 8: Superposition of the three dimensional molecular models of CiSHT1 (pink) and CiSHT2 (blue). Coumaroyl-CoA is docked in the active site and the His153 from the HXXXD motif directly involved in the catalytic activity is represented in white. The specific FYGN motif conserved in the SHT-like enzymes is highlighted in yellow for both proteins.

Fig. 9: Sequence analysis of the SHT-like enzymes. A: Full alignment of the ten SHT-like sequences identified in Asteraceae species with other characterized members of the BAHD family clade Vb. B: Focus on a particular portion of the alignment showing the BAHD motif DFGWG (grey bar), an amino-acid insertion (black bar) and the FYGN motif conserved in the SHT-like sequences (black frame). C: Result of a motif discovery conducted with MEME on all the publicly available predicted SHT-like sequences.

Fig.1

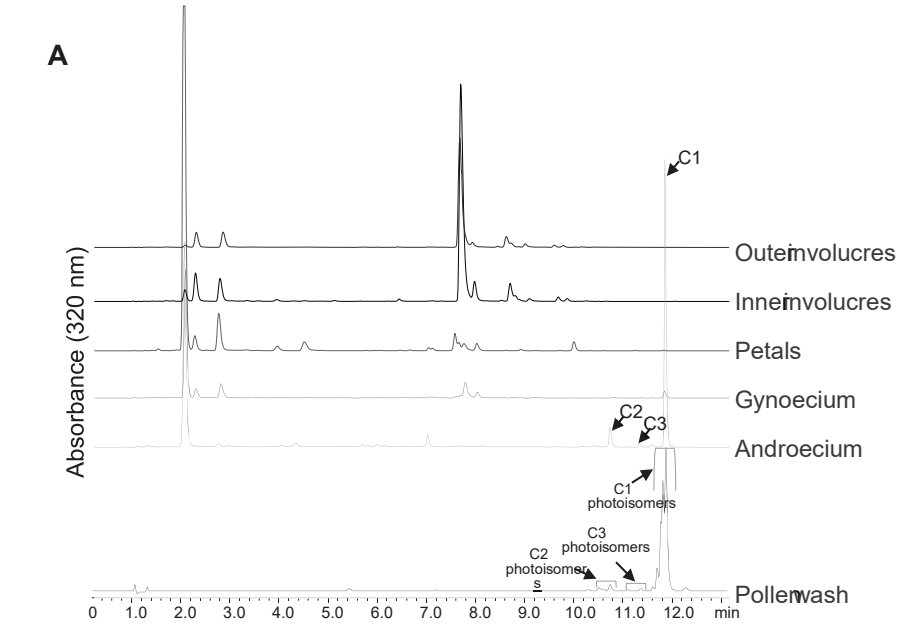
A
Absorbance (320 nm)
C1
Outer involucres
Inner involucres
Petals
Gynoecium
C2
C3
Androecium
C1 photoisomers
C3 photoisomers
C2 photoisomers
Pollen wash
0 1.0 2.0 3.0 4.0 5.0 6.0 7.0 8.0 9.0 10.0 11.0 12.0 min

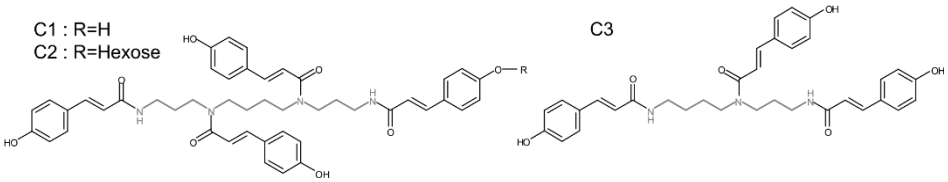
C1 : R=H
C2 : R=Hexose
C3

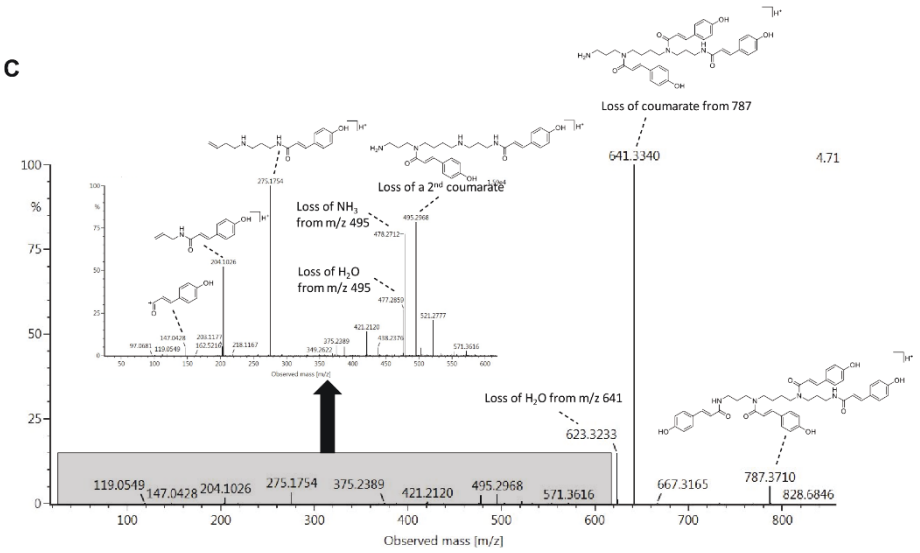
C
Loss of coumarate from 787
641.3340
4.71
Loss of a 2nd coumarate
Loss of NH3 from m/z 495
Loss of H2O from m/z 495
Loss of H2O from m/z 641
623.3233
119.0549
147.0428
204.1026
275.1754
375.2389
421.2120
495.2968
571.3616
667.3165
787.3710
828.6846
Observed mass [m/z]

Fig. 2

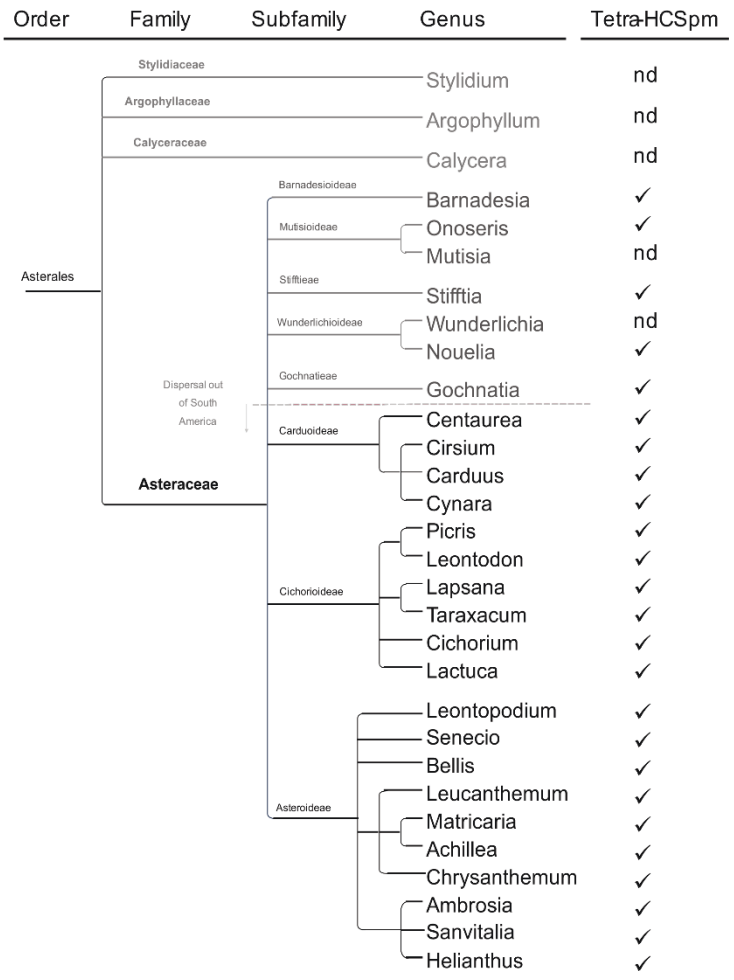
Order
Family
Subfamily
Genus
Tetra-HCSpm
Asterales
Stylidiaceae
Stylidium
nd
Argophyllaceae
Argophyllum
nd
Calyceraceae
Calycera
nd
Asteraceae
Barnadesioideae
Barnadesia
✓
Mutisioideae
Onoseris
✓
Mutisia
nd
Stifftieae
Stifftia
✓
Wunderlichioideae
Wunderlichia
nd
Nouelia
✓
Gochnatieae
Gochnatia
✓
Dispersal out of South America
Carduoideae
Centaurea
✓
Cirsium
✓
Carduus
✓
Cynara
✓
Cichorioideae
Picris
✓
Leontodon
✓
Lapsana
✓
Taraxacum
✓
Cichorium
✓
Lactuca
✓
Asteroideae
Leontopodium
✓
Senecio
✓
Bellis
✓
Leucanthemum
✓
Matricaria
✓
Achillea
✓
Chrysanthemum
✓
Ambrosia
✓
Sanvitalia
✓
Helianthus
✓

Fig. 3

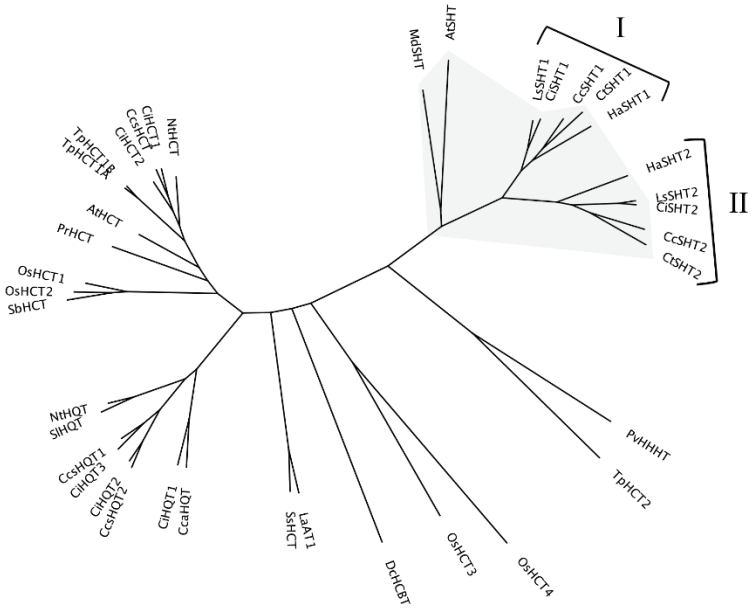
I
II
MdSHT
AtSHT
LsSHT1
CiSHT1
CcSHT1
CtSHT1
HaSHT1
HaSHT2
LsSHT2
CiSHT2
CcSHT2
CtSHT2
NtHCT
ClHCT
CcsHCT
ClHCT2
TpHCT1A
TpHCT1B
AtHCT
PrHCT
OsHCT1
OsHCT2
SbHCT
NtHQT
SlHQT
CcsHQT1
ClHQT3
ClHQT2
CcsHQT2
ClHQT1
CcaHQT
LaAT1
SsHCT
DcHCBT
OsHCT3
OsHCT4
PvHHHT
TpHCT2

Fig. 4

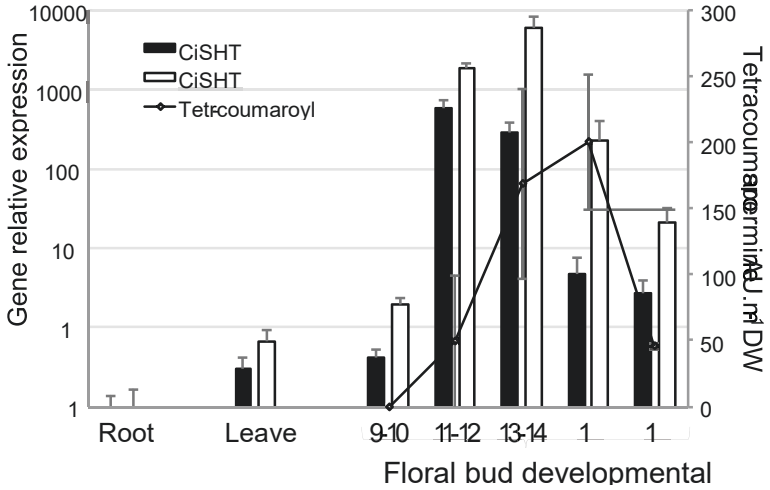
10000
1000
100
10
1
1
Gene relative expression
CiSHT
CiSHT
Tetracoumaroyl
300
250
200
150
100
50
0
Root
Leave
9-10
11-12
13-14
1
1
Floral bud developmental

Fig. 5

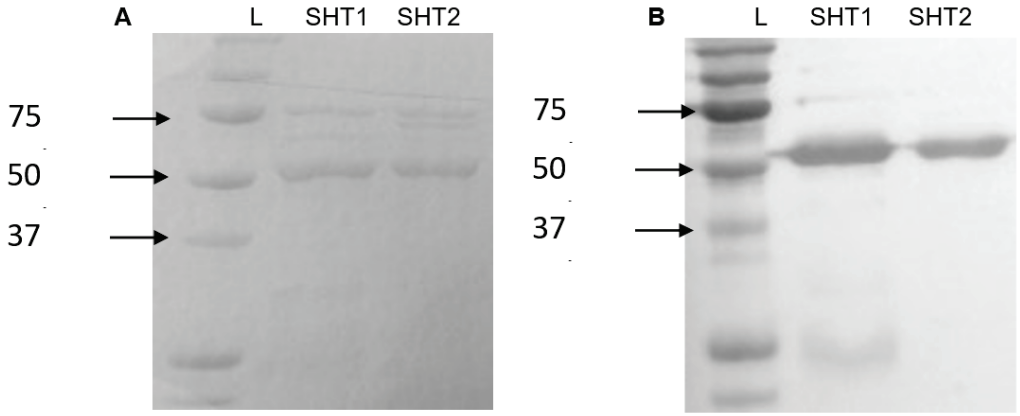
A
L
SHT1
SHT2
75
50
37
B
L
SHT1
SHT2
75
50
37

Fig. 6

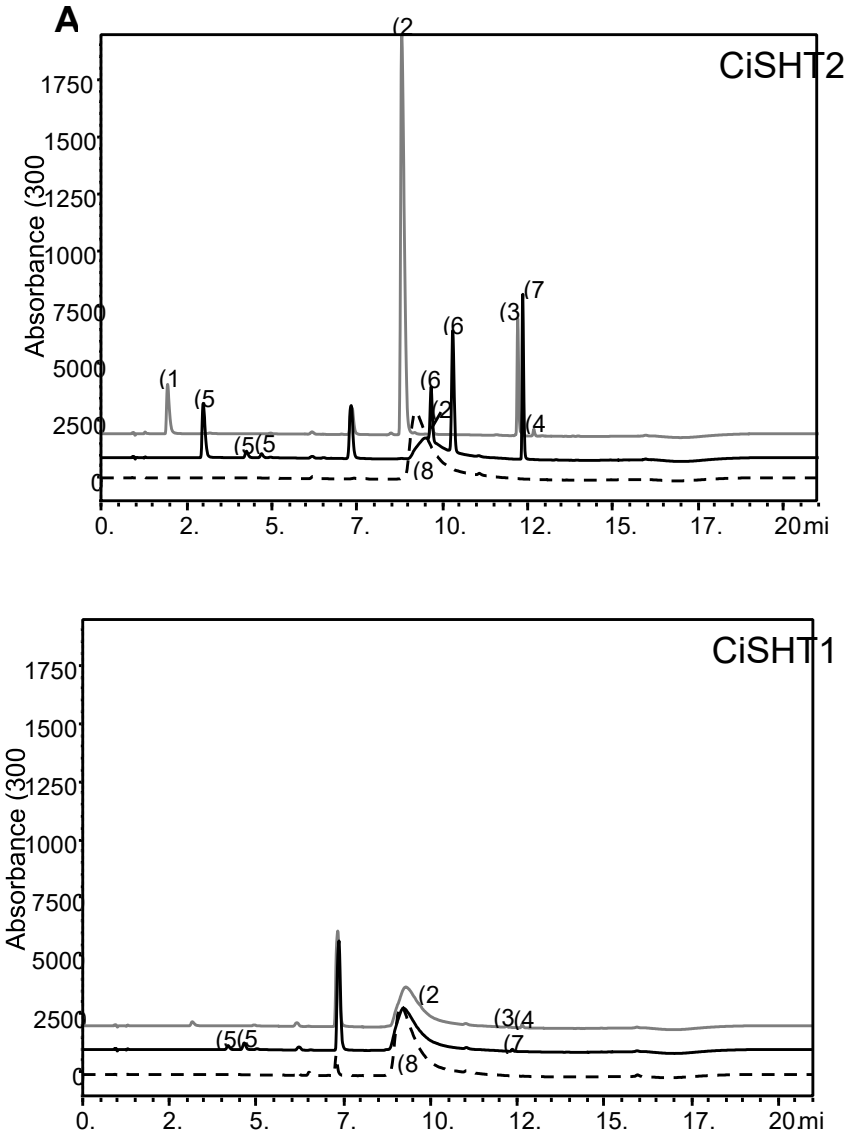
A
CiSHT2
Absorbance (300
1750
1500
1250
1000
7500
5000
2500
0
0.
2.
5.
7.
10.
12.
15.
17.
20 mi
CiSHT1
Absorbance (300
1750
1500
1250
1000
7500
5000
2500
0
0.
2.
5.
7.
10.
12.
15.
17.
20 mi

Fig. 7

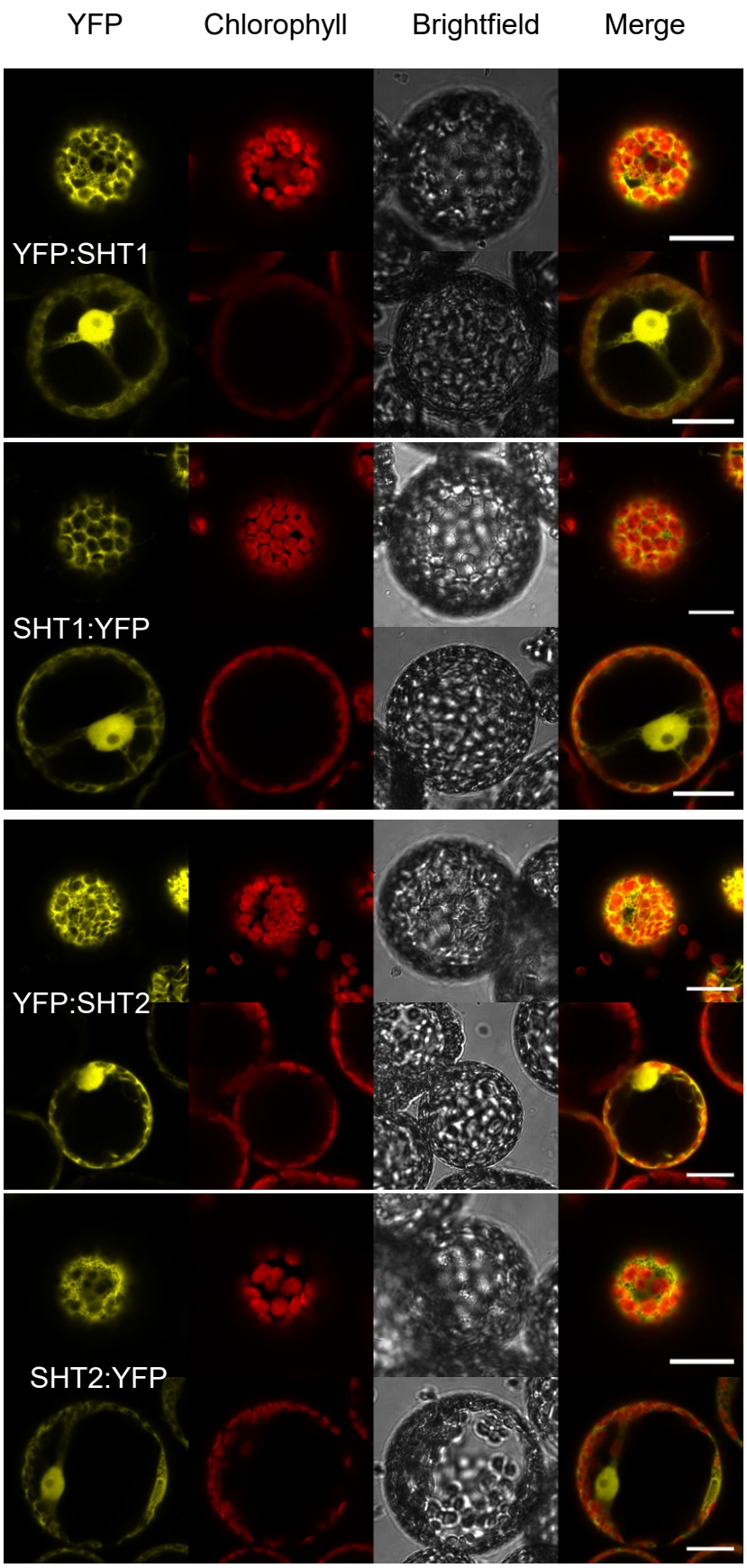
YFP
Chlorophyll
Brightfield
Merge
YFP:SHT1
SHT1:YFP
YFP:SHT2
SHT2:YFP

Fig. 8

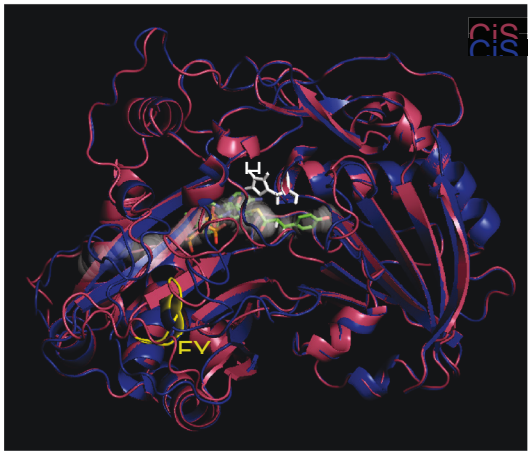

Fig. 9

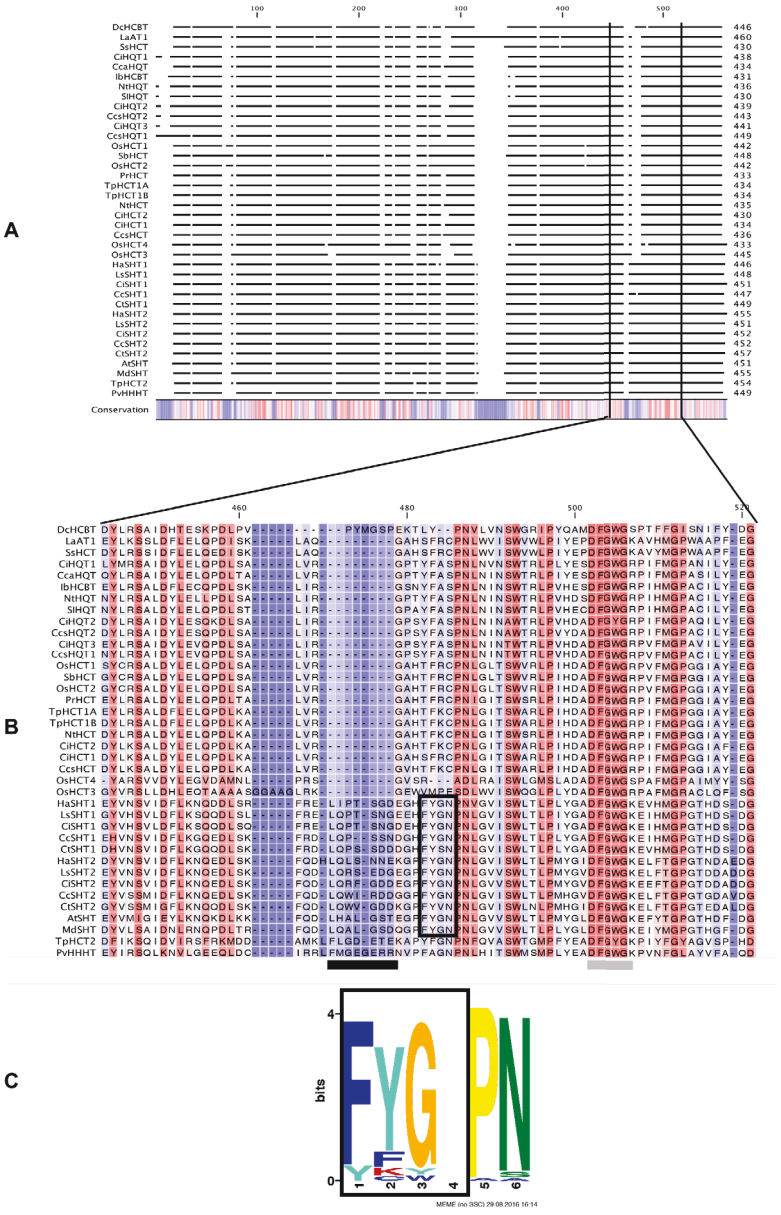

Author contribution

Björn Hielscher performed all sub-cellular localization experiments shown in **Figure 7 Subcellular imaging of YFP-tagged constructs transiently expressed in N. benthamiana leaves** and **Supplemental Figure S4 Subcellular imaging of YFP-tagged constructs stably expressed in *A. thaliana***.

VIII. Acknowledgements

Bei **PD Dr. Nicole Linka** möchte ich mich für die außergewöhnliche Betreuung über die Jahre bedanken. Ohne dich hätte ich nicht so viele Erfahrungen im In- und Ausland machen können, hätte nicht halb so viel gesehen und gelernt.

Prof. Dr. Peter Westhoff danke ich für die Unterstützung im Rahmen des Komitees, wissenschaftliche Diskussionen und die Betreuung während der Lab Rotation im Westhoff Labor.

Prof. Dr. Michael Feldbrügge danke ich für die Unterstützung im Rahmen des Komitees.

Prof. Dr. Andreas Weber möchte ich für die Förderung seit meiner Zeit als Bachelorstudent, sowie die Aufnahme in das iGRADplant Programm und stete wissenschaftliche Impulse danken.

Prof. Dr. Jianping Hu möchte ich für die Betreuung während meines Aufenthalts an der Michigan State University danken. Ebenso bedanke ich mich bei **Dr. Ronghui Pan**, **Dr. Stefanie Tietz** und **Shayna M. Kotzian** für den herzlichen Empfang und die Unterstützung im Hu Lab.

Dr. Petra Fackendahl und **Dr. Sigrun Wegener-Feldbrügge** danke ich für die Koordination des iGRADplant Programms und Unterstützung in allen organisatorischen Fragen.

Dr. Udo Gowik danke ich für die Betreuung während meiner Zeit im Westhoff Labor und die Einführung in die Welt der Transkriptome.

Dr. Tabea Mettler-Altmann danke ich für die gute Zusammenarbeit. Ebenso bedanke ich mich bei **Maria Graf**, **Elisabeth Klemp** und **Katrin Weber** für die praktische Unterstützung im MS Labor.

Dr. Shirin Zamani Nour möchte ich für die Beratung bei allen phänotypischen Analysen danken, sowie **Dr. Alisandra Denton** für die Hilfe bei der Auswertung bioinformatischer Daten.

Dr. Florian Hahn, **Leonie Wirth**, **Julia Schönknecht**, **Yannick Brack** und **Sara Simonte** danke ich für die Mitarbeit an meinen Projekten. Ohne euch gäbe es diese Arbeit in dieser Form nicht.

Dr. Fabio Facchinelli danke ich für die tolle Betreuung während meiner Bachelor- und Masterzeit, sowie die Einarbeitung am Confocal.

Anastasija Plett, **Franziska Kuhnert**, **Samantha Flachbart, Thomas Wrobel** und **Dr. Fabian Brandenburg** danke ich für die allwöchentlichen… wissenschaftlichen… Diskurse.

Lennart Charton, danke! Du warst der beste Kollege, den ich mir hätte wünschen können. Uns bleibt immer Paris!

Bei **Anja Nöcker** möchte ich mich für die unentbehrliche Unterstützung seit Tag 1 bedanken.

Nicht zuletzt danke ich **Dr. Tatjana Goss**, **Dr. Dagbegnon Angelo Romeo Agossou Yao**, **Dr. Nadine Rademacher**, **Dr. Christian Plohmann**, **Meng-Ying Lin**, **Marc-Sven Röll**, **Nils Koppers**, **Eva Maleckova**, **Alessandro Rossoni**, **Dr. Marion Eisenhut**, **Dr. Andres Sadowsky**, **Dr. Urte Schlüter**, **Dr. Berkley Walker, Raja Stracke** und **Kirsten Abel** für die tolle Atmosphäre und Hilfsbereitschaft im Weberlabor.

Dr. Sarah Keßel-Vigelius danke ich für die Vorarbeit am PHT3;3 Projekt.